UNIVERSITÀ
DEGLI STUDI
DI PADOVA

UNIVERSITÀ DEGLI STUDI DI PADOVA

DIPARTIMENTO DI INGEGNERIA INDUSTRIALE

SCUOLA DI DOTTORATO IN INGEGNERIA INDUSTRIALE
INGEGNERIA CHIMICA, MECCANICA E DEI MATERIALI

XXVIII CICLO

PLASMA ELECTROLYTIC OXIDATION COATINGS ON LIGHT ALLOYS

Direttore della Scuola : Ch.^{mo} Prof. Paolo Colombo
Coordinatore d'indirizzo: Ch.^{mo} Prof. Enrico Savio
Supervisore :Ch.^{mo} Prof. Manuele Dabalà

Dottorando : Luca Pezzato

A.A. 2014/2015

ABSTRACT

This thesis summarizes the work carried out during the three-year Ph.D in Industrial Engineering and involve the study and the characterization of coatings obtained on light alloys with the technique known as Plasma Electrolytic Oxidation (PEO). PEO process is, from the practice point of view, similar to the traditional anodic oxidation process as it's based on the electrochemical growth of a protective oxide layer on a metal surface. Compared with the traditional anodizing, PEO process works at higher currents and higher voltages, thus modifying the characteristics of the obtained layer. In recent years the importance of PEO process is increasing both in the research and in the industrial world. In fact the potentiality of the coatings obtained with this type of process are much higher than those of the coatings obtained with the traditional techniques of chemical conversion or anodizing. However, the relatively high cost and some problems related to the process (in particular the need of a post treatment to ensure galvanic corrosion) have now slowed to the widespread use on an industrial scale. So the scientific research on one hand is looking for new solutions to further improve the properties of the coatings, in order to justify the higher costs, on the other is trying to modify the existing process to reduce the above-mentioned costs.

In the first part of this thesis (chapter 1) the PEO process will be generally described with a brief history of the technique and a discussion regarding the chemical and physical principles that underlie the formation of the protective oxide layer. It will be also discussed the micro structural characteristics and technological properties of the obtained coatings, with reference to the current state of art present in the scientific literature. Then the current commercial solutions regarding the coatings obtained by plasma electrolytic oxidation and their main industrial applications will be described.

After, in chapter 2, will be briefly described the experimental apparatus used for the realization and the characterization of the PEO coatings in the laboratories of the Department of Industrial Engineering of the Padua University.

In subsequent chapters the main experimental results obtained during the Ph.D period will be described.

In particular in chapter 3 will be discussed the influence of the main process parameters (current density, time, electrolyte composition) on the characteristics of PEO coatings

obtained on magnesium alloys, with particular reference to the optimization of the above mentioned parameters in order to reduce the overall cost of the process.

In chapter 4 will be discussed the results regarding the addition of additives in order to improve the corrosion resistance of the obtained PEO layer on magnesium and aluminum alloys. In particular, the study will focus on the addition of molybdenum and lanthanum salts in the electrolyte. The choice of this type of additives is linked to their frequent use in surfaces engineering to improve the corrosion resistance as well as to their environmental friendly nature.

In chapter 5 will be instead described the work inherent the addition of additives to improve the wear and corrosion resistance of the coatings produced on magnesium alloys. In particular the effect of the addition of particles and nanoparticles of graphite in the electrolyte will be described.

In chapter 6 will be described the addiction of silver particles in the electrolyte in order to give an antibacterial effect to the coating. The chapter will focus on the mechanism of insertion of the silver particles in the coating and on the corrosion resistance of the obtained samples.

Finally in chapter 7 the possible application of PEO process also on steels (extremely important because of the technological importance of steel) , and particularly on low-alloy steels, will be studied.

The production and the main part of the characterization of PEO coatings was carried out at the metallurgy laboratories in the Department of Industrial Engineering, University of Padua, under the supervision of prof. Manuele Dabalà. Some analysis have, however, been performed at other structures: part of the corrosion resistance tests were carried out at the electrochemical laboratories of the Department of Chemistry, University of Padova with the collaboration of Dr. Cristian Durante, the XPS analysis were carried out at the Department of Chemistry of the University of Padua in collaboration with Prof. Silvia Gross and SIMS analysis were carried out at the Department of Physics of the University of Padua in collaboration with prof. Enrico Napolitani. The analysis of the wear resistance of PEO coatings has been made at the Department of Industrial Engineering of the University of Bologna with the collaboration of Dr. Valerio Angelini and prof. Carla Martini.

The obtained results have allowed an expansion in the knowledge regarding the PEO coatings and in particular to move towards greater industrial development of the technique.

In fact new process parameters that permit to reduce the total time for the obtainment of good PEO coatings were found. Moreover the addiction of news types of additives has permitted to improve the performances of the coating in terms of corrosion resistance and wear resistance and to give an antimicrobial effect to the coating. PEO process was also successfully applied on steels. The obtained results also have a scientific relevance that have allowed their presentation in numerous national and international conferences and publication in scientific journals as reported at the end of the thesis.

SOMMARIO

Questo lavoro di tesi riassume il lavoro svolto durante i tre anni di dottorato in ingegneria industriale e riguarda lo studio e la caratterizzazione di rivestimenti ottenuti mediante la tecnica denominata Plasma Electrolytic Oxidation (PEO) su leghe leggere. Il processo PEO è, dal punto di vista operativo, molto simile ai tradizionali processi di ossidazione anodica in quanto si basa sulla crescita per via elettrochimica di uno strato di ossido protettivo sulla superficie del metallo. Rispetto al tradizionale processo di anodizzazione il processo PEO lavora però a correnti e voltaggi più elevati, modificando così le caratteristiche dello strato ottenuto. Il processo PEO sta assumendo negli ultimi anni sempre maggiore rilevanza sia nell'ambito della ricerca che in quello industriale. Le potenzialità, infatti, dei rivestimenti ottenuti con questo tipo di processo sono molto più elevate rispetto a quelle dei rivestimenti ottenibili con le tradizionali tecniche di conversione chimica o di anodizzazione. Tuttavia il costo abbastanza elevato ed alcune problematiche relative al processo ne hanno per ora frenato la diffusione su larga scala a livello industriale. Dal punto di vista della ricerca scientifica quindi, da un lato si stanno cercando nuove soluzioni che consentano di migliorare ulteriormente le proprietà dei rivestimenti, in modo da giustificare i costi più elevati, dall'altro si stanno cercando delle variazioni al processo che consentano di ridurre i costi sopracitati. In questo lavoro di tesi nella prima parte (capitolo 1) verrà descritto in generale il processo PEO con alcuni cenni storici e verranno discussi i principi chimici e fisici che stanno alla base della formazione dello strato di ossido protettivo. Verranno inoltre descritte le caratteristiche microstrutturali e tecnologiche dei rivestimenti ottenibili, con riferimenti all'attuale stato dell'arte presente nella letteratura scientifica. Verrà poi fatto un breve riferimento a quelle che sono le attuali soluzioni commerciali riguardanti i rivestimenti ottenuti mediante plasma electrolytic oxidation. Successivamente verrà brevemente descritto (capitolo 2) l'apparato sperimentale utilizzato per la realizzazione e la caratterizzazione dei rivestimenti PEO.

Nei capitoli successivi verranno invece descritti i principali risultati sperimentali ottenuti durante il dottorato di ricerca.

In particolare nel capitolo 3 verrà descritto lo studio dell'influenza dei principali parametri di processo (densità di corrente, tempo, composizione dell'elettrolita) sulle caratteristiche

di rivestimenti PEO ottenuti su leghe di magnesio, con particolare riferimento all'ottimizzazione dei parametri sopracitati al fine di ridurre il costo globale del processo.

Nel capitolo 4 verranno illustrati i risultati relativi all'aggiunta di additivi al fine di migliorare la resistenza a corrosione dello strato di ossido ottenuto su leghe di magnesio e di alluminio. In particolare lo studio si concentrerà sull'aggiunta di sali di molibdeno e lantanio nell'elettrolita. La scelta di questo tipo di additivi è legata al loro frequente utilizzo nell'ingegneria delle superfici per migliorare la resistenza a corrosione oltre che alla loro non pericolosità dal punto di vista ambientale.

Nel capitolo 5 verrà invece descritto il lavoro inerente l'aggiunta di additivi per migliorare la resistenza ad usura (oltre che quella a corrosione) dei rivestimenti ottenibili su leghe di magnesio. In particolare verrà descritto l'effetto dell'aggiunta di particelle e di nano particelle di grafite all'elettrolita.

Nel capitolo 6 verrà descritta e studiata la possibile aggiunta di particelle d'argento nell'elettrolita in modo da conferire proprietà battericide al rivestimento PEO. In particolare ci si concentrerà sulle modalità di inserimento di tali particelle nel rivestimento e sulla resistenza a corrosione dei campioni così ottenuti.

Infine nel capitolo 7 verrà studiata la possibile applicazione della tecnica PEO anche sugli acciai ed in particolare sugli acciai basso legati.

La realizzazione e gran parte della caratterizzazione dei rivestimenti PEO è stata effettuata presso i laboratori di metallurgia del Dipartimento di Ingegneria Industriale dell'Università di Padova sotto la supervisione del prof. Manuele Dabalà. Alcune analisi sono però state effettate presso altre strutture: parte dei test di resistenza a corrosione sono stati svolti presso i laboratori di elettrochimica del Dipartimento di Chimica dell'Università di Padova con la collaborazione del dott. Cristian Durante, le analisi XPS sono state realizzate presso il Dipartimento di Chimica dell'Università di Padova con la collaborazione della prof.ssa Silvia Gross e le analisi SIMS sono state realizzate presso il Dipartimento di Fisica dell'Università di Padova con la collaborazione del prof. Enrico Napolitani. La caratterizzazione della resistenza ad usura dei rivestimenti PEO è stata inoltre realizzata presso il Dipartimento di Ingegneria Industriale dell'Università degli Studi di Bologna con la collaborazione del dott. Valerio Angelini e della prof. Carla Martini.

I risultati ottenuti hanno permesso di ampliare le conoscenze inerenti i rivestimenti PEO e in particolare di procedere verso un maggiore sviluppo industriale della tecnica. Infatti è stata sviluppata una nuova sequenza di parametri di processo che permette di ottenere

rivestimenti di ottima qualità con tempi inferiori rispetto a ciò che viene attualmente realizzato. Inoltre l'aggiunta di particolari additivi ha permesso di incrementare notevolmente la resistenza a corrosione e ad usura dei rivestimenti in modo tale da consentire la realizzazione di componenti a più alto valore aggiunto. L'inserimento di altre tipologie di additivi ha poi permesso di conferire proprietà battericide al rivestimento. Infine la tecnica PEO è stata anche con successo applicata agli acciai basso legati aprendo un importante filone di sviluppo a livello tecnologico.

I risultati ottenuti presentano inoltre una rilevanza scientifica tale da averne permesso la presentazione in numerosi convegni nazionali e internazionali e la pubblicazione in riviste scientifiche di settore come riportato nell'elenco delle pubblicazioni che conclude questo lavoro di tesi.

LIST OF CONTENTS

Chapter 1

Plasma electrolytic oxidation (PEO)

1.1 INTRODUCTION [1-2]

Lightweight metals, e.g. aluminum (Al), magnesium (Mg), titanium (Ti) and their alloys are of great importance for applications in various machinery and transportation system, especially in aerospace and automobile products due to their high strength-to-weight ratio and superior physical and chemical performances. However, their poor tribological properties, such as low wear resistance, high friction coefficient and difficulty to lubricate, have seriously restricted their extensive applications. Moreover also the poor corrosion resistance of existing magnesium and aluminum alloys in some service environments has limited the further expansion of their application. In the past decades, various traditional surface treatments, such as physical vapor deposition, chemical vapor deposition, ion beam assisted deposition, and spraying, have been applied to metallic substrates to improve their generally poor tribological and corrosion properties.

However, most of the mentioned methods involve high processing temperature, which may degrade the coatings and/or substrates. Plasma electrolytic oxidation (PEO), also called 'Microarc Oxidation (MAO) is a relatively novel surface modification technique that is attracting ever-increasing interest in fabricating oxide ceramic coatings on light alloys such as Al, Ti and Mg. PEO treatment can enhance their corrosion- and wear-resistance properties, or confer various other functional properties including anti-friction, thermal protection, optical and dielectric, as well as a pre-treatment to provide load support for top layers. PEO is derived from conventional anodizing [3-4]. Anodizing is traditionally carried out using direct current (DC) electrolysis. The work piece is made anodic in an acid electrolyte (sulfuric acid is most commonly used, but phosphoric, oxalic, chromic and other acids can be used, singly or in combination). Typically, the cell voltage is 20 to 80 V DC and the current density is 1 to10 A dm^{-2}, the process usually being controlled at a constant cell voltage. Plasma electrolytic oxidation (PEO) treatment is

usually carried out in high voltage condition which is introduced into the high-pressure discharge area from the Faraday region of traditional anodizing. The applied voltage is increased from tens of volts to hundreds of volts, which is the breakthrough of traditional anodizing. The voltage forms developed from DC to continuous pulse, and then to AC, resulting in corona, glow, spark discharge and even micro-arc discharge phenomenon in the surface of the samples [5]. This allows the formation of coatings composed of not only predominant substrate oxides but of more complex oxides containing the elements present in the electrolyte. The general comparison between conventional DC anodizing and PEO technique was shown in Tab. 1.1.

Tab.1.1 General comparison between conventional direct current anodizing and plasma electrolytic oxidation coating technologies [5]

Properties	**Anodizing**	**PEO technique**
Cell Voltage (V)	20-80	120-300
Current density (A/cm^2)	<10	<30
Substrate pretreatment	Critical	Less Critical
Common electrolytes	Sulfuric, chromic or phosphoric acid	Neutral/Alkaline (pH 7-12)
Coating thickness (µm)	<10	<200
Coating Hardness	Moderate	Relatively High
Adhesion to substrate	Moderate	Very High
Temperature Control	Critical	Not so Important

The PEO technique in detail present many advantages if compared with traditional anodizing [6]:

(i) a wide range of coating properties, including wear-resistance, corrosion-resistance and other functional properties (such as thermo-optical, dielectric, thermal barrier are conferred);

(ii) no deterioration of the mechanical properties of the substrate materials is caused because of negligible heat input;

(iii) high metallurgical bonding strength is measured between the coating and the substrate;

(iv) there is the possibility of processing parts with complex geometric shape or large size;

(v) equipment is simple and easy to operate;

(vi) cost is low, as it has no need of experience vacuum or gas shielding conditions;

(vii) the technique is ecologically friendly, as alkaline electrolytes are employed, and no noxious exhaust emission is involved in the process, meeting the requirement of green environment-friendly surface modification technology.

Moreover conventional anodizing in strongly alkaline solutions can produce coatings up to several microns thick, they are still too thin to provide effective protection against wear and corrosion, and therefore are used mainly for decoration. The PEO method, derived from conventional anodizing but enhanced by spark discharge events when the applied voltage exceeds the critical value of the insulator film, can generate thicker ceramic coatings with excellent properties, e.g. high hardness, good wear and corrosion properties, and excellent bonding strength with the substrate, compared with the conventional anodizing method. The process has demonstrated great successes in offering improved surface oxidation treatment of Mg, Al and Ti alloys, replacing the conventional acid-based anodizing processes and/or conversion treatments, which contain hexavalent chrome and other environmentally hazardous substances. This could be in the future one of the key factors that will cause the increase in the industrial applications of PEO process. The typical equipment used to produce PEO coatings is the same used in conventional anodizing and consist in a power source connected with the cell that contain the electrolyte. A schematic representation of this equipment is reported in Fig.1.1.

Before the PEO treatment, the samples should be ground and polished with abrasive paper, degreased ultrasonically in acetone and cleaned with distilled water. During the treatment, the samples are used as anode plates and immersed in the electrolyte which is cooled by a water cooling system and mechanically stirred by a mixer. After the treatment, the samples should be rinsed with distilled water and air dried. The microstructure and properties of the coatings can be tailored by the careful selection and matching of electrolyte and electrical parameters; thus wide applications can be found in industrial sectors including automotive, aerospace, marine, textile, electronic (3C products), biomedical and catalytic materials [7-9].

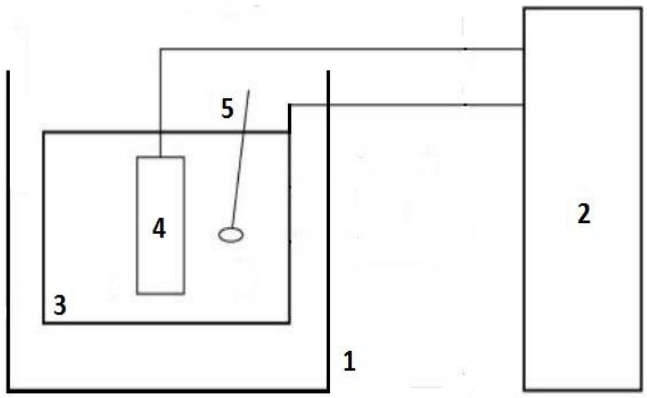

1. Electrolyte bath;
2. DC power supply;
3. Cathode;
4. Sample (Anode);
5. Stirrer.

Fig. 1.1 Schematic representation of the experimental equipment used in PEO process

The PEO technique experienced a long historical development: in the 1930s, Günterschultze and Betz (1934) [10] investigated the phenomenon of spark discharge. It was not until the 1960s, when advances were made for producing cadmium niobate on the cadmium anode in an electrolyte containing Nb using spark discharge by Mcniell and Gruss, that the practical application value of spark discharge was firstly exploited [11-12]. From 1970, utilizing surface discharge to deposit oxide coatings on light metals was studied extensively in Russia, followed by USA, Germany and other countries. The early industrial applications could be traced back to the late 1970s. However, the poor quality and low growth efficiency of the coatings delayed further development of this technique. From the 1980s on, new developments of electrolyte, from acidic to alkaline enabled efficient formation of high quality coatings, especially in the last decade. For example, companies such as Keronite (UK), Magoxid-coat (Germany) and Microplasmic (USA) industrially developed an efficient process. Examples of industrial equipment used in PEO process can be found in Fig.1.2.

Fig. 1.2 Examples of industrial applications of PEO process

1.2 FUNDAMENTALS OF PLASMA ELECTROLYSIS [13]

It is well known that the electrolysis of aqueous solutions is accompanied by a number of electrode processes. In particular, the liberation of gaseous oxygen and/or metal oxidation occurs on the anodic surface. Depending on the electrolyte chemical activity in respect to the metal, the oxidation process can lead either to surface dissolution or to oxide film formation. Liberation of gaseous hydrogen and/or cation reduction can also occur on the cathodic surface. When a 'conventional' electrolytic process is studied (e.g. electroplating, electrochemical machining, anodizing, etc.), the electrode processes are usually considered in the framework of a simplified model, where the electrode-electrolyte interface can be represented by a two-phase system (i.e. metal-electrolyte or oxide-electrolyte couple) with a single phase boundary consisting of a double-charged layer. Concurrent by-product processes (such as gas liberation) are either neglected or taken into account using special correction factors, e.g. 'current yield' or 'electrode shielding' coefficients.

However, as will be shown in the following, such a simplification is not always justifiable, since, under certain conditions, the results obtained from the treatment are influenced considerably by the processes that occur in the gaseous environment surrounding the electrode and/or in its surface layers.

The above-mentioned processes affect the characteristic current-voltage profile of the electrochemical system (Fig. 1.3).

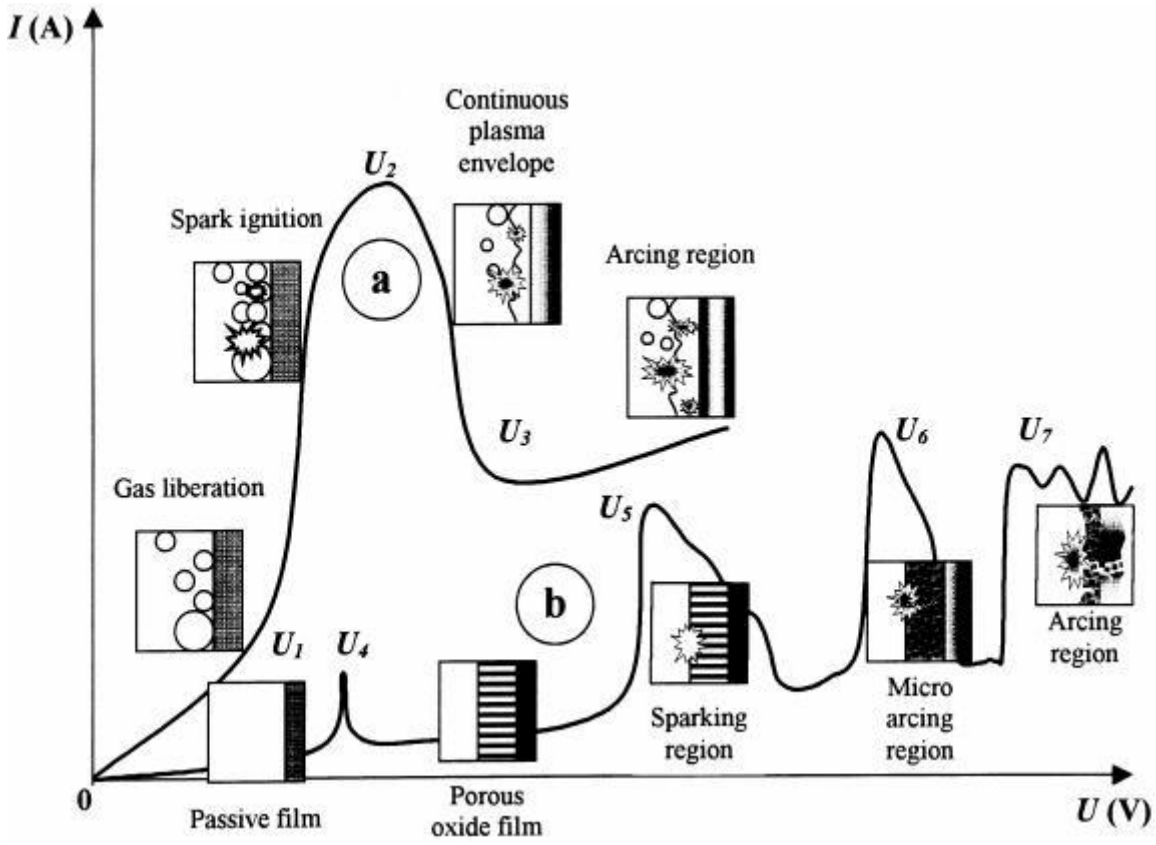

Fig. 1.3 Two kinds of current–voltage diagram for the processes of plasma electrolysis: discharge phenomena are developed (a) in the near-electrode area and (b) in the dielectric film on the electrode surface [13]

A 'type-a' current-voltage plot represents a metal-electrolyte system with underlying gas liberation on either the anode or cathode surface; 'type-b' represents a system where oxide film formation occurs [14-15]. At relatively low voltages the kinetics of the electrode processes for both systems conform to Faraday's laws and the current-voltage characteristics of the cell vary according to Ohm's law. Thus, an increase in voltage leads to a proportional rise in the current (region '0-U_2' in the type-a system and '0-U_4' in the type-b system). However, beyond a certain critical voltage, the behavior of a particular system may change significantly.

For a type-a system in the region U_1-U_2, a potential rise leads to current oscillation accompanied by luminescence. The current rise is limited by a partial shielding action of gaseous reaction products (O_2 or H_2) over the electrode surface. In areas where the electrode remains in contact with the liquid, however, the current density continues to rise, causing local boiling (ebullition) of the electrolyte adjacent to the electrode. Upon progression to point U_2 the electrode is enshrouded by a continuous gaseous vapor plasma envelope of low electrical conductivity. Almost all of the voltage across the cell is now

dropped in this thin, near-electrode region. The electric field strength E within this region therefore reaches a value between 106 and 108 V/m, which is sufficient for initiation of ionization processes in the vapor envelope. The ionization phenomena appear initially as a rapid sparking in scattered gaseous bubbles and then transform into a uniform glow distributed throughout the vapor plasma envelope. Due to the hydrodynamic stabilization of the vapor envelope in the region U_2-U_3, the current drops and, beyond point U_3, the glow discharge transforms into intensive arcing accompanied by a characteristic low-frequency acoustic emission.

The behavior of type-b systems is more complicated. Firstly, the passive film previously formed begins to dissolve at point U_4, which, in practice, corresponds to the corrosion potential of the material. Then, in the region of re-passivation U_4-U_5 a porous oxide film grows, across which most of the voltage drop now occurs. At point U_5, the electric field strength in the oxide film reaches a critical value beyond which the film is broken through due to impact or tunneling ionization [16-17]. In this case, small luminescent sparks are observed to move rapidly across the surface of the oxide film, facilitating its continued growth. At point U_6, the mechanism of impact ionization is supported by the onset of thermal ionization processes and slower, larger arc-discharges arise. In the region U_6-U_7 thermal ionization is partially blocked by negative charge build-up in the bulk of the thickening oxide film, resulting in discharge-decay shorting of the substrate. This effect determines the relatively low power and duration of the resultant arc discharges, i.e. micro-discharges, which are termed 'micro arcs' [13]. Owing to this 'micro-arcing', the film is gradually fused and alloyed with elements contained in the electrolyte. Above the point U_7, the arc micro-discharges occurring throughout the film penetrate through to the substrate and (since negative charge blocking effects can no longer occur) transform into powerful, arcs, which may cause destructive effects such as thermal cracking of the film [15].

In practice, a number of the above electrode processes may occur concurrently over adjacent areas of the electrode surface. The simple two-phase electrode-electrolyte model normally encountered in conventional electrolysis must therefore be replaced by a more complex four-phase system (metal-dielectric-gas-electrolyte) with a number of possible phase boundaries, particularly when electrochemical systems running above the critical voltages of U_1 and U_5 are considered.

Two phases of low conductivity are formed (i.e. dielectric and gas), where the main voltage drop is concentrated. Since the resistance of these phases varies continuously, it is

very difficult to discern in what phase the ionization phenomena are initiated [18]. Thus, the division of electrochemical systems into the two types is not distinct.

1.3 MECHANISM OF FORMATION OF PEO COATINGS [2]

The PEO of metals is a complex process that combines oxide film formation, dissolution and dielectric breakdown and it is developed from the traditional anodic oxidation: the sample (anode) is immersed in an electrolyte and the tank is the cathode, working with higher voltages and current densities [19-20]. Due to the high voltage (that has to be above the dielectric breakdown potential of the oxide layer) persistent anodic micro-discharges are formed on the surface during the PEO treatment. These short-lived micro-discharges are the key factors of the process; they move randomly over the processed surface and produce the growth of an oxide ceramic coating [21]. The typical micro-discharges formed during PEO process can be observed in Fig. 1.4.

Regardless of what kind of electrolyte systems or electrical parameter control modes (constant current or constant voltage) are applied, the basic formation mechanism of PEO coatings is similar. Taking the constant current mode as an example, Fig. 1.5 gives a schematic of the discharge phenomena and coating structure changes during the micro-discharge oxidation process. It is well known that there exists a very thin, natural, passive film on substrate metal surfaces (also shown in Fig. 1.5a), which could provide a very limited protective effect. As the applied voltage increases, a large number of gas bubbles are produced, which is the traditional anodizing stage with the formation of a porous insulation film with a columnar structure perpendicular to the substrate (Fig. 1.5b).

Fig. 1.4 Typical discharges formed during PEO process

When the voltage exceeds a certain threshold (i.e. breakdown voltage), dielectric breakdown occurs in some scattered weak regions across the insulating film, accompanied by the phenomenon of spark discharge (Fig. 1.5c). In this case, a large number of fine, uniform, white sparks are generated on the sample surface which result in the formation of a large number of small uniform micro pores. In constant current mode, in order to ensure effective coating breakdown, the voltage as feedback is forced to increase and reach a relatively stable value (Fig. 1.6).

The color of the sparks also gradually changes from white through yellow to orange-red, while the number decreases. In the yellow to orange-red sparks stage, coating growth rate is faster, this is known as the micro arc stage. With the coating thickness increases, the voltage value increases. Meanwhile the number of sparks reduce but their intensity increases, which induces rather rougher surface morphologies (Figures 1.5d and e). With further increase of the voltage, the strong large dot arc discharge appears and bursts with ear-piercing noise (Fig. 1.5f). This causes a splash of the coating materials and local serious ablation characteristics, thus forming a porous and loose part of the PEO coating. To obtain high-quality coatings, this arc discharge stage should be avoided as far as possible.

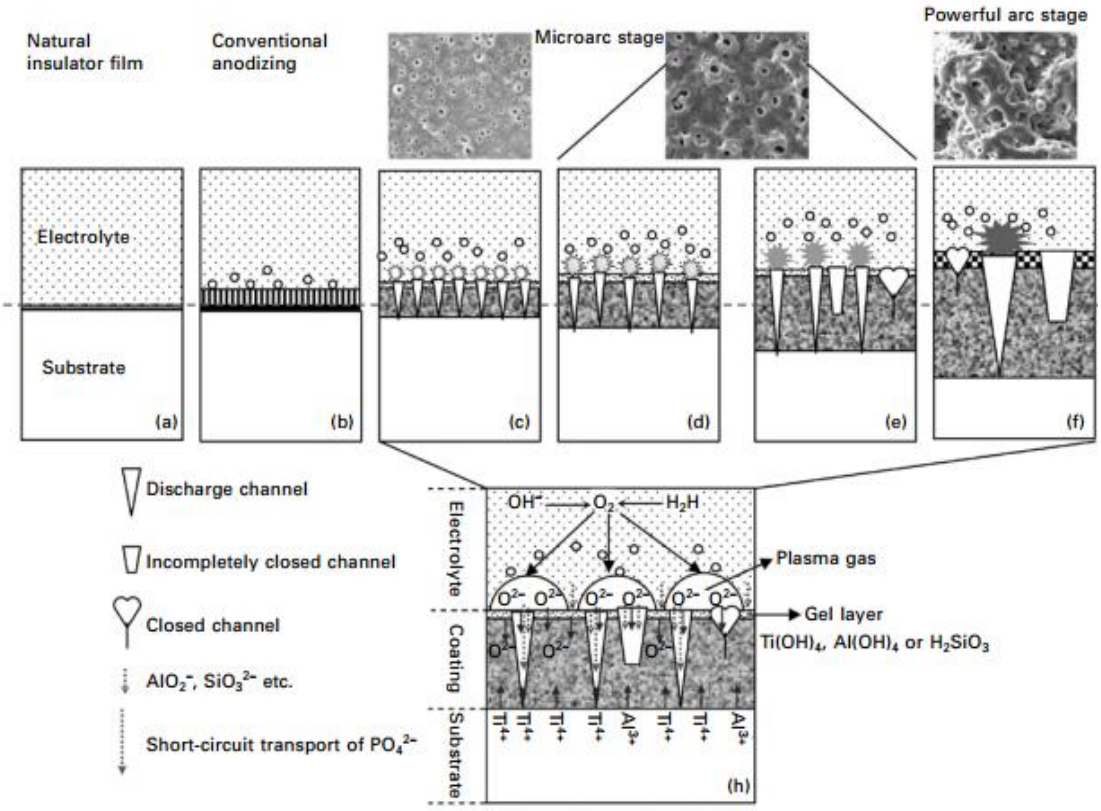

Fig.1.5 Schematic of various chemical reactions and structural evolution developed during plasma electrolytic oxidation process of titanium alloy [2]

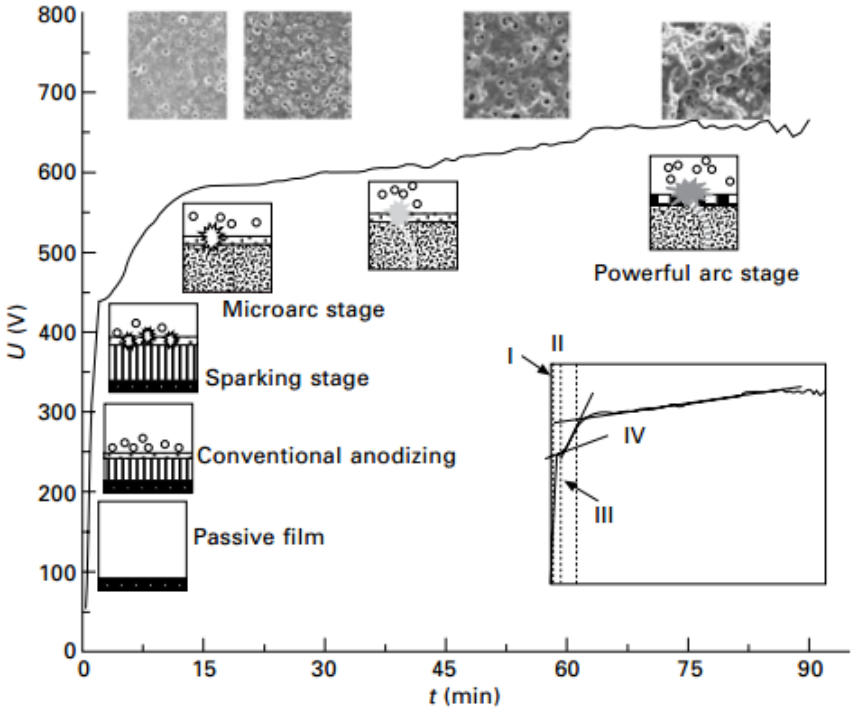

Fig.1.6 Schematic of discharge phenomena and coating microstructure developed during plasma electrolytic oxidation process [2]

The coating formation process under micro-discharge can be broadly classified into the following three steps.

First of all, a large number of dispersed discharge channels are produced as a result of micro-regional instability when the breakdown voltage is reached, as shown in Fig. 5.2c. The induced electron collapse effect makes the coating materials move into the discharge channels rapidly because of the high temperature ($2x10^4$ °C) at, or around, the centre of discharge and the high pressure (10^2 MPa) in less than 10^{-6} s [13]. Under a strong electric field force, anionic components such as $PO_4^{3-}$and SiO_3^{2-} enter the channels through electrophoresis. At the same time, passages, under the effect of high temperature and high pressure, allow alloying elements of the substrate to melt or diffuse into the channels producing the formation of amorphous or meta stable phases.

Secondly, the oxide products are solidified under the rapid cooling of the proximity electrolyte, thus increasing the coating thickness in the local area near to the discharge channels. When the discharge channels become cooled, the reaction products deposit on the channel walls to close the discharge channels.

Finally, the produced gases are driven to escape out of the discharge channels, and as a result, the residual blind holes with 'volcano' shapes are maintained. An example of this volcano shape is shown in Fig.1.7

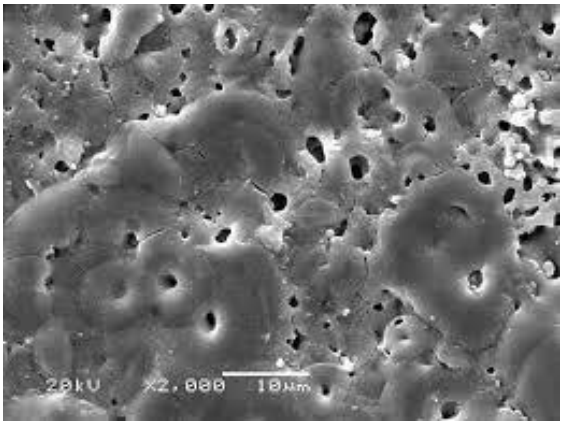

Fig. 1.7 Examples of holes with "volcano" shapes on the surface of a PEO treated sample [2]

When the oxidation continues, the above process repeats in the relatively weak regions of the entire coating surface, thus promoting the overall uniform coating thickness.

In *Region I* of Fig. 1.6, voltage linearly increases with time, corresponding to the traditional anodizing stage, in which a very thin insulating film (as shown in Fig. 1.5b) forms, complying with Faraday's Law of 100% current efficiency. In *Region II*, the voltage increase slows with the decreased oxide film growth rate, which is attributed to the competition of anode coating growth and dissolution. In *Region III*, voltage increases rapidly to exceed the critical value, a large number of dispersed discharge channels (as shown in Fig. 1.5c) are produced as a result of micro-regional instability caused by breakdown and, at the same time, are accompanied by a large release of oxygen. In *Region IV*, the voltage remains stable; this is known as the micro arc stage. At the end of the stage, the strong dot arc discharge appears.

Each spark discharge event corresponds to a discharge channel throughout the coating, resulting in breakdown, channeling, melting and solidification effects, as follows (in the example reported in Fig.1.5 and Fig.1.6 so with a titanium alloy and a phosphate containing electrolyte):

(i) *Discharge induced ion 'short circuit' migration*.

By analyzing element distribution across a section of distinct coatings formed in different electrolyte systems, it is assumed that PO_4^{3-} ion transports by 'short circuit' to the proximity of the substrate-coating interface and participates in chemical reactions, i.e. migrates through the discharge channels rather than through the diffusion effect. Elements, P from P-containing electrolyte and Ti from the substrate, are predominant in the neighboring region of interface between coating and substrate because PO_4^{3-} ion is more easily dragged to the region of the coating–substrate interface through the discharge channel under the high electric field effect.

(ii) *Discharge induced coating in-growth*.

Substrate metal evolves into the discharge channels by dissolution, melting or sputtering. Under the rapid cooling effect of the cold proximity substrate, the generated melting oxide products near to the coating–substrate interface solidify to form a fresh nano-crystalline layer with small uniform nano grains. The nano grains in this layer are subject to gradual growth under the metallurgical process caused by the repeated discharge. It is believed that formation of the very thin nanocrystalline layer is a universal characteristic of the PEO process, regardless of the substrate species. The nanocrystalline layer is constantly

produced by ‘eating’ the substrate and moves towards the substrate; this is also considered as the main inner growth mechanism. It should be noted that the very thin nanocrystalline layer near to the interface is a universal characteristic of the PEO process, regardless of the substrate species, while the grain size and phase composition of bulk coating away from the interface shows great distinction, depending on substrate species and electrolyte components. An example of the nanocrystalline layer is reported in the A zone of the TEM mage in Fig.1.8

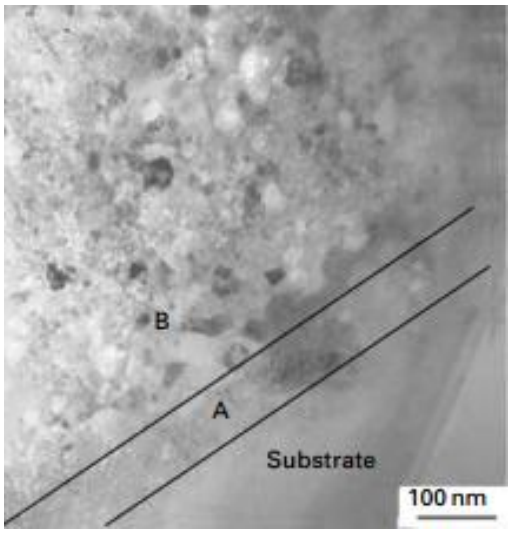

Fig.1.8 TEM images of the inner nanocrystalline layer near coating/substrate interface (A-zone) [2]

(iii) *Discharge induced inner and outer growth of the coating.*

It should be noted that the growth of coating above and below the original substrate surface is simultaneous. The inner growth is attributed to the continuous formation of a nanocrystalline layer by eating the substrate, while the oxide products of the chemical reactions occurring in the discharge. Channels are mainly responsible for the formation of the outer layer. The melting oxide products solidify to deposit on the inner wall of the discharge channel, and tend to close the channel, which enhances the growth of the compact inner layer. However, the produced excessive oxygen gas has to be compressed to escape from the channel, which causes the partial melting products to spray out and deposit on the margin of the channel, thus increasing the outer layer thickness in the local area near to the discharge channels. as a result, the residual blind holes with ‘volcano’ shapes are maintained. Therefore, the outer layer generally has a loose nature. Figure 1.9 presents a scheme of the growth thickness evolution of the PEO coating. It can be seen that in the initial stages of oxidation (Fig. 1.6 Region i), the coating thickness increases rapidly, and the outer growth dominates with a loose and porous structure, as

shown in Figures 1.9 a and b. in the middle stages of oxidation (Fig. 1.6, Regions ii~ iV), the growth rate of the coating slightly decreases, accompanied by the dominant inner growth of a dense coating, as shown in Figures 1.9, d and e.

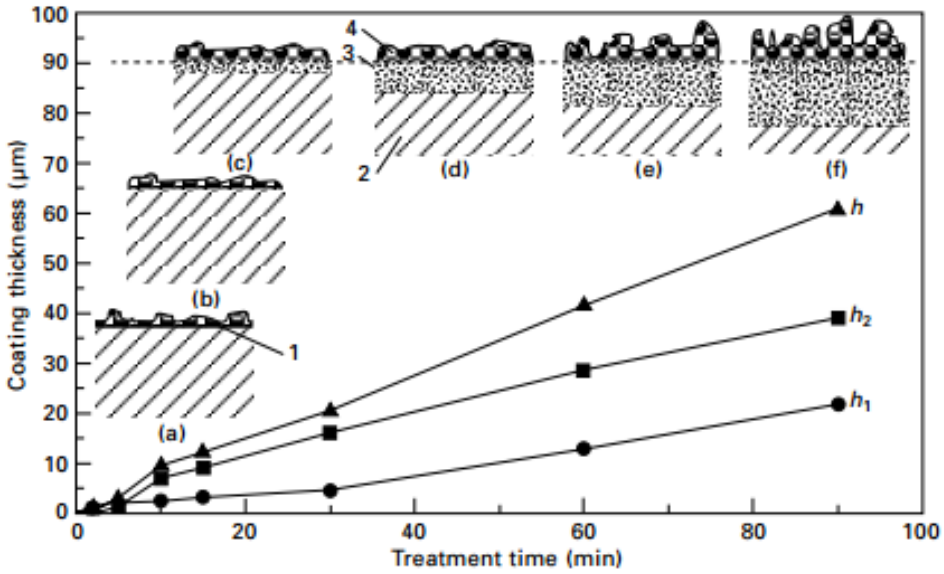

Fig.1.9 Schematic of growth thickness evolution of plasma electrolytic oxidation coating: 1 = conventional anodizing film; 2 = substrate; 3 = inner growth layer; 4 = outer growth layer; (a) (b) in the initial stage; (c) (d) (e) in the medium stage; (f) in the final stage, the surface roughening of the coating is striking. h= whole thickness; h_1= outer growth thickness; h_2= inner growth thickness [2].

With increasing oxidation time, the porous layer thickness in the outer coating increases. in the later Region IV of Fig. 1.6, the appearance of large and long-life sparks results in a looser and rougher coating surface (Fig. 1.9f). During the whole growth process, the inner growth is predominant; generally, the outer growth thickness of the coating registers as low as 30% of the total coating, variations depending on distinct alloy and electrolyte compositions. Therefore, PEO coating causes little change in the finished dimensions, making it suitable for production of precision components. if necessary, the outer growth layer can be polished to return to the original dimensions.

(iv) *Discharge induced involvement of surface sediments into the coating*.

Depending on particular electrolyte systems, insoluble and poorly-movable gels such as $Al(OH)_4$ or H_2SiO_3 continuously deposit on the coating surface, the subsequent discharge process inducing the hydrated polygels to pyrolyse to form oxide products, which further involves the outer layer through channel effect.

(v) *Discharge induced repeated melting–solidification process*.

The coating of nanocrystalline grains combined with a small amount of amorphous phase forms as a result of solidification of melting products under rapid cooling by the cold substrate and electrolyte. The instantaneous temperature gradient around the discharge channel makes it easier to generate the columnar crystal structure along the edge of the discharge channel at the same time, the as-formed coating products are subjected to the melting–cooling–crystallization process under the instantaneous local heating and cooling cycle caused by the repeated discharge which leads to the formation of complex oxides as well as the possible transformation of metastable to high temperature stable phases.

(vi) *Discharge induces no changes of substrate microstructure*.

Generally, the discharge event tends to occur in the coating–substrate interface or regions near the interface, accompanied by the formation of discharge channels through the coating. While the partial high-energy micro area (channel) caused by the discharge is quenched instantly, it is not enough to induce any change of substrate texture neighboring to the coating–substrate interface.

1.4 PRINCIPAL PARAMETERS THAT INFLUENCE PEO COATINGS [1-2]

It is considered that the PEO treatment is a multifactor-controlled process, which is influenced by many factors, intrinsic or extrinsic. The compositions of substrate materials and electrolyte are considered to be intrinsic factors which play crucial role for the structure and composition of PEO coatings, while the extrinsic factors generally consist of electrical parameters, processing temperature, oxidation time and additives [22]. Herein, these influence factors for PEO technique will be introduced and discussed briefly.

a) *Influence of substrate materials*

The difference of substrate materials plays a crucial role in the components and properties of PEO coatings. The predominant compositions of the PEO coatings depend on the substrate materials, for example, the main content of coatings deposited on Al, Mg, Ti and their alloys are Al_2O_3, MgO and TiO_2 respectively. Therefore, the PEO coatings deposited

on different substrate materials generally possess different properties. According to recent studies, the available coating thicknesses are around 300 μm on Al alloy, 150 μm on Mg alloy and 200 μm on Ti alloy respectively. The hardness value ranges for PEO coatings formed on different substrate materials are generally from 300 HV to 2500 HV on Al alloy, from 200 HV to 1000 HV on Mg alloy and from 300 HV to 1100 HV on Ti alloy [13, 22].

It may be observed that aluminum alloys with a high content of Si (such as high-silicon die castings) or Cu (such as high-copper aluminum alloys) are rather difficult to anodize with traditional anodizing processes. This problem can be resolved by using the PEO process although it has the disadvantages of local flaws at Si (or Cu) aggregation sites and slightly higher power wastage. Silicon and copper are the main elements that cause irregular features in the PEO coating [23]. PEO is also very promising as a replacement for conventional anodizing to fabricate high-performance coatings on al or Mg based composites. However, the reinforcement phases (such as particles, whiskers or fibers) in the metal matrix of the composites inevitably affect the microarc discharge process and lower the efficiency of coating growth.

b) *Influence of electrolytes*

The compositions of electrolyte greatly affect the properties of PEO ceramic coatings. Different electrolytes result in different growth rates, structures, phase compositions and element distribution of the PEO coatings [24-27]. Generally, the electrolytes used for PEO treatment are composed of acidic electrolytes and alkaline electrolytes. The acidic electrolytes including concentrated sulfuric acid, phosphoric acid and other salt solutions etc. are seldom used at present due to their great environmental pollution. While the alkaline electrolytes mainly consist of four systems including sodium hydroxide based electrolytes, silicate based electrolytes, phosphate based electrolytes and aluminate based electrolytes [22]. The intrinsic effects of the electrolyte can be summarized as follows:

(i) first and most important, promoting metal passivation to form a thin insulating film, which is a necessary prerequisite for dielectric breakdown to induce spark discharge;

(ii) as the medium for conducting current, transmitting the essential energy needed for anode oxidizing to occur at the interface of metal/electrolyte;

(iii) providing the oxygen source in the form of oxysalt needed for oxidation;

(iv) finally and also interestingly, allowing components present in the electrolyte to be incorporated into the coatings, further modifying or improving the properties of the PEO coatings. To meet the prerequisite for dielectric breakdown, additives to promote strong metal passivation (such as silicates, aluminates and phosphates) are widely used as basic constituents of the electrolytes.

The three groups have the following advantages:

(i) they allow the sparking voltage to be easily reached, thus saving time;

(ii) components present in the electrolyte (such as SiO_3^{2-}, AlO_2 and PO_4^{3-}) are easily incorporated into the coatings by poly-reactions and deposition, thus increasing the coating growth rate;

(iii) usage of environmentally friendly and inexpensive electrolytes produce wear and corrosion-resistant coatings which are beneficial for the commercial producer. it has been proved by experiments that simple alkaline electrolytes are unfeasible for commercialization of the process, because of lower coating growth rates and very high energy consumption.

Thus, a complex electrolyte composition is commonly desirable for investigation and commercial applications.

c)*Effect of electric parameters*

The whole PEO process and the properties of ceramic coatings are greatly affected by electrical parameters including current modes, current density, current frequency, anodic voltage, cathodic voltage, duty cycle etc.

Compared to the unipolar current process, the application of pulsed bipolar current resulted in reducing the high spikes on temperature profiles and the average plasma temperature. The aluminum oxide coating morphology and microstructure were also significantly different under different current modes. The bipolar current mode could improve the coating quality compared with the unipolar current mode, in terms of surface morphology and cross-sectional microstructure. A dense coating morphology could be achieved by adjusting positive to negative current ratio and their timing to eliminate or reduce the strongest plasma discharges and the high temperature spikes, thus resulting in the improvement of coating qualities [28].

The thickness and growth rate of the coatings generally increased with the increasing of applied current frequency [29]. The coating thickness increased with the increased

current density in aluminum alloys and residual stresses in alumina coatings tended to decrease with the increased current density due to increased plasma micro discharge events which promoted stress relaxation through formation of micro crack network and thermal annealing in the coatings [30]. The pore size of PEO coatings increased with the increase of applied voltage. The elastic modulus and residual stress both increased with the increasing of applied voltage [31].

d) *Influence of processing temperature*

The electrolyte temperature can greatly affect the PEO process. If the temperature is too low, the oxidation process becomes weak, resulting in less thickness and lower hardness of the PEO coatings. If the temperature is too high, the dissolution of oxide film will be enhanced, and thus cause the coating thickness and hardness to decrease significantly. Therefore, the processing temperature should also be studied and generally controlled in the range of 20-40℃.

e) *Influence of oxidation time*

With the increasing of oxidation time, the coating thickness increases, while the growth rate decreases. Different oxidation time can result in different coating qualities, such as thickness, roughness, adhesion, hardness, wear resistance and corrosion resistance etc.. Therefore, the oxidation time for PEO treatment should be investigated and optimized.

f) *Influence of additives*

Employing different additives in the electrolyte can greatly affect the PEO process, and thus resulting in different properties of the coatings. For example, Jun Liang et al. [32] studied the effect of KF in Na_2SiO_3-KOH electrolyte on the structure and properties of PEO coatings formed on Mg alloy. It was found that the addition of KF contributed to increase the electrolyte conductivity, decrease the work voltage and final voltage in the PEO process and change the spark discharge characteristics. Furthermore, the addition of KF resulted in a decrease of pore diameter and surface roughness, an increase of the coating compactness and the changes in the phase compositions as well. The hardness and wear-resistance of the coating also enhanced due to the addition of KF. The addition of $NaAlO_2$ to a phosphate-based electrolyte was reported to result in coatings with fine pore sizes. While the coating produced with the conventional phosphate electrolyte was

constituted with only MgO, the formation of $MgAl_2O_4$ spinel was facilitated with the introduction of $NaAlO_2$ into the electrolyte. the conductivity of the electrolyte was reported to increase with increase in $NaAlO_2$, thus resulting in lower breakdown voltages. Due to finer discharges, the coatings produced with 8% $NaAlO_2$ were smoother. Furthermore, a better corrosion resistance was attributed to the higher volume fraction of $MgAl_2O_4$ and reduced structural imperfections in the coating [32].

Addition of CrO_3 to the silicate-based electrolyte was examined by Blawert et al. [33]. The CrO3 in the electrolyte was reported to reduce the coating thickness and also the amount of Forsterite (Mg_2SiO_4) in the coating. Further, the incorporation of chromium species into the layer did not yield any better inhibition capabilities.

1.5 MICROSTRUCTURE OF PEO COATINGS [2]

The micro structural features of PEO coatings are dependent on the processing conditions, and the thickness of the coatings can range from 5 µm to 200 µm. The coatings have a jagged/wavy interface in most cases, which makes them an integral part of the substrate. Characteristically, all PEO coatings have a very thin barrier, with a thickness ranging from a few nm to a maximum of 2 µm. The core ceramic oxide layer is found above the barrier layer, growing in thickness with prolonged PEO processing. As the layer grows by the continuous discharge process, there are pores being formed and incorporated into the coating. Blawert *et al.* [34] have described the micro structural features of a 120 µm thick PEO layer obtained from a silicate-based electrolyte. In detail they found that the coating can be divided into four distinct regions:

(i) a thin inner *barrier layer* of < 1 µm;

(ii) a relatively compact *intermediate layer* just next to the barrier layer with a lower number of pores and cavities;

(iii) a region of *pore bands* with visible craters and pore channels;

(iv) the outermost *porous layer* with craters on top.

The above features are schematically represented in Fig. 1.10.

This build-up of a PEO coating is more or less typical for many PEO coatings produced using Si-based electrolytes.

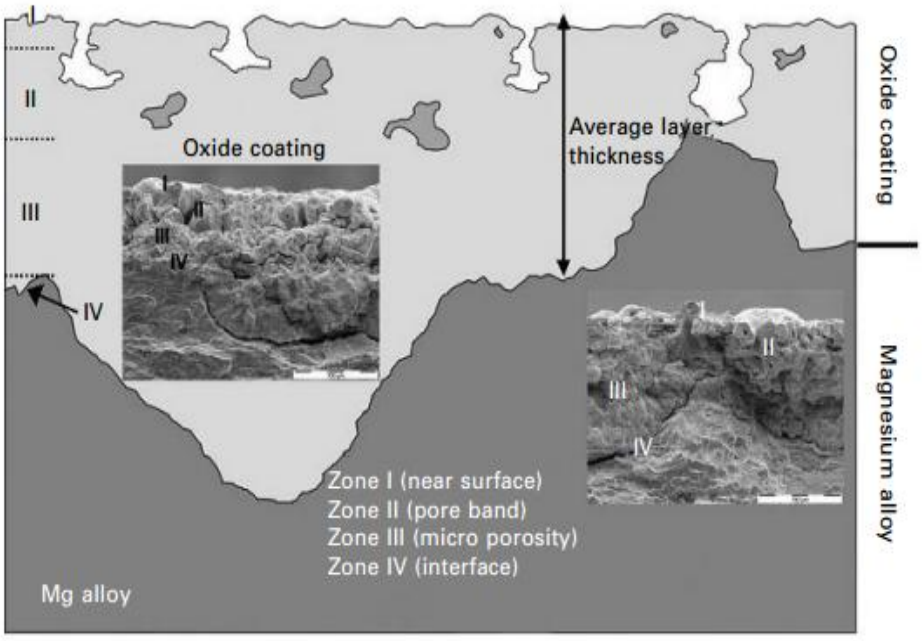

Fig.1.10 Schematic representation of cross-section of PEO coatings on magnesium alloys (typical features of the layer obtained by SEM micrographs are inserted) [2]

The zone called zone IV is the inner barrier layer or transitional layer that gives the main protection against corrosion. The zone called zone III is the functional layer, with high hardness, that give the main part of the wear resistance. Zone II and zone I forms the external porous layer or technological layer. This last layer could be very important; the pores in fact can be sealed in order to improve the corrosion resistance, or this layer can be the substrate for another one. Moreover the pores can be filled with lubricant or used to color the obtained surfaces. The pores can also be used to improve the biocompatibility of the coatings for example with the growth of osteoblastic cells or to introduce in the coating an antimicrobial agent.

To simplify the structure of PEO coatings in literature can be often found the reference to the double layer structure of PEO coatings, where the functional layer is considered the non-porous zone of the technological layer.

An example of the cross section of a PEO coating obtained on an AZ91 magnesium alloys where are clearly visible the three different layers is reported in Fig.1.11

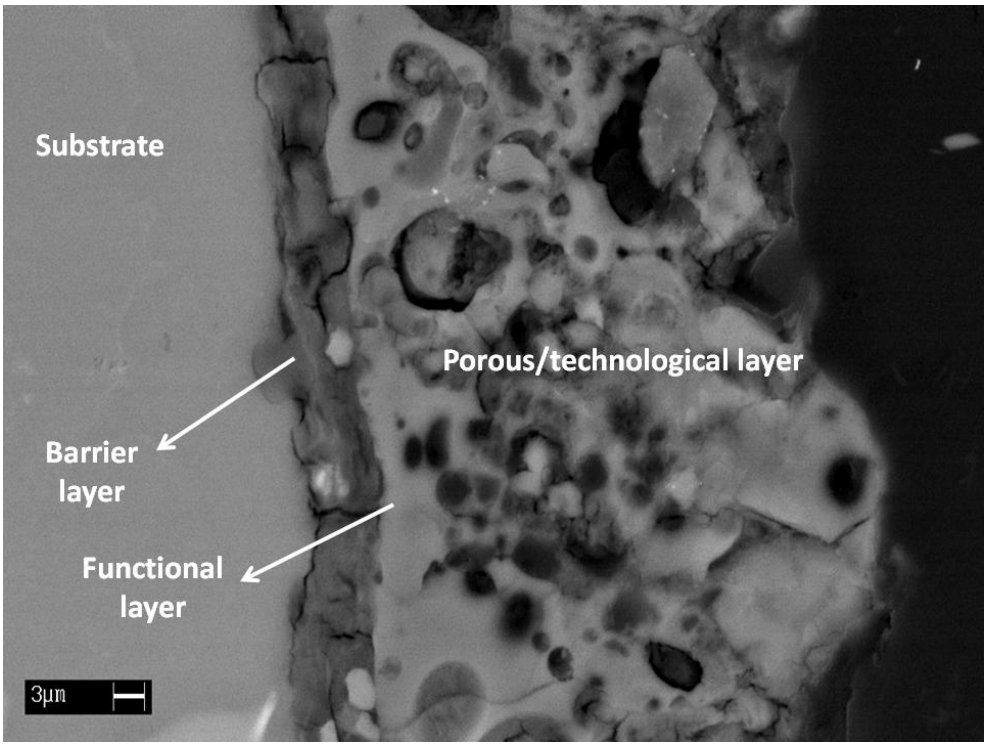

Fig. 1.11 Example of the microstructure obtained in the cross section of an AZ91 magnesium alloy PEO treated in a solution containing silicates and phosphates

Depending on the spark discharge essence pore formation in the coatings during PEO process is inevitable. Evidence is presented by Curran and Clyne [35] for the presence of sub-micrometer, surface-connected porosity in such coatings on aluminum alloys, at levels in the order of 20%. High porosity (up to 40%) was found on coatings formed on Mg alloys [36]. This porosity has an important influence on various properties and characteristics of coatings [35]. The pores on the coating surface are largely inter-connected, which can provide natural 'cages' for surface impregnation with a wide variety of compounds, including paints, lubricants, sol–gels and polymers (such as PTFE), to achieve duplex coatings for enhanced properties. The porosity may by partially responsible for the low stiffness and the low thermal conductivity of the coatings. A reduced stiffness limits the differential thermal expansion stresses and a low conductivity favors an effective thermal barrier function, which is beneficial for the thermal protection of the substrates. Porosity in the coating can induce adverse effects, such as reduced hardness leading to low wear resistance, and poor corrosion resistance from the penetration of corrosive liquids through the pores

The porosity in PEO coatings is a function of discharge intensity and processing duration. Pores of sizes (diameters) ranging from as low as 0.5 µm to as high as 50 µm

have been observed for various types of PEO coatings on magnesium alloys. The scanning electron micrograph of a typical PEO coating of 5–8 μm thickness obtained from a silicate electrolyte at low processing voltages (380 V) under conditions of fine discharges shown in Fig. 1.12 reveals fine and uniformly distributed pores on the surface of an AM50 magnesium alloy.

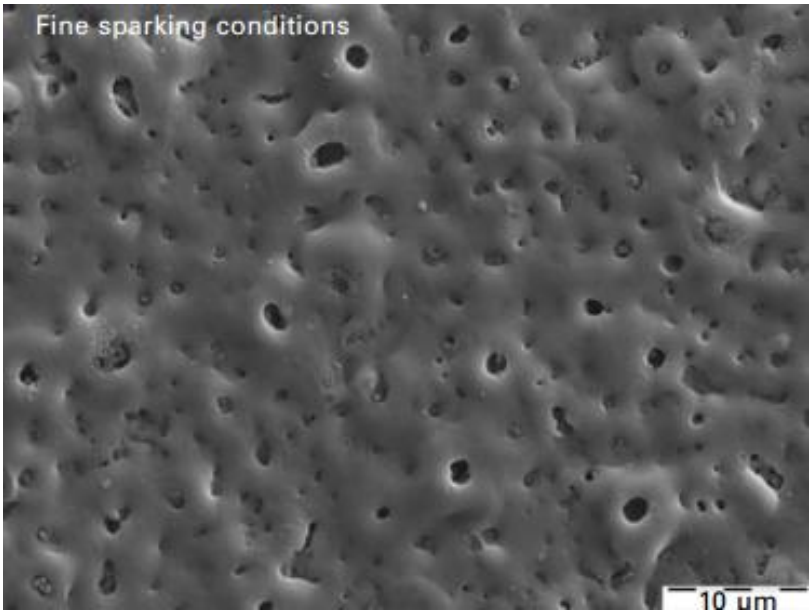

Fig.1.12 Scanning electron micrograph showing the surface morphology of PEO coatings obtained in fine sparking conditions [2]

On the other hand, the surface morphology of a 12–15 μm thick coating obtained in coarse sparking conditions in Fig. 1.13 shows large coarse oxide deposits with large pores on the surface.

The cross-sectional features of the PEO coatings differ greatly depending on the electrolyte and also on the processing conditions.

Coatings from silicate-based electrolytes (Si-PEO) are, in general, reported to be more compact than those produced in phosphate electrolytes (P-PEO) typical scanning electron micrographs of Si-PEO and P-PEO coatings from the work of Liang *et al.* [37] are shown in Fig. 1.14.

Arrabal et al. [38] and Liang *et al.* [39] have observed similar features in P-PEO and Si-PEO coatings produced by them.

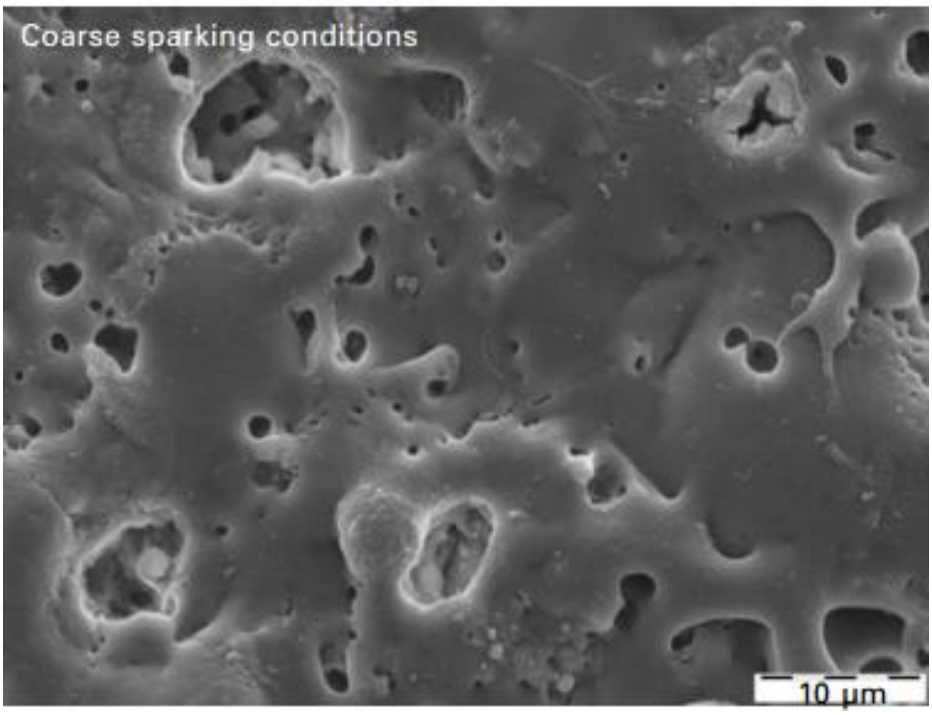

Fig.1.13 Scanning electron micrograph showing the surface morphology of PEO coatings obtained in coarse sparking conditions [2]

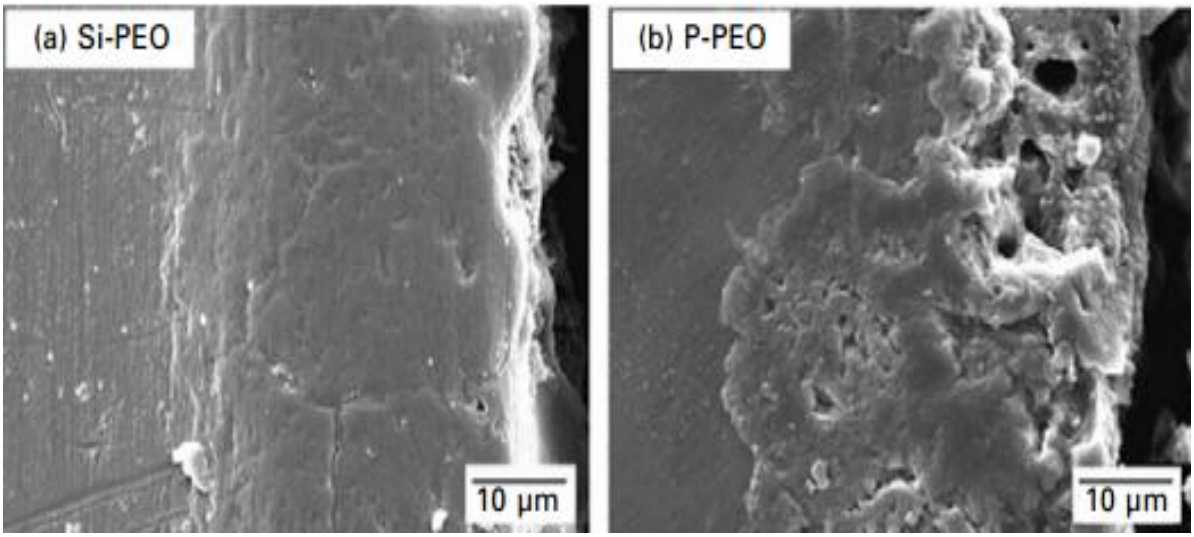

Fig.1.14 Scanning electron micrographs showing the cross-sections of Si-PEO and P-PEO coatings [37]

This different structure in the cross section of the coating cause significant differences in the corrosion resistance. In detail as will be later described coatings obtained with silicates exhibits improved corrosion performances if compared with the ones obtained with phosphates.

The phase composition of the PEO coating on magnesium alloys is mainly influenced by the electrolyte composition, and the energy intensity during the discharge is also

considered to play a role. Coatings produced on an AZ91D alloy using an aluminate–fluoride electrolyte were found to be constituted with $MgAl_2O_4$ and Al_2Mg. A large number of research publications on PEO using silicate based electrolytes have shown the formation of Mg_2SiO_4 as the major phase [40-41]. In addition, the coatings from silicate-based electrolytes were reported to also contain MgO, $MgAl_2O_4$ and MgF_2, depending on the alloy, processing conditions and additives employed. Liang *et al*. [40] reported the presence of only MgO in the coatings obtained from a phosphate-based electrolyte. However, a few other publications have documented the presence of $Mg_3(PO_4)_2$, as well, along with MgO in coatings from similar electrolytes [39-42]. A typical XRD profile showing the results of phase composition analysis performed on silicate- and phosphate-based PEO coatings on AM50 magnesium alloy by Liang *et al*. [39] is presented in Fig. 1.15.

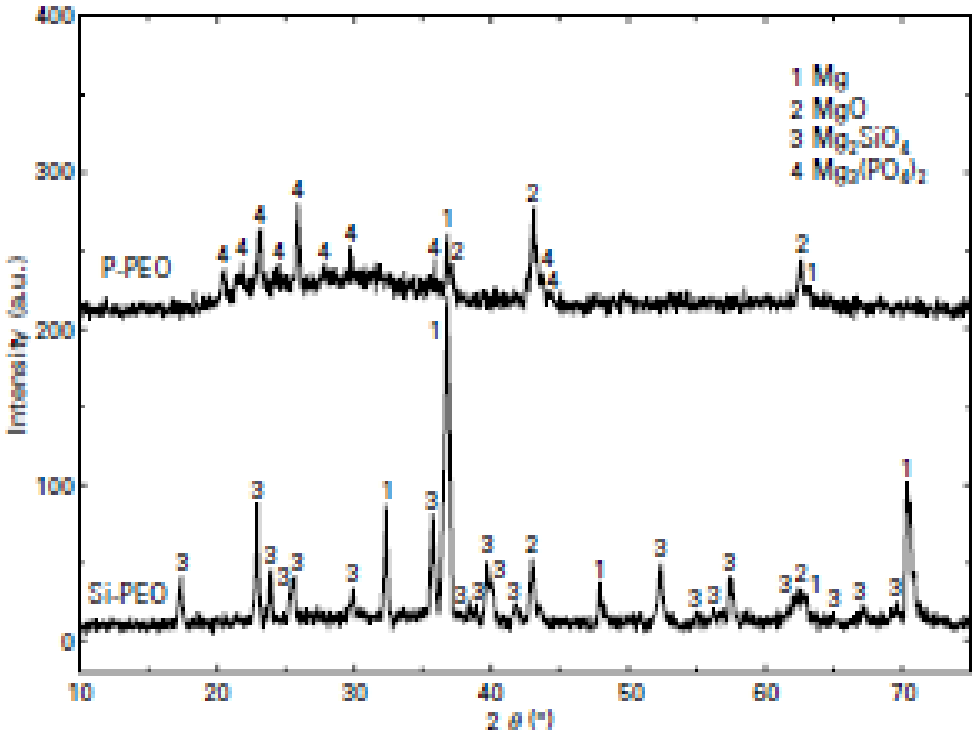

Fig.1.15 XRD patterns showing the phase composition of PEO coatings on AM50 magnesium alloy obtained from a silicate (Si-PEO) and a phosphate (P-PEO) based electrolyte [39]

The phase composition of PEO coatings obtained on aluminum and titanium alloys strongly depends on the electrolyte composition. A brief summary of the composition of the coatings with different electrolytes is reported in Tab.1.2 and Tab.1.3.

Tab. 1.2 Coating phase constituents formed on Al alloy in complex electrolytes mainly containing strong passive silicates (or phosphates) [2]

Ref.	Electrolyte group	Substrate	Electrolyte composition	Phase composition of coating	Potential applications
Voevodin *et al.*, 1996	Silicate	B95 alloy	Na_2SiO_3, 2–20g/L KOH, 2–3 g/L	Al_2O_3, SiO_2 Al-Si-O compound	Wear resistance, corrosion resistance
Wu *et al.*, 2005	Silicate	Al-Zn-Mg alloy	NaOH, 2 g/L Na_2SiO_3, 4 g/L	α-Al_2O_3 dominated, γ-Al_2O_3	Wear resistance, corrosion resistance
Lv *et al.*, 2006	Phosphate	Pure Al	$(NaPO_3)_6$, 0.008 M NaOH, 0.025 M	α-Al_2O_3 γ-Al_2O_3 $AlPO_4$	Biocidal, corrosion resistance

Tab. 1.3 Coating phase constituents formed on Ti alloy in complex electrolytes mainly containing strong passive silicates (aluminates or phosphates) [2]

Ref.	Electrolyte group	Substrate	Electrolyte composition	Phase composition of coating	Potential applications
Wang *et al.*, 2006a	Silicate	Ti6Al4V	Na_2SiO_3 $(NaPO_3)_6$ $NaAlO_2$	Rutile dominated, anatase	Wear resistance, corrosion resistance
Wang *et al.*, 2005b	Aluminate	Ti6Al4V	$NaAlO_2$ Na_2CO_3	Al_2TiO_5	Wear resistance, corrosion resistance
Wang *et al.*, 2004	Phosphate	Ti6Al4V	$(NaPO_3)_6$ NaF $NaAlO_2$	$AlPO_4$ dominated, TiO_2	Biocidal, corrosion resistance

1.6 PROPERTIES OF PEO COATINGS [1,2,43]

1.6.1 Adhesive strength between substrate and coating [2]

It has been mentioned that high adhesive strength of coatings can be achieved using the PEO process. However, such statement is mostly based on experimental observations rather than on direct experimental data. Recently, scratch tests have been applied to evaluate the adhesive strength of PEO coatings formed on titanium alloys. However,

various conclusions have been drawn. Yerokhin *et al*. [44] measured the adhesive strength of coatings formed in different electrolytes, and found that the highest critical load (96 N) was obtained in coatings formed in $KAlO_2/Na_3PO_4$ electrolyte. However, using the same method, other investigators [45-46] and this author found no effective data owing to lack of the distinct acoustic launching signals caused by coatings failure. Possibly, this is attributed to the higher adhesion strength of coating to substrate compared with the internal strength of the coatings. A shear test conducted by Wang *et al*. to evaluate the adhesion property indicated that PEO coatings have a high adhesion strength of 110 MPa for an Al_2TiO_5 dominated coating [47] and 40 MPa for an AlPO4 predominant [48], respectively. The $AlPO_4$ predominant coating, mainly relying on the deposit of external components, showed the lower adhesion. Generally, the more prevailing the cohesive failure, the stronger is the adhesive strength of coating to substrate is. In general, the thicker the coating, the weaker the adhesion strength of coating to substrate is.

1.6.2 Internal stress of the coating [2]

It is well known that the internal stress of a coating affects physical and mechanical properties such as hardness, adhesion, wear resistance and fatigue cracking. Therefore, evaluating the residual stress in the PEO coating is very valuable as a measure for mechanical damage. Recently, $Sin^2\,y$ X-ray diffraction technique was conducted by Khan *et al*. [49] to evaluate the residual stresses in oxide ceramic coatings produced on BS Al 6082 alloy, indicating that internal normal stress in the coatings ranged from –111 (±19) MPa to –818 (±47) MPa and shear stress ranged from –45 (±27) MPa to –422 (±24) MPa, depending on the applied duty cycle and frequency parameters used during pulsed unipolar PEO treatment. Guan *et al*. [50] reported, based on a finite element method, that the compression strength of the coating is about 600 MPa. In addition, a four-point bending test was conducted to reveal the mechanism of cohesive cracking and spallation in the coating. This indicated that plastic deformation in the substrate is due to interfacial crack extension, so the interface crack mode of the coatings is ductile.

1.6.3 Dielectric properties [2]

Ceramic products (such as Al_2O_3, SiO_2, ZrO_2) formed on light alloy surfaces have high electrical resistance and breakdown strength, so possess a great potential for insulating coatings. The coatings formed in silicate-rich electrolytes have a greater thickness with a higher mass rate, especially if components containing SiO_2 are incorporated into the coating, and this is beneficial for increasing dielectric strength. Dielectric strength up to

2500 V can be reached, depending on the coating specification and the alloy. As an example, a PEO coating can replace the commonly used electric insulation painting material to make sensors, which not only simplifies the sensor structure, but also increases the stiffness reliability and accuracy.

1.6.4 Optical properties [2]

The color of PEO coatings can be changed over a wide range, depending on the process conditions such as substrate metal types, electrolyte composition and concentration, and electrical, and temperature parameters. Among them, alloying elements in the substrate and the composition and concentration of electrolyte play a crucial role for the formation of a specific color. Some coloring additives such as $KMnO_4$, $FeSO_4$, Cr_2O_3 and NH_4VO_3 are also being developed to offer unique colors, which provide a wide range for decorative architecture or optical applications in aerospace. Black absorptive coatings formed in eco-friendly electrolytes containing blackening additives finds a great potential on Al alloys as thermal control layers applied to aerospace components (e.g. in satellite). PEO coatings with vanadium oxide predominating on the surface have been obtained on aluminum alloys in phosphate–vanadate and silicate–vanadate electrolyte. It is thought that this V_2O_3 layer results in the black appearance observed. Compared with conventional blackening processes using Ni-P coating, sulphuric acid anodizing coating or spraying black paints, PEO can be applied to more alloy types and the properties of the coatings are satisfactory with low reflectance values (<0.1%) and good environmental stability. The porous feature of the PEO coating is beneficial for infrared reflection applications. The porous and rough surface influences the infrared reflection efficiency and significantly decreases the reflection of infrared waves from 780 nm to 3000 nm.

1.6.5 Biomedical properties [2]

Titanium and its alloys (e.g. Ti6Al4V) have been widely used for orthopedic and dental implants due to their good biocompatibility, excellent corrosion resistance and high strength-to-weight ratio; however, their bio-inert nature restricts their wider clinical applications. PEO can form TiO_2-based bioactive coatings on titanium substrates by incorporating Ca and P into the coating, firstly developed by Ishizawa and Ogino [51-53]. To prepare the bioactive coatings, electrolytes containing calcium salts such as calcium acetate, calcium glycerophosphate and calcium dihydrogen phosphate have been explored in the PEO process [54-57]. Recent investigations indicate that the formation of bioactive components in the coatings partially depends on the applied voltage.

To stimulate bone formation and enhance osteointegration, PEO has also been applied to porous titanium surfaces [58], which is beneficial for bone in growth into the porous structure, thus achieving a strong chemical bonding at the bone/implant interface.

1.6.6 Color [43]

The natural color of the surface after PEO treatment is generally grey, as reported in Fig. 1.16 but the color can be easily changed to black as reported in the previous section.

Fig. 1.16 PEO treated sample of AZ91 magnesium alloy

Further coloring of anodized layers can be achieved by organic dyes or inorganic pigments, immediately after anodizing. In situ electrolytic coloring can be obtained also by electrolytic deposition of inorganic metal oxides and hydroxides into the pores of the film or by adding organic constituents to the anodizing electrolyte that decompose and form particles which become trapped as the anodic film grows [59].

1.6.7 Thermal protection properties [2]

Thermal barrier coating requires a property combination of low thermal conductivity, good oxidation resistance and thermal shock resistance. PEO coatings are becoming attractive for the thermal protection [60-61] of metals working in high temperature environments. PEO coatings formed on metal substrates exhibit a low thermal conductivity, good thermal shocking and oxidation resistance properties, which gives them great potential for thermal barrier coating applications at high temperatures. The high heat resistance of the PEO coatings may be valuable in manufacturing protective barrier coatings for spacecraft and missiles.

1.6.8 Corrosion resistance properties [2,43]

Among light alloys, Mg alloy is most active and thus sensitive to corrosion, followed by Al alloy and Ti alloy. PEO can significantly improve the corrosion resistance properties of Mg and Al alloys. PEO coatings can readily offer good protection to magnesium alloys in mild environments and/or for short durations. The corrosion resistance of PEO coatings in aggressive environments and for long-term exposures is dictated by many factors, including the coating composition, thickness, and defect levels. As is well known, these coatings are porous in nature, and the extent of porosity and other defects such as cracks can influence the corrosion behavior. Nevertheless, all anodized layers play two basic roles in corrosion prevention (at least to some extent): *Firstly*, the layer is separating the magnesium surface from the surrounding environment. With a generally higher corrosion resistance of the layer, the lifetime of a magnesium component can be increased. *Secondly*, the layer is more or less an insulator with high dielectric strength, so that the flow of current between dissimilar metals can be drastically reduced, which offers a better protection against contact corrosion. Although the various anodizing processes result in different layers, there is a clear agreement in the literature that none of these can protect magnesium alloys from corrosion in aggressive environments for a longer period without being sealed and coated with an organic top layer. This can be clearly seen in Fig.1.17, which demonstrates the effect of salt spray and galvanic coupling on PEO coated and uncoated pencil sharpeners.

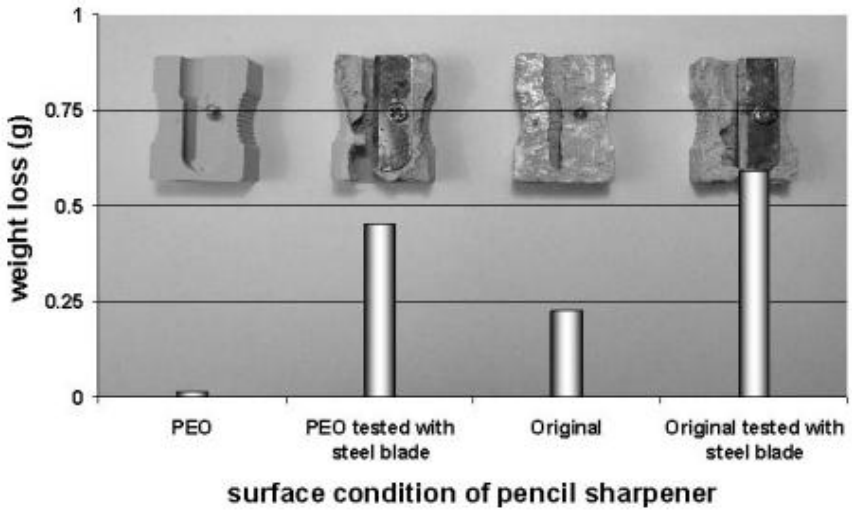

Fig. 1.17 Salt spray performance of PEO treated and original pencil sharpeners with or without galvanic coupling to the steel blade [43]

Since anodized magnesium alloys are generally designed to be sealed or can be also covered by other protective layers, testing in most cases was not performed on anodized surfaces only, but on the layer systems build up on anodized layers. Thus, it is sometimes difficult to assess the corrosion prevention of the anodized layers alone. However, it is admitted that in a more severe environment the open pore structures of the anodized layers on magnesium have to be sealed to give adequate corrosion resistance. General corrosion, galvanic corrosion and pitting are the predominantly examined forms of corrosion. A number of corrosion fatigue results have been reported, but much fewer studies on stress corrosion cracking of anodized surfaces have been carried out.

Nevertheless, to prevent galvanic corrosion, not only the anode (magnesium), but also the cathode, the electrical contact between anode and cathode and the contact with the electrolyte should be considered. In many cases it is even better to coat the contact partner rather than the magnesium.

Electrochemical impedance spectroscopy results show that the porous outer layer of the coating formed on AM50 magnesium alloy is inconsequential with respect to corrosion, as the corrosion resistance depends on the compact inner layer of the coating [62]; exactly the same is true for PEO treated al and Ti alloys. This is largely because corrosive liquids can easily penetrate through the porous outer layer to contact the compact inner layer, so the inner layer plays the critical role in the inhibition of corrosion.

The process parameters, the electrolyte composition and the substrate can influence the corrosion properties. For example Mizutani *et al.* [63] reported a much better corrosion resistance of $Mg(OH)_2$ layers produced by anodizing at 3 V in NaOH rather than of their higher voltage counterparts (10 and 80 V) containing MgO [63]. For the same type of alloy, the impurity level (Fe, Ni, Cu content) can determine the corrosion performance of an anodized coating applied on these. A primary HP AZ91 alloy coated showed much better corrosion resistance than a low purity secondary AZ91 with the same coating [64]. Furthermore, it has been found that the corrosion resistance of the same anodized coating can be different on different magnesium alloys [65-67]. In detail the corrosion resistance of the anodized coating was closely associated with the corrosion performance of the substrate alloy: an increase in the corrosion resistance of the substrate alloy produce an increase also in the corrosion resistance of the coating. This fact can be linked with the corrosion mechanism of an anodized layer that can be seen in Fig.1.18.

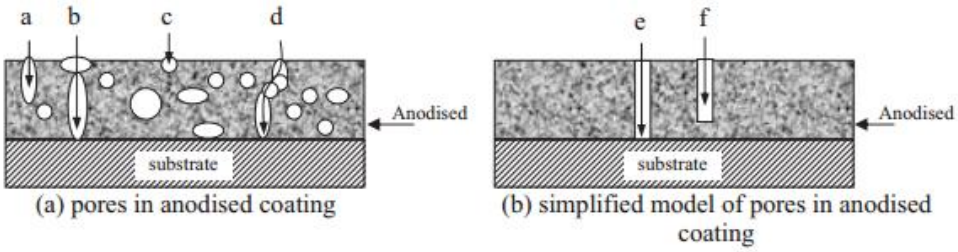

Fig. 1.18 Schematic diagrams of (a) the microstructure of an anodized coating on magnesium alloys and (b) the simplified microstructure of the coating [43]

As there are some "through holes" in the anodized coating which allow the aggressive media to reach the substrate, the corrosion of the anodized alloy should be determined by the corrosion resistance of the substrate alloy at the bottoms of the "through holes". Therefore, the corrosion performance of the substrate has a significant influence on the corrosion resistance after it has been anodized.

Atmospheric corrosion tests and particularly the accelerated salt spray test (ASTM B117) or equivalent tests represent most of the existing corrosion performance data. The performance of magnesium AZ91D specimens with different commercial anodizing surface treatments and some with a additional paint coating was studied in literature [43] under atmospheric exposure and compared with uncoated material. The results of the study in terms of hours of resistance in salt spray are reported in Tab.1.4 It can be clearly observed the importance of the sealing treatment in the improvement of the corrosion resistance: the presence of an unsealed anodized film on the AZ91 alloy surface does not offer any protection against galvanic corrosion. Only when the film is sealed and painted, superior protection against galvanic corrosion is obtained.

Tab.1.4 Salt Spray Corrosion Resistance of Some Anodized Coatings [43]

Coating system	Corrosion resistance (h)
AZ91 HP untreated	0–10
AZ91 HP + Magoxid(MC) 25 m	80–100
AZ91 HP + MC + sealing water glass	250–300
AZ91 HP + MC + sealing Silane	430–600
AZ91 HP + MC + EP-powder paint 60–80 m	750–1000
AZ91 HP + MC + silane + EP-powder paint 60–80 m	1000

Accelerated electrochemical test (anodic polarization) results of AZ91D uncoated and coated with 35µm Keronite are shown in Fig. 1.19. The results demonstrate contrasting behavior of the coated specimens compared to uncoated alloy. The coated specimen displayed a more noble rest potential "E_{corr}" compared to that shown by the uncoated specimen. A more noble rest potential in deaerated electrolyte generally signifies less susceptibility to corrosion attack. Moreover, the coated specimen displayed greater resistance to initiation of corrosion attack shown by the presence of a breakdown potential "E_b" and a passive potential range "E_b-E_{corr}" [68].

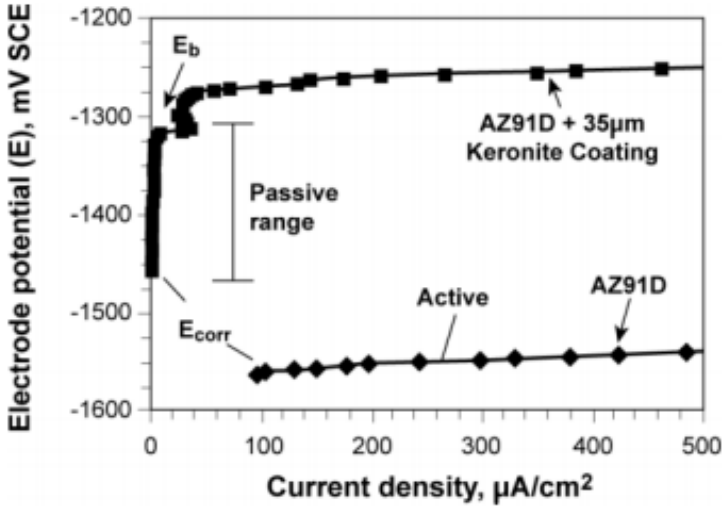

Fig. 1.19 Accelerated electrochemical test (anodic polarization) results of AZ91D uncoated and coated with 35lm Keronite [68]

Corrosion tests on rather thick anodized specimens revealed a clear correlation between pore density and corrosion resistance. Potentiodynamic polarization curves obtained in 5 % NaCl aqueous solution (pH 10 adjusted by NaOH, scanning rate 0.2 mV/s) gave a corrosion rate of 3.2 mm/y for the substrate and 0.001 mm/y for the 55 min treated sample [69].

It is interesting to note that the thicker layer obtained after 50 min treatment offered less protection than the layer obtained through 20 min anodizing. This indicates that the defect density is the dominating influence rather than the layer thickness. Increasing the layer thickness to more than 100 µm did not reduce the amount of open defects that provided detrimental contact between the magnesium substrate and the electrolyte. Sealing the coating appeared absolutely necessary to enable long term exposure in aggressive environments [69].

An interesting study regarding the comparison of the corrosion resistance of different PEO coated sample and samples treated with traditional conversion coatings has been performed by Wang *et al.* [70] and the results are reported in Fig.1.20.

The performance of these anodizing coatings was better than that of chromate treatment. The best corrosion protection could be achieved by an Anomag/sealant system, followed by Magoxid/sealant and Cr-free passivation treatments. Visual analysis showed that the corrosion resistance of these anodizing coatings was comparable to a chromate/powder coating system examined by the author. The results confirmed the improved corrosion performances of PEO coatings if compared with traditional chromate conversion coatings.

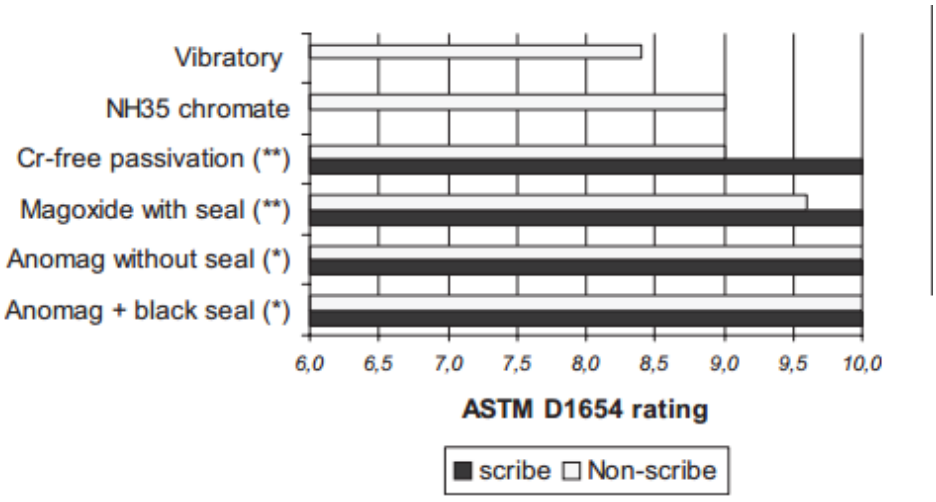

Fig. 1.20 Ratings of selected anodizing treatments on AZ91D after 80 days exposure to GM9540P. The degradation is evaluated according to ASTM D 1654 with "10" representing no degradation and "0" severe degradation.[70]

1.6.9 Wear resistance properties [1]

Employing PEO technique to form ceramic oxide coatings on Ti, Mg, Al and their alloys can significantly enhance the mechanical and tribological properties, such as high hardness, superior wear resistance and good adhesion to the substrate. In recent years, investigations on the phase composition, mechanical and tribological properties of PEO coatings on Ti, Mg, Al and their alloys were done by many researchers. However, the tribological performances of PEO coatings are not only affected by the intrinsic properties of PEO coatings, but also affected by many extrinsic factors, such as sliding loads, sliding speed, counterpart materials, lubricated conditions, temperature and humidity etc. Herein, the sliding loads are emphasized and classified into three levels: low loads (0-5 N), medium loads (5-50 N) and heavy loads (above 50 N). And then, the friction and wear

behaviors of different PEO coatings in different conditions will be introduced and discussed under different load levels.

-Low loads

The investigations of structure, composition, mechanical and tribological properties under low loads of PEO coatings formed on AM60B Mg alloy in silicate and phosphate electrolyte have been done by Jun Liang *et al.* [37]. The samples were fabricated in the electrolyte containing Na_2SiO_3(10g/L),KOH (1g/L) or Na_3PO_4(10 g/L), KOH (1 g/L). The friction and wear properties of the PEO coatings were evaluated on a reciprocal sliding UMT-2MT tribometer in dry sliding conditions under a load of 2 N, using Si3N4ball as counterpart material, with a siding speed of 0.1 m/s and sliding amplitude of 5 mm. The wear life of PEO coatings formed in two different electrolytes was compared with the thin coatings and results showed that the wear life of coating formed in silicate electrolyte is about four times as long as that of coating formed in phosphate electrolyte. The uncoated Mg alloy has a friction coefficient of about 0.3 and exhibits a high wear rate of 3.81×10^{-4} mm^3/Nm. While for both the oxide coatings, the friction coefficients are in the range of 0.6-0.8 and the wear rates are only in the range of $3.55\text{-}8.65\times10^{-5}$ mm^3/Nm. These evidences demonstrate that the PEO coatings formed on Mg alloy in both electrolytes have greatly enhanced the wear resistance but exhibit higher friction coefficients compared with the uncoated Mg alloy. Furthermore, the oxide coating formed in silicate electrolyte has a higher friction coefficient but exhibit a better wear resistance than that formed in phosphate electrolyte. It also suggests that the structure and phase composition of coatings are indeed the dominant factors which influence the mechanical property and friction and wear behaviors of PEO coatings.

-Medium loads

P. Bala Srinivasan *et al* [71] studied the dry sliding wear behavior of PEO coatings with different thickness of 10 μm and 20 μm on cast AZ91 magnesium alloy. The samples were fabricated by PEO treatment in silicate based electrolyte containing Na_2SiO_3 (10 g/L) and KOH (10 g/L). The dry sliding wear behavior of the untreated Mg alloy, PEO coated specimen A and B was assessed on a ball-on-disc oscillating tribometer. The results indicated that the thickness of coatings played a crucial role in enhancing the wear resistance. At higher initial stress levels, the deformation of the substrate causes the cracking and flaking-off of the coating, especially when it is thin. Under such

circumstances the increased thickness of PEO coating provided a better load bearing capacity, thus resulting in a superior wear resistance.

-Heavy loads

Some studies [72-73] revealed that the PEO ceramic coatings under heavy loads can sharply increase the wear resistance and decrease the wear rate, compared to the uncoated substrates. However, the PEO coatings normally exhibit higher friction coefficients which can cause not only the wear of sliders, but also the wear damage of counterpart materials in many tribological applications. Thus, it is necessary to fabricate the PEO coatings with both good wear resistance and low friction coefficient. This is valid for all the loads but is particularly important under heavy loads. The possible ways for the reduction of the friction coefficient will be further discussed in chapter 5.

1.7 COMMERCIAL EXAMPLES OF PEO COATINGS [43]

Parallel to extensive scientific research around the world, PEO coating technology is readily available on a commercial basis. Commercial processes such as Anomag, Keronite, Magoxid, Tagnite, and others have been developed.

The *Anomag Process* was developed by Magnesium Technology Ltd in New Zealand. The anodizing bath consists of an aqueous solution of ammonia and sodium ammonium phosphate. So the process is environmentally friendly and does not use chromium or other heavy metals, nor are fluorides used [74]. Anodizing is obtained without the formation of high energy plasma discharges (spark discharge), offering smoother layers [75]. Coatings applied to magnesium alloy substrates may vary in thickness from as little as 5 microns to a maximum of around 25 microns.

The *Magoxid-Coat* process has his origins in Russia and was further developed by AHC-Oberflächentechnik GmbH in Germany. The plasma is generated by an external power source in a slightly alkaline electrolyte near the surface of the work-piece (anode). The discharging (by arcing) and formation of oxygen plasma in the electrolyte causes partial short term surface melting and ultimately the formation of an oxide-ceramic layer. It is preferable to work with a voltage that increases to 400 volts. The current density is in particular 1 – 2 A/dm^2. Normally, layers with 15–20 micrometer thickness are produced with a growth rate of 1.5 micrometer per minute.

The *Tagnite Coating System* was developed in the 1990's in the USA by Technology Applications Group Inc. as a chromate-free anodic surface treatment, and they claim, that it is providing significantly more corrosion and abrasion resistance than any chromate based coating. Like typical anodizing coatings, the part to be coated is connected to a conductive rack which carries the part throughout the coating process. The electrolyte used to form the coating is an alkaline solution clear in color, containing no chromium (VI) or other heavy metals and operates below room temperature.

It mainly consists of an aqueous solution containing hydroxide, fluoride and silicate species which are also incorporated into the layer. To ensure maximum corrosion resistance and high dielectric strength, the Tagnite coating is applied at voltages exceeding 300 volts DC. The coating consists mostly of hard magnesium oxide with minor surface deposition of hard fused silicates and has a white color. The Tagnite coating can be applied as thin as 0.10 mil (~2.5µm) or as thick as 0.9 mil (~22.5µm) depending upon the alloy being coated.

Keronite technology was conceived in Russia and developed in the UK by Isle Coat Ltd, a subsidiary of CFB plc. The process results in hard, wear-resistant coatings, which also provide good corrosion resistance and a good thermal barrier. Light alloys such as aluminum, titanium and magnesium can all be treated, and the technology offers significant improvements compared with traditional methods such as hard anodizing or coating with nickel-silicon carbide. Keronite also compares favorably with spark-anodizing processes currently being developed around the world. Electrical bipolar (positive and negative) pulsed electrical current of a specific wave form in a proprietary electrolyte is used, and the electrical current creates the plasma discharge near the surface of the part to be coated. The electrolyte is a non hazardous, low concentrated alkaline solution (98 % demineralized water, chrome and ammonia free), which can easily be disposed. The layer thickness can range from 10 to 80µm. In order to create surfaces with advanced properties Keronite ceramic matrix can be impregnated with different materials.

Fundamentally it can be said that currently, PEO processes are in a transition phase from research to commercial applications, mainly focused on the corrosion- and wear-protection of light alloys. it is necessary to further study the fundamentals of the PEO technique to advance scientific understanding and to explore new functional PEO coatings for high-tech applications.

1.8 INDUSTRIAL APPLICATIONS OF PEO COATINGS [2,43]

The main purpose of PEO oxide layers applied on magnesium components is to improve their wear and corrosion resistance. They are used alone, as a base for further build up of coating systems, e.g. promoting the adhesion of paint and powder coating systems to the magnesium substrate, or as a pretreatment for adhesive bonding. One early example where a PEO coat was industrially used in combination with a paint finish is shown in Fig.1.21 (high speed milling cutter)

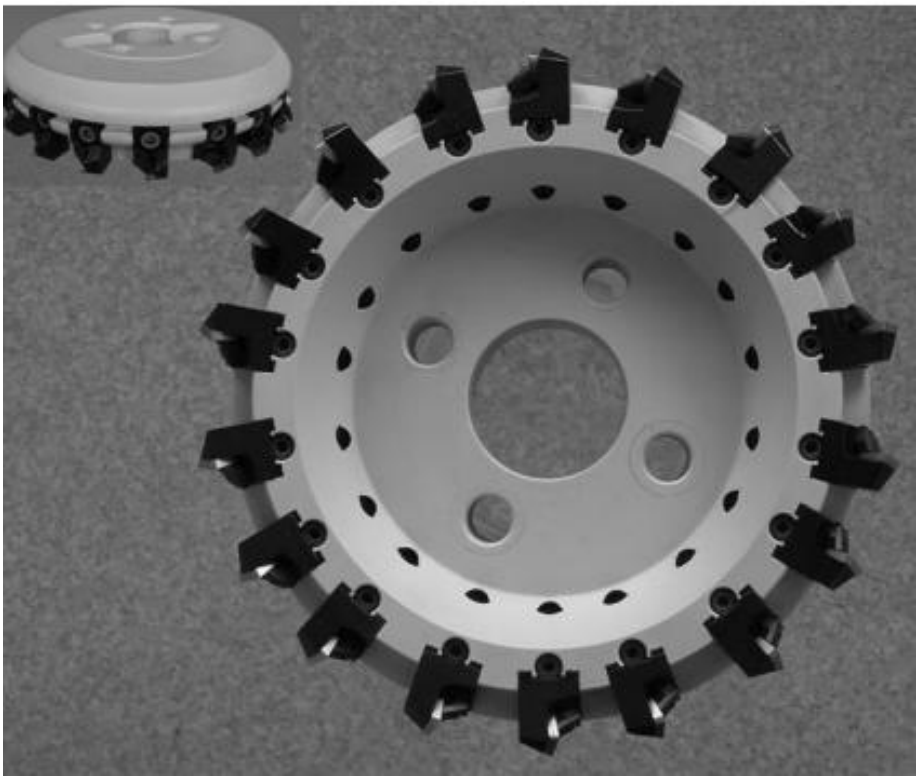

Fig.1.21 PEO (Magoxid provided by AIMT) and paint-coated magnesium body of a high-speed milling cutter [2]

Basically, all commercial magnesium alloys independent of their production process (cast or wrought) can be treated; thus, there is a large range of possible applications across all industrial sectors (automotive, consumer, aviation, medical, food, electronics, etc.) which use magnesium for weight reduction and have to fight poor wear and corrosion resistance.

However, despite more favorable properties compared to conversion coatings, the disadvantage is clearly the higher cost involved with PEO, limiting the number of

actual applications thus, main competitors of the PEO coatings are conversion coatings that are inexpensive and simple in comparison with PEO processes. Never less in spite of being more expensive than conversion coatings, the properties of PEO coatings regarding paint adhesion and the prevention of undermining of paint films are much superior.

The main sectors where PEO coatings are currently used are:

- Auto motive Sector
- Valves and fittings
- Office and data technology
- Food processing industry (to improve the corrosion resistance of magnesium alloys)
- Energy technology (turbine components, bearing surfaces in belt pulleys)
- Household appliance industry (doors, panels, covers)
- Aviation and space industry (gearbox of helicopters are one the first applications of PEO process)
- Telecommunication
- Sport sector (on the rims of the bikes for aesthetic reason and to improve breaking performances)
- Glasses and industrial fashion

Some real examples of industrial applications of PEO treatments are reported in the photos below.

Fig.1.22 PEO treated rim with Keronite process

Fig.1.23 PEO coated yacht winch drum

Fig.1.24 PEO process applied on a gear and on a piston head

The main problems regarding a large industrial application of the PEO process remain:

-The capital costs, electricity consumption and the chemicals adopted in the process if compared with traditional conversion coatings
-The need of a post-treatment. There is no question that the anodizing treatments can produce the better properties, but like conversion coatings they are not good enough to get along without a post treatment to seal their porous surface.

It is expected that these problems will be solved through further optimization of the current anodizing processes (e.g., new additives in the bath solutions, introduction of a better power control, acoustic vibrations and air micro-bubbles, etc.). In particular an optimization of the now well known process with some variations on the main process parameters could obtain a reduction in the costs. From this point of view the objective are the costs of traditional conversion coatings. From the other hand further improvement in the mechanical and corrosion properties of the final coatings, could also justify an increase in the costs.

Chapter 2

Experimental system

After the study of the scientific and industrial state of art regarding PEO process, briefly described in the previous chapter, the first part of the experimental work was devoted to the development of a laboratory-system to produce PEO coatings on little samples. As power supply to obtain PEO coatings a TDK-Lambda GEN-300-8-1P230 rack mount programmable power supply (Fig.2.1) was used.

Fig.2.1 Power supply used to produce PEO coatings.

The generator was connected with different types of cathodes in order to obtain PEO coatings on different materials. In detail to produce PEO coating on steels two bars of SAF2507 duplex stainless steel were used instead for aluminum and magnesium alloy a carbon steel wire mesh was used. In order to control the temperature of the system the cell was connected with a thermostatic bath. In the treatments where suspended particles are present in the electrolyte magnetic stirring is possible. The whole system works under an extractor wood. All the treatments were performed with a fixed current density (depending from the substrate and from the electrolyte) and letting the potential free to vary. The potentials can however be recorded during the tests. An image of the system used to produce PEO coatings in the laboratory can be seen in Fig.2.2

The typical samples that can be produced with this system are little bars 4x2 cm or anyway samples with small areas. To obtain bigger samples a more powerful generator has to be connected to the system in order to generate the necessary current density to perform the treatment. However the use of a metallic mesh as cathode permit to obtain good coatings also on samples with a complex geometry.

Fig.2.2 Laboratory system used to produce PEO coatings.

The characterization of the surfaces and of the cross sections (obtained after metallographic preparation) of the various samples was mainly performed with with a Cambridge Stereoscan 440 scanning electron microscope (SEM), equipped with a Philips PV9800 EDS (Fig.2.3) and a D500 X-ray diffractometer (XRD) using Cu Kα radiation (Fig.2.4). With SEM-EDS analysis the thickness and composition of the protective layer can be studied. Moreover from surface analysis also the morphology and in particular the porosity and the presence of micro-cracks can be evaluated.

XRD analysis permit to evaluate the different phases present in PEO coatings in particular the effect of the influence of the electrolyte composition on this phases was studied.

The presence of different phases could also produce variations in the mechanical properties of the coatings, mainly evaluated with Vickers micro-hardness tests.

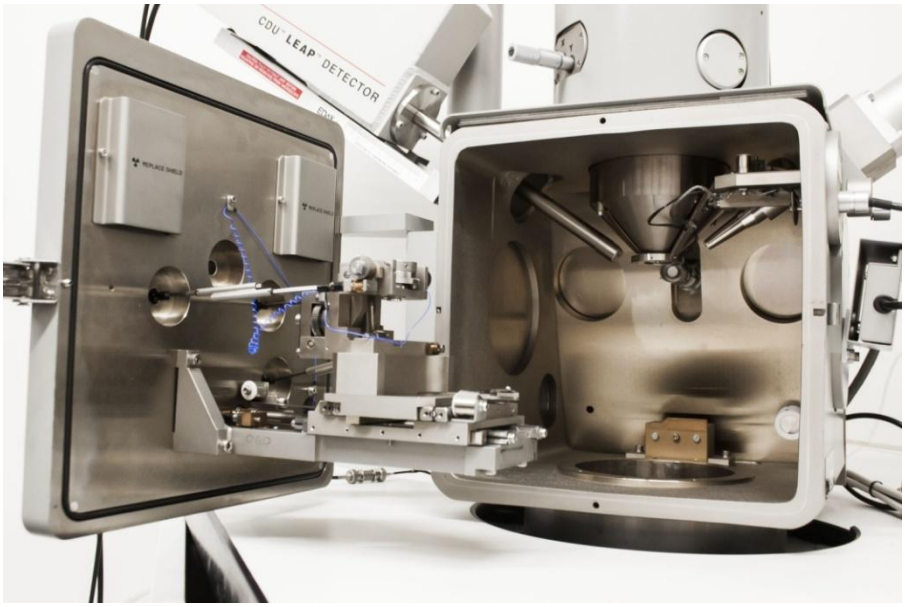

Fig.2.3 Scanning electron microscope (SEM) used in the characterization of the samples.

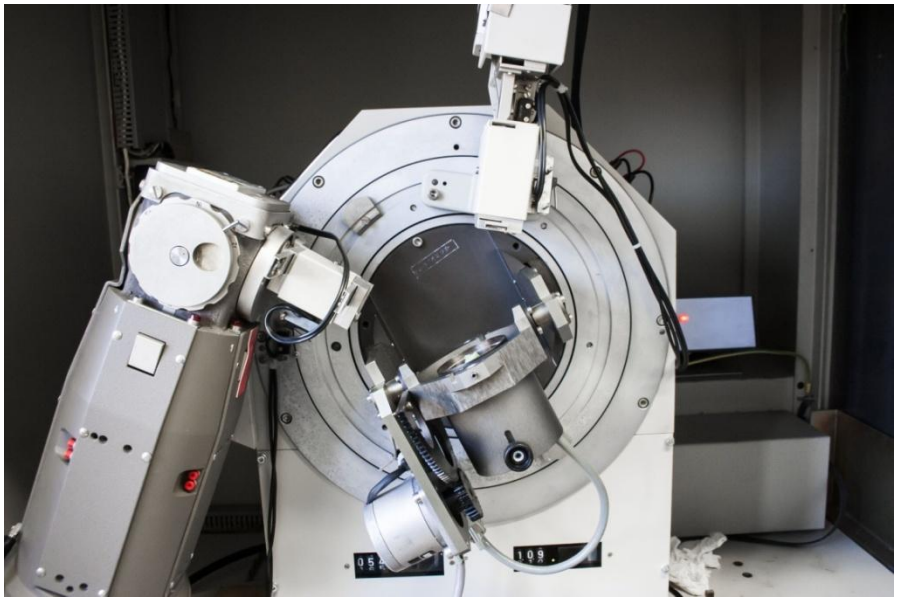

Fig.2.4 X-Ray diffractometer used in the characterization of the PEO coated samples.

On certain particular samples in order to verify the elemental distribution and the oxidation state of the elements also secondary ion mass spectrometry (SIMS) and X-ray photoelectron spectroscopy (XPS) were performed. Secondary ion mass spectrometry (SIMS) analysis were performed with a CAMECA IMS-4f spectrometer, using a Cs+ 14.5 KeV 3 nA primary beam rastered over an area of 100x100 μm^2, while collecting,

$^{18}O^-$, $^{27}Al^-$, $^{24}Mg^-$, $^{11}Na^-$, $^{14}Si^-$ and $^{42}Mo^-$ secondary ions from a central area of 60 µm diameter. Depth calibration were carried out measuring the crater depth after the analyses with a profilometer TENCOR P10 and assuming constant sputtering rates. X-ray photoelectron spectroscopy (XPS) spectra were run on a Perkin-Elmer Φ5600ci spectrometer using standard Al radiation (1486.6 eV) working at 250 W. The assignments of the peaks were carried out by using the values reported in the reference handbook [76], in the NIST XPS Database [77-78] and in the references reported in [79-82]. Survey scans (187.85 pass energy, 1 eV/step, 25 ms per step) were obtained in the 0 - 1300 eV range. The atomic composition, after a Shirley type background subtraction [83], was evaluated using sensitivity factors supplied by Perkin [76]. The spectra have been corrected according to charging effect, assigning to C1s peak 284.8 eV binding energy. Deconvolution of the peaks was performed with XPSpeak 4.1 software.

The corrosion resistance of the different samples was evaluated with electrochemical tests to obtain relevant information regarding the corrosion resistance in reasonable time. In detail Potentiodynamic polarization tests and electrochemical impedance spectroscopy (EIS) tests were performed using an AMEL 2549 Potentiostat for the potentiodynamic tests and a Materials Instrument Spectrometer coupled with the 2549 Potentiostat for the EIS tests. The experimental setup used for corrosion tests can be observed in Fig.2.5

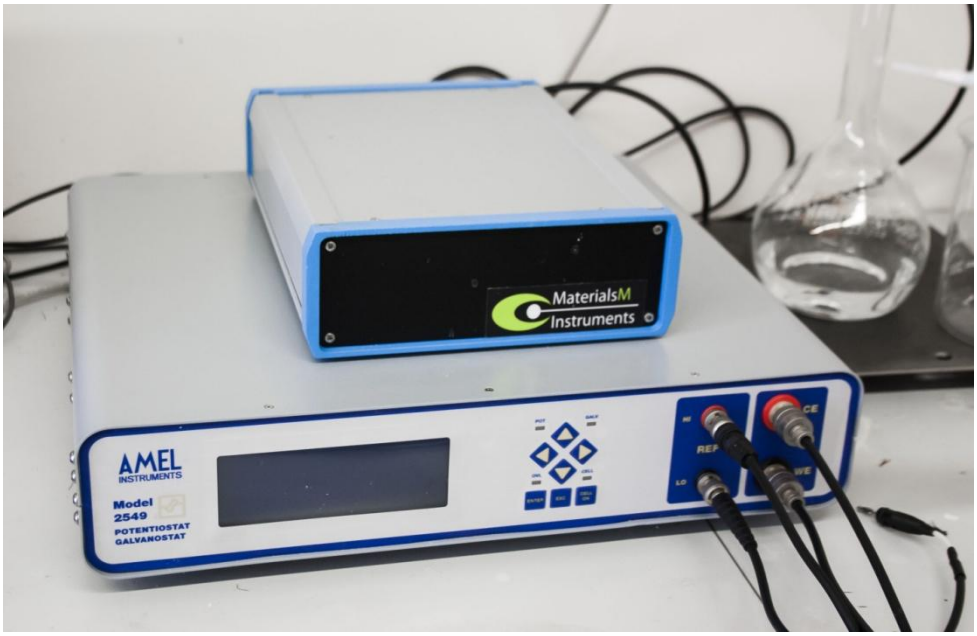

Fig.2.5 Experimental setup used for corrosion tests on PEO samples

In detail a three electrode cell was employed using a saturated calomel electrode as reference electrode (SCE) and a platinum electrode as counter electrode. The working electrode is the PEO treated sample. As reference, in all the test also an untreated sample was tested. All the potentiodynamic corrosion tests were performed in a solution containing 0.1 M Na_2SO_4 and 0.05 M NaCl in order to simulate an aggressive environment containing both chlorides and sulphates. This kind of environment is one of the most aggressive for light alloys. The scan rate was 0.5 mV/s.

The EIS measurements were performed in a solution containing 0.1 M Na_2SO_4 and 0.05 M NaCl, at the value of the open circuit potential and in a frequency range between 10^5 Hz and 10^{-2} Hz, with a perturbation amplitude of 5 mV. Experimental data were fitted with the software Z-view using the equivalent circuits reported in Fig.2.6. In particular, for some samples was used the Randles circuit (Fig.2.6a), one of the simpler circuits that can be employed; for the others was used the circuit reported in Fig. 2.6b. This last type of circuit is the one typically used to fit EIS data from PEO coated samples [114-115]. In fact the two time constants represented in the equivalent circuit correspond to the porous and the barrier layer that, as was reported in chapter 1, schematically represent the PEO coatings. Though Blawert et al. [43] reported more in detail the presence of four types of layers for PEO coatings from a microstructural point of view, it was not possible to fit the data to such a physical model from an electrochemical response point of view [62]. In fact attempts to include more elements gave rise to unrealistically large errors for the additional elements [62].

However in each single case discussed in the following chapters was employed the circuit that permit to have the best fit of the experimental data.

Considering the parameters of the equivalent circuits: the value of R_1 represents the resistance of the solution; R_2 the polarization resistance of the external porous layer; R_3 the polarization resistance of the internal barrier layer; and CPE (CPE_2 for the barrier layer and CPE_1 for the porous layer) a constant phase element, which is used in the equivalent circuit instead of a capacitance, because often the measured capacitance is not ideal.

The impedance representation of CPE is given by:

$$Z(CPE) = 1/[Q(j\omega)^n] \qquad (2.1)$$

where Q is a constant phase element and ω is the angular frequency. The number n is an empirical exponent and can vary between 1 (perfect capacitor) and 0 (perfect resistor). A value of n less than 1 would represent a somewhat capacitor and it is generally thought to arise from the presence of heterogeneities, both laterally and within the depth of the coating. If the values of the exponent n are approximately 1, Q can be said to behave similar to a pure capacitor and the Eq.2.2 can be considered valid:

$$C = \varepsilon_0 \varepsilon A / d_{ox} \tag{2.2}$$

Where C is the capacitance, ε_0 is the permittivity of vacuum, ε is the dielectric constant, A the effective area and d the distance of the plates that can be used to estimate the thickness of the coating.

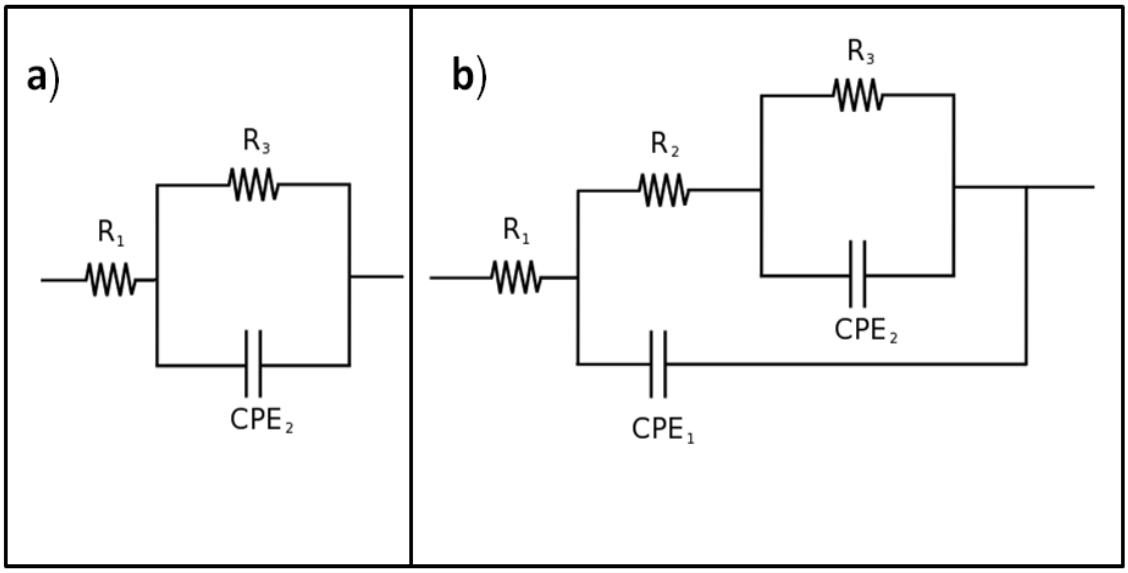

Fig. 2.6 Equivalent circuits employed for curve fitting of the untreated sample and the sample treated with 0.3 g/l of sodium molybdate (a) and of the other treated samples (b)

The wear resistance of the PEO treated samples was analyzed with a block on ring tribometer (ASTM G77) using as ring of 100Cr6 as antagonist. A scheme of the tribometer and the experimental layout used in the tests can be observed in Fig.2.7

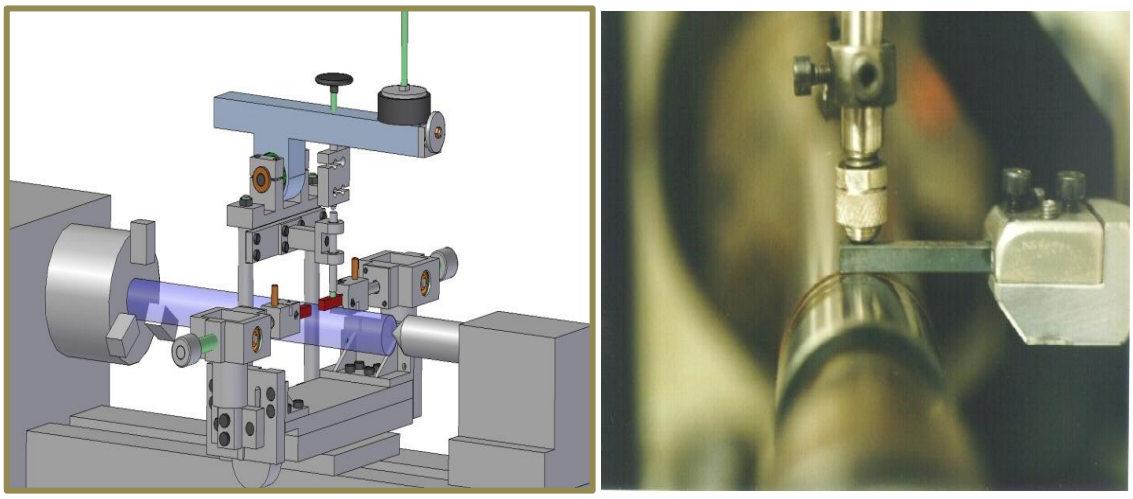

Fig.2.7 Scheme of the tribometer (on the left) and experimental layout of the tests (on the right)

Two different loads (5 and 10 N) were used during the wear test with a sliding rate of 0.3 m/s .

The geometry of the PEO treated samples used in tribological tests is the one reported in Fig.2.8

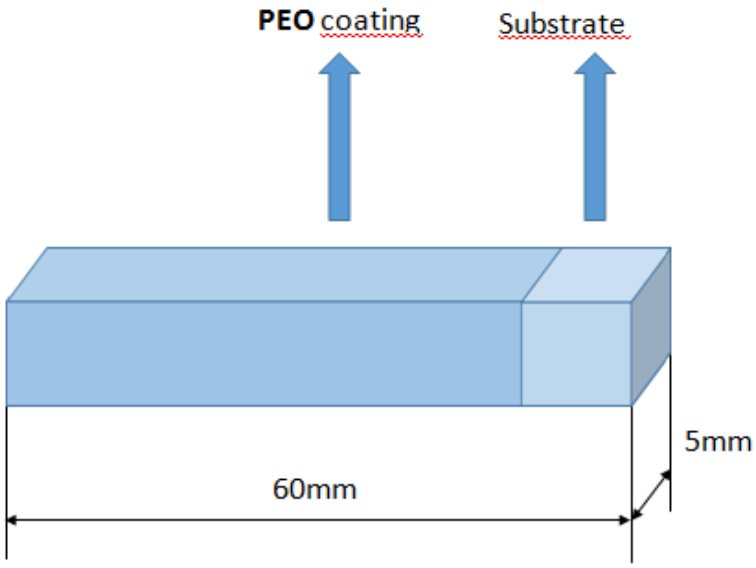

Fig.2.8 Geometry of PEO treated samples used in tribological tests

The tribometer evaluate also the coefficient of friction during the test. After the test the samples (an example in Fig.2.9) were analyzed to gain more information regarding the wear resistance and the wear mechanism.

Fig.2.9 Sample after the wear test

In particular the samples were analyzed with T2000 profilometer (Fig.2.10) in order to quantify the maximum depth of wear. The morphology of the wear lines was instead studied with an Hirox KH 7700 multifocal microscope (Fig.2.9).

Fig.2.10 Profilometer (on the left) and multifocal microscope (on the right) used for the characterization of the samples after the wear tests.

Chapter 3

Study of the effects of process parameters on PEO coatings

The first part of the work in the Ph.D project was devoted to the study of the PEO process itself. In particular the experimental tests were focused on PEO treatments on magnesium and magnesium alloys and the effect of the main process parameters on the obtained oxide ceramic films were studied.

In literature, several works about PEO of magnesium alloys can be found. In particular, the effects of additives in the electrolyte and of the operating conditions were studied [84-89]. In previous works PEO processes were performed mainly using low current densities (0.01 - 0.1 A cm^{-2}) and long treatment times (5 - 60 minutes) [90-93].

In this chapter, PEO process was performed on pure magnesium and magnesium alloys (AM50 and AZ91). The effects of the current density and treatment time on the morphology, thickness, chemical composition and corrosion resistance of the coatings, were investigated. In respect to previous studies, it was chosen to work with higher current densities (0.1 - 0.45 A cm^{-2}) and shorter treatment times (20 - 60 s). This choice was done in order to facilitate an industrial application of PEO process, reducing the whole production time of the component. In the second part of this chapter the effect of the electrolyte composition on the corrosion resistance of PEO coatings obtained on commercially pure magnesium was briefly studied.

3.1 PRODUCTION OF PEO COATINGS

Samples of commercially pure magnesium, AZ91 and AM50 alloy were used as substrate for PEO coatings in order to study the effects of the current density, treatment time and electrolyte composition on the morphology, thickness, chemical composition and corrosion resistance of the coatings. The nominal composition of the alloys is reported in Tab.3.1

Tab.3.1 Chemical composition of the alloys

Alloy	Al%	Zn%	Mn%	Si%	Fe%	Cu%	Ni%	Other%
AM50	5.0	<0.22	0.25	<0.10	<0.005	<0.010	<0.002	<0.030
AZ91	9.0	0.65	0.15	<0.10	<0.005	<0.010	<0.002	<0.030

The samples were cut from ingots and, before PEO treatment, were polished following standard metallographic techniques and then degreased using acetone in ultrasound. The PEO electrolyte was constituted in the first part of the study by an aqueous alkaline solution with 100 g L^{-1} of $Na_5P_3O_{10}$, 40 g L^{-1} of NaOH and 42 g L^{-1} of NaF.

The formation of the oxide ceramic layer was obtained using:

i) different current densities (0.1 - 0.2 - 0.25 - 0.35 - 0.45 A cm^{-2}) with the same treatment time (60 s);

ii) the same current density (0.25 or 0.45 A cm^{-2}) with different treatment times (20 - 40 - 80 s).

The initial and final voltages, achieved during the experiment at the different current density values, are reported in Tab.3.2

After the treatment, the samples were washed with deionized water and ethanol and dried with compressed air.

During the PEO process a large number of sparks/micro-discharges occurred on the surface of the samples; the number of these sparks increased with the current density and the treatment time. The treatments were performed working at constant current density, and monitoring the potential. A potential increase was observed during the process of 60 s, and depended quantitatively on the current density applied. In fact, for low current densities a potential increase of about 10 - 20 V was measured, whereas the increase was more important (about 40 - 50 V) for the treatments carried out at high current densities (see Tab.3.2).

Tab.3.2 Final and initial polarization voltages achieved for different samples under various current density values in the electrolyte 100g L^{-1} of $Na_5 P_3O_{10}$, 40g L^{-1} of NaOH and 42g L^{-1} of NaF

	Initial potential [V]	**Final potential [V]**
Commercially pure magnesium treated at 0.1 A cm^{-2}	55	58
Commercially pure magnesium treated at 0.25 A cm^{-2}	55	65
Commercially pure magnesium treated at 0.35 A cm^{-2}	55	75
Commercially pure magnesium treated at 0.45 A cm^{-2}	55	80
AZ91 alloy treated at 0.1 A cm^{-2}	50	60
AZ91 alloy treated at 0.25 A cm^{-2}	50	70
AZ91 alloy treated at 0.35 A cm^{-2}	50	90
AZ91 alloy treated at 0.45 A cm^{-2}	50	100
AM50 alloy treated at 0.1 A cm^{-2}	55	65
AM50 alloy treated at 0.25 A cm^{-2}	55	70
AM50 alloy treated at 0.35 A cm^{-2}	55	85
AM50 alloy treated at 0.45 A cm^{-2}	55	95

3.2 EFFECT OF THE CURRENT DENSITY AND OF THE TREATMENT TIME

3.2.1Surface Analysis

The morphology of the surface layers, on commercially pure magnesium, obtained with PEO process at different current densities for the same time (60 s), are shown in Fig.3.1.

The surfaces of all samples showed numerous craters and pores and the number of pores decreased with the increase of the current density applied during the treatment. In detail, passing from the sample treated at 0.1 A cm^{-2} to the sample treated at 0.45 A cm^{-2}, there was a significant reduction in the number of pores. In the sample treated at the lowest current density (0.1 A cm^{-2}) also some zones that were not completely coated during the PEO treatment were visible, and indeed, from EDS analysis, they resulted to be constituted only by Mg. Moreover, a large number of micro-cracks were observed, probably caused by residual stress resulting from rapid quenching of the molten materials at the solid/electrolyte interface, during the plasma discharges.

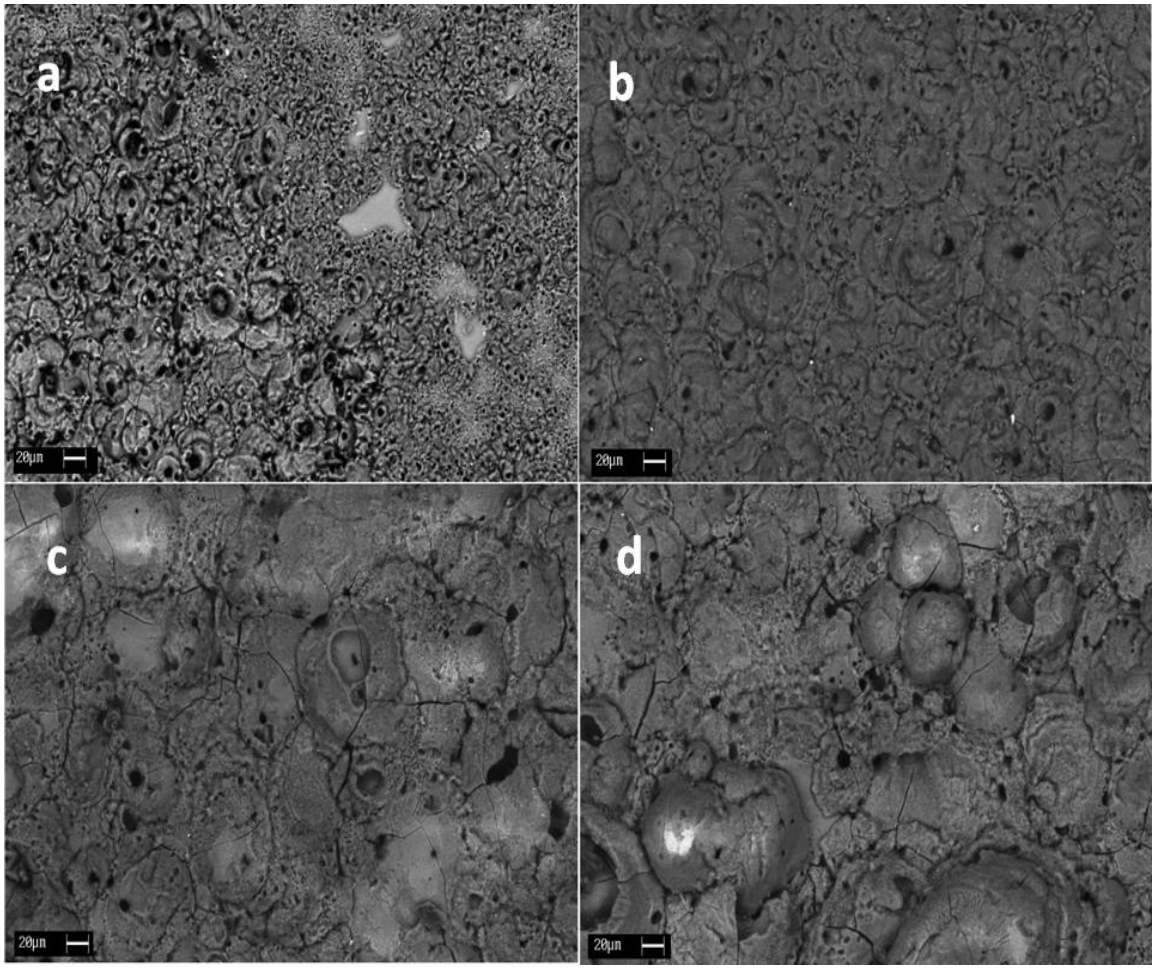

Fig.3.1 Scanning electron micrographs (backscattered electrons, 650X) of the surface of PEO coatings formed on commercially pure magnesium. All the samples were treated for 60s at 0.1 A cm^{-2} (a), 0.25 A cm^{-2} (b), 0.35 A cm^{-2} (c) and 0.45 A cm^{-2} (d)

The layers obtained by PEO process, at different current densities for the same time (60 s), on the surface of AZ91 and AM50 alloys showed the same morphology seen on the surface of pure magnesium: a decreasing porosity occurred with the increase of the current density applied in the treatment (Fig.3.2, Fig.3.3).

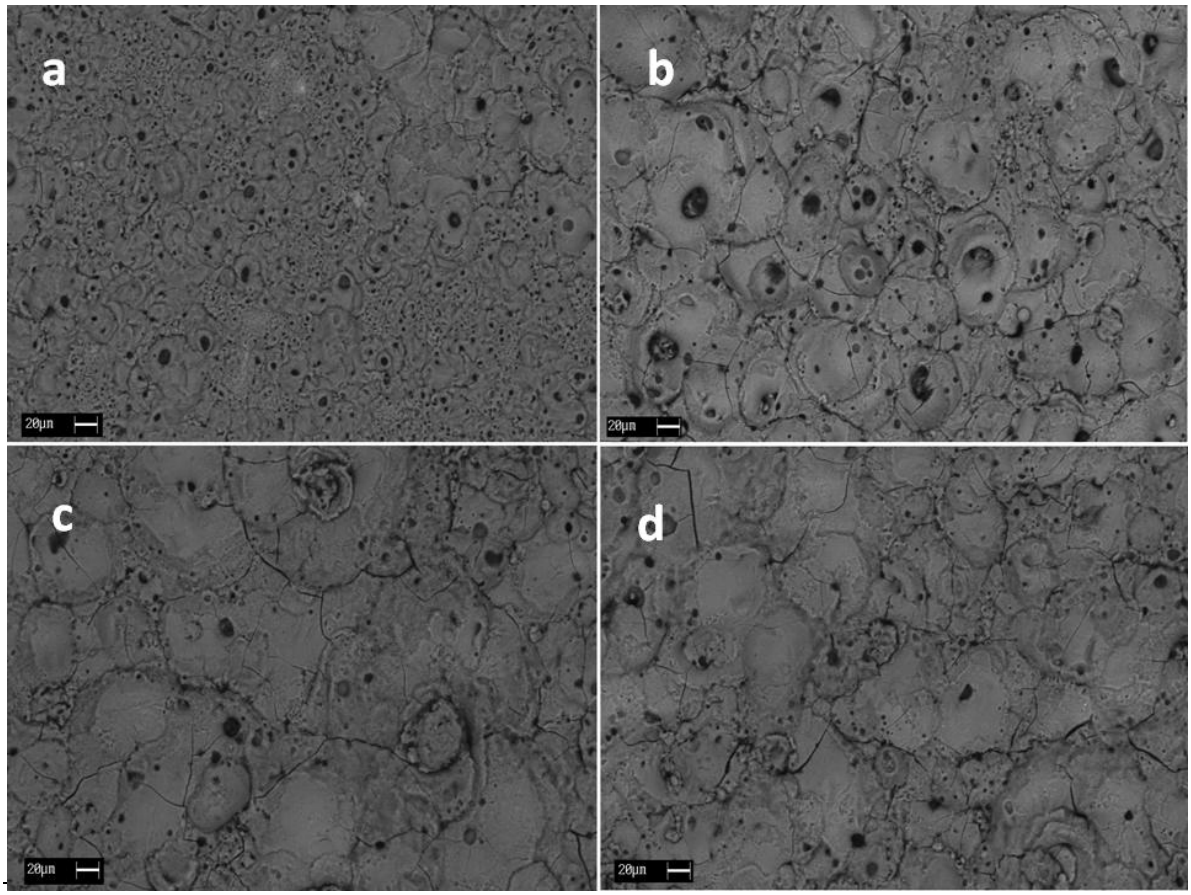

Fig.3.2 Scanning electron micrographs (backscattered electrons, 650X) of the surface of PEO coatings formed on AZ91 magnesium alloy. All the samples were treated for 60s at 0.1 A cm^{-2} (a), 0.25 A cm^{-2} (b), 0.35 A cm^{-2} (c) and 0.45 A cm^{-2} (d)

The cross-section images of the PEO coated sample for pure magnesium at different current densities are presented in Fig.3.4. An increase in the thickness of the surface layer passing from the sample treated at 0.1 A cm^{-2} (6 μm thick) to the one treated at 0.35 A cm^{-2} (47 μm thick) was observed. The detachment of the layer and the presence of cracks could be due to the damage occurred during the sample preparation (cutting and grinding). The thickness of the oxide layer in the sample obtained at 0.45 A cm^{-2} was lower than the one of the sample treated at 0.35 A cm^{-2}, (30 μm *vs*. 47 μm, respectively), but the last resulted more continuous and homogenous.

In the cross-section images of the PEO coated samples of AZ91 and AM50 alloy a continuous surface layer was observed, except for AZ91 treated with the current density at 0.1 A cm^{-2}, where only isolated islands were visible. The thicker layer grew with the current applied in the treatment: 2 μm and 7 μm at 0.1 A cm^{-2}, 30 μm and 17 μm at 0.35 A cm^{-2}, and 60 μm and 55 μm at 0.45 A cm^{-2}, for AZ91 and AM50 respectively (Fig.3.5,

Fig.3.6). Therefore, from SEM analysis, it resulted that working at high current density with relatively short treatment times allowed the formation of a thick oxide layer.

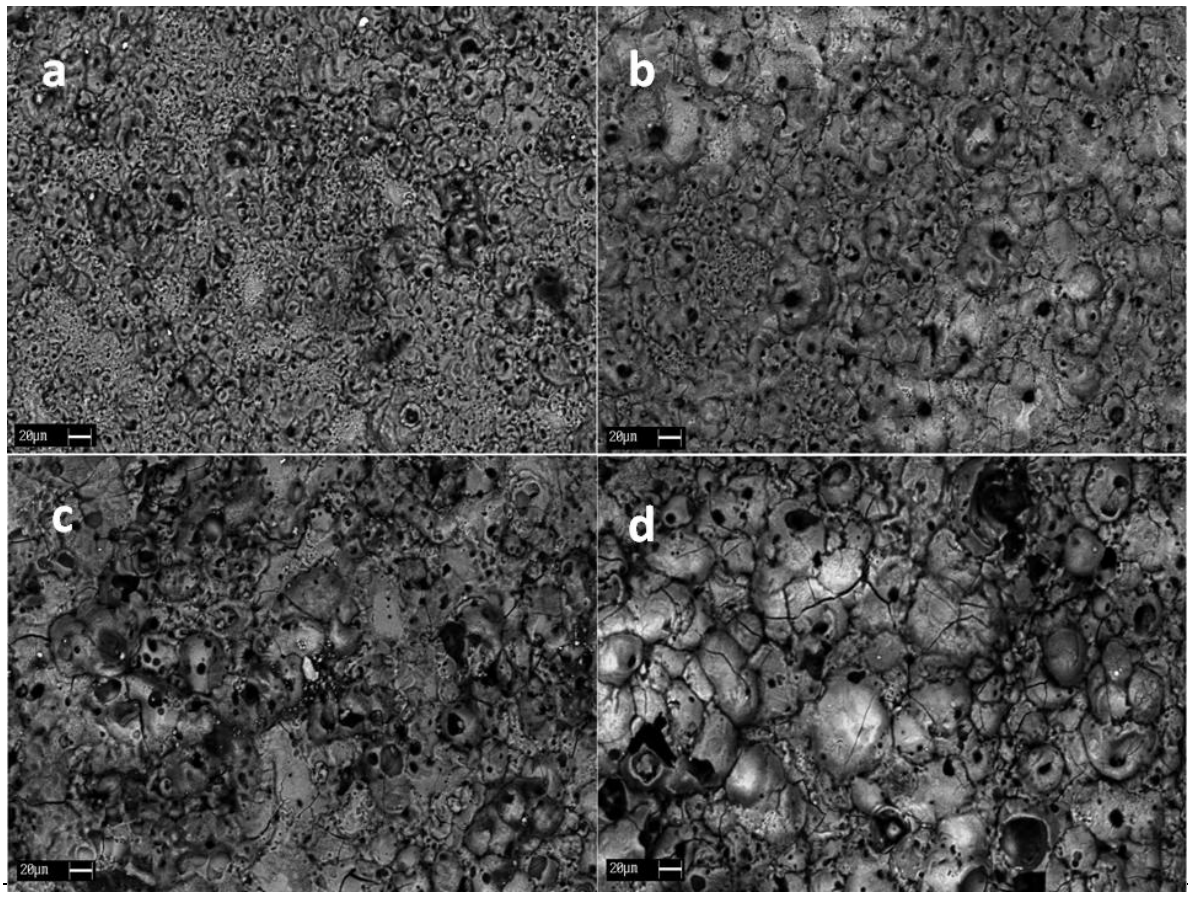

Fig.3.3 Scanning electron micrographs (backscattered electrons, 650X) of the surface of PEO coatings formed on AM50 magnesium alloy. All the samples were treated for 60s at 0.1 A cm^{-2} (a), 0.25 A cm^{-2} (b), 0.35 A cm^{-2} (c) and 0.45 A cm^{-2} (d)

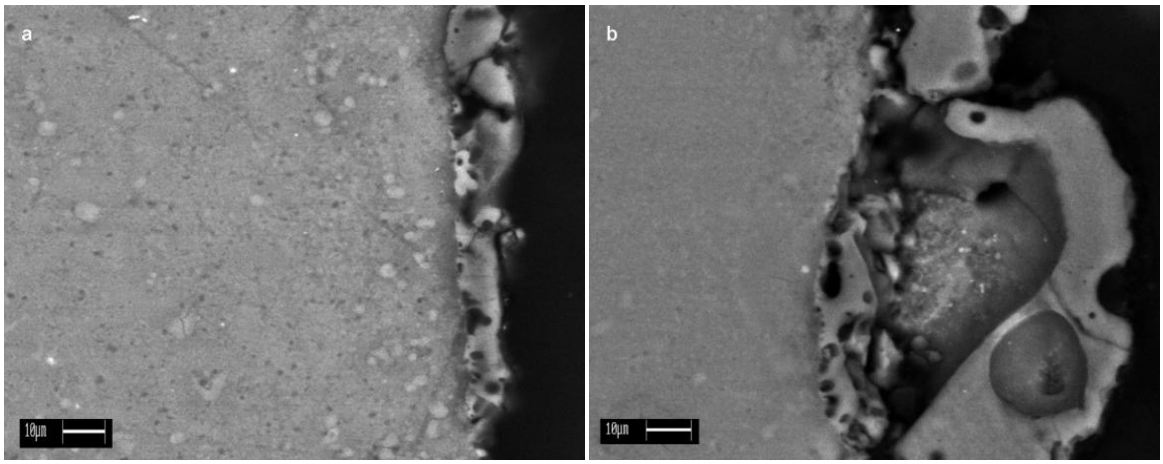

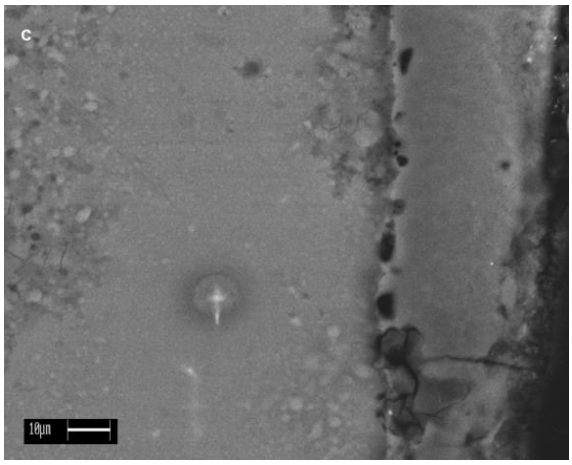

Fig.3.4 Scanning electron micrographs (backscattered electrons, 750X) of the cross section of PEO coatings formed on commercially pure magnesium samples treated for 60s at 0.1 A cm^{-2} (a), 0.35 A cm^{-2} (b) and 0.45 A cm^{-2} (c)

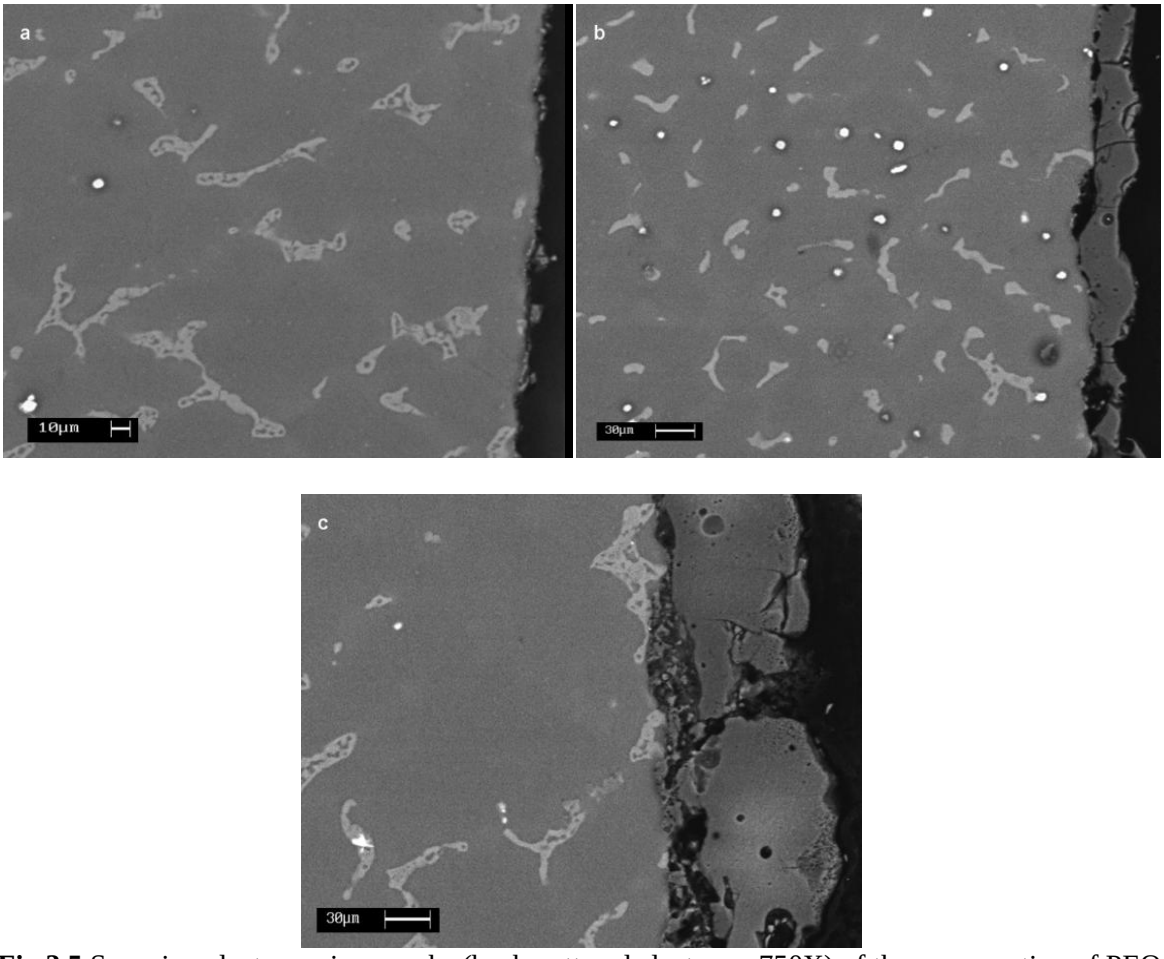

Fig.3.5 Scanning electron micrographs (backscattered electrons, 750X) of the cross section of PEO coatings formed on AZ91 magnesium alloy samples treated for 60s at 0.1 A cm^{-2} (a), 0.35 A cm^{-2} (b) and 0.45 A cm^{-2} (c)

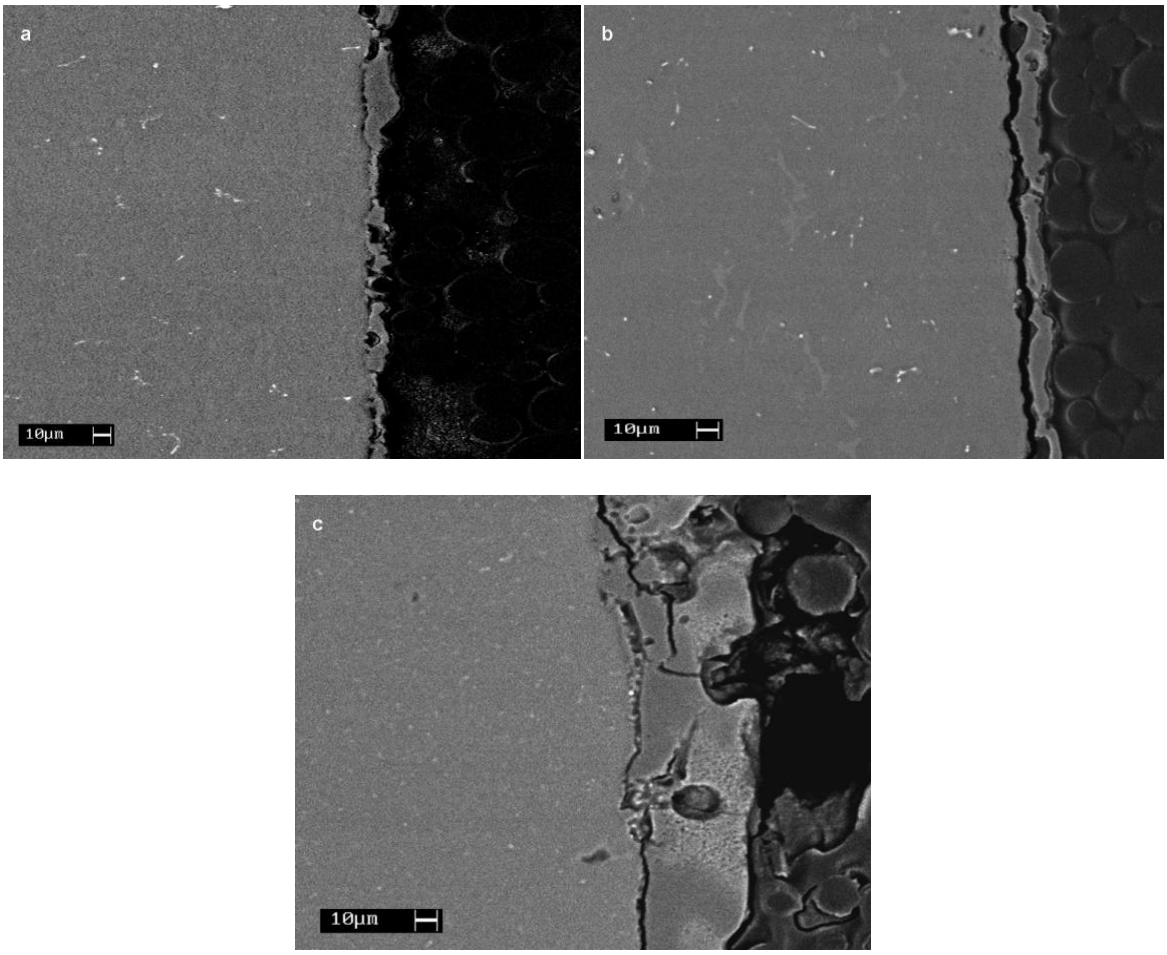

Fig.3.6 Scanning electron micrographs (backscattered electrons, 750X) of the cross section of PEO coatings formed on AM50 magnesium alloy samples treated for 60s at 0.1 A cm^{-2} (a), 0.35 A cm^{-2} (b) and 0.45 A cm^{-2} (c)

The chemical composition and the phase analysis of the layers were investigated by EDS and XRD, respectively. EDS analysis, carried out on the surface, revealed that the composition of the coating was not significantly influenced by the current density applied during the treatment, and the EDS spectra of the various samples were substantially the same. The surface of the coating formed on commercially pure Mg was principally composed by O, Na, Mg, P and F, whereas in AM50 and AZ91 alloys, besides the elements cited, also Al was registered, due to its presence in the alloy. The quantitative results of EDS analysis of the cross-sectioned surface layers (excluding oxygen that forms with the other elements oxides and phosphates) are reported in Tab.3.3.

Tab.3.3 Quantitative results (wt%) of EDS analysis of the cross-sectioned surface layers

Alloy	Mg%	P%	Na%	Al%	F%
Pure Magnesium	60.51	21.41	9.63	-	8.44
AZ91	47.44	31.17	7.64	7.28	6.46
AM50	43.16	43.81	7.72	2.27	3.05

EDS elemental profiles were performed among the cross-section of the samples in order to evaluate the composition of the layer along the thickness. The elemental profile carried out in the layer of AZ91, obtained at 0.45 A cm^{-2} for 60 s, showed that no variations in elemental concentration along the cross-section of the coating was registered, except for sodium, whose concentration increased near the surface (Fig.3.7). In addition, a slight increase of F, in proximity of the surface was observed. The tests on AM50 and commercially pure magnesium gave the same results obtained for AZ91 alloy with an enrichment of sodium and F (less marked for this last element) in the portion of the layer near the surface.

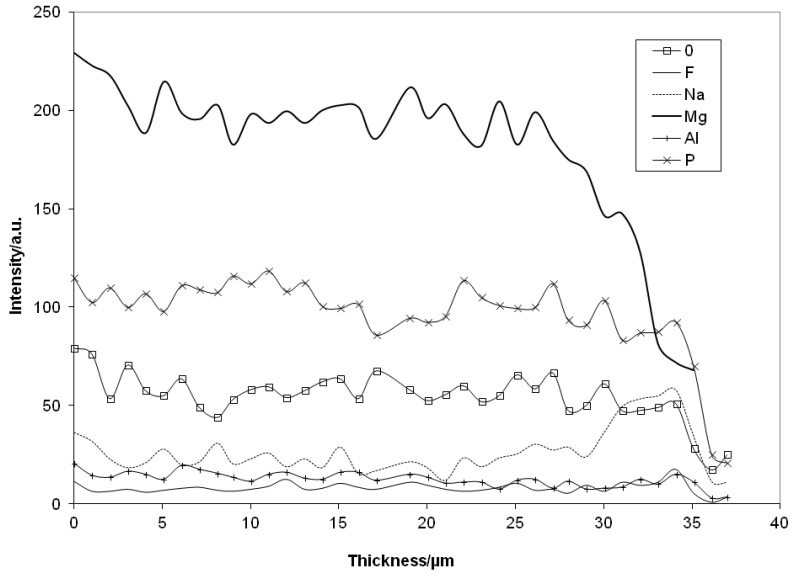

Fig.3.7 EDAX line microanalysis for the cross section of an AM50 sample treated at 0.35 A cm^{-2} for 60s. The plot goes from the interface metal-coating to the surface

XRD analysis was performed only on the samples of pure commercially magnesium and of AZ91 and AM50 alloys treated at 0.45 A cm^{-2} for 60 s. The patterns are presented in Fig.3.8. In all patterns the presence of the Mg peak was observed, due to the reflection from the substrate. The peaks of magnesium phosphate $Mg(PO_3)_2$, magnesium oxide MgO, and sodium fluoride NaF, were visible in all the alloys. In AM50 and AZ91 alloys also the presence of aluminum oxides (Al_2O_3) and mixed aluminum-magnesium oxides ($MgAl_2O_4$) were detected. The composition of the layer was clearly connected with the electrolyte used in this PEO process, constituted by an alkaline solution of sodium phosphate and sodium fluoride. Therefore, in the coating phosphates and fluorides could be found. The

presence of NaF could be due to the adsorption effect on the surface. As a matter of fact, from EDS analysis an enrichment of these two elements resulted near the surface.

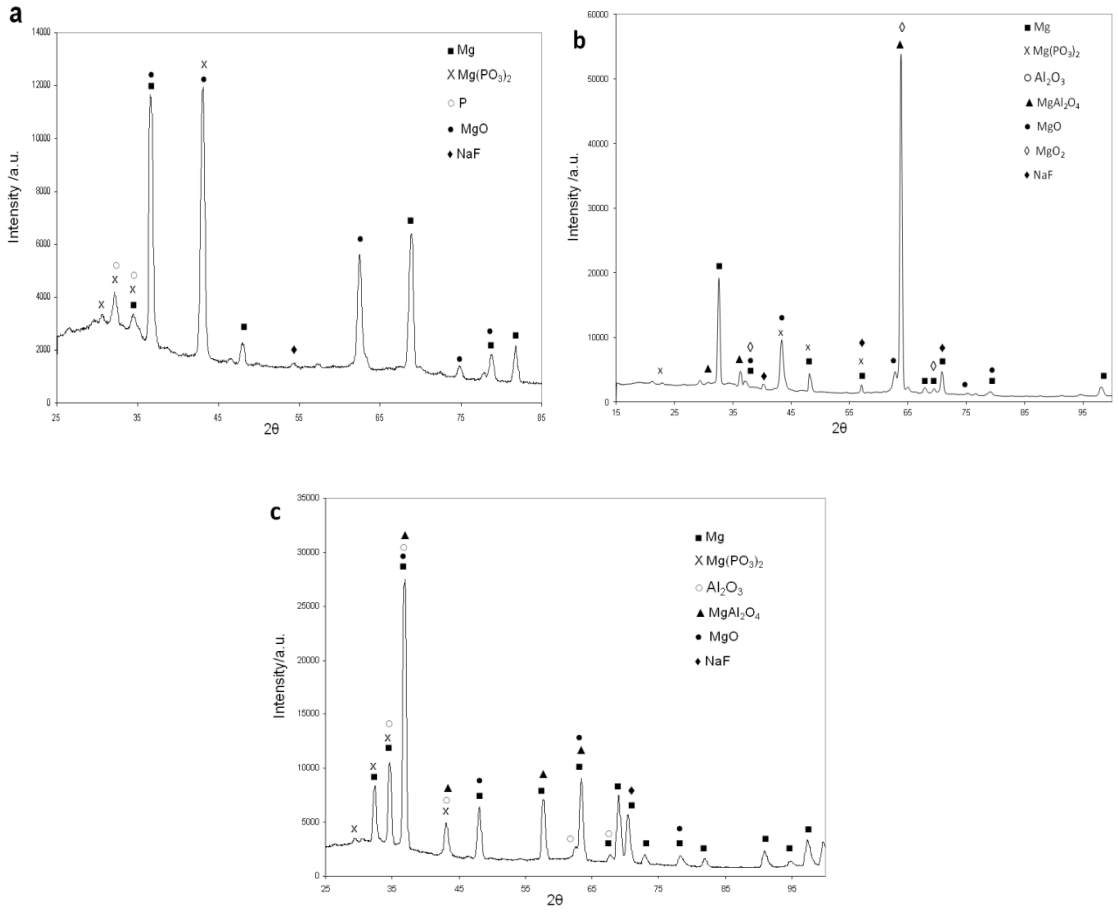

Fig.3.8 X-ray diffraction patterns for (a) commercially pure magnesium; (b) AZ91 alloy and (c) AM50 alloy PEO coated at 0.45 A cm^{-2} for 60s

In order to obtain information about the composition and the state of oxidation of the elements in the ceramic oxide layer obtained with PEO process, XPS analysis (without sputtering) were performed on the sample of pure commercial Mg treated at 0.45 A cm^{-2}. The survey spectrum of the sample is shown in Fig.3.9. From the collected spectrum of the main photoelectron lines (C1s, O1s, F1s, Na1s, Mg1s and P2p), the atomic percentages of the elements present in the external surface of the coating were calculated. The layer resulted to be principally constituted by O, Mg, F, P and Na, in agreement with the previous analysis. The presence of C is attributable to ambient contamination. The peak of Mg2s binding energy of 89.1 eV and the peak of Mg2p binding energy of 50.4 eV were assigned to the presence of MgO [76-77]. The peak of Na1s binding energy of 1071.6 eV

was attributed to the NaF compound [77] and the peaks of P2s and P2p binding energy 191.0 eV and 133.9 eV, respectively, were associated to the presence of $Mg_3(PO_4)_2$ [94]. The presence of NaF is probably due to the adsorption effect on the surface, in agreement with EDS and XRD analysis.

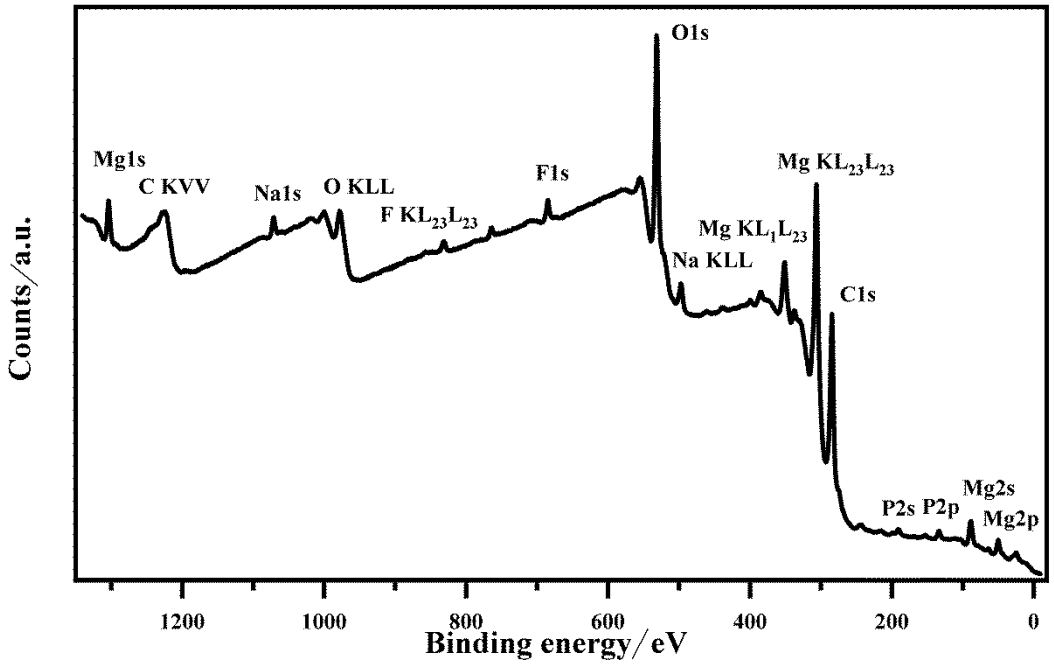

Fig.3.9 XPS survey spectra for commercially pure magnesium PEO coated at 0.45 A cm^{-2} for 60s

3.1.2 Corrosion behavior

To study the corrosion properties of the layers produced by the PEO process, potentiodynamic anodic polarization and EIS test were performed in a solution containing both sulphates and chlorides (0.1 M Na_2SO_4 and 0.05 M NaCl).

3.1.2.1 Potentiodynamic polarization tests

The anodic polarization plots for commercially pure magnesium treated with different current densities for 60 s are reported in Fig.3.10 and the corrosion current densities i_{corr} and corrosion potentials E_{corr} for the different treatments are reported in Tab.3.4.

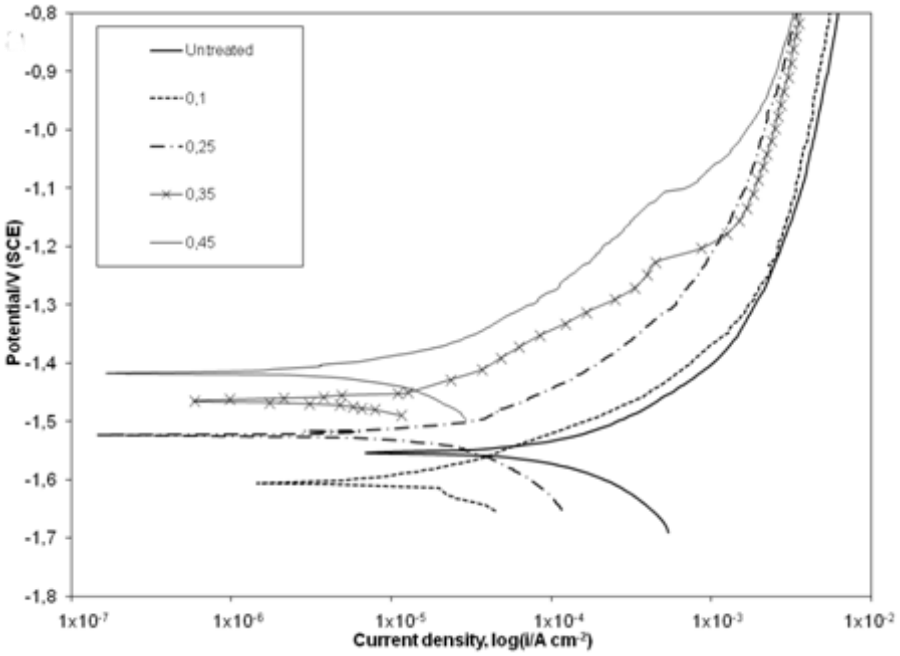

Fig.3.10 Potentiodynamic polarization plots for commercially pure magnesium PEO coated at different current densities for 60s (test electrolyte: 0.1M Na_2SO_4 + 0.05M NaCl)

Tab.3.4 Results of the anodic polarization test in 0.1M Na_2SO_4 + 0.05M NaCl solution for samples treated at different current densities for 60s. The values of E_{corr} are given versus SCE

	i_{corr} [A cm^{-2}]	E_{corr} [V]
Commercially pure magnesium untreated sample	$1x10^{-4}$	-1.55
Commercially pure magnesium treated at 0.1 A cm^{-2}	$3x10^{-5}$	-1.6
Commercially pure magnesium treated at 0.25 A cm^{-2}	$2x10^{-5}$	-1.52
Commercially pure magnesium treated at 0.35 A cm^{-2}	$5x10^{-6}$	-1.46
Commercially pure magnesium treated at 0.45 A cm^{-2}	$5x10^{-6}$	-1.41
AZ91 alloy untreated sample	$2.6x10^{-5}$	-1.56
AZ91 alloy treated at 0.1 A cm^{-2}	$1x10^{-5}$	-1.44
AZ91 alloy treated at 0.25 A cm^{-2}	$4x10^{-6}$	-1.3
AZ91 alloy treated at 0.35 A cm^{-2}	$3x10^{-6}$	-1.34
AZ91 alloy treated at 0.45 A cm^{-2}	$2x10^{-6}$	-1.14
AM50 alloy untreated sample	$7x10^{-5}$	-1.6
AM50 alloy treated at 0.1 A cm^{-2}	$4x10^{-6}$	-1.6
AM50 alloy treated at 0.25 A cm^{-2}	$3x10^{-6}$	-1.5
AM50 alloy treated at 0.35 A cm^{-2}	$4x10^{-6}$	-1.42
AM50 alloy treated at 0.45 A cm^{-2}	$5x10^{-6}$	-1.42

The corrosion resistance of the PEO treated samples was significantly improved compared with the untreated one. As a matter of fact, a decrease in the current density and an increase in the corrosion potential were observed. In particular, from the untreated sample to the one treated at 0.45 A cm^{-2}, the decrease of i_{corr} was higher than one order of magnitude. In terms of corrosion potential, in comparison with the untreated sampled,

there was a slight decrease for the sample treated at 0.1 A cm^{-2}, whereas an increase for all the other treated samples was registered, with ennoblement of 0.14 V for the sample treated at 0.45 A cm^{-2}. The better corrosion properties of the samples treated with higher current densities can be directly connected with the thicker layer and the reduction of the porosity on the surface, that both were previously observed by SEM for high current densities applied in the treatment.

The anodic polarization plot and the resulting data for AM50 alloy treated at different current densities for 60 s are reported in Fig.3.11 and Tab.3.4.

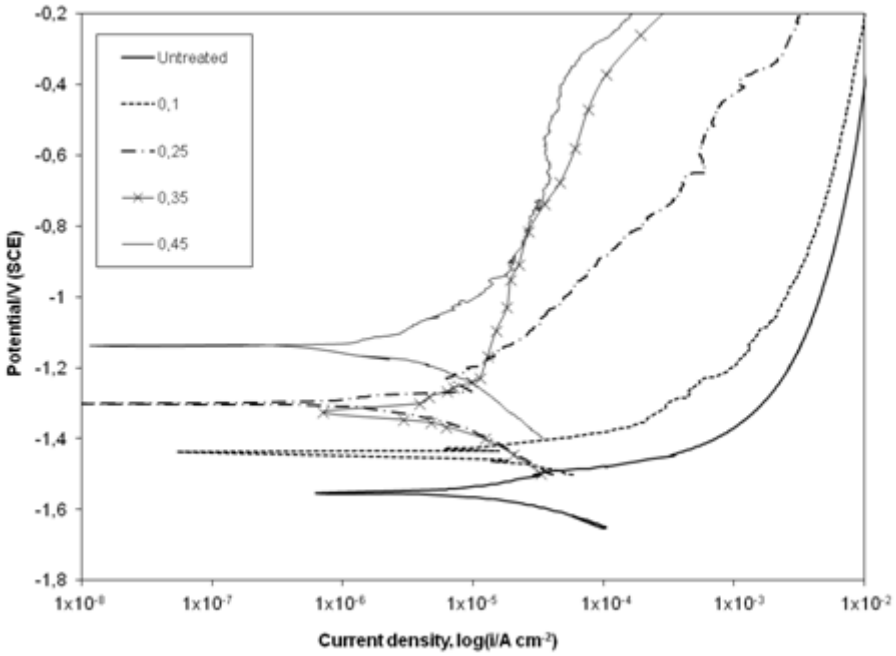

Fig.3.11 Potentiodynamic polarization plots for AM50 alloy PEO coated at different current densities for 60s (test electrolyte: 0.1M Na_2SO_4 + 0.05M NaCl)

Also for this alloy the values of E_{corr} indicated that PEO treatment caused an increase in the corrosion potential in comparison with the untreated sample and that this effect was more evident with high current densities applied (an ennoblement about 0.18 V for the sample treated at 0.45 A cm^{-2} was observed). For AM50 alloy it can be observed that the values of i_{corr} of the treated samples were more or less the same and one order of magnitude lower than the one of the untreated sample, indicating the improvement in corrosion resistance due to PEO treatment. In this alloy, a passivation phenomenon can be observed for the sample treated at 0.1 A cm^{-2}. For AZ91 the anodic polarization plot and the values of E_{corr} and i_{corr} are reported in Fig.3.12 and Tab.3.4 As it was observed for the previous materials, the PEO treatments caused an ennoblement in the corrosion potential and it increased the current density applied in the treatment. An ennoblement of 0.42 V was measured for the

sample treated at 0.45 A cm^{-2}. The values of i_{corr} for AZ91 alloy for the samples treated at 0.25, 0.35 and 0.45 A cm^{-2} are more or less the same and one order of magnitude lower than the values of the untreated sample and the sample treated at 0.1 A cm^{-2}. Also for AZ91 alloy, the samples treated at 0.35 and 0.45 A cm^{-2} showed a passivation phenomenon.

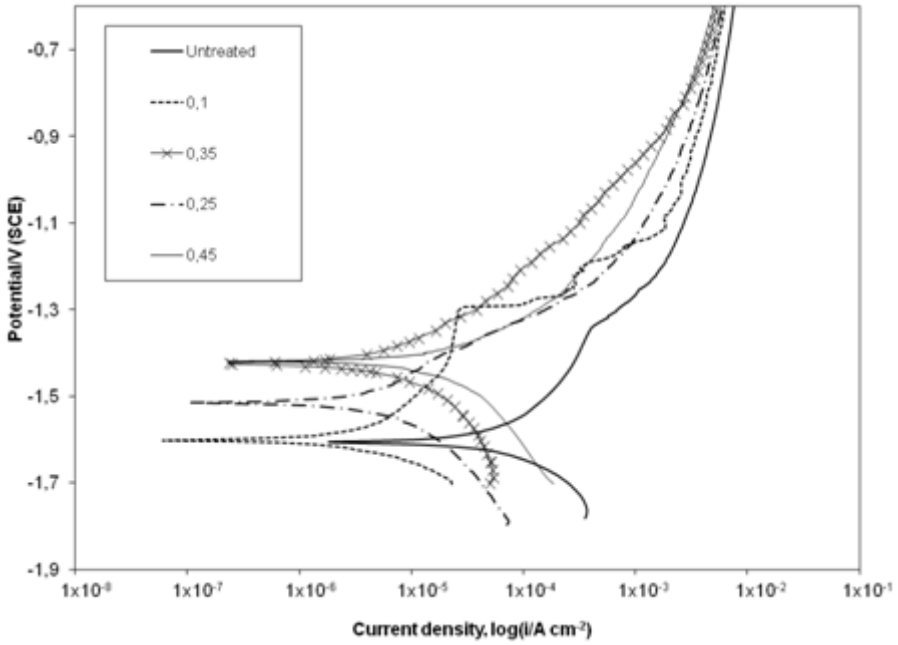

Fig.3.12 Potentiodynamic polarization plots for AZ91 alloy PEO coated at different current densities for 60s (test electrolyte: 0.1M Na_2SO_4 + 0.05M NaCl)

Potentiodynamic polarization tests were also performed on samples treated with the same current density (0.25 or 0.45 A cm^{-2}) but with different treatment times (20, 40, 60, 80 s). These tests were carried out to evaluate the effect of the treatment time on the corrosion properties of the coatings. The results of this tests for AZ91 alloy treated at 0.25 A cm^{-2} for various treatment times were reported in Fig.3.13, where the sample treated for 60 s showed the better corrosion resistance, even if its values of i_{corr} and E_{corr} were very similar to the ones of the samples treated for 40 and 80 s. Only the sample treated for 20 s presented values of i_{corr} and E_{corr} significantly lower than the others. A similar behavior was found for AZ91 alloy treated at 0.45 A cm^{-2} and for commercially pure magnesium and AM50 alloy at both current densities.

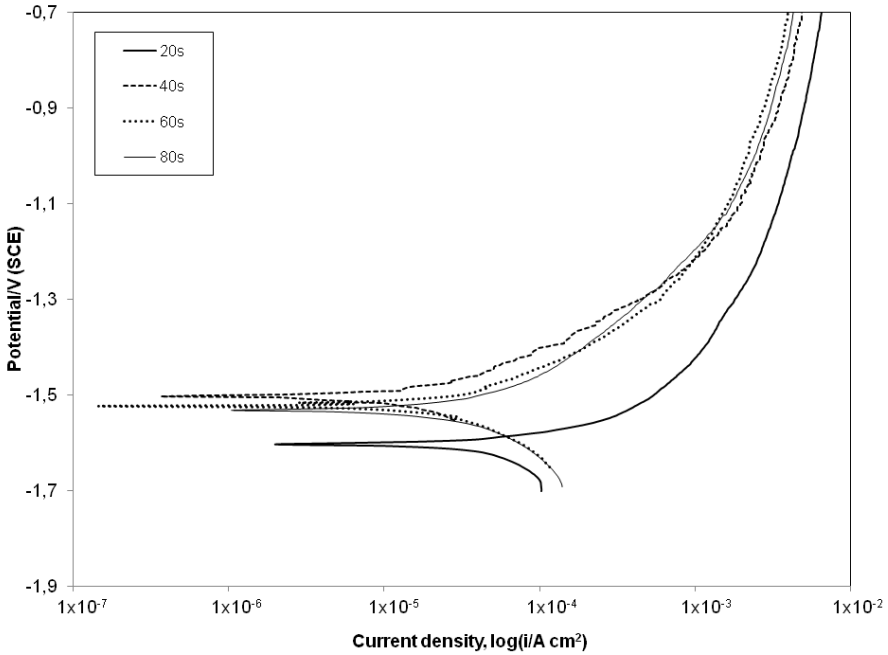

Fig.3.13 Potentiodynamic polarization plot for AZ91 alloy PEO coated at 0.25 A cm^{-2} and different treatment times (test electrolyte: 0.1M Na_2SO_4 + 0.05M NaCl)

These results showed that increasing the treatment time causes only a slight improvement in the corrosion resistance of the samples. Therefore, the effect of the treatment time was quantitatively less important than the effect of the current density. Increasing the current density applied in the PEO treatment caused a good improvement in the corrosion resistance with ennoblement in the corrosion potential and a decrease of more than one order of magnitude in the current density.

3.1.2.2 Electrochemical impedance spectroscopy

To better understand the corrosion characteristics of the PEO coated specimens, EIS tests were performed on the alloys treated at 0.1 and 0.45 A cm^{-2} for 60 s. The data coming from EIS tests were fitted for quantitative evaluation with the software Z-view using the equivalent circuit, shown in Fig.2.6a.

A good fitting quality was obtained, as it can be observed in Fig.3.15, where continuous lines represent simulation data (chi-squared values varied between 0.005 and 0.05). The simpler circuit was used due to the good fitting results obtained.

For the samples of commercially pure magnesium, the Nyquist impedance plot and the fitting results are reported in Fig.3.14a and Tab.3.5

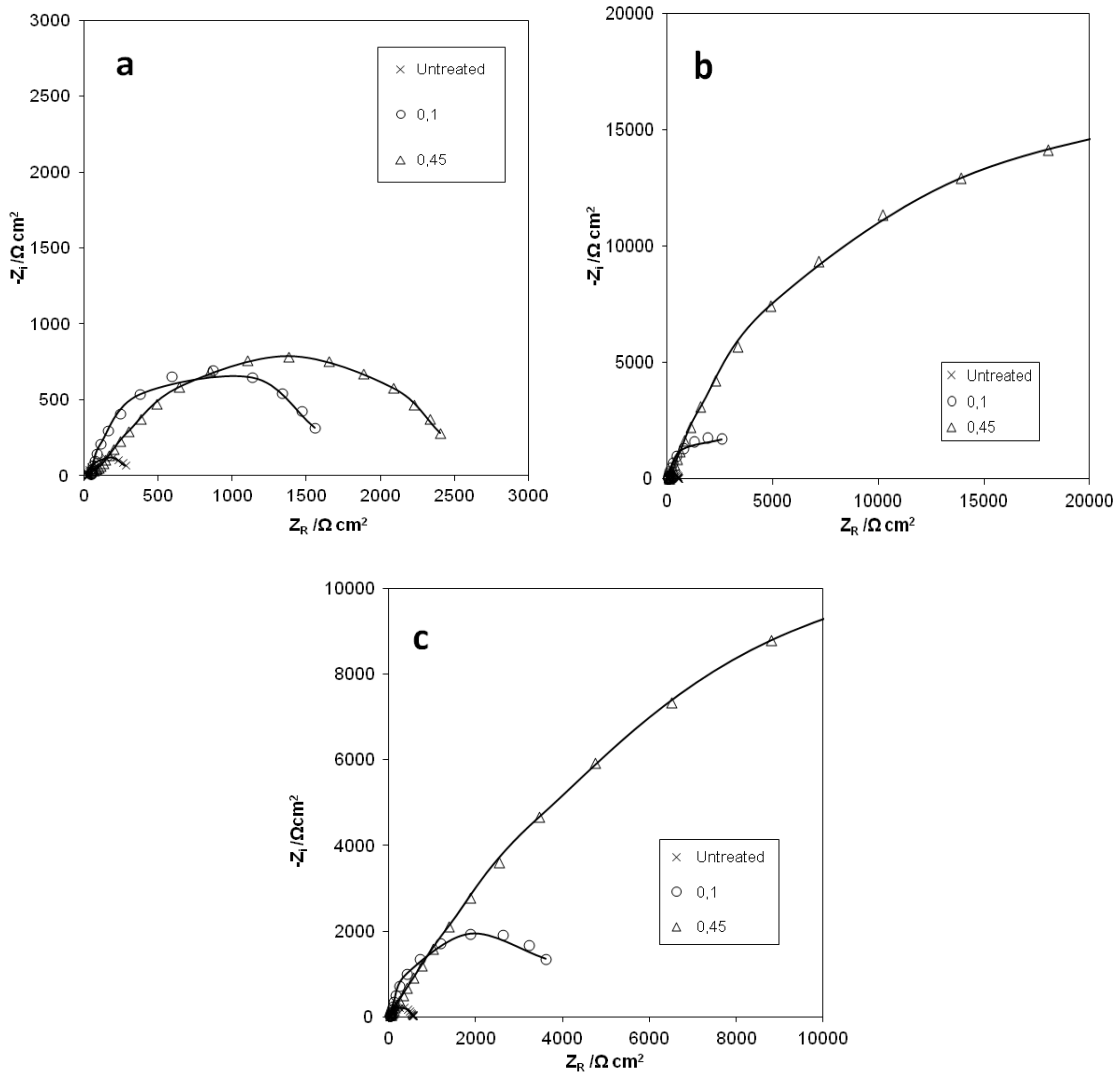

Fig.3.14 Nyquist plots for (a) commercially pure magnesium; (b) AZ91 alloy and (c) AM50 alloy PEO coated at different current densities for 60s (test electrolyte: 0.1M Na_2SO_4 + 0.05M NaCl). Continuous lines represent simulation data and points experimental data

Tab.3.5 Equivalent circuit data for samples treated at different current densities for 60s

	R_1 [Ω cm^2]	Q_2[F Hz^{1-n}]	n	R_3 [Ω cm^2]
Commercially pure magnesium untreated	25.46	1.71×10^{-5}	0.93	274
Commercially pure magnesium treated at	26.12	6.21×10^{-6}	0.74	1937
Commercially pure magnesium treated at	26.13	3.24×10^{-6}	0.74	2667
AZ91 alloy untreated sample	23.36	1.72×10^{-5}	0.88	519
AZ91 alloy treated at 0.1 A cm^{-2}	25.75	3.49×10^{-6}	0.86	4473
AZ91 alloy treated at 0.45 A cm^{-2}	25.48	1.86×10^{-6}	0.84	20639
AM50 alloy untreated sample	25.32	9.83×10^{-5}	0.78	632
AM50 alloy treated at 0.1 A cm^{-2}	23.18	2.14×10^{-6}	0.81	4993
AM50 alloy treated at 0.45 A cm^{-2}	25.12	4.22×10^{-6}	0.76	40035

Increasing the current density of the PEO process, induced also an increase in the value of R_3, the polarization resistance, which is inversely proportional to i_{corr}. In detail, the R_2 of the sample treated at 0.45 A cm^{-2} was one order of magnitude higher than the one of the untreated sample. Moreover, a decrease in the value of Q_2 can be observed passing from the untreated sample to the sample treated at 0.45 A cm^{-2}. From Eq. 2.2, the lower value of Q_2, obtained for the samples treated at high current density, can be correlated with an increase in the thickness, in agreement with the results from SEM observation.

The Nyquist impedance plots and the results of the data fitting, for AZ91 alloy, are reported in Fig.3.14b and in Tab.3.5, respectively. Similarly to the results obtained for pure commercially magnesium, a decrease in the values of Q_2 and an increase in the values of R_3 were found for the samples with PEO treatment, in comparison with the untreated sample, suggesting the presence of a thicker and more protective layer. It should be noted, that the value of R_3 for the sample treated at 0.45 A cm^{-2} was two order of magnitude higher than the one of the untreated sample, whereas for commercially pure magnesium, at the same operative conditions, this value was only one order of magnitude higher than the one of the untreated sample. The Nyquist impedance plots and the results of fitting of the data for AM50 alloy are reported in Fig3.14c. and Tab.3.5, where a behavior very similar to AZ91 alloy can be observed. These results evidenced that the PEO process caused an enhancement in the corrosion resistance of both pure magnesium and magnesium alloys, but the improvement was more evident for magnesium alloys, in agreement with the results coming from anodic polarization tests.

3.2 EFFECT OF THE ELECTROLYTE CONCENTRATION AND COMPOSITION

After the study of the influence of the current density and of the treatment time previously reported during a second part of the work the corrosion behavior of samples of commercially pure magnesium treated for one minute at 0.3 A/cm^2 with different electrolytes was studied. At first the sample obtained with the previously described solution (100 g L^{-1} of $Na_5P_3O_{10}$, 40 g L^{-1} of NaOH and 42 g L^{-1} of NaF) was compared with a sample obtained with a more dilute solution: 50 g L^{-1} of $Na_5P_3O_{10}$, 20 g L^{-1} of NaOH and 21 g L^{-1} of NaF. The results of the anodic polarization tests are reported in Fig.3.15 and Tab.3.6. From this data it can be found that no significant differences in the

corrosion behavior of the two samples can be observed. So is better to work with dilute solution due to the saving in regents.

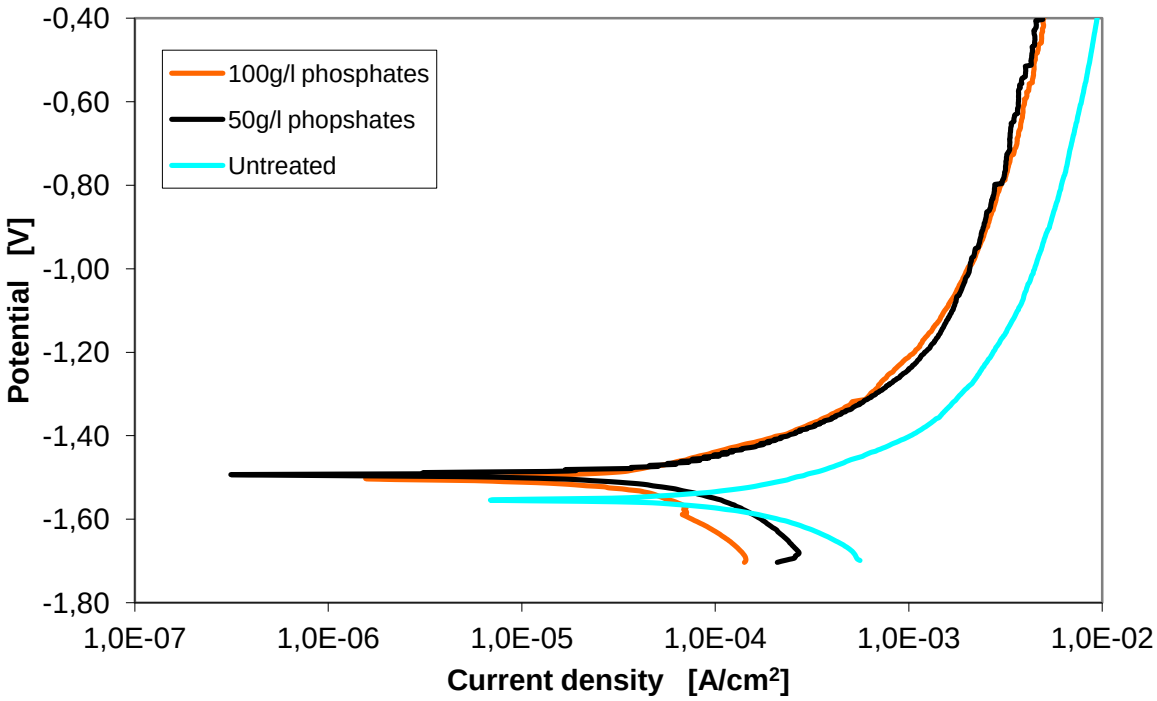

Fig.3.15 Potentiodynamic polarization plot for commercially pure magnesium PEO coated at 0.3 A cm^{-2} and one minute with different electrolyte concentration (test electrolyte: 0.1M Na_2SO_4 + 0.05M NaCl)

Tab.3.6 Results of the anodic polarization test in 0.1M Na_2SO_4 + 0.05M NaCl solution for samples treated with different electrolyte concentrations for 60s at 0.3 A/cm^2 The values of E_{corr} are given versus SCE

	Untreated	**100g/l $Na_5O_{10}P_3$ + 1M NaOH + 1M NaF**	**50g/l $Na_5O_{10}P_3$ + 0.5M NaOH + 0.5M NaF**
I_{corr} [A/cm^2]	$9x10^{-5}$	$2x10^{-5}$	$2x10^{-5}$
E_{corr} [V]	-1.55	-1.5	-1.5

The sample obtained with the previously described electrolyte (50 g L^{-1} of $Na_5P_3O_{10}$, 20 g L^{-1} of NaOH and 21 g L^{-1} of NaF) at 0.3 A/cm^2 for one minute was also compared with one obtained with an electrolyte containing sodium silicates instead of sodium phosphates (50 g L^{-1} of Na_2SiO_3, 20 g L^{-1} of NaOH and 21 g L^{-1} of NaF) treated with the same electric conditions and the results of corrosion tests are reported in Fig.3.16 and Tab.3.8. It can be observed that the sample obtained with the electrolyte containing sodium silicates is characterized by a lower value of corrosion current density and an higher value of

corrosion potential, so this sample is characterized by better corrosion performances. The improved corrosion resistance of the sample treated with silicates was predictable, in fact as reported in literature and as was remarked in chapter 1, coatings obtained with silicates are more compact and homogeneous than the ones obtained with phosphates.

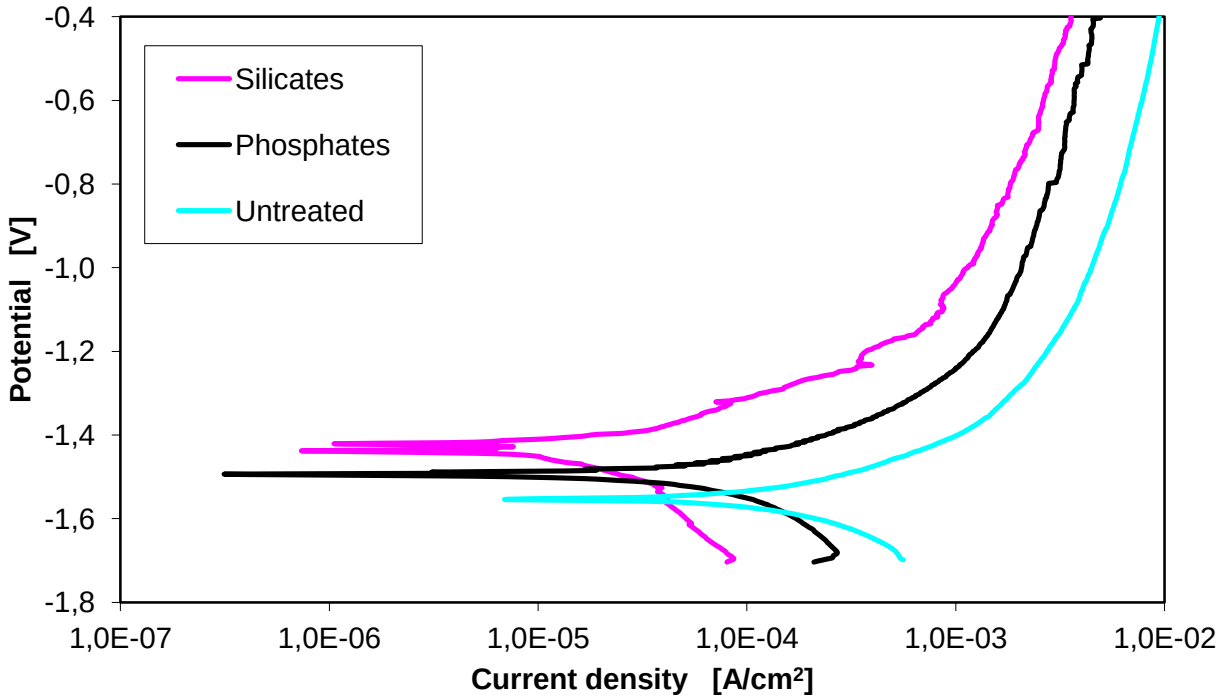

Fig.3.16 Potentiodynamic polarization plot for commercially pure magnesium PEO coated at 0.3 A cm^{-2} and one minute with different electrolyte compositions (test electrolyte: 0.1M Na_2SO_4 + 0.05M NaCl)

Tab.3.8 Results of the anodic polarization test in 0.1M Na_2SO_4 + 0.05M NaCl solution for samples treated with different electrolyte compositions for 60s at 0.3 A/cm^2 The values of E_{corr} are given versus SCE

	Untreated	**Electrolyte with Phosphates**	**Electrolyte with Silicates**
I_{corr} [A/cm^2]	$9x10^{-5}$	$5x10^{-5}$	$1x10^{-5}$
E_{corr} [V]	-1.55	-1.5	-1.45

3.3 CONCLUDING REMARKS

The plasma electrolytic oxidation (PEO) process performed, using as electrolyte an aqueous alkaline solution containing phosphates and fluorides, produced on magnesium and magnesium alloy a thick ceramic layer, principally constituted by oxides, phosphates and fluorides. Working with high current densities and very short times allowed the

formation of a thick surface layer. The current density applied during the treatment influenced the morphology, the thickness, and the corrosion properties of the layers but not the composition. The increase of the current density caused a reduction in the number of pores on the surface and an increase in the thickness of the coating. The effect of the treatment time was quantitatively less important than the one of the current density. PEO coated samples exhibited improved corrosion properties as evidenced by potentiodynamic anodic polarization tests and EIS tests, in comparison with untreated samples. EIS tests in particular evidenced that both magnesium and magnesium alloys showed an enhancement in the corrosion resistance due to the PEO treatment, but the improvement was higher for magnesium alloys compared with the one of commercially pure magnesium. Moreover was found that an electrolyte containing silicates produce an increase in the corrosion resistance of the samples if compared with one containing phosphates instead working with dilute electrolytes (up to 50% of dilution) do not significantly affect the corrosion resistance of the obtained coatings. However the most innovative finding of this research was the possibility to obtain coatings with optimal corrosion performances working with shorter treatment times if compared with the known literature. This could be a big advantage in industrial applications due to the increase in the production rate and the consequent reduction of costs.

Chapter 4

Study of additives to improve the corrosion resistance

After studying the influence of process parameters on the obtained PEO coatings the second part of the Ph.D. project was devoted to study the possible addition of additives in the electrolyte in order to improve the corrosion resistance of the coatings obtained both on aluminum and magnesium alloys. One of the most important advantages of PEO process is the use of environmental friendly electrolytes, so the choice of the additives is very difficult in order to keep this important property. In detail the choice was oriented on molybdate salts and rare earth salts. These compounds do not cause problems to the environment and to humans (instead for example Cr(VI)) and were already used in literature to increase the corrosion resistance of different kinds of coatings. Cerium and lanthanum salts were employed to prepare solutions that produce a conversion precursor film on aluminum and magnesium alloys [95-96]. Particles of insoluble cerium oxide were also used in literature suspended in the electrolyte to obtain their co-precipitation during PEO process and improve the properties of the oxide layer [97-98]. Cerium salts were used to produce solutions used as post-treatment to seal the characteristic pores on coatings obtained by PEO [99]. All these treatments have positive effects on the corrosion resistance of the obtained coatings. Molybdenum is well known as a corrosion inhibitor when present in the solutions as Mo(VI) [100-102], moreover due to its strong oxidation character, its reduction product is stable and can form a passive film [103-104]. The incorporation of Mo(VI) ions provide also a potential self-healing ability when the film is damaged [105]. In several researches, conversion coatings using molybdate salts to improve the corrosion resistance of magnesium alloy, have been investigated [106-108].

In this Ph.D work lanthanum and molybdenum salts were directly dissolved in the electrolyte used to produce the PEO coatings in order to reduce the whole treatment time

and to obtain the final coating in only one step. Regarding this particular solution there aren't a lot of works in literature. The use of molybdate salt for PEO process in fact has been poorly studied. Molybdenum was used to produce post-treatment solutions to seal the pores that characterize coatings obtained with PEO [109], and only in one research it was added to the electrolyte for the PEO process [110]. Moreover in literature rare earth salts are often employed in treatments produced on metals to improve the corrosion resistance, especially with the formation conversion coatings [103], but only few works reported the dissolution of rare earth salts in the electrolyte to produce a PEO coating [111].
In this thesis will be described firstly the addiction of molybdenum salts in the electrolyte in order to improve the corrosion resistance of PEO treated AZ91 magnesium alloys. In the second part will be described the results of the addiction of lanthanum salts in the electrolyte used to produce PEO coatings on a 7075 aluminum alloy.

4.1 EFFECT OF THE ADDICTION OF MOLYBDENHUM SALTS IN THE ELETROLYTE

In this chapter will be described the experimental analysis carried out in order to study the influence of the addiction of sodium molybdate in the electrolyte used to produce PEO coatings on magnesium alloys

4.1.1 Production of molybdenum-containing PEO coatings

Samples of AZ91 magnesium alloy were cut from bars and used as substrate for PEO treatment. The nominal composition of the alloy is reported in Tab.4.1

Tab.4.1 Chemical composition of AZ91 magnesium alloy

Alloy	Al%	Zn%	Mn%	Si%	Fe%	Cu%	Ni%	Other%
AZ91	9.0	0.65	0.15	<0.10	<0.005	<0.010	<0.002	<0.030

Before PEO treatment, the samples were polished following standard metallographic techniques (grinding with abrasive papers and polishing with cloths) and then degreased using acetone in ultrasound. The base electrolyte used in the PEO process was constituted by an aqueous alkaline solution with 15 g/l of Na_2SiO_3, 3 g/l of NaOH and 10 ml/l of diethylamine. To this solution different concentrations of sodium molybdate Na_2MoO_4

(0.3, 0.6, 1, 3 g/l) were added in order to evaluate the effect of the presence of this compound on the final coating.

All the samples were treated using the same treatment time (15 minutes) and the same current density (0.05 A/cm^2) letting the potential free to vary. After the treatment, the samples were washed with deionised water and ethanol and dried with compressed air.

The voltage versus time plot recorded during the process for the various samples is reported in Fig.4.1.

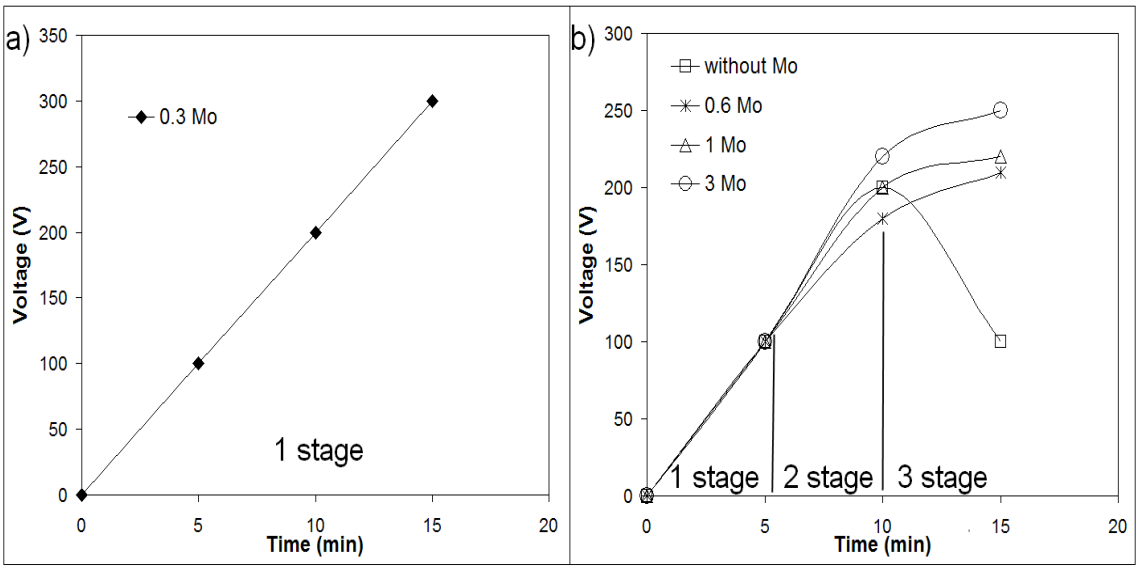

Fig. 4.1 Voltage versus Time plot and different stages of PEO coating for the sample treated with 0.3 g/l of sodium molybdate in the electrolyte (a) and for the other samples (b)

Considering the typical four stages of the PEO process reported in literature [112], with the treatment here described only the early stages are performed on the samples due to the low current density applied during the process. Thanks to this, the early stages of the formation of the protective layer (the inner barrier layer and the initial formation of the porous layer) can be studied [113,86]. In particular, in the sample treated with 0.3 g/l of sodium molybdate in the electrolyte (Fig. 4.1a) only the first stage, with the voltage that increased linearly and the formation of a thin barrier layer, can be observed. The formation of micro-discharges was not observed in this sample. For the other samples (Fig. 4.1b) the formation of micro-discharges occurred during the treatment and the process entered in the second and third stages, which correspond to the beginning of the porous layer growth. In the sample treated without molybdate salt the process entered in the second stage but a decrease in the recorded potential can be observed before the third stage, indicating a partial dissolution of the protective layer and of the substrate.

4.1.2 Analysis of the Corrosion behaviour

The corrosion resistance of the samples was evaluated by potentiodynamic polarization tests and EIS tests performed in a solution containing both sulphates and chlorides (0.1 M Na_2SO_4 and 0.05 M NaCl).

4.1.2.1 Potentiodynamic polarization tests

The anodic polarization plots of the samples treated with low and high molybdate concentrations are reported respectively in Fig.4.2a and Fig.4.2b. The curves were in both cases compared with the one of the untreated sample. The values of the corrosion current densities i_{corr} and of the corrosion potentials E_{corr} for the samples treated with electrolytes containing different sodium molybdate concentrations are reported in Tab.4.2.

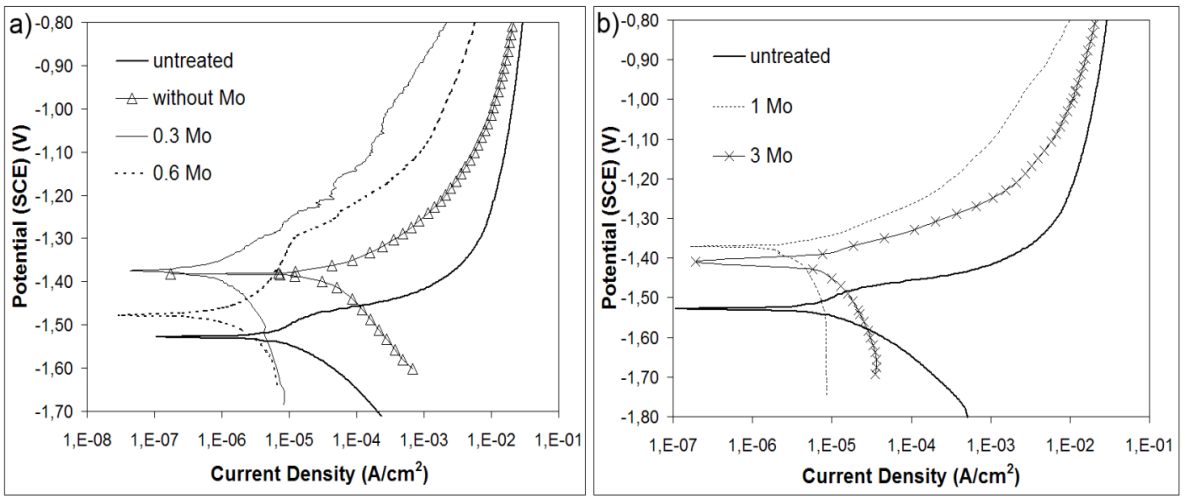

Fig. 4.2 Anodic polarization plot of AZ91 samples treated with an electrolyte containing low (a) or high (b) amounts of sodium molybdate (test electrolyte: 0.1M Na_2SO_4 + 0.05M NaCl)

Tab.4.2 Values of the corrosion current density and of the corrosion potential of AZ91 samples treated with an electrolyte containing various concentrations of sodium molybdate obtained in chlorides and sulphates solution

	Untreated	**NoMo**	**0.3Mo**	**0.6Mo**	**1Mo**	**3Mo**
I_{corr} [A/cm^2]	1.5 x10^{-5}	3.5 x10^{-5}	1x10^{-6}	2.5 x10^{-6}	4.5 x10^{-6}	7 x10^{-6}
E_{corr} [V]	-1.55	-1.39	-1.37	-1.5	-1.37	-1.41

The previously reported table and figures show that adding Na_2MoO_4 in the electrolyte used to produce PEO coating had a positive effect on the corrosion resistance of the

samples. In fact, all the samples treated with the electrolyte containing molybdate show a lower current density than the one treated without molybdate.

In terms of E_{corr} all the PEO treated samples exhibited an ennoblement in comparison with the untreated sample. The higher potential values were observed for the samples obtained with 0.3 g/l and 1 g/l of Na_2MoO_4, with an ennoblement of about 0.15 V.

The data reported in Tab.4.2 also indicate that the concentration of sodium molybdate influenced the corrosion resistance of the coated samples: the lowest addition of Na_2MoO_4 (0.3 g/l) in the electrolyte produced coatings with better corrosion resistance if compared with coatings obtained with the highest addition (3 g/l) of Na_2MoO_4. In fact, a decrease in the corrosion current was observed with the decrease of sodium molybdate in the electrolyte. However, the total removal of Na_2MoO_4 showed a negative effect on the corrosion resistance: the sample treated with the electrolyte without Na_2MoO_4 was characterized by the highest corrosion current density and so by the worst corrosion performances.

4.1.2.2 Electrochemical impedance spectroscopy

To better understand the corrosion behavior also EIS tests were performed on the samples treated with and without Na_2MoO_4 in the electrolytes. A good fitting quality was obtained for all samples, with chi-squared values varying between 0.006 and 0.04. The circuit reported in Fig. 2.6a was used to fit data coming from the untreated sample, where only the natural oxide layer is present, and from the sample treated with 0.3 g/l of sodium molybdate, where only the initial barrier layer should be formed, because the PEO process was stopped at the first stage. The equivalent circuit reported in Fig.2.6b was used to fit data coming from the other treated samples, in order to consider also the presence of the external porous layer, typical of PEO coatings. This choice permit to minimize the error in the fitting of the experimental data.

Nyquist impedance plots and results of the fitting of the experimental data for the samples treated using electrolytes containing different concentrations of Na_2MoO_4 are reported in Fig.4.3a, Fig.4.3b and Tab.4.3.

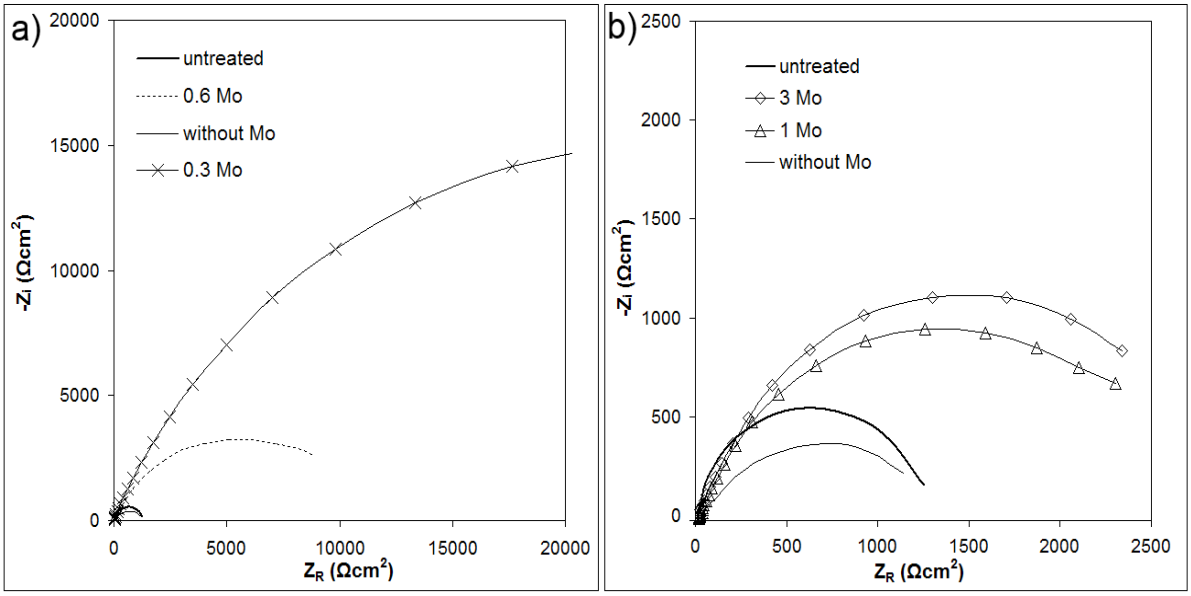

Fig.4.3 Nyquist plots for AZ91 samples PEO coated with an electrolyte containing low (a) or high (b) amounts of sodium molybdate (test electrolyte: 0.1M Na_2SO_4 + 0.05M NaCl)

Tab.4.3 Equivalent circuit data for AZ91 alloy treated with an electrolyte various containing concentrations of sodium molybdate obtained in chlorides and sulphates solution

	Untreated	**NoMo**	**0.3Mo**	**0.6Mo**	**1Mo**	**3Mo**
R_1 [Ω*cm^2]	14.71	13.45	16.46	14.07	15.54	15.1
R_2 [Ω*cm^2]	-	565.3	-	10310	2777	2528
R_3 [Ω*cm^2]	1259	800	42721	7500	2640	2800
Q_1 [F*Hz^{1-n}]	-	4.78×10^{-7}	-	1.07×10^{-5}	8.54×10^{-6}	1.34×10^{-6}
n_1	-	0.86	-	0.69	0.71	0.77
Q_2 [F*Hz^{1-n}]	1.11×10^{-5}	8.03×10^{-5}	9.37×10^{-7}	8.4×10^{-5}	4.3×10^{-5}	4.8×10^{-5}
n_2	0.91	0.84	0.73	0.84	0.76	0.81

Adding Na_2MoO_4 in the electrolyte produced an increase in the value of R_3, if compared with the untreated sample and the sample treated without molybdate. R_3 and R_2 are inversely proportional to i_{corr} and so they are directly related to the corrosion resistance of the barrier layer and the porous layer, respectively. The values of R_3 are the most relevant to evaluate the corrosion resistance, because the barrier layer gives the major protection against corrosion. Comparing the values of R_3 of the samples treated with the electrolyte

containing Na_2MoO_4, a decrease in the value of R_3 with the increase of Na_2MoO_4 amount can be observed. In fact, the highest value of R_3 is the one measured on the sample treated with the lower molybdate amount (0.3 g/l); for this sample the polarization resistance is one order of magnitude higher. This behavior can be related to the formation of a thin but dense and protective coating in the sample treated with 0.3 g/l of sodium molybdate. These results are in agreement with the anodic polarization plots, where the sample treated with 0.3 g/l of sodium molybdate in the electrolyte was the one with the lower value of i_{corr}. Regarding the values of R_2, which corresponds to the polarization resistance of the porous layer, it can be observed that the sample treated with 0.6 g/l of sodium molybdate was characterized by the maximum value of R_2. The decrease of the polarization resistance of the porous layer with the increase of molybdate content can be explained with the greater number of pores and micro-cracks. The minimum value of R_2 measured for the sample treated without molybdate can be due to the partial dissolution of the protective layer and of the substrate, which occur during the PEO process without molybdate.

4.1.3 Surface analysis

The SEM images of the surface of the coated samples obtained with backscattered electrons are shown in Fig.4.4. As it's possible to observe, some samples did not show the typical surface of PEO coatings that are characterised by the presence of a continuous porous ceramic coating. This can be correlated with the evolution of the process previously described; in fact, the typical porous PEO coating can be observed after the whole four stages process whereas in this case only earlier stages occurred.

In the sample treated without molybdenum in the electrolyte, the coating was irregular with surface covered by large agglomerates of about 200 μm (Fig.4.4a). From EDS analysis, these agglomerates resulted be constituted by Mg, Si, Al, Na and O, whereas in the uncoated zone only the presence of the elements belonging to the AZ91 alloy were detected. The presence of uncoated zones can be correlated with the partial dissolution of the protective layer and of the substrate due to the decrease of the potential observed at the end of the second stage.

The presence of 0.3 g/l of sodium molybdate in the electrolyte allowed the formation of a thin but more homogeneous coating, as reported in Fig. 4.4b and Fig. 4.4f.

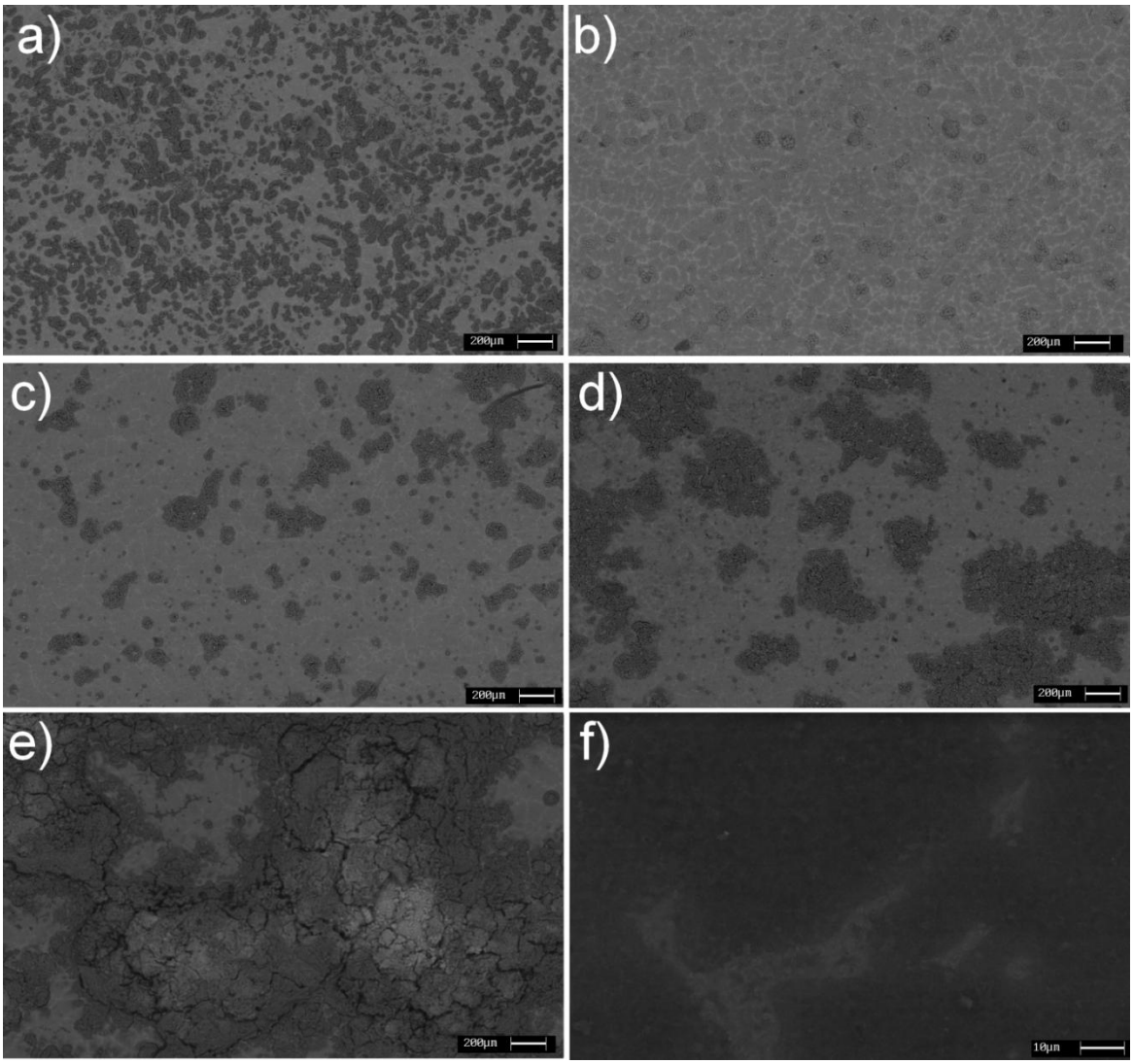

Fig. 4.4 SEM-BSE images of the surfaces after PEO process: a) without sodium molybdate, b) 0.3 g/l; c) 0.6 g/l; d)1 g/l; e) 3g/l; f) higher magnification of b).

From the EDS analysis performed in correspondence of the thin film, resulted the presence of Mg, Al and Si, but not of Mo (Fig.4.5a). This thin and homogeneous layer is the typical inner barrier layer of PEO coatings formed after the first stage of the treatment and is the one that gives the major protection against corrosion.

Increasing the molybdate content in the electrolyte, induced the growth of the agglomerates, until to cover the whole surface in the case of the sample treated with 3 g/l of the salt (Fig. 4.4c, 4.4d, 4.4e). The agglomerates showed the typical feature of the PEO coating, with the presence of porous microstructures and some volcano top-like pores. The formation of these agglomerates is in accordance with the evolution of the PEO process previously reported in Fig. 4.1b. In fact during the second and third stage the production of the anodic micro-discharges induced the growth of the external porous layer of the PEO coatings; but only some agglomerates are visible because the formation of this film is

completed only after the fourth stage of the process that were not performed with our process parameters. In the sample treated with 3 g/l, a lot of cracks are also present on the surface of the coating. The EDS analysis carried out on the surfaces evidenced that Mo is present in the samples treated with 1 and 3 g/l of salt (Fig. 4.5b).

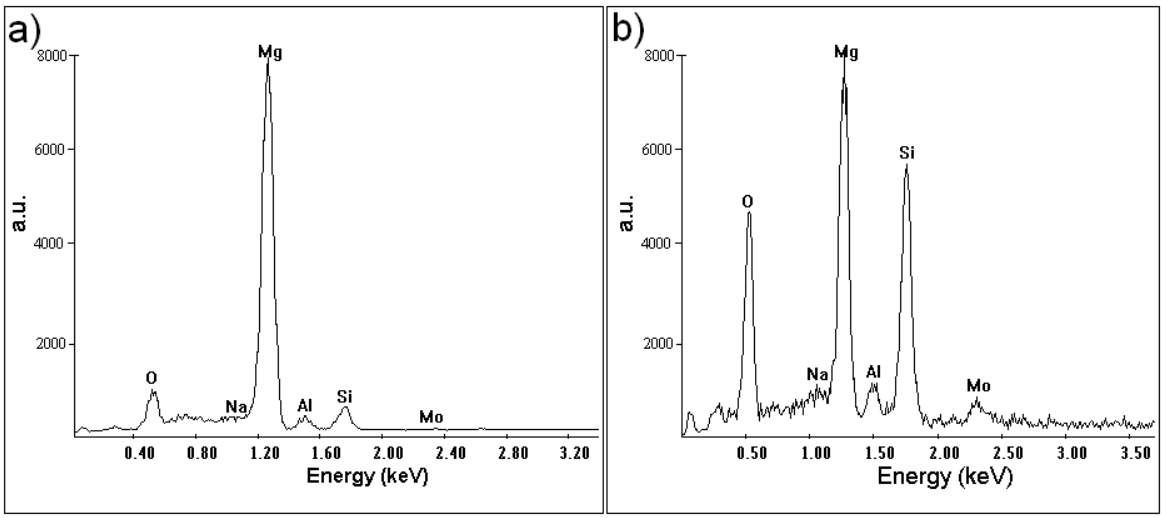

Fig.4.5 EDS spectrum of surface analysis of: a) sample with 0.3g/l; b) sample with 3 g/l.

The cross-sections of the coated samples were examined by SEM using backscattered electrons mode, and the images of the samples obtained with the various concentrations of sodium molybdate, previously described, are shown in Fig. 4.6. It can be observed that in the sample treated with the electrolyte without sodium molybdate (Fig. 4.6a), the layer is not continuous and only isolated zones of material are coated, in correspondence of the zones where dissolution of the substrate occurred. The thickness of the coating in these zone is about of 40 μm, and it was composed by Mg, Si, Al and Na. In the sample treated with 0.3 g/l of Na_2MoO_4 (Fig. 4.6b, Fig. 4.6f) the presence of a continuous coating can be observed. The oxide layer is thin, about 1 μm, but dense and homogeneous, with the presence of isolated agglomerates of ceramic coating. This type of structure corresponds to the first stages of PEO coating process and the presence of this thin barrier layer can be correlated with the high corrosion resistance showed by this sample and previously observed with anodic polarization tests and EIS tests. The cross-section of the samples reported in Fig. 4.6c and 4.6d confirmed that in the samples treated with 0.6 and 1 g/l of sodium molybdate the coating was not homogenous and the formation of agglomerates rich of pores, typical of the third stage of PEO treatment, can be observed.

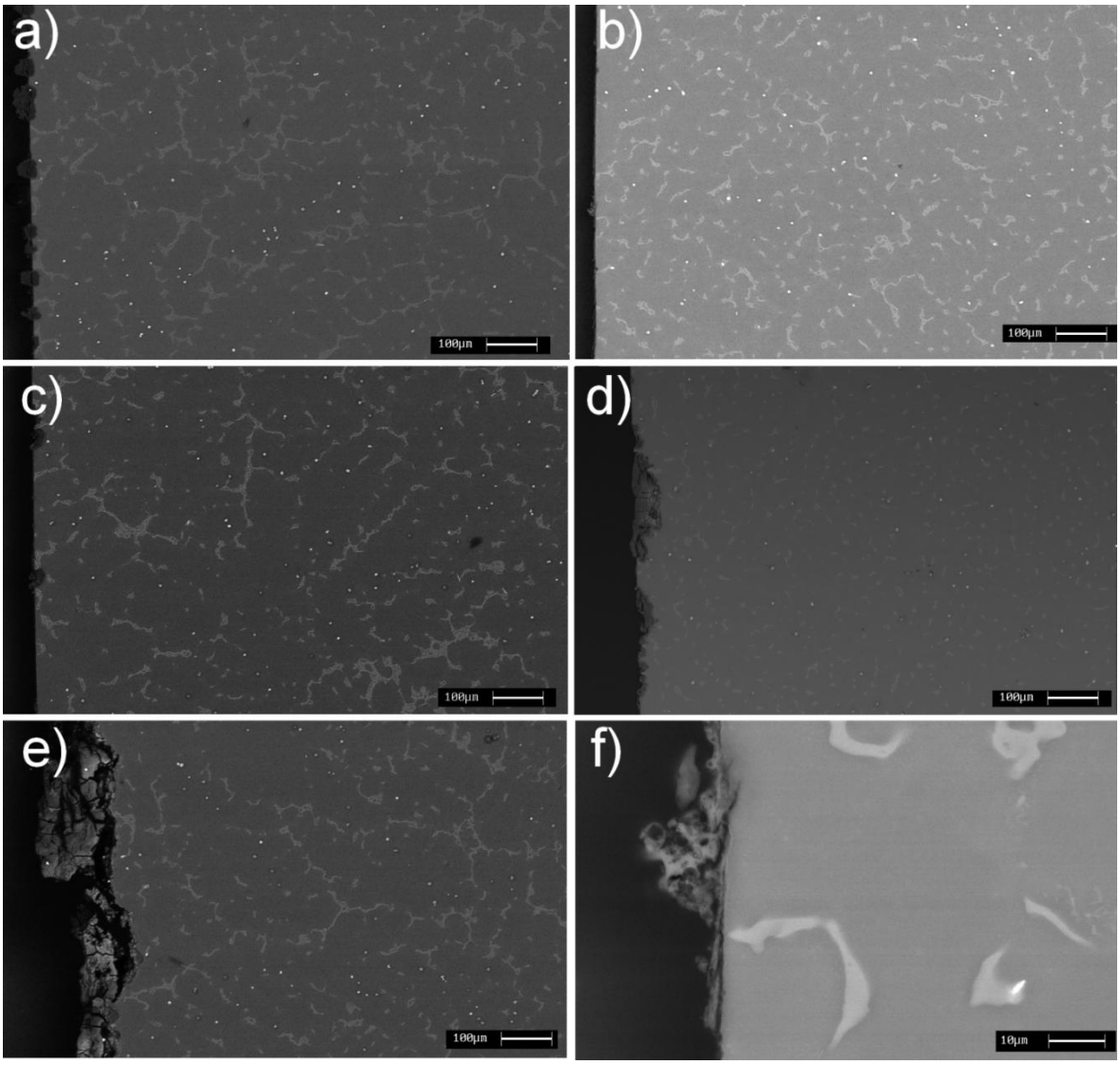

Fig. 4.6 SEM-BSE images of the cross-sections of the sample PEO coated using as electrolyte a base alkaline solution containing 0 g/l of sodium molybdate.

In the sample treated with 3 g/l of sodium molybdate (Fig. 4.6e) a continuous, and also thicker (about 40 µm) layer can be observed. However, the thicker layer was characterized by the presence of several micro-cracks in the section of the coating as was already observed on the surface. The presence of these micro-cracks can explain the poor corrosion performances of this sample if compared with the one treated with 0.3 g/l of molybdate.

The EDS analysis performed on the cross-section of the samples in correspondence of the coating were in agreement with the analysis carried out on the surfaces. They evidenced that the coatings are constituted mainly by oxygen, magnesium, silicon, aluminium and sodium. The presence of molybdenum was only detected in the samples treated with the electrolyte containing 1 and 3 g/l of sodium molybdate.

The XRD analysis performed on the samples showed that the coating was constituted mainly by MgO and Mg_2SiO_4, in agreement with the composition of the alloy and of the electrolyte. Molybdenum compounds were not detected, due to the low concentration of the salt in the electrolyte. The presence of the peaks of Mg was observed, due to the reflection from the substrate of AZ91 alloy. In Fig. 4.7a and 4.7b are shown the diffraction patterns of the sample treated with 0.3 g/l and of the one treated with 3 g/l of sodium molybdate, respectively. The diffraction pattern of the sample treated with 0.3 g/l (Fig. 4.7a) was enlarged to allow a better view of the minor phases present in the sample.

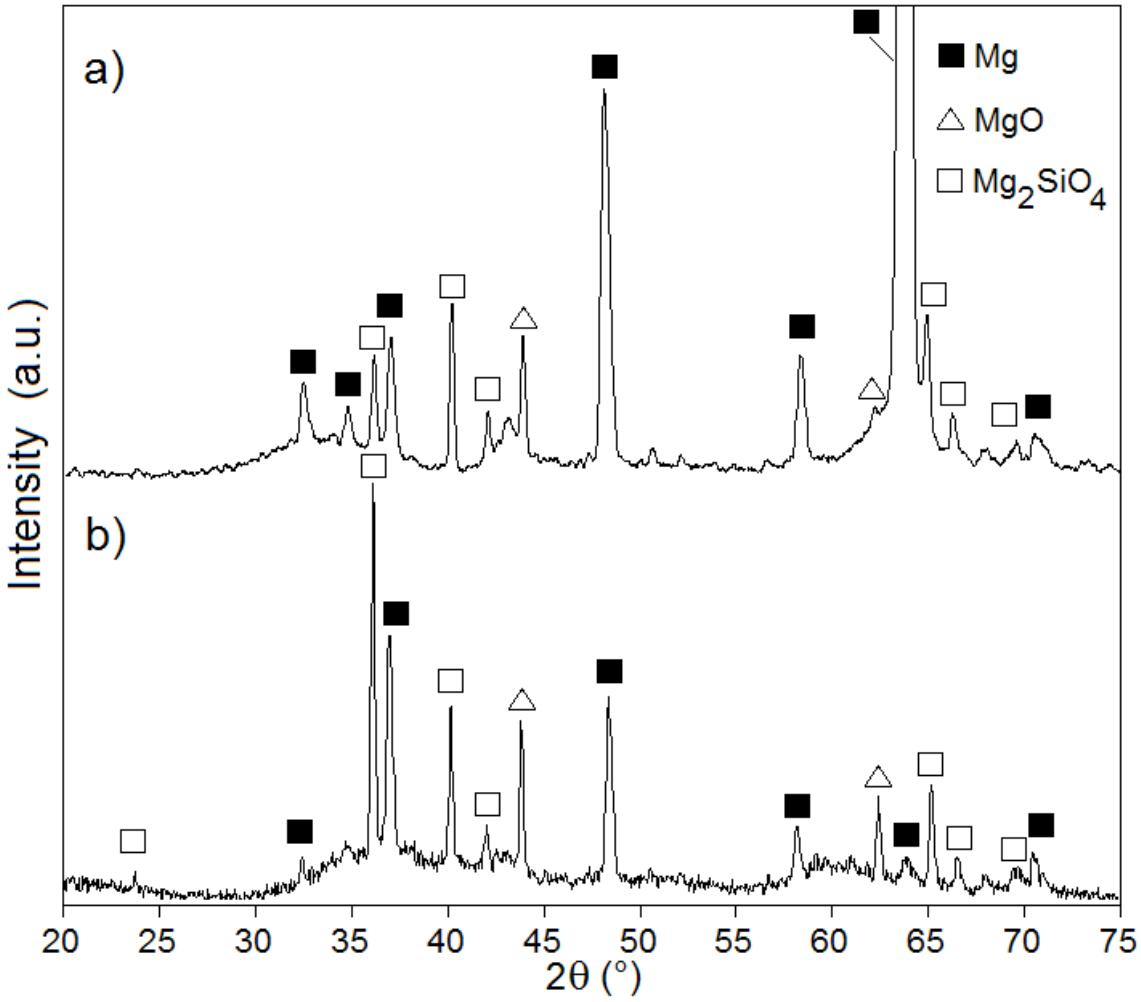

Fig. 4.7 X-ray diffraction pattern for AZ91 alloy PEO coated using an electrolyte with (a) 0.3 g/l and (b) 3 g/l of sodium molybdate.

The comparison of the patterns revealed that in the coating were present the same phases, but it was different the amount of these, due to the different thicknesses of the two coatings. In the sample treated with 3 g/l of sodium molybdate the coating was thick about 40 μm and the signal coming from the substrate is relatively low, whereas in the sample

treated with 0.3 g/l of sodium molybdate the thickness was about 1 μm, and the peaks corresponding to the substrate (Mg) are predominant.

Summarizing the study of the surface morphology, the analysis of the cross sections and the identification of the phases of the coated samples evidenced that the sample characterized by the best surface characteristics in terms of homogeneity, integrity and adhesion of the coating was the one obtained with 0.3 g/l of sodium molybdate in the electrolyte that was also the sample characterized by the best corrosion performances as was previously described.

To better understand the properties of the coating produced using 0.3 g/l of sodium molybdate, SIMS and XPS analysis were conducted on the surface of this sample.

SIMS chemical profiles of the various elements that constituted the protective layer in the sample obtained with an electrolyte containing 0.3 g/l of sodium molybdate are reported in Fig. 4.8a.

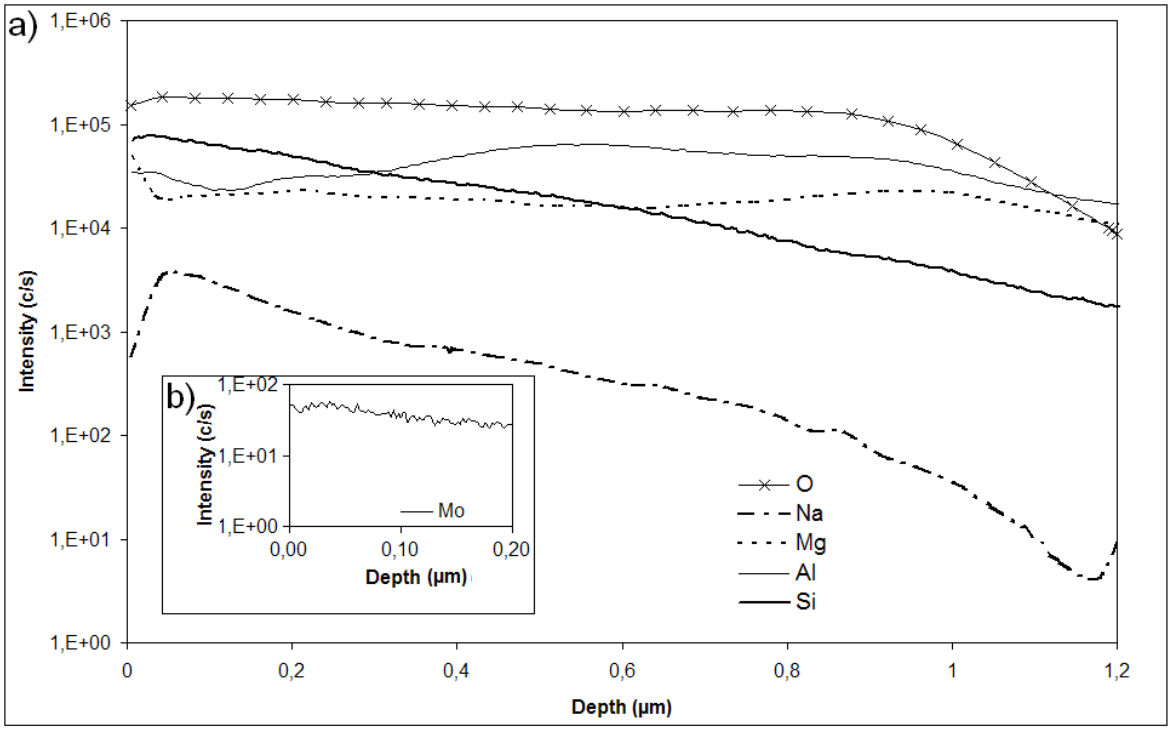

Fig. 4.8 SIMS depth profiles for (a) the elements that mainly compose the protective layer and (b) molybdenum in the sample PEO treated with an electrolyte containing 0.3 g/l of sodium molybdate.

The oxygen profile indicates that the thickness of the protective layer was is about 1 μm, in fact at this depth the counts for the oxygen start to decrease. It can be observed that Al and Mg are more or less constant in the whole sample. On the other hand Na and Si level

decrease significantly near the base material and this indicates are more concentrated in the external part of the coating. Also molybdenum is visible but with low signal; the chemical profile reported in Fig. 4.8b indicates that molybdenum concentration was constant in the protective layer.

XPS analysis (without sputtering) were performed on the sample of AZ91 alloy treated with the electrolyte containing 0.3 g/l of Na_2MoO_4. The survey spectrum of the sample is shown in Fig. 4.9.

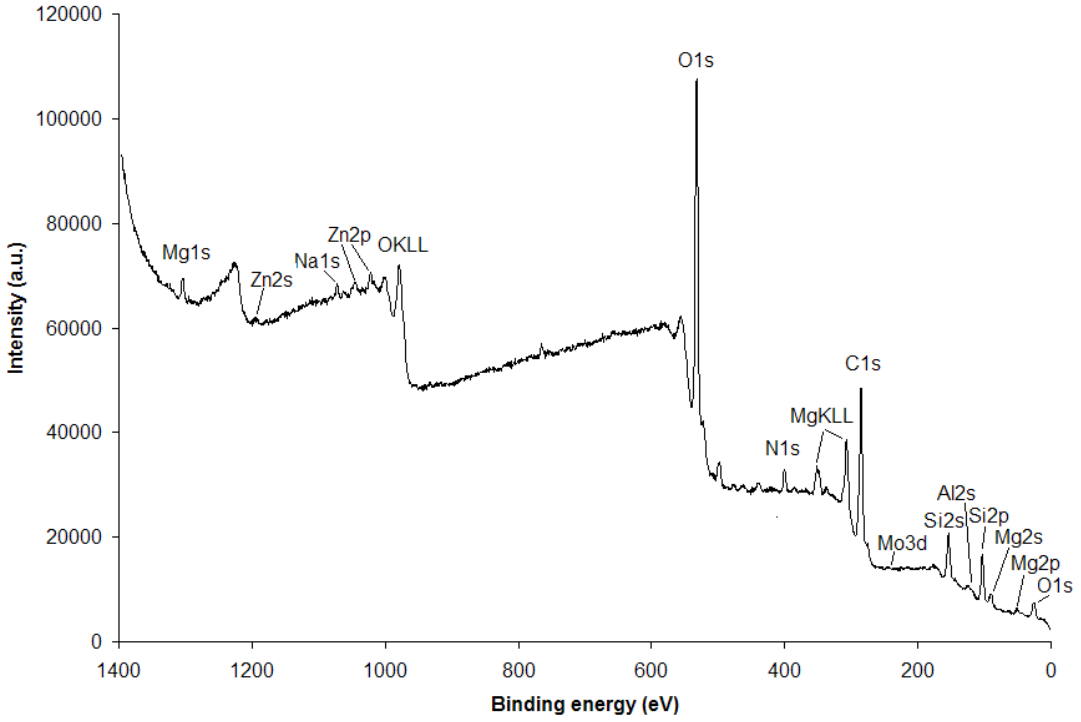

Fig. 4.9 XPS survey spectra for AZ91 magnesium alloy PEO coated using an electrolyte containing 0.3 g/l of sodium molybdate

Tab.4.4 Quantitative XPS analysis of the external layer formed on the sample treated with 0.3 g/l of sodium molybdate

C%	O%	Mg%	Si%	Al%	Na%	Zn%	Mo%
45.1	37.4	4.5	10.7	0.6	1.0	0.4	0.2

From the collected spectrum of the main photoelectron lines, the atomic percentages of the elements present in the external surface of the coating were calculated. The layer resulted to be principally constituted by O, Mg, Si, Al, Na, Zn and Mo. The presence of C is attributable to ambient contamination. The results of the quantitative analysis are reported in Tab. 4.4. The high resolution O 1s spectra of the PEO coated sample is shown in

Fig.4.10a. Oxygen spectra can be deconvoluted in three main components: the peak located at 530 eV BE corresponding to metal oxides (Mg, Al, Zn); the peak located at 531.7 eV BE to the metal hydroxides and to Mg_2SiO_4; the peak located to 533 eV BE to SiO_2. The high resolution Si 2p peak is shown in Fig. 11b. It resulted by the sum of three peaks: the one situated at 101.8 eV BE attributed to the α-Mg_2SiO_4; the one at 102.9 eV BE corresponding to γ-Mg_2SiO_4 and the one at 103.6 eV BE corresponding to SiO_2 [116]. The high resolution peak of Mg 2p is shown in Fig. 10c. This peak is the sum of three peaks: the one at 49.6 eV BE was attributed to the $Mg(OH)_2$, the one at 50.4 eV BE corresponded to MgO and $MgAl_2O_4$ [27], while the last at 51.7 eV BE to the Mg_2SiO_4 and $MgMoO_4$ [117]. The high resolution Mo 3d peak (Fig. 4.10d) showed that the Mo was in the form of MoO_3 and $MgMoO_4$. The peak of Na 1s binding energy of 1071.70 was attributed to $(SiO_2)_{0.7}(Na_2O)_{0.3}$, whereas the peak of Zn $2p_{3/2}$ binding energy of 1022.1 was correlated to the presence of ZnO [77].

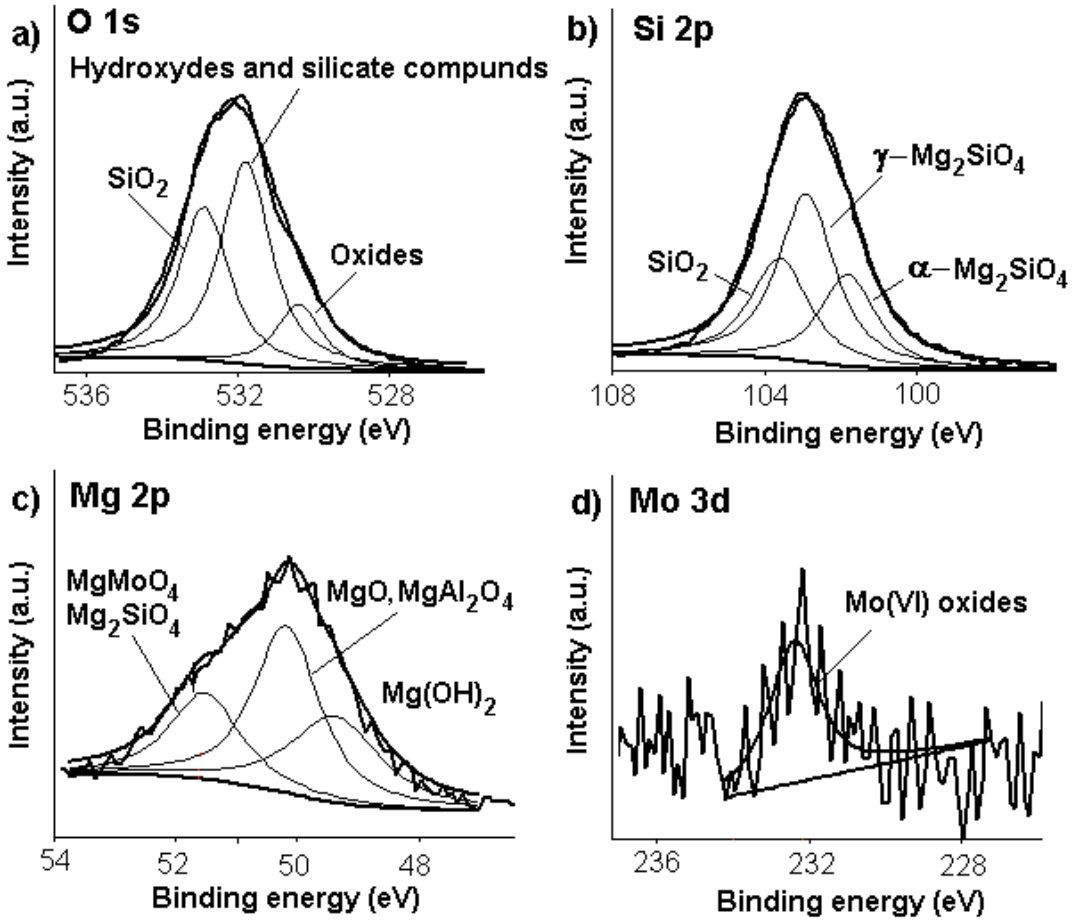

Fig.4.10 High resolution single peak of: (a) O 1s; (b) Si 2p; (c) Mg 2p; (d) Mo 3d, of the samples treated with 0.3 g/l of sodium molybdate.

Therefore, from XPS analysis it is possible that conclude that the external coating was constituted principally by MgO, $Mg(OH)_2$, Mg_2SiO_4 and SiO_2. The other minor components were $MgAl_2O_4$, $MgMoO_4$, MoO_3, ZnO and $(SiO_2)_{0.7}(Na_2O)_{0.3}$.

Despite the smaller thickness of the coating in this sample, in comparison with the common PEO coatings, this coating allowed to noticeably reduce the corrosion rate. The improvement in the corrosion resistance of the sample treated with 0.3 g/l of sodium molybdate can be attributed to the presence of Mg_2SiO_4, MgO and MoO_3.

The presence of molybdenum can be correlated with the improved corrosion performances due to the self-healing ability and the inhibition properties of this element.

4.1.4 Concluding remarks

The evolution of the PEO process, and consequently the morphology of the coatings and their corrosion properties, was influenced by the molybdate concentration. Considering the fourth steps involved in the formation of a PEO coating, without molybdate in the electrolyte only the first and the second step occurred along with a decrease in potential values at the end of the second stage. With low concentrations of molybdate the process stopped after the first stage of PEO treatment, whereas with higher concentrations of the salt also the second and third stage occurred. The layer formed with the higher molybdate amount was thicker but rich of micro-cracks and pores; the one obtained with the lower molybdate amount was thinner but more dense; the one formed without molybdate was irregular.

The corrosion resistance of the coated samples was related to the morphology. In general, an increase in the corrosion resistance can be observed with the decrease of the molybdate content in the electrolyte; however, the sample obtained without sodium molybdate presented the worst corrosion performance. The sample treated with 0.3 g/l of sodium molybdate, characterised by a thin and dense layer, corresponding to the protective inner layer of typical PEO coatings, showed the best corrosion resistance. Increasing the molybdate amount decreased the corrosion resistance due to the presence of a not homogenous coating. The main phases in the coatings were Mg_2SiO_4, MgO. The SIMS and XPS analysis preformed on the sample treated with 0.3 g/l of molybdate revealed the presence of Mo, even if in low amount, in the form of MoO_3 and $MgMoO_4$. The presence of Mo(VI) contributed to improve the corrosion resistance of this sample.

4.2 EFFECT OF THE ADDICTION OF LANTHANUM SALTS IN THE ELETROLYTE

In this second part of the chapter will be described the experimental analysis carried out in order to study the influence of the addiction of lanthanum nitrate in the electrolyte used to produce PEO coatings on aluminum alloys

4.2.1Production of lanthanum-containing PEO coatings

Samples of 7075 aluminum alloy were used as substrate for PEO coatings. The nominal composition of the alloy is reported in Tab.4.5 and the microstructure of the initial alloy in Fig.4.11 .

Tab. 4.5 Chemical composition of 7075 alloy (wt%)

Al	Mg	Zn	Cu	Others
90.7	3.1	4.1	0.9	1.2

Fig. 4.11 Microstructure of 7075 alloy

The samples were polished following standard metallographic technique before the PEO treatment and then degreased using acetone in ultrasound. The electrolyte used in the PEO process was constituted by an aqueous alkaline solution with 25 g/L of Na_2SiO_3, 2.5 g/L of NaOH and different concentrations (0, 0.025, 0.05, 0.075, 0.1 g/L) of $La(NO_3)_3$.

The treatments were performed maintaining the current constant, letting the potential free to vary. In detail, the current density was fixed at 0.5 A/cm^2 and the samples were treated for 30 seconds. After the treatment, the samples were washed with deionized water and ethanol and dried with compressed air.

During the PEO process a large number of sparks/micro-discharges were observed on the surface of the samples; the number of these sparks depended on the lanthanum amount in the electrolyte: increasing lanthanum nitrate in the electrolyte produced an increase in the number of micro-discharges until 0.075 g/l of $La(NO_3)_3$, whereas a further increase in lanthanum nitrate caused a decrease in the number of sparks. In Fig.4.12 are reported as example the samples treated without lanthanum nitrate (Fig.4.12a) and with 0.075 g/l of lanthanum nitrate in the electrolyte (Fig.4.12b) at the end of the treatment.

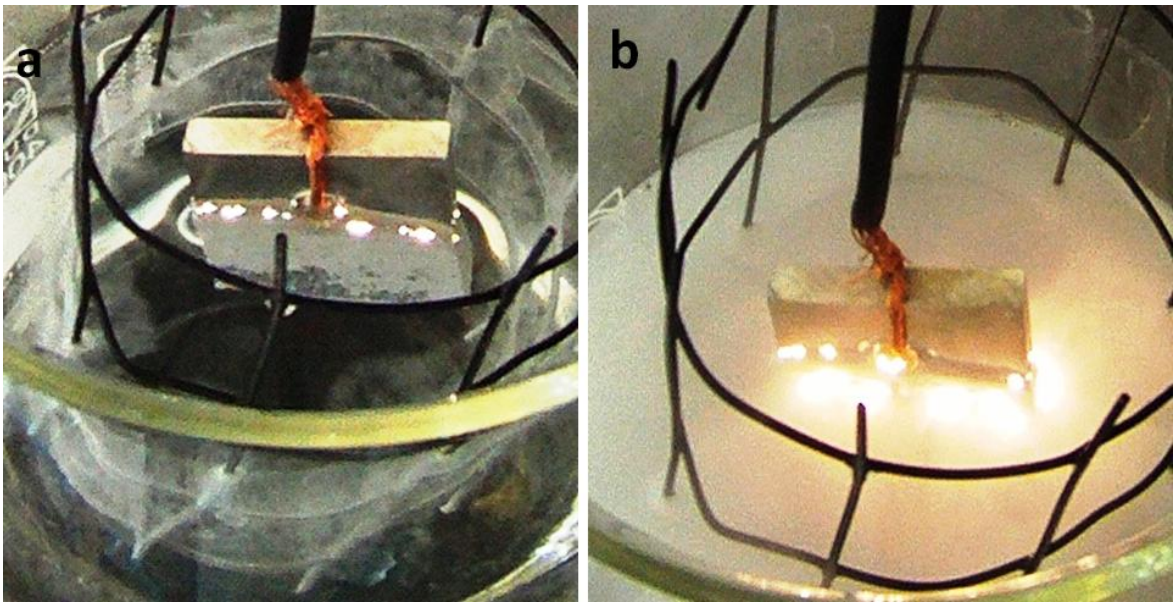

Fig. 4.12 Images of PEO process during the treatment of the sample treated a) without lanthanum nitrate and b) with 0.075 g/L of lanthanum nitrate in the electrolyte.

The voltage vs time plot is reported in Fig.4.13 and can be observed that the lanthanum concentration influence the final potential of the PEO process. The sample treated without lanthanum in the electrolyte is characterized by the minimum value of the potential at the end of the process and can be observed an increase in the potential with the increase of lanthanum content with a maximum at 0.075 g/l. Further increase in the lanthanum concentrations cause a decrease in the final potential. The voltage during the treatment is directly connected with the number of micro-discharges previously observed: higher final potential cause a larger number of micro-discharges and consequently the formation of a thicker protective layer.

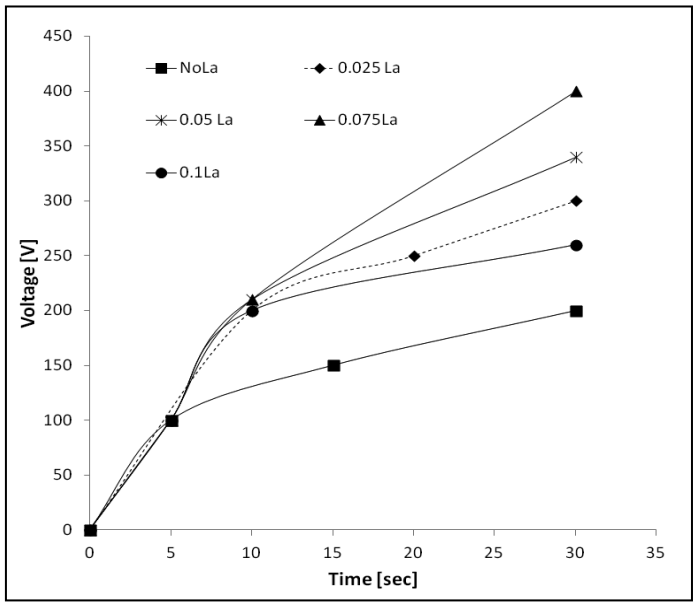

Fig.4.13 Voltage *vs* time plot for the different PEO treatments

4.2.2 Analysis of the Corrosion behaviour

4.2.2.1 Potentiodynamic polarization tests

The anodic polarization plots for 7075 aluminium alloy treated with electrolytes containing different concentrations of $La(NO_3)_3$ for 30 s are reported in Fig.4.14 and corrosion current densities i_{corr}, corrosion potentials E_{corr} and passivation ranges are reported in Tab.4.6.

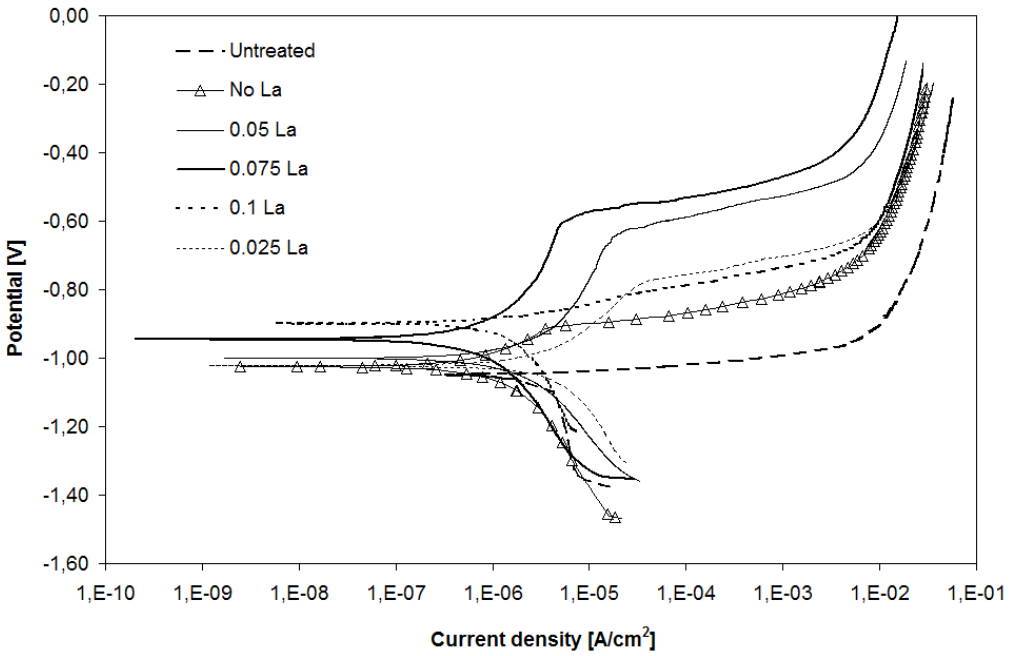

Fig. 4.14 Potentiodynamic polarization plot of 7075 alloy PEO coated at 0.5 Acm^{-2} with different concentrations of lanthanum nitrate in the electrolyte (test electrolyte: 0.1M Na_2SO_4 + 0.05M NaCl).

Tab.4.6 Values of the corrosion current density, of the corrosion potential and of the passivation range for 7075 samples treated with an electrolyte containing various concentrations of lanthanum nitrate obtained in chlorides and sulphates solution.

SAMPLE	E_{corr} [SCE] [V]	i_{corr} [A/cm^2]	Passivation range [V]
Untreated	-1.05	7.0 x10^{-6}	-
No La	-1.02	1.5 x10^{-6}	0.1
0.025 g/L La	-1.02	2.0 x10^{-6}	0.2
0.05 g/L La	-1.00	1.0 x10^{-6}	0.3
0.075 g/L La	-0.94	8.0 x10^{-7}	0.3
0.1 g/L La	-0.90	2.1 x10^{-6}	0.05

The results show that the presence and the concentration of lanthanum nitrate in the electrolyte influenced the corrosion resistance of the coated samples: increasing the amount of lanthanum nitrate until the value of 0.075 g/l induced a decrease in the corrosion current densities, whereas a further increase produced a worsening in the corrosion resistance. The samples treated with 0.075 g/l of lanthanum nitrate was characterized by a value of corrosion current density ($8x10^{-7}A/cm^2$) one order lower than the other samples. The i_{corr} values of the other PEO treated samples with 0, 0.025, 0.05 and 0.1 g/L of $La(NO_3)_3$ are more or less the same, whereas the untreated sample is the one with the higher value of corrosion current density.

Also the corrosion potential is influenced by the presence of lanthanum nitrate: the sample treated with 0.1 g/L of this compound in the electrolyte had the higher value of E_{corr} and this value decreased with the amount of lanthanum nitrate. The presence of a strongly correlation between the passivation range and the lanthanum concentration in the electrolyte can be also observed. In particular, in the samples with the lower values of i_{corr} (0.05 and 0.075 g/L of $La(NO_3)_3$) also a large passive zone (about 0.3 V) can be observed. This zone was also present but less evident in the samples treated with 0 and 0.025 g/L and is only slightly visible in the sample treated with 0.1 g/L of lanthanum nitrate.

4.2.2.2 Electrochemical impedance spectroscopy

To better understand the corrosion behavior also EIS tests were performed on the samples treated with different concentrations of $La(NO_3)_3$ in the electrolytes. Experimental data were fitted with the software Z-view using the same equivalent circuits used for PEO coating obtained in molybdate solutions. For the untreated sample the simple Randles circuit (Fig. 2.6a) was chosen due to the only presence of the natural oxide layer, for the

other samples the circuit reported in Fig.2.6b was used. A good fitting quality was obtained for all the samples with chi-squared values varying between 0.001 and 0.005

Regarding the parameters of the equivalent circuit, the physical meaning of the different electrical parameters is the same as reported before.

Nyquist impedance plots and results of the fitting of the experimental data for the samples treated using electrolytes containing different concentrations of lanthanum nitrate are reported in Fig.4.15 and Tab.4.7.

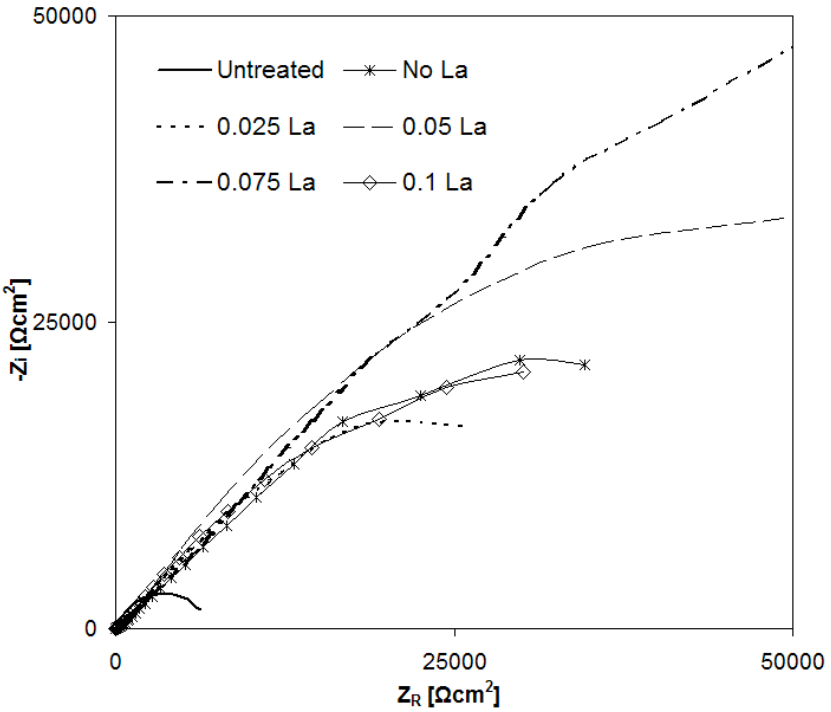

Fig.4.15 Nyquist plots of 7075 alloy PEO coated with different concentrations of lanthanum nitrate in the electrolyte (test electrolyte: 0.1M Na_2SO_4 + 0.05M NaCl).

For the untreated sample the values of R_2, Q_1 and n_1 are not reported because was used for the fitting a simpler circuit due to the only presence of the natural oxide layer. The values of R_2 and of R_3 permit to evaluate the resistance of the porous and barrier layer respectively and so they are directly connected with the corrosion resistance of the samples. As expected, the untreated sample was characterized by the lowest value of R_3 because the protection was given only by the natural oxide coating. It can be observed that the sample with the higher value of R_2 and the second higher of R_3 is the one obtained with 0.075 g/l of lanthanum nitrate, in agreement with the results of the anodic polarization tests. The sample obtained with 0.05 g/l of the salt had the higher value of the polarization resistance for the barrier layer and the second higher for R_2, so this sample can be

considered as the second in term of corrosion resistance. The samples obtained with 0, 0.025 and 0.1 g/l of the salt, were characterized by values of R_2 and R_3 of the same order of magnitude.

Tab.4.7 Equivalent circuit data for 7075 aluminium alloy treated with an electrolyte containing various concentrations of lanthanum nitrate obtained in chlorides and sulphates solution

	Untreated	**No $La(NO_3)_3$**	**0.025 g/L $La(NO_3)_3$**	**0.05 g/L $La(NO_3)_3$**	**0.075 g/L $La(NO_3)_3$**	**0.1 g/L $La(NO_3)_3$**
R_1 [$\Omega*cm^2$]	20	20	23	24	24	20
R_2 [$\Omega*cm^2$]	-	312	267	332	3217	117
R_3 [$\Omega*cm^2$]	7050	124000	292000	630000	595000	169000
Q_1 [$F*Hz^{1-n}$]	-	6.39×10^{-5}	6.90×10^{-5}	3.55×10^{-5}	7.1×10^{-6}	4.81×10^{-5}
n_1	-	0.54	0.54	0.68	0.6	0.55
Q_2 [$F*Hz^{1-n}$]	1.65×10^{-5}	1.07×10^{-5}	2.59×10^{-5}	2.04×10^{-5}	1.18×10^{-5}	2.92×10^{-5}
n_2	0.84	0.69	0.5	0.56	0.55	0.57

The capacitance C_1 and C_2 of the two CPE can be calculated using the values of Q and R reported in Tab.4.7 using Eq.4.1 [115,118-119]:

$$C = \sqrt[n]{\frac{Q}{R^{n-1}}} \tag{4.1}$$

It can be observed that the minimum value of C_1 and C_2 was found for the sample treated with 0.075 g/l of lanthanum salts in the electrolyte. The values of the capacitances calculated for the sample obtained with 0.05 g/l of lanthanum nitrate are slightly higher while the samples treated with 0, 0.025 and 0.1 g/l of salt, had the maximum values of C_1 and C_2. The value of C can be correlated with the thickness of the protective oxide layer, using Eq.2.2, valid for a parallel-plate capacitor, corresponding to a homogenous oxide

layer. Therefore, the lower value of *C* calculated with the Eq.4.1 for the sample obtained with 0.075 g/l of lanthanum nitrate, can be related to a thicker layer of this sample.

4.2.3 Surface analysis

Secondary electron images of the surface of the PEO coatings are shown in Fig.4.16. The coating surface show the typical feature of PEO coatings with the presence of pores of different dimension [120-121], and differences were observed in the five samples.

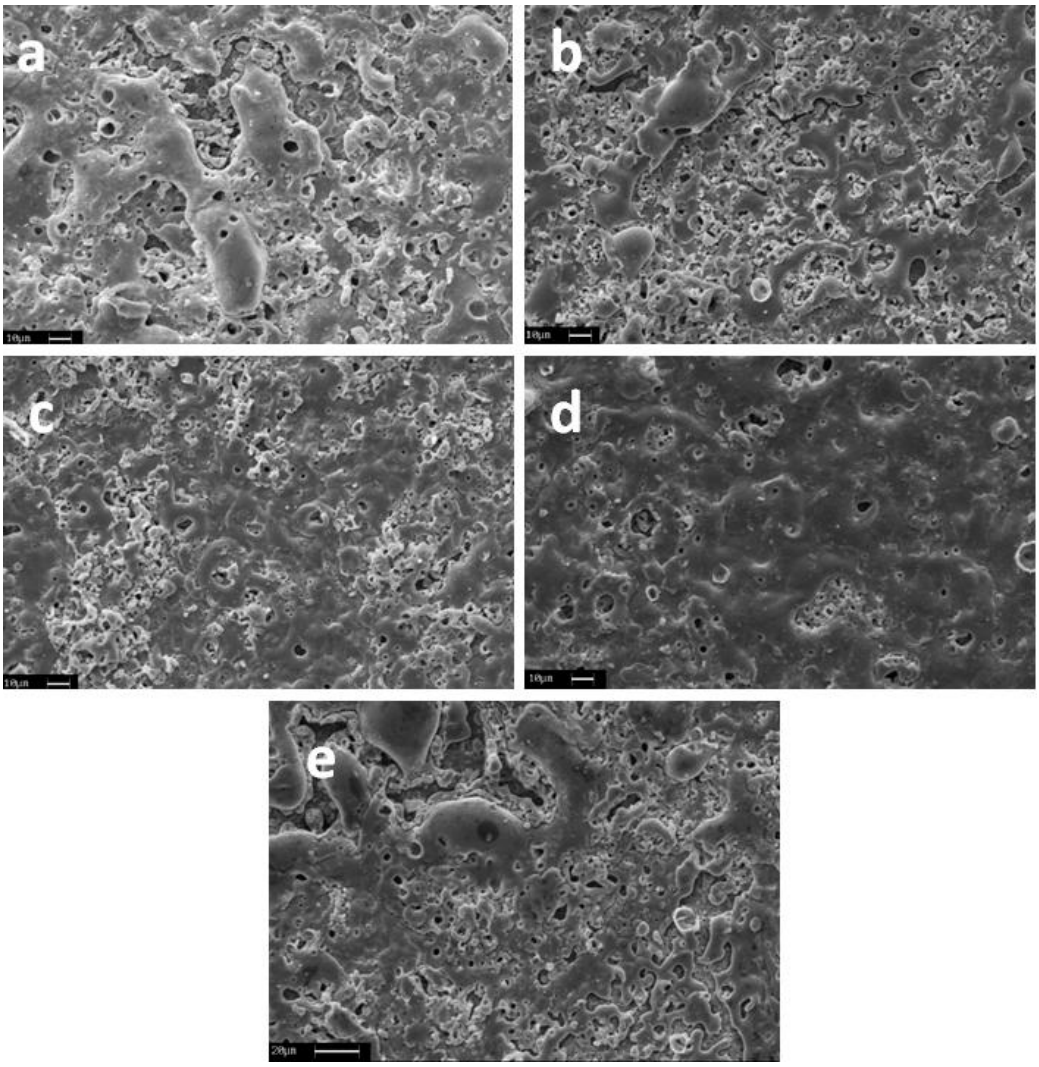

Fig.4.16 Scanning electron micrographs (secondary electrons) of the surface of PEO coatings formed on 7075 aluminium alloy with different concentrations of lanthanum nitrate in the electrolyte: a) 0 g/L; b) 0.025g/L; c) 0.05g/L; d) 0.075 g/L; e) 0.1 g/L.

In particular, in the samples treated with 0.05 and 0.075 g/L of lanthanum nitrate (Fig. 4.16c and 4.16d) a reduction in the number of pores and the presence of extended areas without pores can be observed, in comparison with the other samples. Therefore, the

lanthanum nitrate seemed to influence the morphological characteristic of the coating and the improvement in the corrosion performances of the samples treated with 0.05 and 0.075 g/L of lanthanum nitrate could be due to the low porosity of their surface.

The cross-sections of the coated samples were examined by SEM using backscattered electrons, and the images of the samples obtained with the various concentrations of lanthanum nitrate, previously described, are shown in Fig. 4.17.

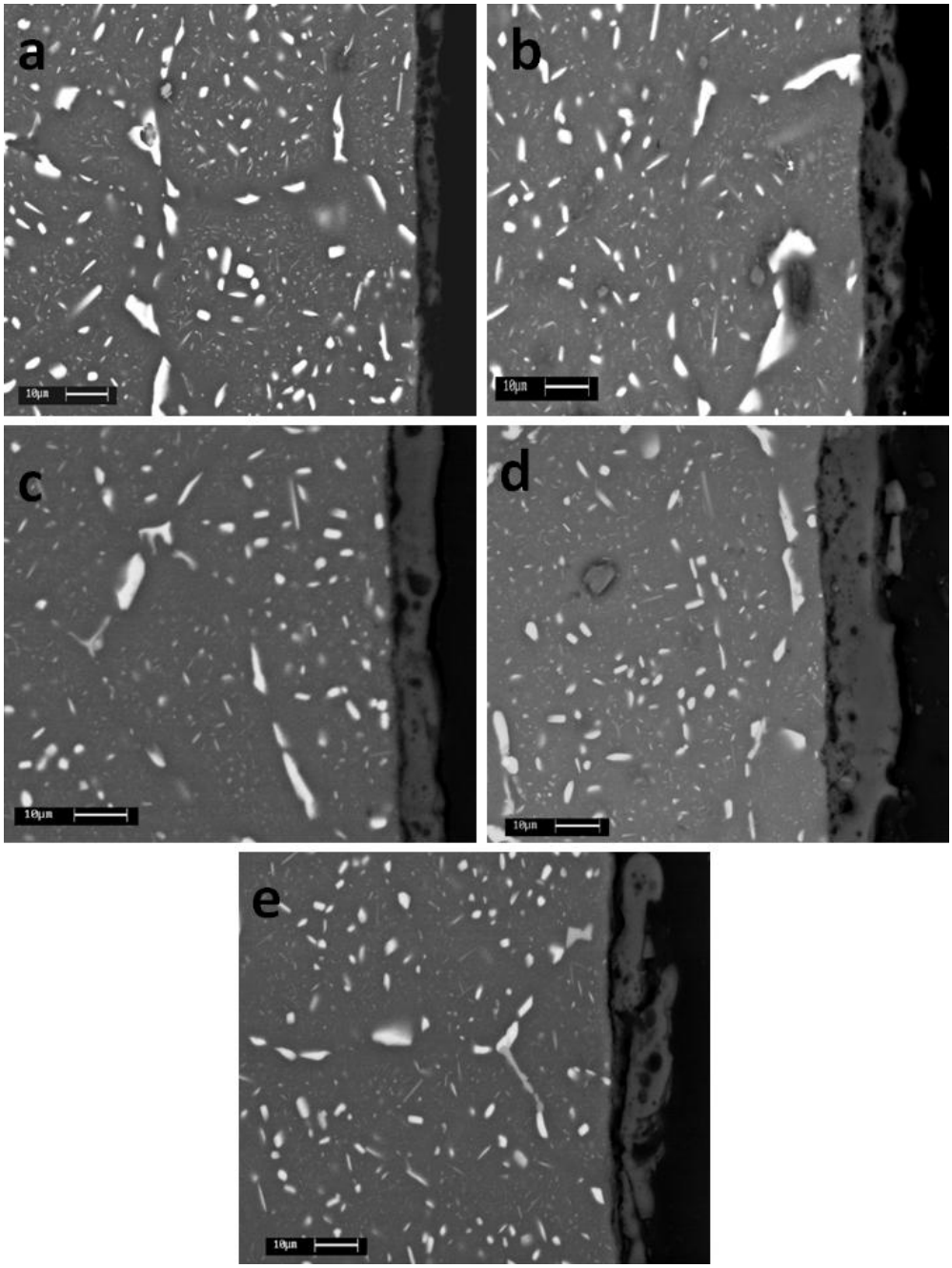

Fig. 4.17 Scanning electron micrographs (backscattered electrons) of the cross section of PEO coatings formed on 7075 aluminium alloy with different concentrations of lanthanum nitrate in the electrolyte: a) 0 g/L; b) 0.025g/L; c) 0.05g/L; d) 0.075 g/L; e) 0.1 g/L.

It can be observed that the concentration of lanthanum nitrate in the electrolyte significantly influenced the thickness of the oxide layer that is about 5 µm in the sample treated without lanthanum nitrate (Fig.4.17a), 10 µm in the samples treated with 0.025 and 0.05 g/L of lanthanum nitrate (Fig. 4.17b and 4.17c) and 16 µm in the sample with 0.075 g/L (Fig. 4.17d). A further increase in the lanthanum concentration caused a decrease in the thickness of the coating to about 12 µm as can be observed in the Fig. 4.17e for the sample treated with 0.1 g/L. Moreover, an important variation in the adhesion of the coating can be observed among the various samples: in fact, the protective layer is particularly adherent in the samples treated with 0.05 and 0.075 g/L of lanthanum nitrate and a good adhesion can be still observed in the sample treated with 0.025 g/L, whereas in the samples obtained with no lanthanum in the electrolyte or with the highest concentration of this compound the adhesion is very poor. Moreover, in the samples treated with 0.05 and 0.075 g/L of lanthanum nitrate in the electrolyte the protective layer seems to be more uniform and homogeneous in comparison with the other samples, where several cracks and heterogeneities are present.

EDS analysis was performed both on the surface and the cross sections of the PEO coated samples and the results are reported for the sample treated with 0.075 g/L of the salt in Fig. 4.18.

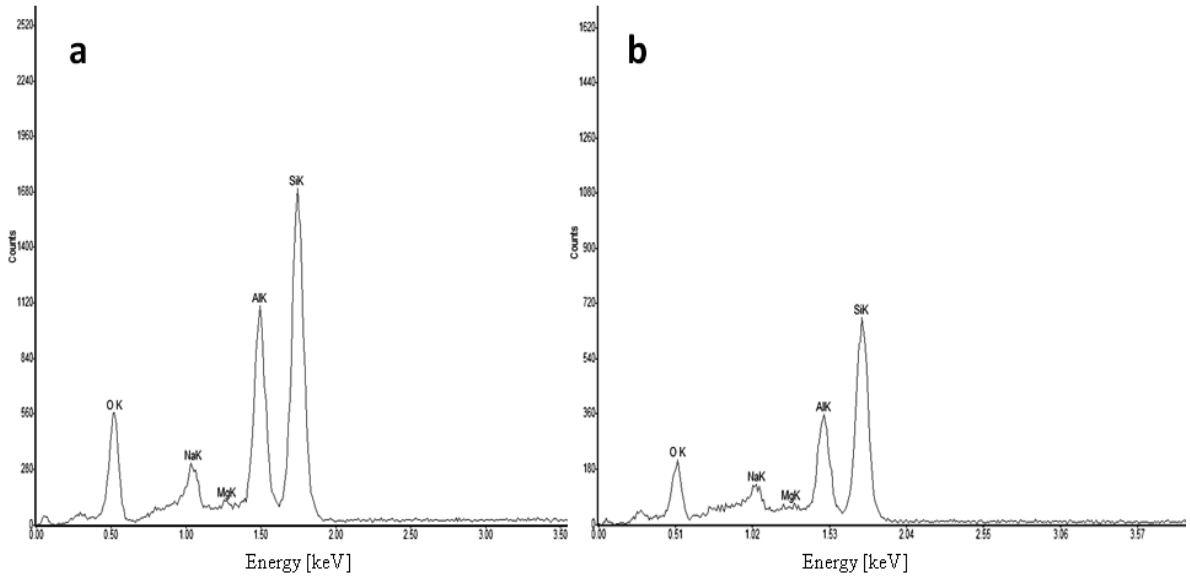

Fig. 4.18 EDS spectra collected on a) the surface, and on b) the cross section of the sample treated with 0.075 g/L of lanthanum nitrate in the electrolyte.

The protective layer resulted be constituted mainly by O, Si, Al, Na and Mg, but no La was detected, due to the low concentration of this element in the electrolyte (Tab. 4.8). The EDS analysis performed on the other samples confirmed the results reported for the one obtained with 0.075 g/L of lanthanum nitrate.

Tab. 4.8 Semi-quantitative elemental composition (wt%) from EDS analysis of the sample treated with 0.075 g/L of lanthanum nitrate.

	O	**Si**	**Al**	**Na**	**Mg**
Surface	38.5	34.5	18.2	7.4	1.4
Section	36.6	38.5	16.6	7.2	1.5

GDOES analysis were performed to evaluate the elemental distribution in the cross section of the coatings. The analysis were performed on the sample without lanthanum in the electrolyte, on the sample with the highest concentration of lanthanum (0.1 g/L) and on the sample obtained with 0.075 g/L of $La(NO_3)_3$. The results are reported in Fig. 4.19a, Fig. 4.19c and Fig. 4.19b, respectively.

The profile of the Na and La are not shown, since they cannot be detected by this instrument. The coatings are mainly constituted by O, Si and Al. In all the samples can be observed an enrichments in Si near the surface, after that the presence of silicon is constant in the protective layer up to the interface with the substrate, where it gradually decreases. The thickness were estimated as a depth at which the oxygen concentration dropped to 50% of its maximum value. GDOES analysis confirmed what was previously observed about the thickness of the coating: the sample obtained with 0.075 g/L of lanthanum nitrate in the electrolyte is the one characterized by the thicker protective layer (about 16 µm), and the sample obtained without lanthanum salts by the thinner (about 5 µm).

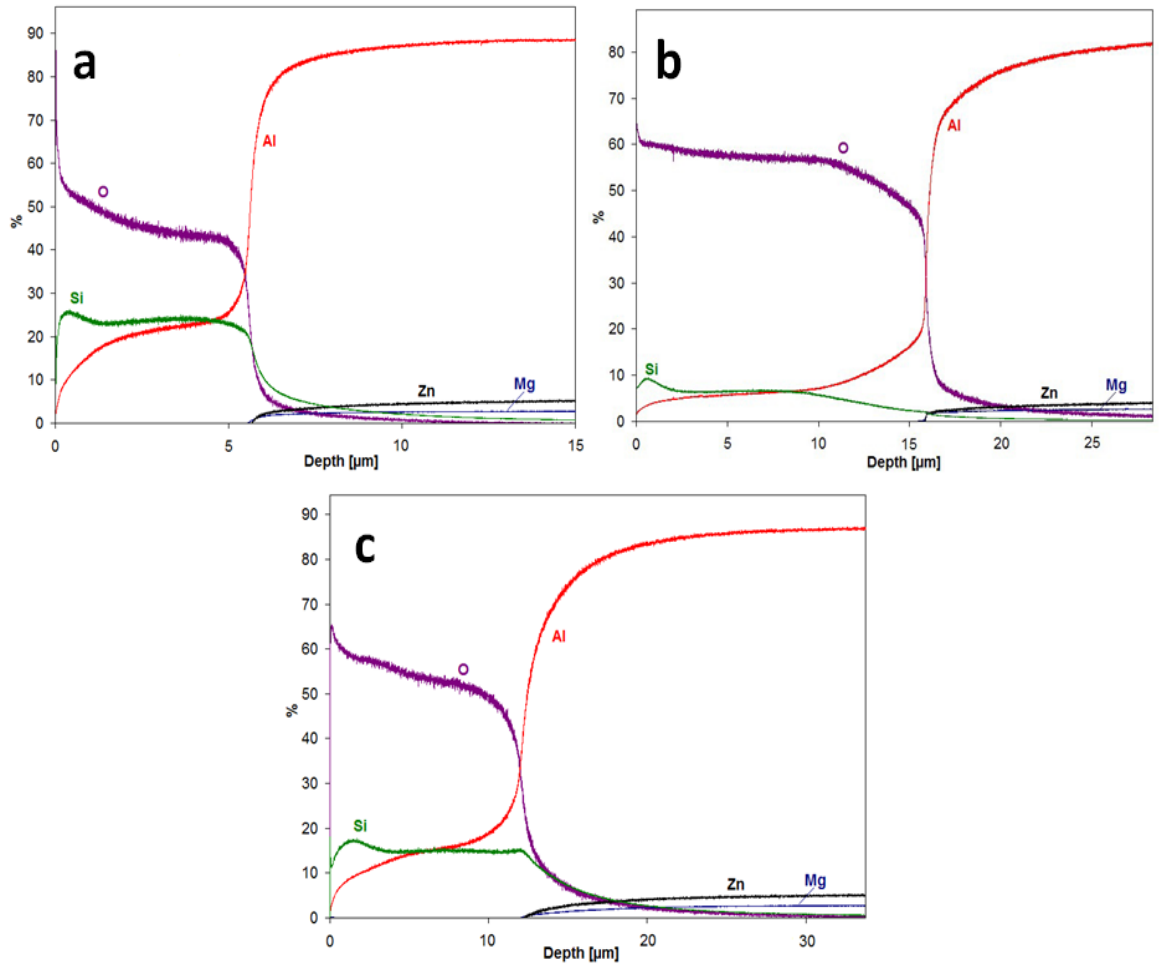

Fig.4.19 GDOES elemental profiles for the samples of 7075 aluminium alloy treated with different concentration of lanthanum nitrate: a) 0 g/L; b) 0.075 g/L; c) 0.1 g/L.

The XRD analysis performed on the samples showed that the coatings were constituted mainly by Al_2SiO_5, Al_2O_3, in accordance with the composition of the alloy and of the electrolyte. Lanthanum compounds were not detected, due to the low concentration of the salt in the electrolyte. The presence of the peaks of Al was observed, due to the reflection from the substrate. In Fig.4.20 are reported the XRD patterns for the samples treated with 0, 0.075 and 0.1 g/L of lanthanum nitrate.

The comparison of the different patterns evidenced that in the coating are present the same phases. The different intensities of the peaks can be attributable to the different thickness of the coating in the different samples. In the sample treated with 0.075 g/L of lanthanum salts the coating was thick about 16 µm and the signal coming from the substrate is relatively low if compared with the sample treated with 0 g/L of lanthanum nitrate, whose coating was about 5 µm.

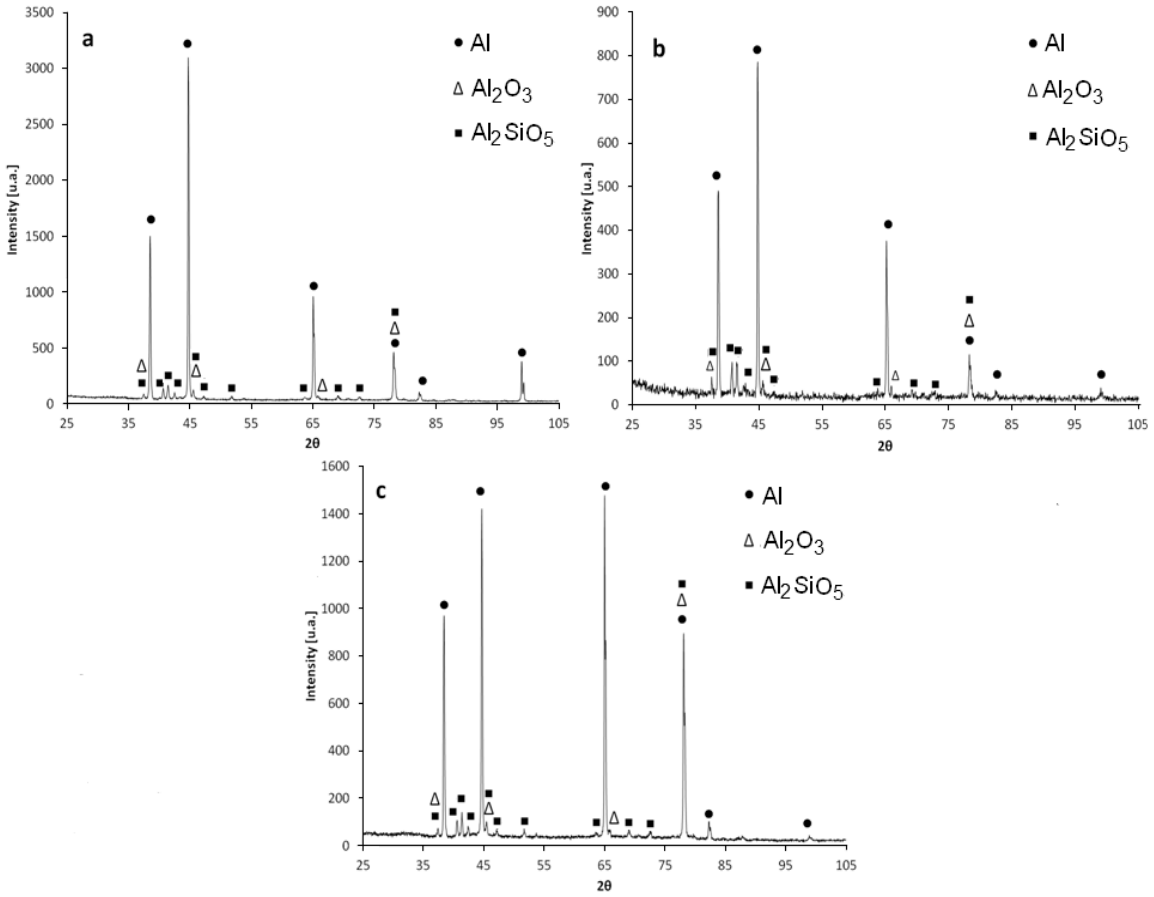

Fig. 4.20 X-ray diffraction patterns for the samples of 7075 aluminium alloy treated with a) 0 g/L; b) 0.075 g/L; c) 0.1 g/L of lanthanum nitrate in the electrolyte

To better understand the properties of the coating produced using 0.075 g/L of lanthanum nitrate, XPS analysis (without sputtering) was performed on the surface of this sample and the results were compared with the ones obtained by the samples treated with 0 and 0.1 g/L. The survey spectra of the samples are shown in Fig. 4.21. From the collected spectrum of the main photoelectron lines, the atomic percentages of the elements present in the external surface of the coating were calculated. The layer resulted to be constituted by O, Si, Al, Na, Mg, Zn and La (Tab. 4.9). The presence of C is attributable to ambient contamination. Lanthanum was present in the samples treated with 0.075 and 0.1 g/L of lanthanum nitrate, but with a low amount, 0.2% and 0.3%, respectively.

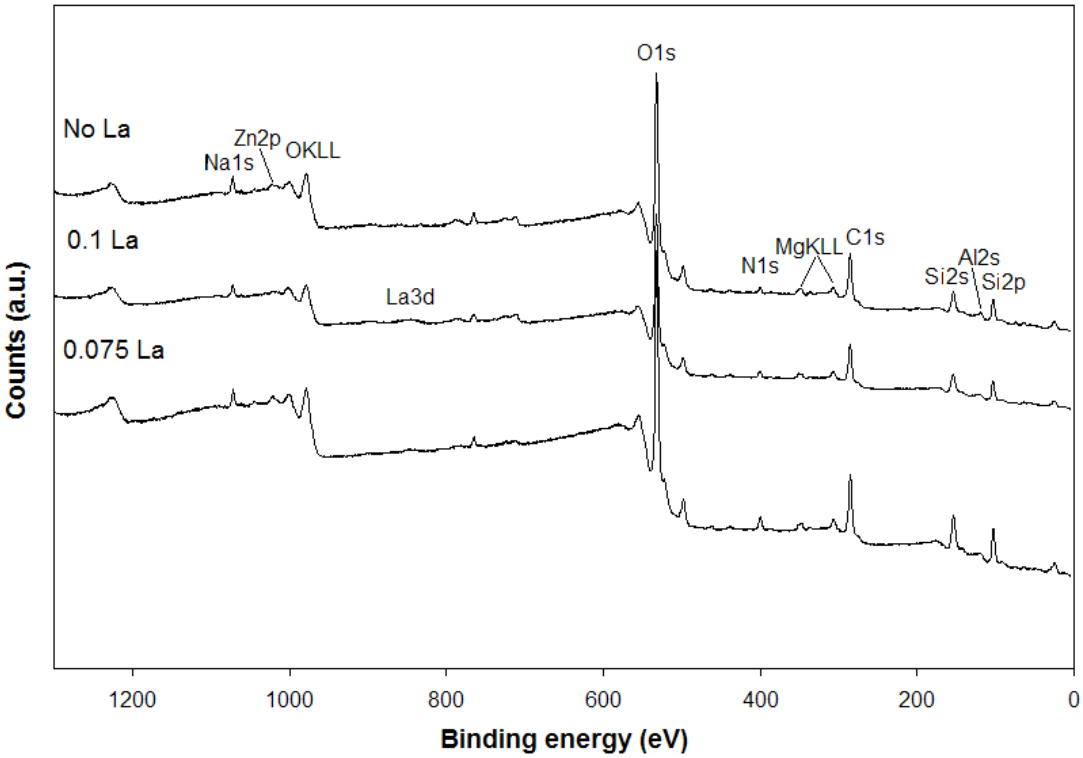

Fig. 4.21 XPS survey spectra for 7075 aluminium alloy treated with different concentration of lanthanum nitrate in the electrolyte.

Tab. 4.9 Quantitative XPS analysis of the external layer formed on the samples treated with different amounts of lanthanum nitrate (wt%).

Sample	**C**	**O**	**Na**	**Mg**	**Al**	**Si**	**Zn**	**La**
Region	**C1s**	**O1s**	**Na1s**	**Mg2s**	**Al2p**	**Si2p**	**$Zn2p_{3/2}$**	**La3d**
Without La	32.7	46.9	2.7	1.2	4.6	11.2	0.7	-
0.075 g/L La	32.6	45.4	2.6	1.3	4.2	13.0	0.7	0.2
0.1 g/L La	32.4	46.4	3.1	1.1	4.7	11.5	0.5	0.3

The high resolution O 1s spectra of the sample treated with 0.075 g/L is shown in Fig. 4.22a. Oxygen spectra can be deconvoluted in two main components: the peak located at 530 eV BE corresponding to metal oxides; the peak located at 531.7 eV BE to the metal hydroxides and to aluminosilicate compounds [122].

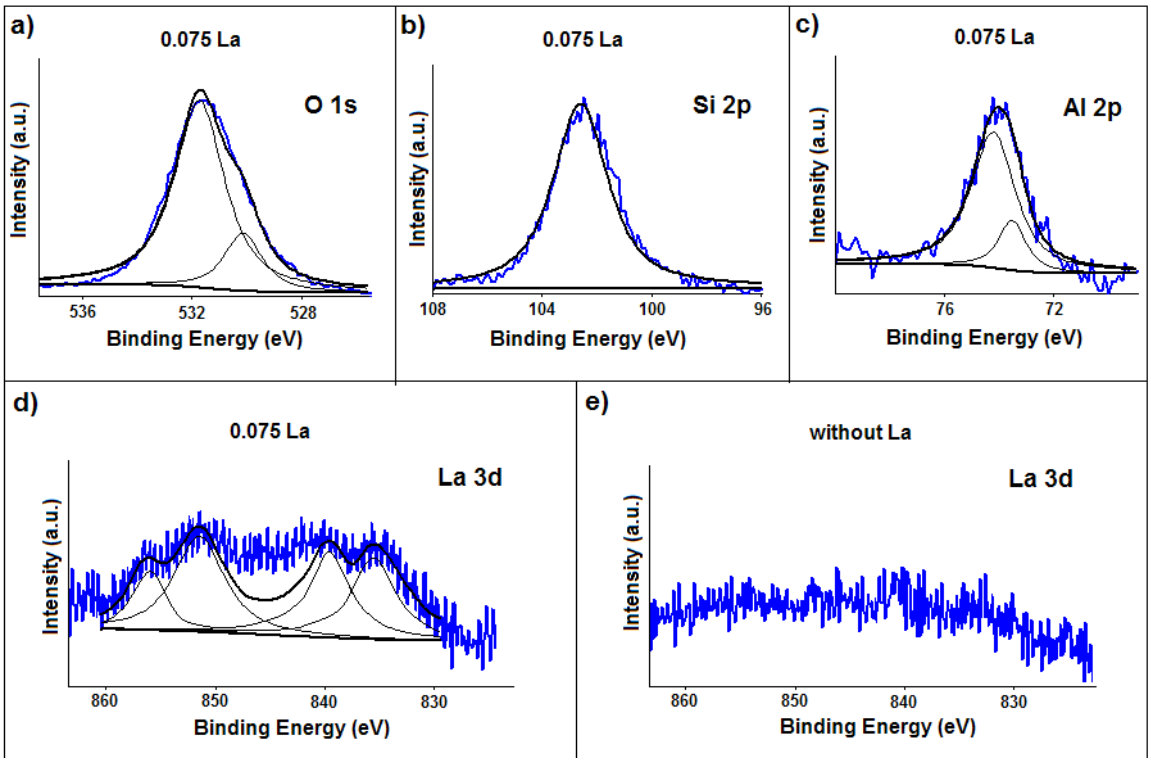

Fig. 4.22 High resolution single peak of: (a) O 1s; (b) Si 2p; (c) Al 2p; (d) La 3d of the sample treated with 0.075 g/L of lanthanum nitrate and e) La 3d of the sample treated without lanthanum nitrate.

The high resolution Si 2p peak of the sample treated with 0.075 g/L is shown in Fig. 4.22b, and the main peak located at 102.7 eV BE suggested that Si is mainly present as aluminosilicate, and not as SiO_2 [122]. The high resolution peak Al 2p peak of the sample treated with 0.075 g/L is shown in Fig. 4.22c.

The main peak located at 74.2 eV BE with 82% of area corresponds to aluminosilicate, whereas the small peak at 73.5 eV BE is consistent with Al_2O_3 [76]. The peak of Na 1s binding energy of 1071.70 eV BE was attributed to $(SiO_2)_{0.7}(Na_2O)_{0.3}$.

The high resolution O 1s, Si 2p, Al 2p and Na 1s spectra of the sample treated without and with 0.1 g/L of lanthanum salt did not show evident differences with the sample treated with 0.075 g/L.

The high resolution La 3d peak of the sample treated with 0.075 g/L, is shown in Fig.4.22d. From the background and the noise it was possible to distinguish the presence of four peaks: the peaks located at 835.1 eV BE and 851.6 eV BE corresponding to $La(OH)_3$, whereas the peaks 839.2 eV BE and 855.7 eV BE are the two satellites peaks [123]. For comparison, in Fig. 4.22e is shown the La 3d region of the sample treated without lanthanum salt, where no peaks can be observed.

Therefore, from XPS analysis it was possible to conclude that the external coating of the sample obtained with 0.075 g/L of lanthanum salt, was constituted principally by aluminosilicate (Al_2SiO_5), Al_2O_3, $(SiO_2)_{0.7}(Na_2O)_{0.3}$ and $La(OH)_3$.

Summarizing, the addition of lanthanum nitrate in the electrolyte produced and improvement in the surface characteristics of the oxide layer produced during PEO process: all the samples treated with this compound in the electrolyte were characterized by a thicker and denser coating in comparison with the sample obtained without lanthanum nitrate. Moreover, the sample obtained with 0.075 g/L of lanthanum nitrate was characterised by the thickest, most dense and uniform oxide layer and by the highest corrosion resistance. Further additions of $La(NO_3)_3$ did not produce an improvement in the protective layer. In fact, the coating obtained with 0.1 g/L of lanthanum nitrate was thinner, not adherent and with several cracks. Further additions of lanthanum nitrate in the electrolyte was not possible due to the lack of solubility of this compound in alkaline solutions. XPS analysis revealed the presence of lanthanum in the samples treated with 0.075 and 0.1 g/L of lanthanum nitrate in the electrolyte. Therefore, the formation of the large passive zone in the anodic polarization curve registered for the samples treated with lanthanum nitrate, and more marked with the 0.075 g/L concentration, can be probably correlated to the presence in the coatings of hydroxide lanthanum, which is known to be a corrosion inhibitor [124]. The anomaly observed for curve of the sample obtained the concentration of 0.1 g/L, it is likely attributable to the poor adherence of the coating and the presence of the cracks.

4.2.4 Concluding Remarks

The composition of the electrolyte, and in detail the $La(NO_3)_3$ amount, strongly influenced the characteristics of the layer in terms of corrosion resistance and surface morphology. The addition of lanthanum salts produced an increase in the corrosion performances of the coated samples, as shown from the results of anodic polarization and EIS tests. All the samples treated with electrolyte containing lanthanum salts were characterized by lower corrosion current density and higher polarization resistance, if compared with the ones obtained without lanthanum. The improvement in the corrosion performances can be correlated with the formation of a thicker, more dense and uniform oxide layer in the samples PEO treated using lanthanum salts. The concentration 0.075 g/L of $La(NO_3)_3$ induced the formation of the most homogeneous, adherent and thickest coating,

characterised by the highest corrosion resistance. This protective layer was mainly composed by Al_2SiO_5 and Al_2O_3 with a thickness of about 16 µm. The XPS analysis revealed that La, even if in low amount, was present as $La(OH)_3$ in the coating obtained with 0.075 and 0.1 g/L of lanthanum nitrate.

In conclusion the addition of lanthanum in the electrolyte caused an increase in the corrosion resistance first of all due to the increase of the barrier effect of the coating: in fact the presence of lanthanum cause an increase in the final potential and in the number of micro-discharges causing the formation of a thicker film. Moreover, the presence of lanthanum in the coating produced an increase of the corrosion resistance and in particular the formation of a large passive zone probably due to the inhibition properties of this element.

Chapter 5

Study of additives to improve the wear and corrosion resistance

It is known that PEO coatings are harder than the magnesium substrate and can offer a superior wear resistance, as demonstrated by several researchers. But it is also believed that the introduction of secondary phases into the porous PEO coating may offer even better tribological characteristics. In fact regarding the wear properties of PEO coatings, they consist of hard crystalline ceramic phases, which have good adherence to the substrate. However, they are porous and rough and exhibit high coefficient of friction under dry sliding conditions. The open and interconnected pore structure, in fact, makes them vulnerable to fracture failure under load and reduced corrosion resistance, especially in the long run. Dry sliding wear tests have revealed that the friction coefficient values for PEO coating/steel and PEO coating/ceramic (Si_3N_4) couples are higher than that for couples of the parent magnesium substrates [40,71]. In many tribological applications, high friction coefficient could lead not only to the wear of the slider, but also to the wear damage of the counter material. It would be beneficial if the friction coefficient could be reduced by some means for example producing PEO composite coatings using particles that could improve the tribological properties. There is not much literature on composite PEO coatings. Mu and Han [125] developed composite coatings comprising MgF_2 and ZrO_2 from a K_2ZrF_6 based electrolyte with some additives. The processing voltage was found to be instrumental in governing the thickness and composition, and thus the micro hardness of the coatings. The coatings were found to consist of MgF_2, tetragonal and monoclinic ZrO_2, and MgO. The bond strength, hardness and corrosion resistance were found to be better for the coatings obtained with a higher processing voltage (550 V). Arrabal *et al.* [38] and Matykina *et al.* [126] have experimented with the incorporation of particles of monoclinic zirconia during the PEO processing, and have investigated the

mechanism of coating formation. The coatings obtained using a DC power source in alkaline silicate–phosphate electrolytes comprised MgO, $Mg_2SiO_4$and $Mg_3(PO4)_2$ phases, and zirconia particles were found to get incorporated preferentially into the inner regions and at the coating surface. Due to local heating at the micro discharge regions, these monoclinic zirconia particles were found to transform into tetragonal zirconia. also, a $Mg_2Zr_5O_{12}$ phase was identified in the PEO coatings when zirconia incorporation was attempted in the phosphate-based electrolyte.

Recently, an alternative approach to obtain PEO coatings with low friction property was to introduce low friction materials into the coating by modifying the electrolytes with the solid lubricants additives. In this approach, solid lubricant particles, such as graphite, PTFE, MoS_2, WS_2 etc. are added into the electrolyte and dispersed with mechanical stirring to form a suspension. During the PEO process, solid lubricant particles can move from the electrolyte to the surface of the specimen, and be adsorbed on the surface, then be embedded into the ceramic coating.

It is important for this approach that solid lubricant particles should be sufficiently and uniformly dispersed in the electrolyte. So sufficient and constant mechanical stirring is inevitable. What's more, if necessary, a dispersant (such as acetone, ethanol etc.) is used to wet and disperse the solid lubricant particles. A kind of anionic surfactant (e.g. Sodium dodecyl sulfonate, etc.) is also used as additive to help the solid lubricant particles to be negatively charged and be suspended in the electrolyte. But the quantity of added dispersant and surfactant should be controlled and optimized. Too much additive can greatly affect the original properties of electrolyte and the whole coating process, resulting in low qualities of the coatings, such as non uniformity, high roughness, poor adhesion to the substrate, less thickness, more inclination to breakdown and burn out, etc. However, lower concentration of additive can't wet and disperse the solid lubricant particles in the electrolyte sufficiently. So the specific and accurate quantity of additives should be decided by different coating processes.

It is generally considered that the embedding of solid lubricant particles into the ceramic coating matrix depends on concentration diffusion and electrophoretic deposition. The embedding of particles may be recognized by the adsorption of particles on the surface of the specimen, so higher concentration can help to enhance the adsorption rate, thus lead to more particles embedded into the ceramic coating. To be negatively charged are beneficial to the electrophoresis of particles in the electrolyte, thus resulting in more

particles incorporated into the ceramic coatings. On the other side, the concentration of solid lubricant particles in the electrolyte and the quantity of solid lubricant particles incorporated into the coating should also be controlled and optimized. Too higher concentration of particles in the solution may greatly affect the original properties of electrolyte, causing poor qualities of the coatings. Too much solid lubricant particles incorporated into ceramic coatings may cause the destruction of the original coating structure and less ceramic component which plays the role as wear-resistant substrate, resulting in poorer qualities and lower wear resistance of the coatings. It is also considered that the embedding of nanoparticles into the PEO coatings depends on current density, frequency, duty cycle and coating time. Aliofkhazraei *et al.* [127-128] investigated the effects of concentration, current density, frequency, duty cycle and coating time on the embedding of Si_3N_4 nanoparticles into TiO_2 coatings. Results showed that the wear/mass loss rate decreased with the increasing of relative content of Si_3N_4 in the coatings. And the relative content of Si_3N_4 in the coatings increased by increasing of concentration, frequency and coating time, while it decreased by increasing of duty cycle and current density.

Up to now, some researchers have successfully incorporated solid lubricant particles (such as graphite, PTFE, MoS_2, etc.) into the PEO ceramic coatings formed on Al and Ti alloys. In the friction and wear process, the ceramic oxide coating plays the role as wear-resistant substrate while solid lubricant particles act as friction reducing agent during the sliding. Compared with the single PEO coatings, the yielded self-lubricating composite coatings can sharply decrease the friction coefficient and wear loss during the long-term sliding. Furthermore, the wear damage of counterpart materials can also be reduced greatly due to lower friction coefficient.

Xiaohong Wu *et al.* [129] have successfully incorporated graphite into Al_2O_3 ceramic coating fabricated on 2024Al alloy by PEO technique in a graphite-dispersed sodium aluminate electrolyte. The thickness of the composite coating produced was in the range 22±1 μm. Ball-on-disk tribological tests showed that the self-lubricating composite coating formed in the electrolyte containing 4g/L graphite exhibited a lowest friction coefficient of 0.09, under a normal load of 1 N, with a sliding time of 8 min and linear sliding speed of 0.08m/s, using a ball of Si_3N_4 as counterpart material.

Ming Mu *et al.* [130] have also successfully incorporated graphite into TiO_2 ceramic coating fabricated on Ti6Al4V alloy by PEO technique in a graphite-dispersed phosphate

electrolyte. The tribological evaluation was carried out on a ball-on-flat UMT-2MT tribometer, under a constant normal load of 2N, with a frequency of 5 Hz, an oscillating amplitude of 5 mm and a sliding time of 30 min, using AISI52100 steel balls as counterpart materials. And the results of friction and wear tests showed that the friction coefficient of the PEO coating reduced from nearly 0.8 to about 0.15 and the wear resistance improved significantly under dry sliding conditions, due to the presence of the graphite particles in the coating. Recently, Ming Mu *et al*. [131] have once again successfully incorporated MoS_2 into TiO_2 ceramic coating fabricated on Ti6Al4V alloy by PEO technique in MoS_2 dispersed phosphate electrolyte. Results showed that the TiO_2/MoS_2 composite coating exhibited improved tribological properties compared with the TiO_2 coating under dry sliding condition, which reduced the friction coefficient from 0.8 to about 0.12.

From above studies, it is clear that the approach to prepare self-lubricating composite coating was the most effective for the PEO coatings. This because coatings contained low friction materials could be obtained by only one step. Besides, the coatings were expected to integrate the advantages of wear resistance of the PEO coating and low friction property of solid lubricants.

As reported a lot of literature can be found regarding the preparation of self-lubricant PEO coatings on aluminum and titanium alloys but a lack of works was found regarding magnesium alloys.

In this thesis will be described the results obtained suspending graphite particles and nanoparticles into the electrolyte in order to reduce the maximum wear depth and the friction coefficient during tribological tests on the samples. PEO process will be applied with the innovative approach described in the previous chapters that permit to obtain good coatings working with at high current densities and short treatment times.

5.1 PRODUCTION OF THE GRAPHITE-CONTAINING PEO COATINGS

Samples of AZ91 and AZ80 magnesium alloy were used as substrate for PEO coatings in order to study the effects of the addiction of graphite particles and nanoparticles on the morphology, thickness, chemical composition, corrosion and wear resistance of the coatings. The nominal composition of the alloys is reported in Tab.5.1

Tab.5.1 Chemical composition of the alloys

Alloy	Al%	Zn%	Mn%	Si%	Fe%	Cu%	Ni%	Mg%
AM80	8.0	0.5	0.12	0.1	0.005	0.05	0.005	Bal.
AZ91	9.0	0.65	0.15	<0.10	<0.005	<0.010	<0.002	Bal.

The samples were cut from ingots and, before PEO treatment, were polished following standard metallographic techniques and then degreased using acetone in ultrasound. The PEO electrolyte was an aqueous alkaline solution with 50 g L^{-1} of $Na_5P_3O_{10}$, 50 g L^{-1} of Na_2SiO_3 , 40 g L^{-1} of NaOH and 3 g/l of graphite particles or nanoparticles. The nanoparticles were dispersed in acetone before the use in PEO electrolyte.

First of all two different sizes (30 µm average on the left, 15 µm average on the right) of graphite particles were tested and the SEM images of these particles are reported in Fig.5.1

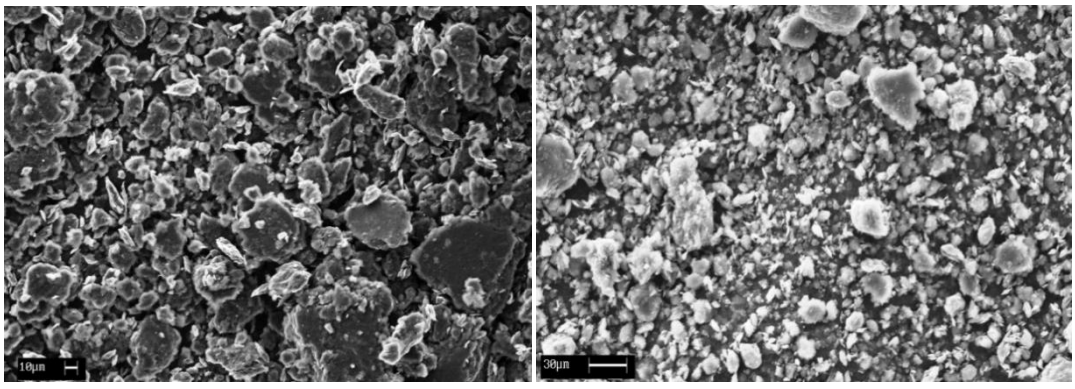

Fig.5.1 SEM images of the graphite particles (30 µm average on the left, 15 µm average on the right)

Also the use of graphite nanoparticles (<100nm) was tested and the TEM image of the nanoparticles is reported in Fig.5.2

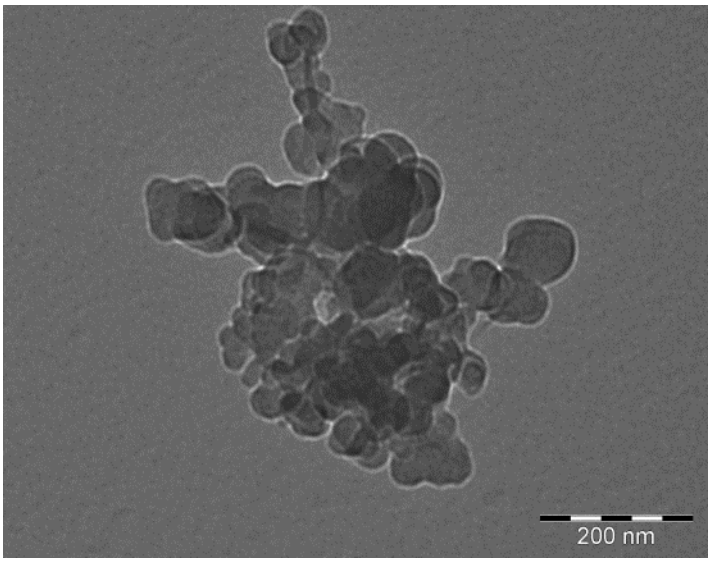

Fig.5.2 TEM image of the graphite nanoparticles

During the treatment, the sample worked as anode and the cathode was a steel mesh. The electrolyte was contained in a Becker and agitated with magnetic stirring during the treatment. The electrolyte was maintained at room temperature by a link with a cooling bath. The treatments were performed maintaining the current constant at 0.5 A/cm^2, letting the potential free to vary. Two different treatment times were used: 1 minute and 3 minutes.

The initial and final voltages, achieved during the experiment are reported in Tab.5.2

Tab. 5.2 Final and initial polarization voltages achieved for different samples

	Test	Initial voltage (V)	Final Voltage (V)
AZ80	1 min without graphite	80	90
	3 min without graphite	80	100
	1 min with graphite	80	90
	3 min with graphite	90	100
AZ91	1 min without graphite	70	80
	3 min without graphite	80	95
	1 min with graphite	70	90
	3 min with graphite	70	100

After the treatment, the samples were washed with deionized water and ethanol and dried with compressed air.

5.2 SURFACE ANALYSIS

First of all the effect of the addiction of the graphite particles reported in Fig.5.1 will be discussed.

Samples of AZ91 magnesium alloy were PEO treated at 0.5 A/cm^2 for one minute. The cross sections of the samples treated with the electrolyte containing graphite particles with average dimension of 15 and 30 µm and of the sample treated without graphite particles in the electrolyte are reported in Fig.5.3a,b and c.

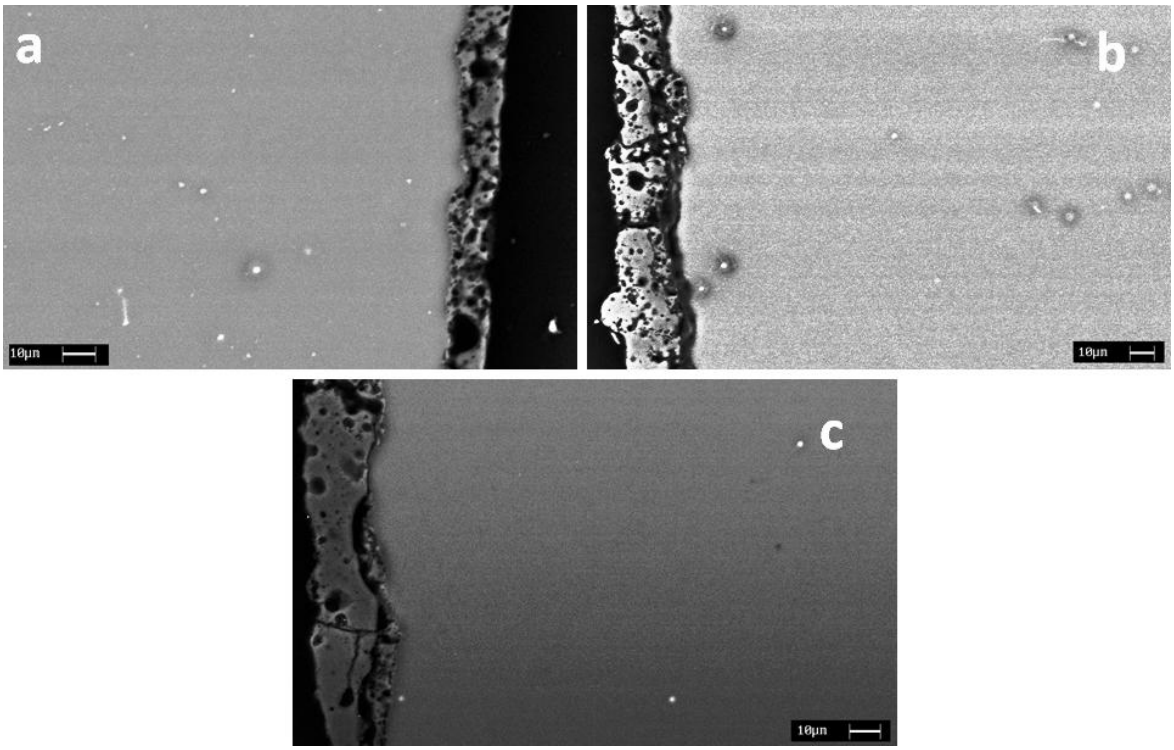

Fig.5.3 SEM image of the cross sections of the samples of AZ91 PEO treated for one minute at 0.5 A/cm^2 with graphite particles with average dimension of 15 µm (a), 30 µm (b) and no graphite particles (c)

No significant differences in the three samples can be observed if not a little variation in the thickness of the protective layer. Also the results of EDS analysis reported in Fig.5.4 did not reveal significant differences and more importantly did not reveal the presence of graphite in the coatings.

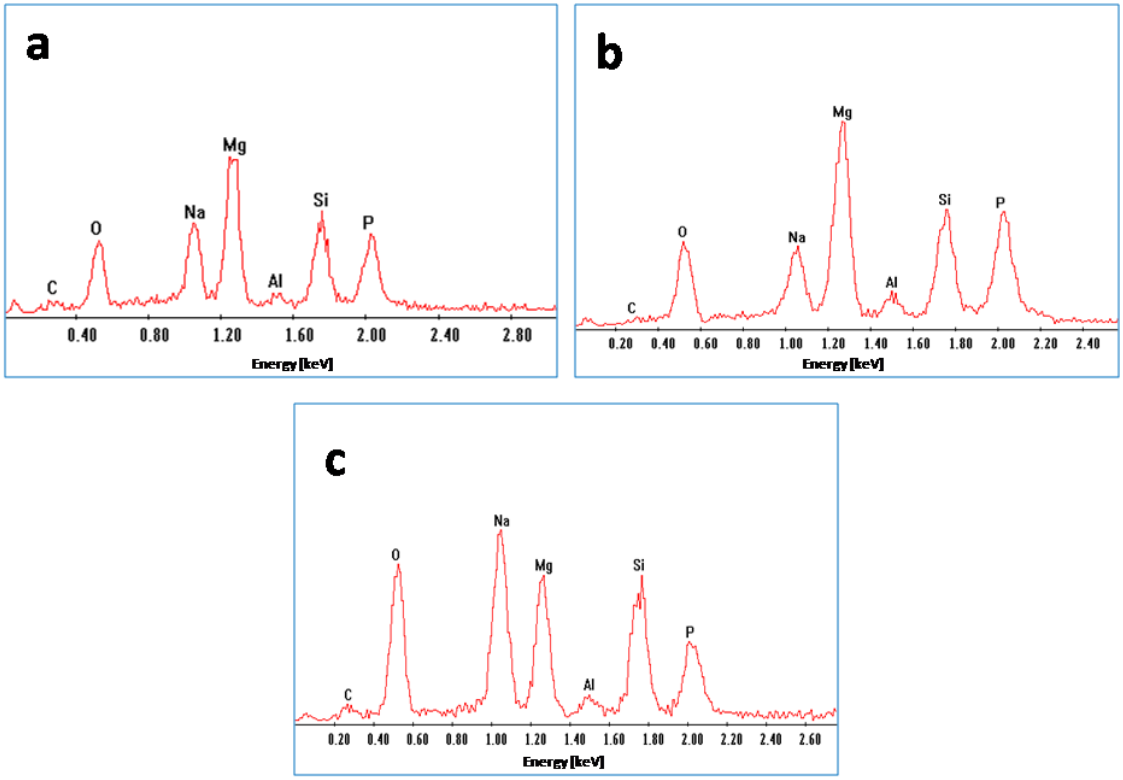

Fig.5.4 EDS micro-analysis recorded on the cross sections of the oxide protective coating in the samples of AZ91 PEO treated for one minute at 0.5 A/cm^2 with graphite particles with average dimension of 15 µm (a), 30 µm (b) and no graphite particles (c)

This fact can be related with the dimensions of the graphite particles. In fact the graphite particles has an average dimension of 15 or 30 µm but the dimensions of the pores that characterize the surface of the PEO coating for AZ91 treated in the conditions previously described are lower as can be observed in Fig.5.5

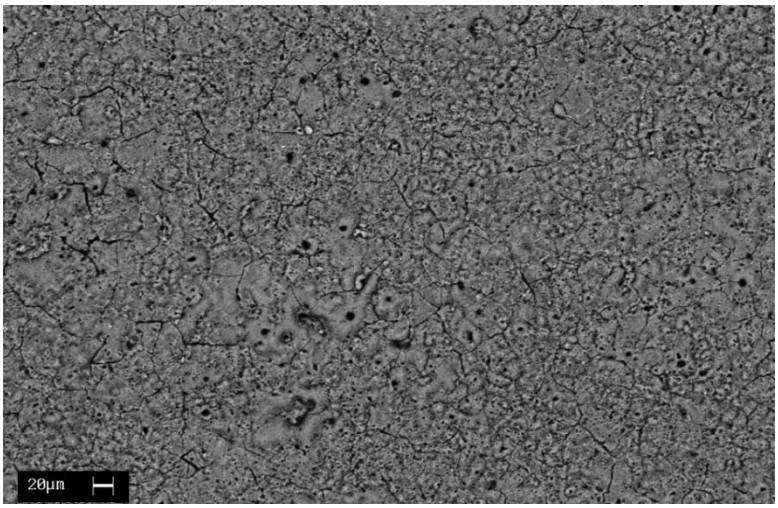

Fig.5.5 SEM image of the surface of the sample of AZ91 PEO treated for one minute at 0.5 A/cm

Due to this evidence the graphite particles cannot fill the pores and cannot be sealed into the coating.

Due to this problem all the other tests were performed using graphite nanoparticles instead of graphite particles..

The samples of AZ91 and AZ80 magnesium alloy were treated at 0.5 A/cm^2 for one and three minutes in the previously described solutions with and without graphite nanoparticles.

The SEM images of the cross section and the surface of the different AZ91 samples are reported in Fig.5.6 and Fig.5.7. It can be observed that both the treatment performed for 1 and 3 minutes produce the formation of a continuous coating characterized by the typical porous surface of PEO treated samples. The adhesion in all the samples seems good and the main difference between the various samples is the thickness of the protective layer. The thickness of the oxide ceramic coating for the different samples are summarized in Tab.5.3

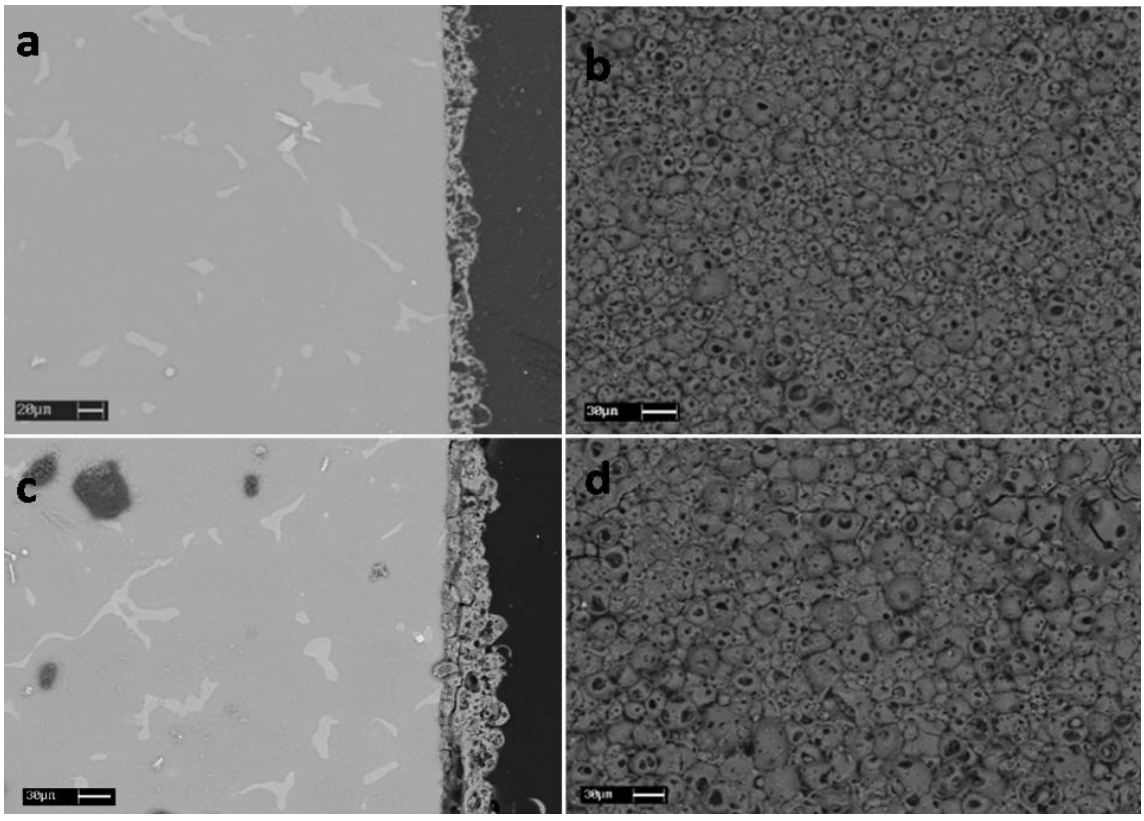

Fig.5.6 SEM image of the cross section (a) and the surface (b) of the sample of AZ91 PEO treated for one minute at 0.5 A/cm^2 and of the cross section (c) and the surface (d) of the sample of AZ91 PEO treated for three minutes at 0.5 A/cm^2. Both the treatments are performed without graphite nanoparticles in the electrolyte

It can be clearly seen from the table and figure reported that the increase in the treatment time produce an increase in the thickness of the protective layer, this in accordance with the previously reported results obtained on magnesium alloy reported in Chapter 3. Moreover was found that also the presence of graphite has a main role in the thickness of the oxide ceramic coating: the comparison between the samples produced with the same treatment time with and without graphite nanoparticles evidenced that the presence of the graphite produce an increase in the thickness of the coating. This behavior can be linked with the electrical conductivity of the graphite particles that influence the discharge process during PEO treatment and produce an increase in the thickness of the coating.

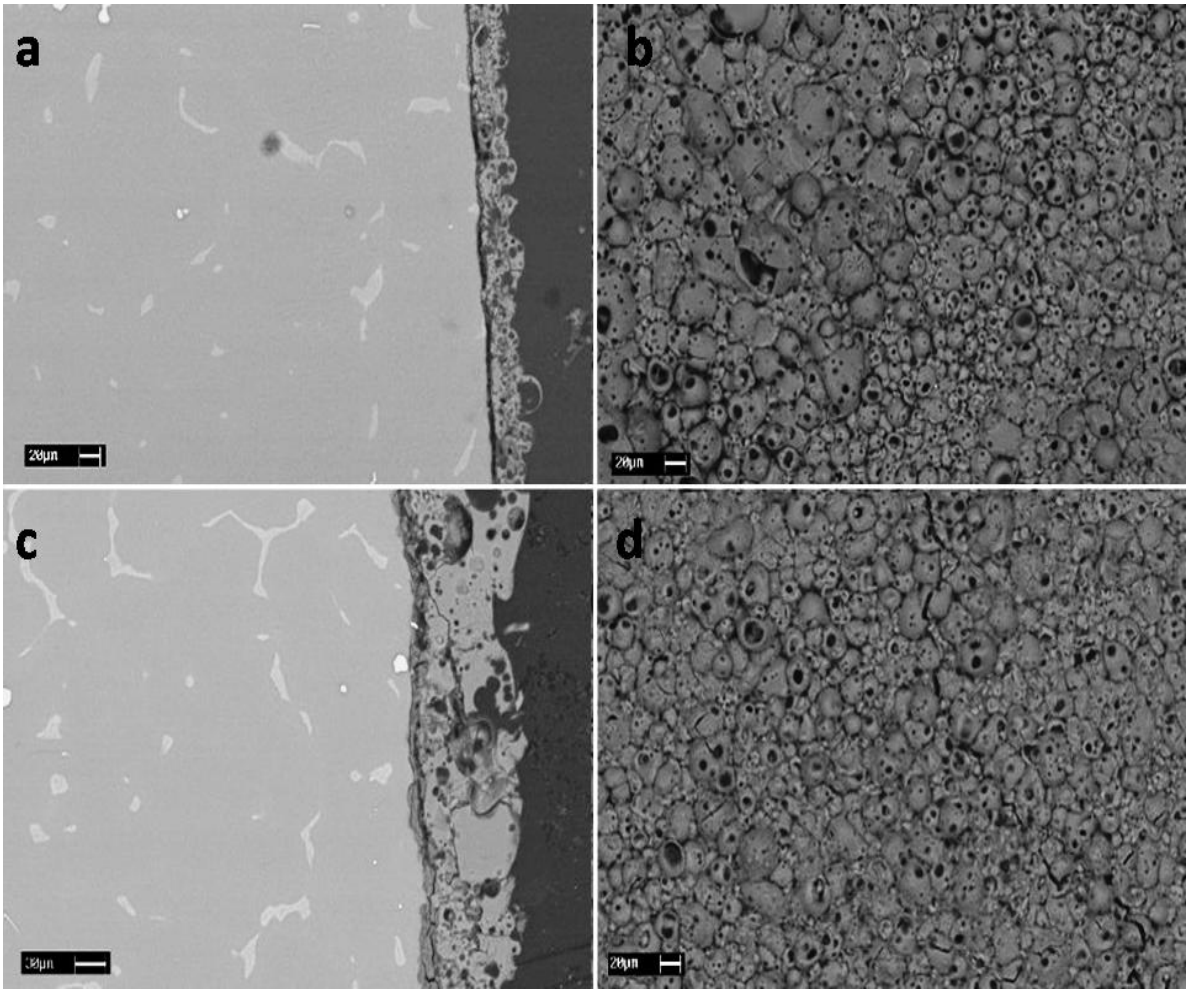

Fig.5.7 SEM image of the cross section (a) and the surface (b) of the sample of AZ91 PEO treated for one minute at 0.5 A/cm^2 and of the cross section (c) and the surface (d) of the sample of AZ91 PEO treated for three minutes at 0.5 A/cm^2. Both the treatments are performed with graphite nanoparticles in the electrolyte

Tab.5.3 Thickness of the coating in the different PEO treated samples of AZ91 magnesium alloy

Test	Thickness (µm)
1 min without graphite	20
3 min without graphite	35
1 min with graphite	30
3 min with graphite	70

An analysis of the cross section of the different samples evidence that for the samples treated for three minutes the traditional microstructure of the coating is obtained; in fact, as reported in Fig.5.8 the presence of both the inner barrier layer and of the external porous/technological layer is clearly visible. Instead in the samples treated for one minute only the presence of the external layer can be revealed in the SEM micrographs due to the low thickness of the barrier layer.

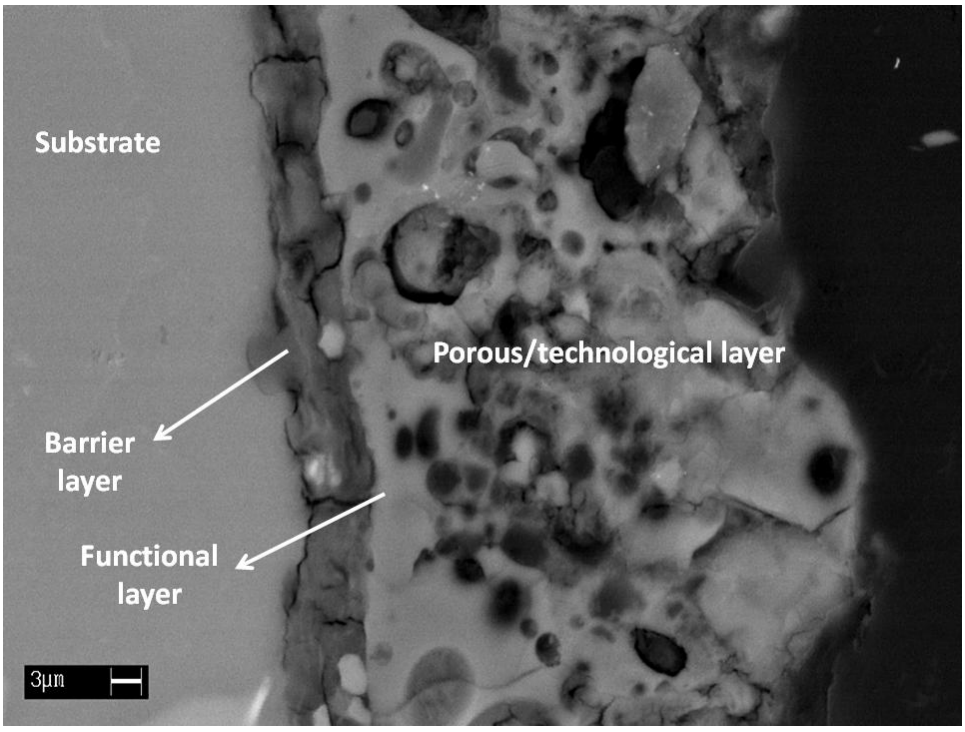

Fig.5.8 SEM image of the cross section of the sample of AZ91 PEO treated for 3 minutes at 0.5 A/cm^2 with graphite nanoparticles in the electrolyte

The comparison of the cross section of the different samples (at high magnification) is reported in Fig.5.9

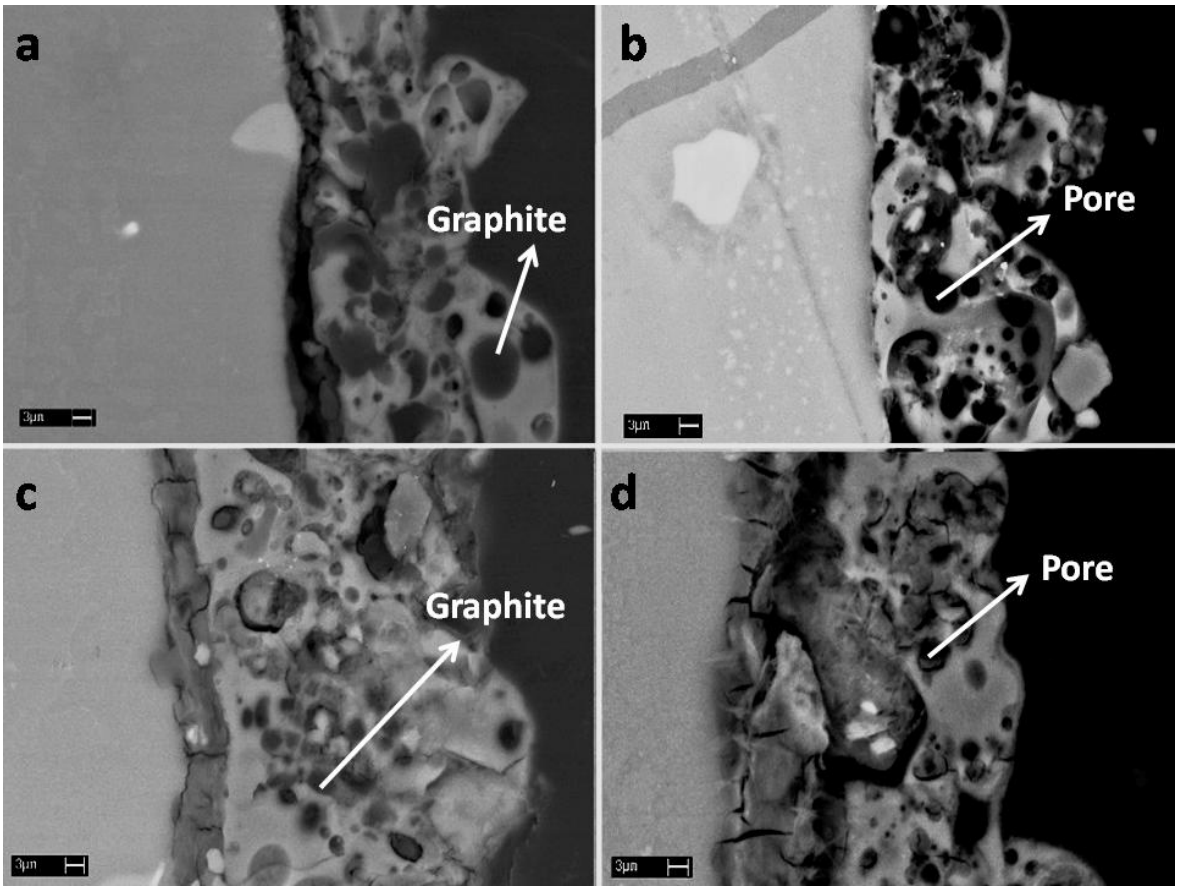

Fig.5.9 SEM image of the cross section of the samples of AZ91 PEO treated at 0.5 A/cm^2 for one minute with graphite nanoparticles (a) and without graphite nanoparticles (b) and of the samples of AZ91 PEO treated at 0.5 A/cm^2 for three minutes with graphite nanoparticles (c) and without graphite nanoparticles (d)

From Fig.5.9 can be clearly observed that the use of graphite nanoparticles instead of graphite particles overcome the previously reported problem that the particles were too big to fill the pores that characterize the PEO coating. In fact for both the treatment times (one minute and three minutes) it can be observed that the pores (visible on the images b and d) are filled with graphite as can be seen in images a and c.

The presence of graphite in the pores is confirmed by EDS micro-analysis. The obtained spectra collected in the cross section of the sample of AZ91 treated for three minutes in the barrier layer (a), in the porous layer (b) and in a pore filled with graphite (c) are in fact reported in Fig.5.10 It can be clearly seen the presence of the graphite inside of the pores (Fig.5.10c).

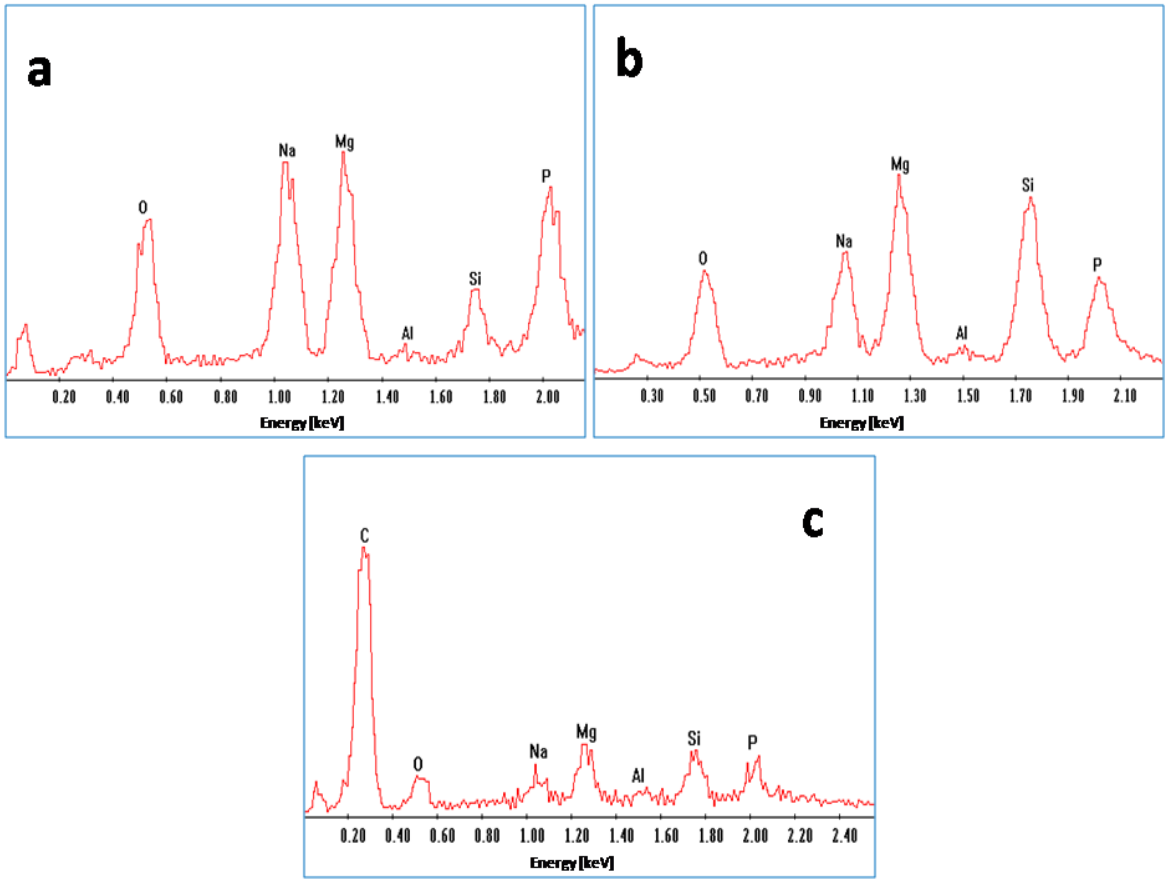

Fig.5.10 EDS micro-analysis of the barrier layer (a), porous layer (b) and of the graphite inside the pore (c) in the cross section of the sample of AZ91 PEO treated for 3 minutes

It can be also observed that the barrier layer is rich in phosphates (Fig.5.10a) instead the porous layer is rich in silicates (Fig.5.10b).

For AZ80 magnesium alloy the results in terms of thickness and morphology of the oxide ceramic coating are more or less the same as the one obtained for AZ91. The SEM images of the cross section and the surface of the different AZ80 samples are reported in Fig.5.11 and Fig.5.12

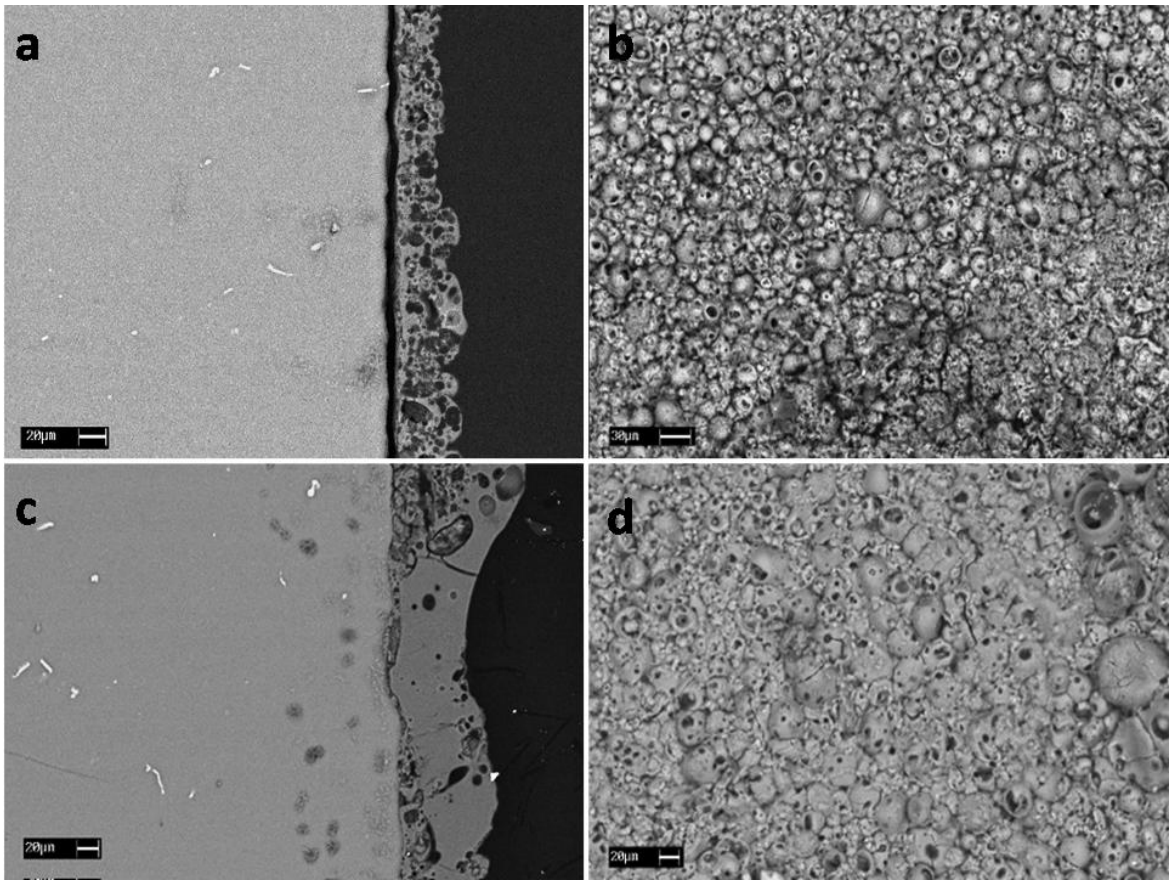

Fig.5.11 SEM image of the cross section (a) and the surface (b) of the sample of AZ80 PEO treated for one minute at 0.5 A/cm^2 and of the cross section (c) and the surface (d) of the sample of AZ80 PEO treated for three minutes at 0.5 A/cm^2. Both the treatments are performed without graphite nanoparticles in the electrolyte

Also for AZ80 magnesium alloy in all the samples can be observed the typical porous surface of PEO coatings. Moreover in all the samples a good uniformity of the coating and a good adhesion with the substrate can be observed. Only in the sample treated without graphite for one minute some adhesion problems can be found probably due to the metallographic preparation. Also in this case the thickness of the protective layer is influenced by the treatment time and by the presence of graphite nanoparticles; the thickness of the different samples are summarized in Tab.5.4. As predictable an increase in the thickness of the protective layer was obtained with the increase of the treatment time. Moreover, as was found for AZ91 magnesium alloy, the presence of the graphite nanoparticles produced a remarkable increase in the thickness of the oxide layer in the sample treated for one minute. For the sample treated at three minutes the graphite do not influence the thickness of the coating. Also in this case this behavior can be connected with the electrical conductivity of the graphite particles.

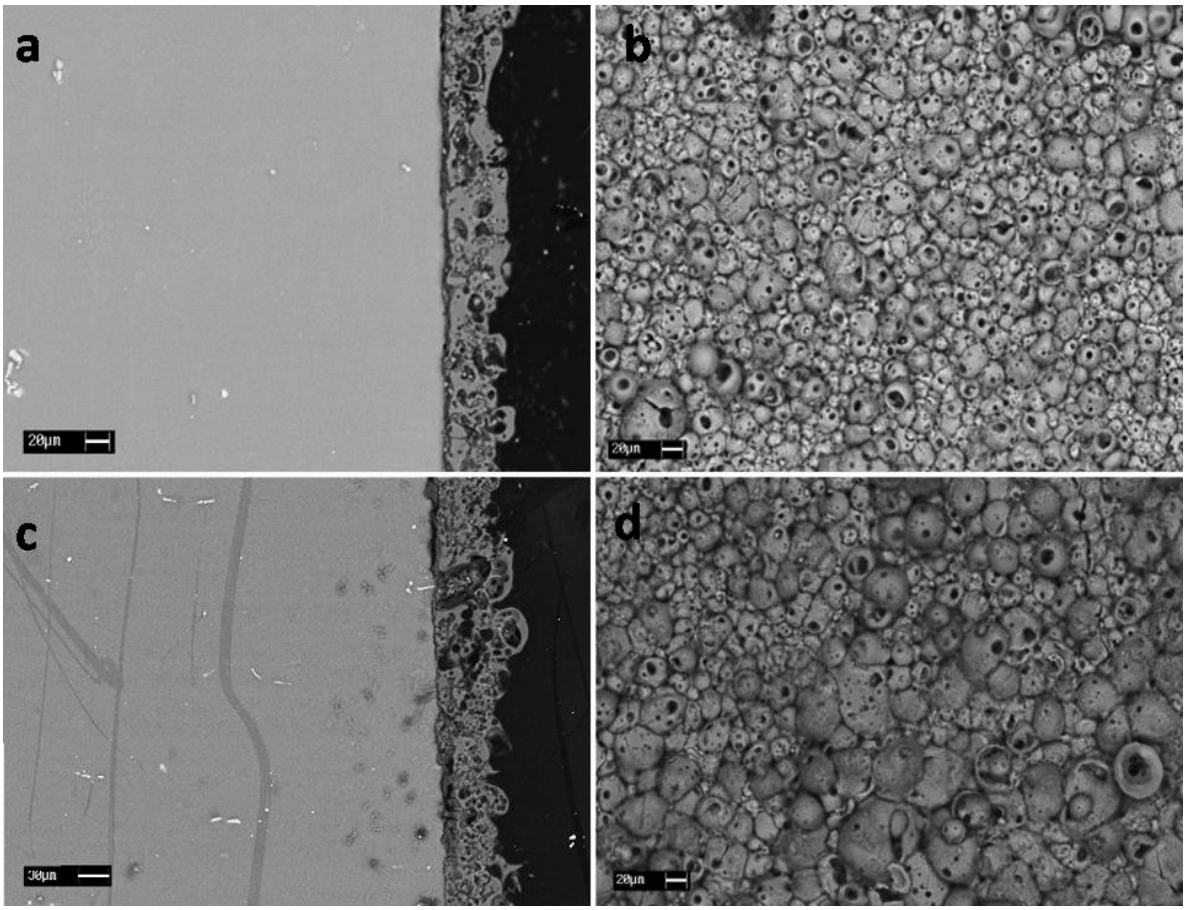

Fig.5.12 SEM image of the cross section (a) and the surface (b) of the sample of AZ80 PEO treated for one minute at 0.5 A/cm^2 and of the cross section (c) and the surface (d) of the sample of AZ80 PEO treated for three minutes at 0.5 A/cm^2. Both the treatments are performed with graphite nanoparticles in the electrolyte

Tab.5.4 Thickness of the coating in the different PEO treated samples of AZ80 magnesium alloy

Test	Thickness (µm)
1 min without graphite	30
3 min without graphite	60
1 min with graphite	50
3 min with graphite	60

To better understand the microstructure of the coating and the influence of the graphite on this microstructure also an analysis of the cross section of the samples of AZ80 alloy at higher magnifications was performed and the results are reported in Fig.5.13

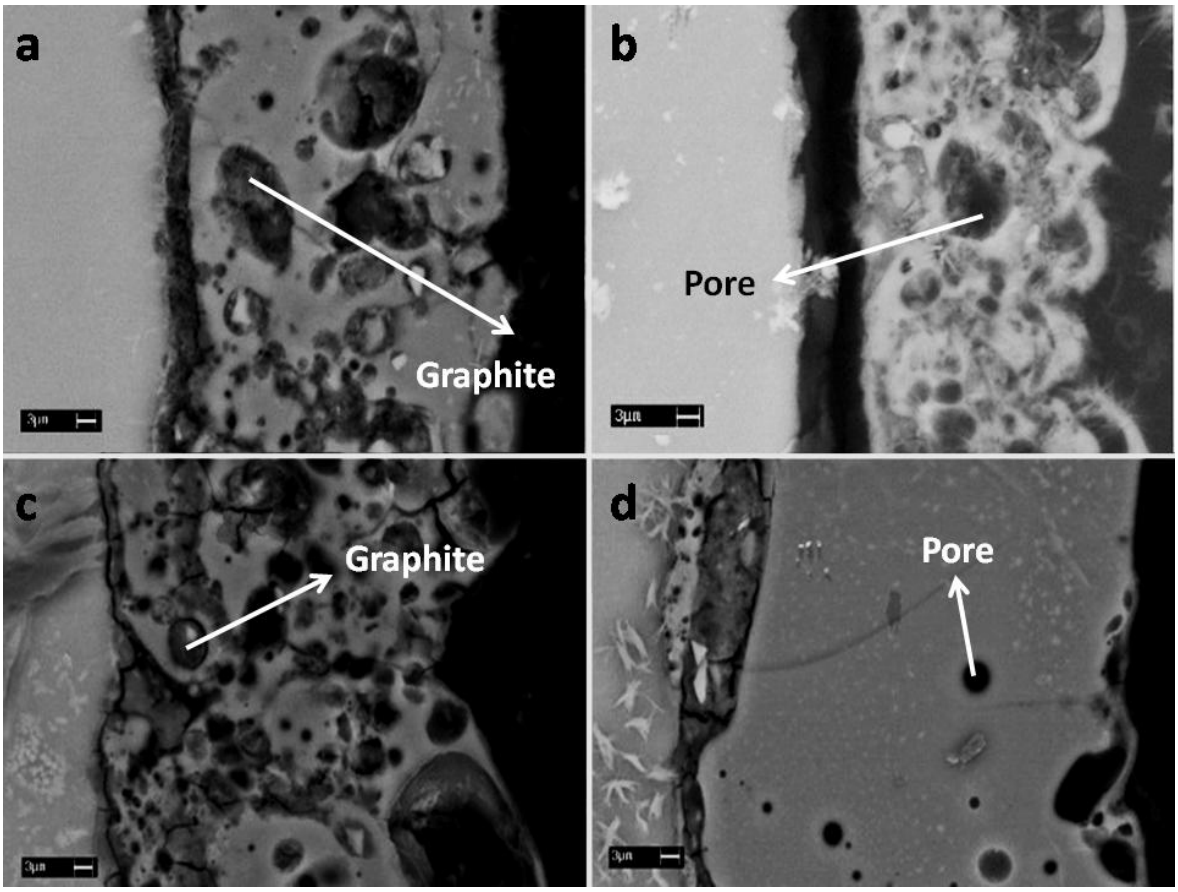

Fig.5.13 SEM image of the cross section of the samples of AZ80 PEO treated at 0.5 A/cm^2 for one minute with graphite nanoparticles (a) and without graphite nanoparticles (b) and of the samples of AZ80 PEO treated at 0.5 A/cm^2 for three minutes with graphite nanoparticles (c) and without graphite nanoparticles (d)

Also for AZ80, in analogy with the results obtained for AZ91 magnesium alloy, it can be observed that for both the treatments the graphite particles fill the pores that characterize the PEO surface. Also for this alloy the typical double layer structure of the PEO coatings can be found in the samples treated for three minutes (as evidenced in Fig.5.14 for the sample treated with graphite), instead in the samples treated for one minute the inner barrier layer is less visible due to the low thickness.

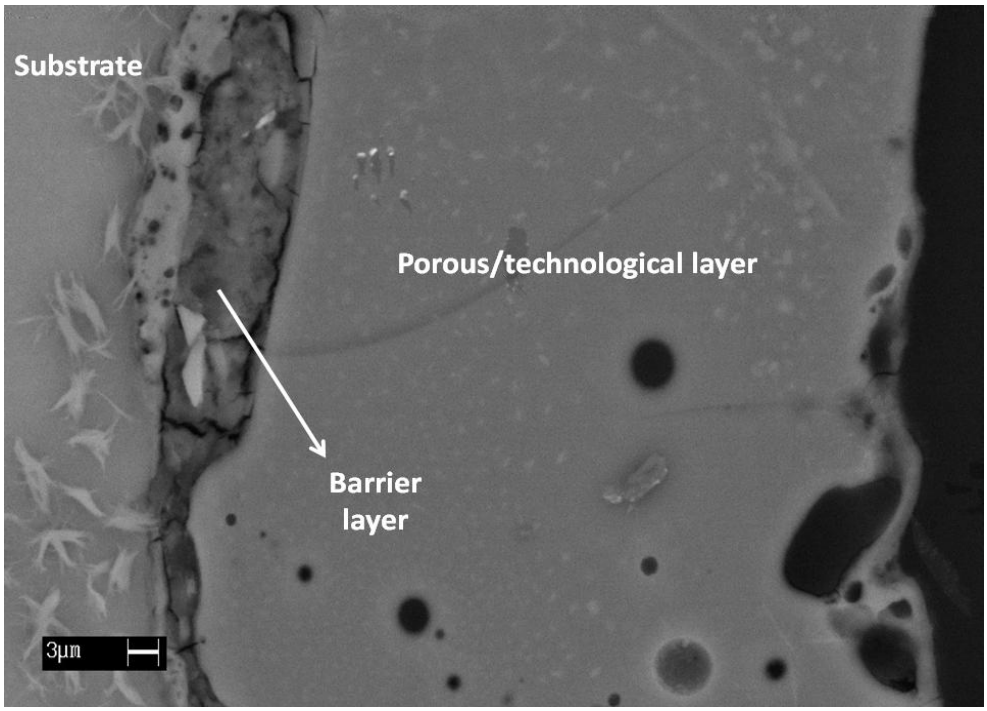

Fig.5.14 SEM image of the cross section of the sample of AZ91 PEO treated for 3 minutes at 0.5 A/cm^2 without graphite nanoparticles in the electrolyte

The presence of graphite in the pores is also in this case confirmed by EDS micro-analysis. In detail in Fig.5.15 it can be seen the results of the extended micro-analysis conducted on the oxide protective coating of the sample treated for three minutes without graphite nanoparticles (Fig.5.15a) and of the sample treated for three minutes with graphite particles (Fig.5.15b). It can be clearly seen that the carbon peak is visible only in the sample treated with graphite nanoparticles.

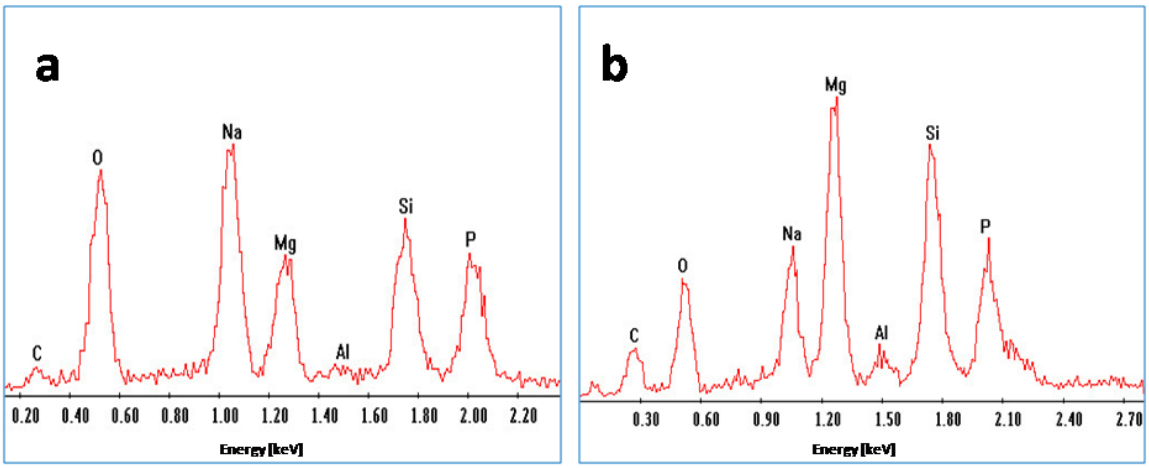

Fig.5.15 EDS micro-analysis of the sample of AZ80 PEO treated for 3 minutes without graphite nanoparticles (a) and with graphite nanoparticles (b)

5.3 CORROSION BEAHVIOUR

The corrosion resistance of the different PEO treated samples was evaluated with potentiodynamic polarization tests and EIS tests. The polarization curves for the samples of AZ91 and AZ80 are reported in Fig.5.16 and Fig.5.17 respectively and the values of corrosion current densities and corrosion potentials, extrapolated from the curves are summarized in Tab.5.5

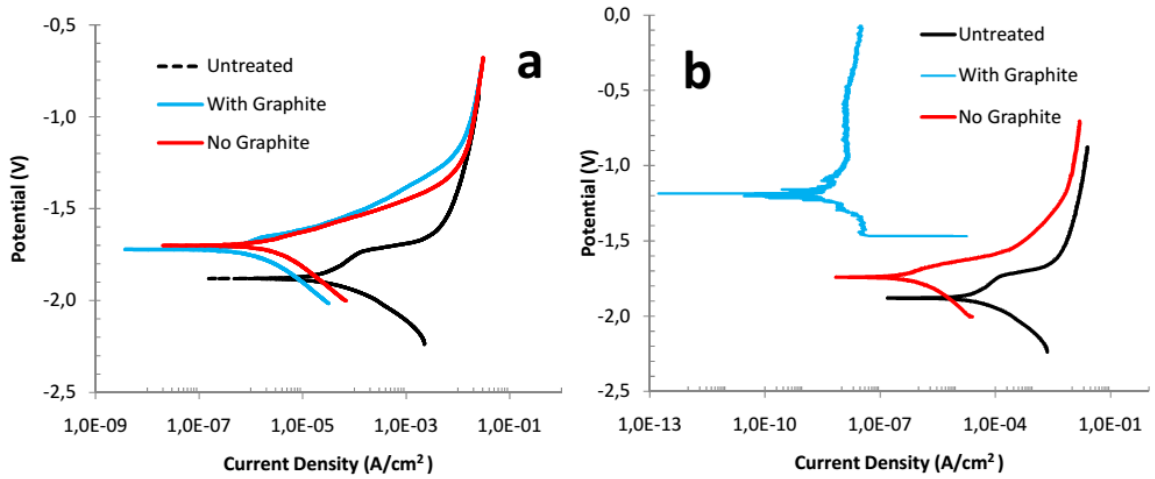

Fig.5.16 Potentiodynamic polarization plots of samples of AZ91 PEO treated for 1 minute (a) and with 3 minutes (b) with and without graphite nanoparticles compared with the untreated sample (test solution: 0.1M Na_2SO_4 + 0.05 M NaCl)

In detail it can be observed that for AZ91 all the PEO treated samples have an improved corrosion resistance if compared with the one of the untreated sample. In fact all the PEO treated samples are characterized by a corrosion current density, that is directly linked with the corrosion rate in the Faraday law, over one order of magnitude lower than the untreated sample. Moreover also an increase in the corrosion potential can be observed in the PEO treated samples. Regarding the comparison between the different treatments it can be observed that, for the treatment performed without graphite nanoparticles in the electrolyte, the corrosion behavior of the samples, treated for one or three minutes, is very similar. Also the sample treated for one minute with graphite nanoparticles has a corrosion resistance of the same order of magnitude if compared with the one of the two samples previously described. However the sample treated for three minutes with graphite nanoparticles in the electrolyte (Fig. 5.16b) is characterized by improved corrosion performances: this sample in fact has a corrosion potential 0.5 V higher, and a corrosion current density two order of magnitude lower than the other PEO treated samples. This

behavior can be connected with the surface morphology previously described: the coating obtained at three minutes is thicker than the one obtained at one minute but with a lot of pores; this pores in the treatment with graphite nanoparticles are filled by the graphite and so the barrier effect of the oxide ceramic coating results improved. This behavior is not clearly visible in the samples treated for one minute (Fig.5.16a) due to the reduced thickness of the coating.

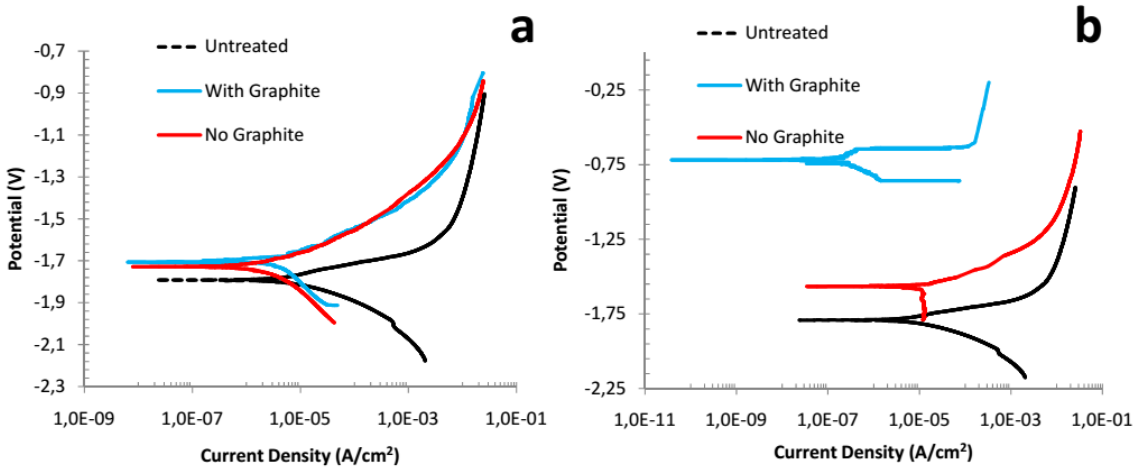

Fig.5.17 Potentiodynamic polarization plots of samples of AZ80 PEO treated for 1 minute (a) and with 3 minutes (b) with and without graphite nanoparticles compared with the untreated sample (test solution: 0.1M Na_2SO_4 + 0.05 M NaCl)

For the samples of AZ80 magnesium alloy the anodic polarization plots can be observed for the samples treated for one minute in Fig.5.17a and for the samples treated for three minutes in Fig. 5.17b. Also for this alloy all the PEO treated samples exhibit improved corrosion resistance if compared with the untreated sample with a decrease of more than one order of magnitude in the corrosion current density and an increase in the corrosion potential. Also for AZ80 the samples treated for one minute with and without graphite nanoparticles in the electrolyte and the sample treated for three minutes without graphite nanoparticles have the same corrosion behavior (corrosion current density about one order of magnitude lower than the untreated sample and corrosion potential 0.2 V higher). Also for this alloy a higher improvement in the corrosion resistance can be observed in the sample treated for three minutes with graphite nanoparticles in the electrolyte with a decrease of one order of magnitude in the corrosion current density and an increase of about 1.1 V in the corrosion potential if compared with the other PEO treated samples. Also in this case the corrosion performances can be connected with the surface

morphology, and in particular with the thicker and "graphite filled" oxide ceramic coating of the sample treated for three minutes with graphite nanoparticles in the electrolyte.

Tab.5.5 Corrosion potentials and corrosion current densities obtained for the different PEO treated samples from potentiodynamic polarization tests

Material	Treatment	Corrosion Current Density (A/cm^2)	Corrosion Potential (V)
AZ80	Untreated	$3.5x10^{-5}$	-1.82
AZ80	PEO: 1 min with graphite	$3.5\ x10^{-6}$	-1.70
AZ80	PEO: 3 min, with graphite	$2.0\ x10^{-7}$	-0.67
AZ80	PEO: 1 min without graphite	$2.2\ x10^{-6}$	-1.72
AZ80	PEO: 3 min without graphite	$9.0\ x10^{-6}$	-1.56
AZ91	Untreated	$4.0\ x10^{-5}$	-1.87
AZ91	PEO: 1 min with graphite	$6.0\ x10^{-7}$	-1.72
AZ91	PEO: 3 min, with graphite	$4.1\ x10^{-9}$	-1.18
AZ91	PEO: 1 min without graphite	$2.0\ x10^{-6}$	-1.70
AZ91	PEO: 3 min without graphite	$6.0\ x10^{-7}$	-1.75

To better understand the corrosion behavior of the different samples also EIS test were performed. In analogy with the considerations reported in the previous chapters regarding the fitting of the experimental data two different equivalent circuits were chosen: the one in Fig.2.6a for the untreated sample and the one in Fig. 2.6b for the PEO treated samples in order to consider the double layer structure of PEO coatings.

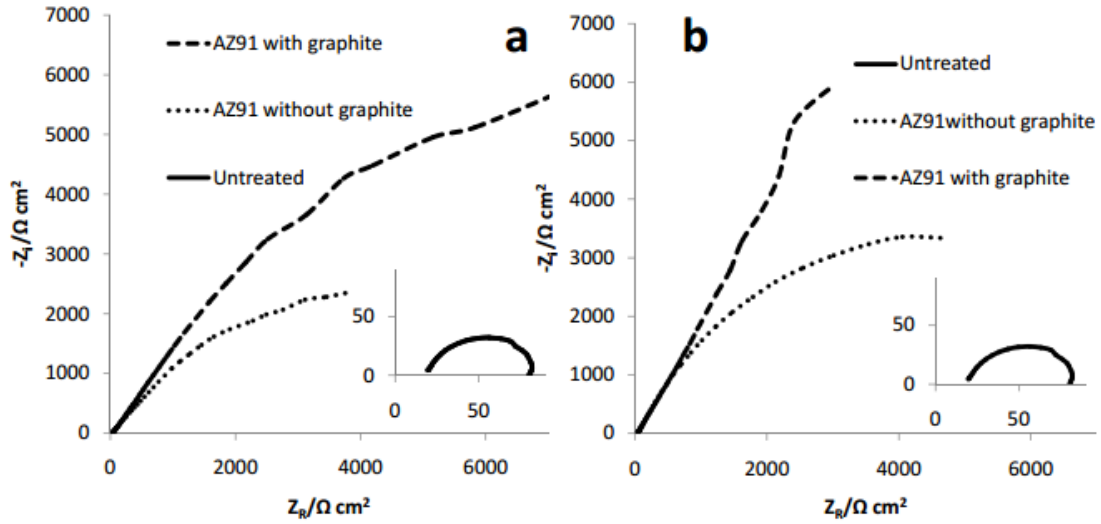

Fig.5.18 Nyquist plots of samples of AZ91 PEO treated for 1 minute (a) and with 3 minutes (b) with and without graphite nanoparticles compared with the untreated sample (test solution: 0.1M Na_2SO_4 + 0.05 M NaCl)

The results for AZ91 magnesium alloy, reported in terms of Nyquist plots, and the results of the fitting of the experimental data (where a good fitting quality was obtained with a chi square value that vary between 0.001 and 0.01) are reported in Fig.5.18 and Tab.5.6.

Tab.5.6 Results of the fitting of the experimental data for the samples of AZ91 magnesium alloy after EIS tests

	R_1 [$\Omega*cm^2$]	R_2 [$\Omega*cm^2$]	R_3 [$\Omega*cm^2$]	Q_1 [$F*Hz^{1-n}$]	Q_2 [$F*Hz^{1-n}$]	n_1	n_2
Untreated	19.2	67	-	$1.9x10^{-5}$	-	0.91	-
AZ91 1 minute without graphite	22.4	401	8436	$9.3x10^{-4}$	$9.74x10^{-6}$	0.84	0.91
AZ91 1 minute with graphite	21.3	5623	50426	$1.5\ x10^{-5}$	$1.9\ x10^{-7}$	0.87	0.9
AZ91 3 minutes without graphite	20.5	501	10868	$2.1x10^{-5}$	$9.86x10^{-7}$	0.87	0.96
AZ91 3 minutes with graphite	24.3	8003	100580	$3.9x10^{-5}$	$3.6x10^{-8}$	0.86	0.86

From the previously reported data it can be observed that EIS confirmed the results coming from potentiodynamic polarization tests but also gains some more important information. In fact the behavior of the different samples can be more clearly distinguished due to the higher precision of the technique. First of all is clearly confirmed that the PEO treated samples are characterized by higher corrosion performances if compared with the untreated one. An increase of several orders of magnitude in the polarization resistance can in fact be recorded. It can be observed that the samples treated without graphite nanoparticles in the electrolyte have a very similar behavior, with the sample treated for 3 minutes that is characterized by only slightly higher values of R_2 and R_3. However the difference in the thickness of the coatings, that was found during SEM analysis, is confirmed by the fact that the value of Q_2 in the sample treated for one minute is one order of magnitude higher than the sample treated for three minutes. The difference in the values of Q_1 is less important so it can be confirmed that the main difference in the two treatment is an increase in the thickness of the barrier layer in the sample treated for three minutes. Considering the samples treated with graphite nanoparticles in the electrolyte it can be observed that for both the treatments (one minute and three minutes) a remarkable increase

in the corrosion resistance is recorded if compared with the samples treated without graphite. An increase both in the values of R_2 and R_3 can in fact be noted as a decrease in the values of Q_2. This fact, as was previously said, can be linked with the presence of the graphite that from one hand close the pores present on the surface of the sample, from the other cause a variation in the discharge mechanism and permit to obtain thicker protective coatings if compared with the correspondent sample treated without graphite. EIS tests so permit to better evaluate the corrosion behavior of the sample treated for one minute with graphite nanoparticles that result better than the samples treated without graphite. This fact was not noted in potentiodynamic polarization tests due to the more precision of EIS tests. The sample with the best corrosion performance remain however the one treated for three minutes with graphite nanoparticles in the electrolyte: this sample is in fact characterized by the higher values of R_2 and R_3. Moreover the sample is also the one with the lower value of Q_2 and so is characterized by the presence of the thicker protective layer confirming what was previously described in the surface analysis.

EIS tests were also performed on the samples of AZ80 magnesium alloy and the results, reported in terms of Nyquist plots, and the fitting of the experimental data (where a good fitting quality was obtained with a chi square value that vary between 0.008 and 0.01) are reported in Fig.5.19 and Tab.5.7.

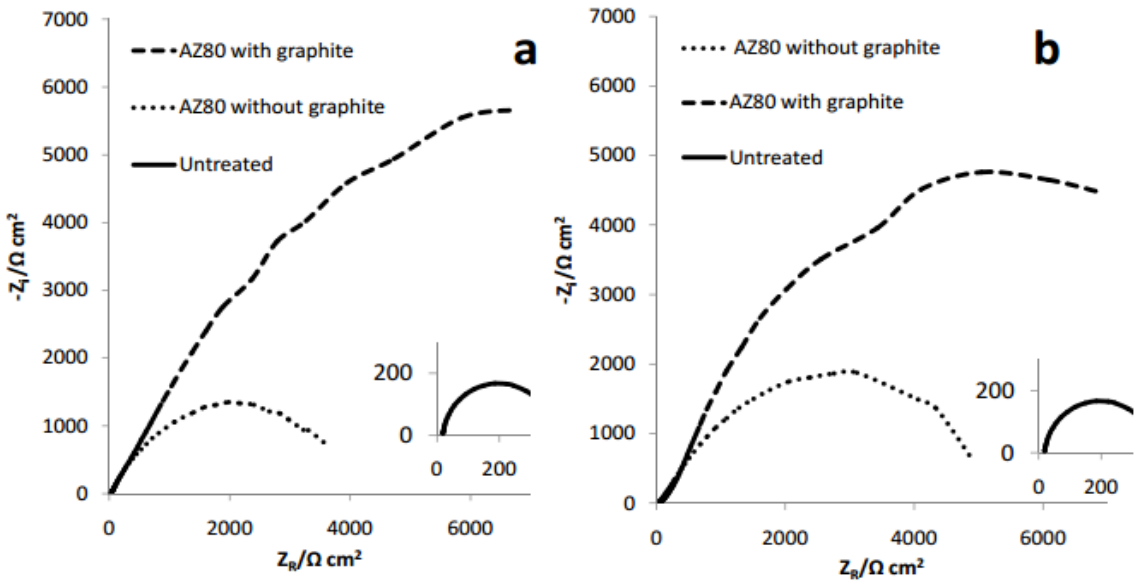

Fig.5.19 Nyquist plots of samples of AZ80 PEO treated for 1 minute (a) and with 3 minutes (b) with and without graphite nanoparticles compared with the untreated sample (test solution: 0.1M Na_2SO_4 + 0.05 M NaCl)

Also for AZ80 magnesium alloy EIS test permit to better evaluate the corrosion performance of the different samples. From Nyquist plots is clearly observable that all the PEO treated samples exhibits sensibly higher corrosion performances than the untreated sample with an increase of several orders of magnitude in the polarization resistance.

Tab.5.7 Results of the fitting of the experimental data for the samples of AZ80 magnesium alloy after EIS tests

	R_1 [$\Omega*cm^2$]	R_2 [$\Omega*cm^2$]	R_3 [$\Omega*cm^2$]	Q_1 [$F*Hz^{1-n}$]	Q_2 [$F*Hz^{1-n}$]	n_1	n_2
Untreated	18.6	350	-	$8.53x10^{-5}$	-	0.93	-
AZ80 1 minute without graphite	20.4	400	3940	$7.4\ x10^{-5}$	$9.2x10^{-5}$	0.93	0.88
AZ80 1 minute with graphite	19.2	476	19312	$3.4\ x10^{-5}$	$2.59x10^{-5}$	0.94	0.91
AZ80 3 minutes without graphite	20.2	450	5365	$1.67x10^{-5}$	$2.03x10^{-5}$	0.92	0.91
AZ80 3 minutes with graphite	19.6	2882	18459	$5.1x10^{-5}$	$4.5x10^{-6}$	0.96	0.96

The samples treated for one and three minutes without graphite in the electrolyte have a similar corrosion behavior and only a slight increase in the value of R_3 and a slight decrease in the value of Q_2 can be observed in the sample treated for three minutes characterized by a thicker protective layer. Instead both the samples treated without graphite in the electrolyte are characterized by a remarkable lower corrosion resistance if compared with the ones treated with graphite nanoparticles. In fact the samples treated for 1 and 3 minutes with graphite nanoparticles show a similar corrosion resistance and are characterized by a value of R_3 almost one order of magnitude higher if compared with the samples treated without graphite. This fact can be explained with the presence of the graphite particles that fill the pores increasing the barrier effect of the coating. Regarding the values of Q_2 a comparison of the samples treated for the same time with and without graphite nanoparticles evidence that the presence of graphite produce a decrease in the value of Q_2 and so an increase in the thickness of the coating (confirming the SEM observation). This fact can be, also for AZ80 alloy, connected with the modification in the

discharge phenomena produced by the conductive graphite particles. However the maximum in the thickness of the coating is obtained for the sample treated for three minutes with graphite nanoparticles. Also for AZ80 EIS test permit to better evaluate the corrosion resistance of the different samples due to his higher precision than anodic polarization tests and in particular the behavior of the sample treated for one minute with graphite particles was better explained.

5.4 MECHANICAL BEHAVIOUR

In order to understand the effect of the treatment time and of the presence of graphite nanoparticles on the mechanical resistance of the obtained coatings the micro-hardness of the oxide layer was measured with a Vickers microdurometer. The results of the test ($HV_{0.1}$) for both AZ91 and AZ80 are reported in Tab.5.8. The values of the micro-hardness were measured on the cross section of the coating in order to not affect the measure with the hardness of the metallic substrate.

Tab.5.8 Results of the micro-hardness tests for the different PEO treated samples

AZ91 1 min No C	**AZ91 1 min C**	**AZ91 3 min No C**	**AZ91 3 min C**	**AZ80 1 min No C**	**AZ80 1 min C**	**AZ80 3 min No C**	**AZ80 3 min C**
320	450	333	566	370	400	437	468

For both the alloys an increase in the treatment time produce an increase in the hardness of the coating, this in accordance with the fact reported in literature that an increase in the thickness of the coating produce an increase in the hardness but also in the fragility. Also the presence of graphite in the electrolyte produce a variation in the hardness. This fact can be partially linked with the higher thickness of the coatings obtained with graphite in the electrolyte but also with an effect of the graphite particles itself. The increase in the hardness due to the presence of the graphite particles is however more significant for AZ91 than for AZ80.

5.5 TRIBOLOGICAL BEHAVIOUR

All the obtained samples were tested with a block on ring tribometer at two different loads (5 and 10 N).

First of all was analyzed the effect of the presence of graphite particles on the friction coefficient recorded during the tribological tests. One of the problems of PEO coatings is, in fact, the increase in the friction coefficient if compared with the untreated alloy. The graphite present in the coating (in forms of graphite nanoparticles inside of the pores, as was described in the previous section) could work as solid lubricant and cause the decrease of the friction coefficient. The results of the analysis of the friction coefficient for the different samples are reported in Fig.5.20 Some tests were not performed at 10 N because the failure of the oxide coating begin already at 5N. This tests are signed as N.E. in the graph.

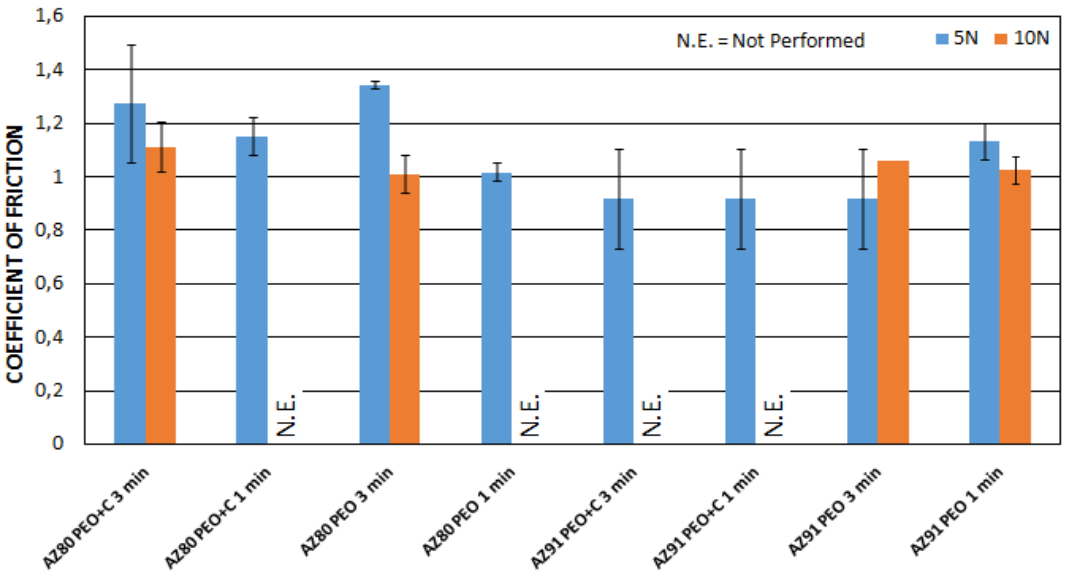

Fig.5.20 Results of the tribological tests in terms of friction coefficient for all the PEO treated samples

It can be observed from the previously reported data that the presence of graphite do not significantly influence the friction coefficient. In fact a comparison between the samples treated for the same time with and without graphite nanoparticles show variations in the friction coefficient inside the error bar. This fact can be explained in two different ways for the samples treated for one and three minutes. In the samples treated for one minute the layer is too thin and the graphite inside the pores is too low to have a significant effect as solid lubricant. The samples treated for three minutes are instead characterized by a fragile

failure (as reported in the images below in Fig.5.22 and Fig.5.23) so there are a lot of fragments of the oxide coating between the block and the ring, and the graphite could not work as solid lubricant.

After tribological tests the wear lines were analyzed with a profilometer in order to individuate for each sample the max depth of wear. This measure can be considered as an evaluation of the wear resistance of the sample and the obtained values for the PEO treated samples are reported for the two different loads in Fig.5.21. Also in this case the symbol N.E. means that the test was not performed because the failure was recorded at lower loads. Instead the symbol N.D. means that the depth of the wear is under the detection limit of the profilometer.

The values reported in the graph has to be compared with the reference values of maximum depth of wear obtained for the untreated AZ91 and AZ80 magnesium alloys at 5N that are respectively *140 and 160 µm*. The tests at 10N were not performed on the untreated samples because at 5N the maximum depth of wear was already remarkable.

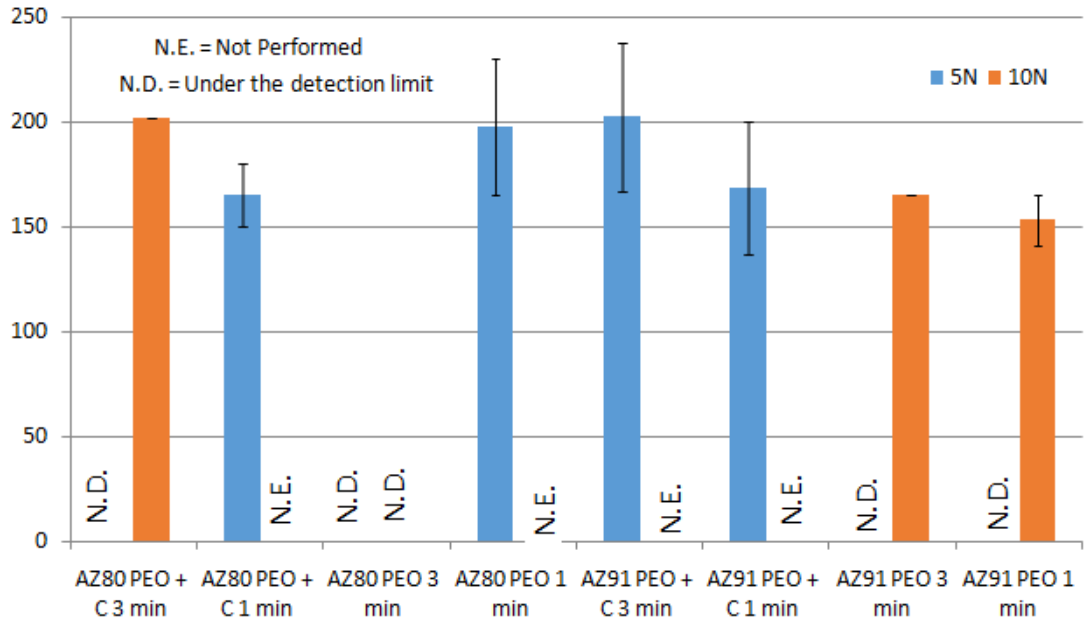

Fig.5.21 Results of the tribological tests in terms of maximum depth of wear for all the PEO treated samples

After the tribological tests the samples were also observed at multifocal microscope in order to better understand the mechanism of wear and failure, and the results are reported in Fig.5.22 for AZ91 and in Fig.5.23 for AZ80

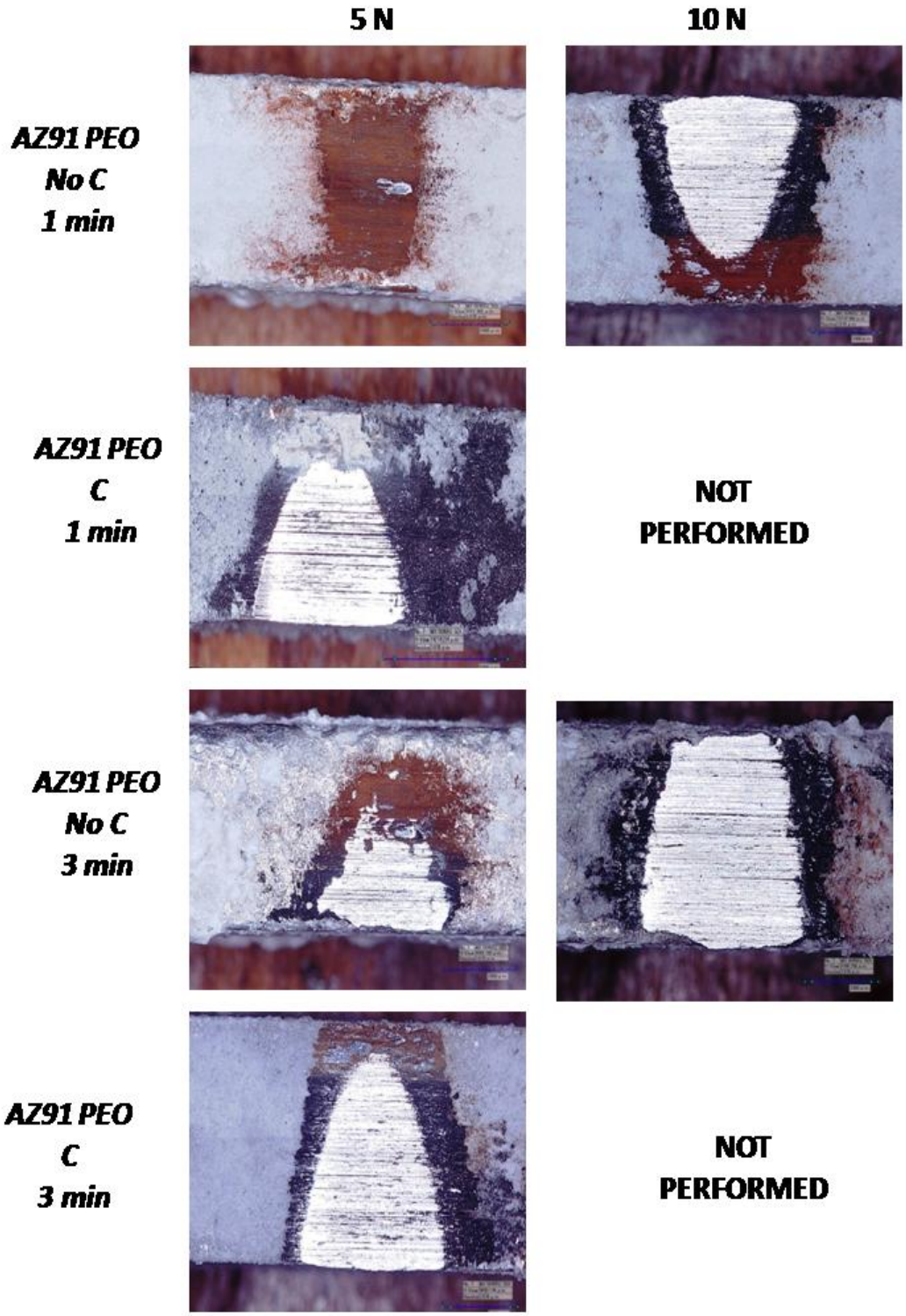

Fig.5.22 Images at the multifocal microscope of the different samples of PEO treated AZ91 after tribological test

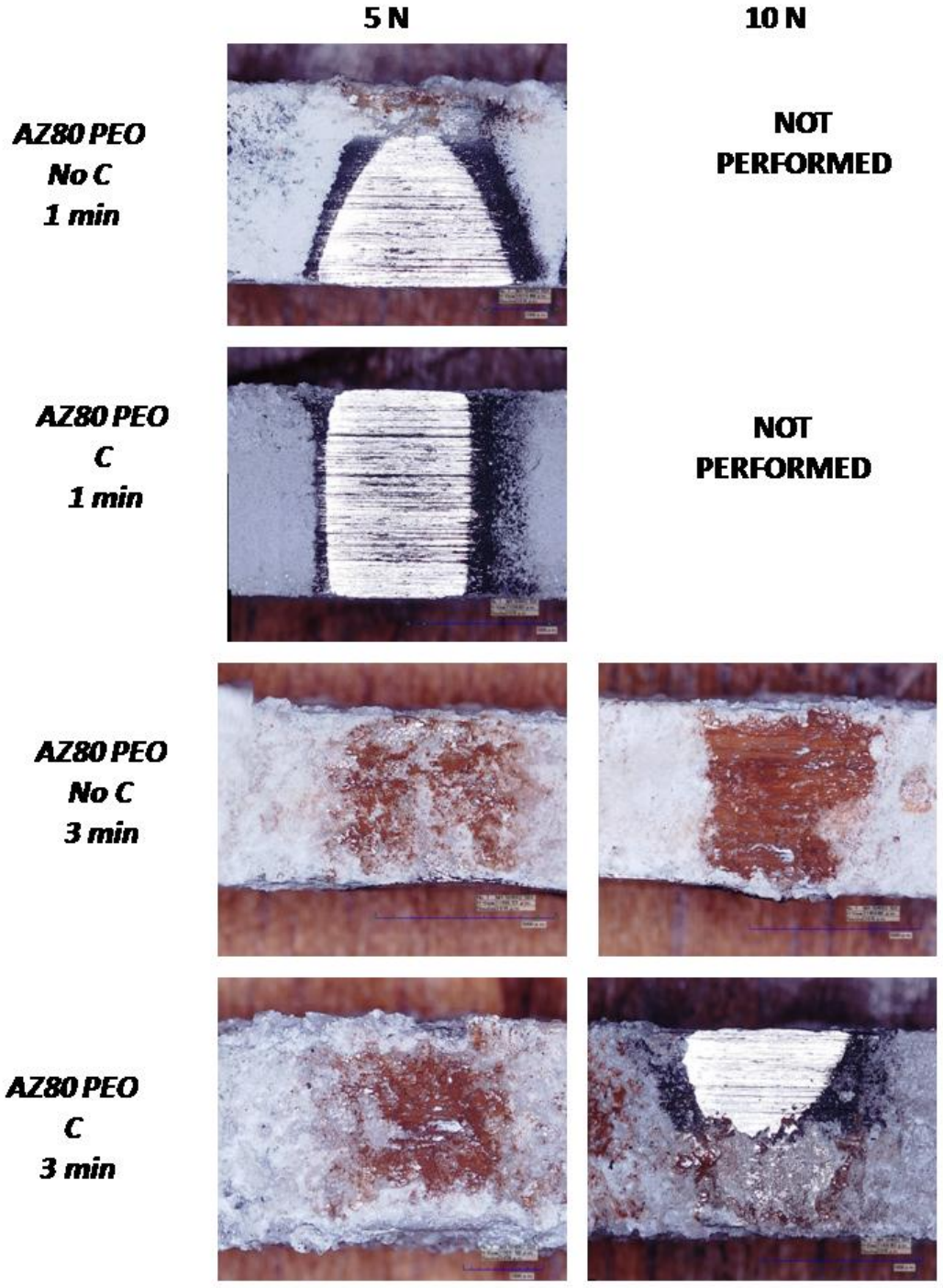

Fig.5.23 Images at the multifocal microscope of the different samples of PEO treated AZ80 after tribological tests

Considering the samples of AZ91 magnesium alloy, it can be observed that only the samples treated without graphite nanoparticles in the electrolyte exhibit a decrease in maximum depth of wear if compared with the untreated sample. This fact can be connected with the behavior of the coatings obtained with graphite in the electrolyte on this alloy: the

presence of graphite nanoparticles produce, in fact, an increase in the thickness and also in the hardness of the protective coating, but also an increase in the fragility of the oxide layer. This fact produce a decrease in the wear resistance because fragile failure can occur. The presence of fragile cracks can be detected in both the images recorded after the test at 5N in the samples treated with graphite in the electrolyte. For the samples treated without graphite nanoparticles in the electrolyte for 1 and 3 minutes improved wear resistance can be observed if compared with the untreated sample but only in the sample treated for 1 minute tested at 5N the PEO coating is still present on the surface of the sample after the tribological test (the red zone are zones rich of Fe_2O_3 coming from the antagonist). In the samples treated for 3 minutes without graphite nanoparticles tested at 5 and 10 N and in the sample treated for one minute tested at 10 N the uncoated substrate is instead clearly visible after the test.

Considering the samples of AZ80 magnesium alloy, it can be observed that the samples treated for three minutes with and without graphite nanoparticles in the electrolyte showed a remarkable decrease in the maximum depth of wear if compared with the untreated one. Instead both the samples treated for one minute with and without graphite nanoparticles show a decrease in the wear resistance, probably due to the low thickness of the protective coating combined with the fragility of the coating itself. From the images at the multifocal microscope it can be noted that in the sample treated for 3 minutes without graphite nanoparticles the PEO coating is still present on the surface after the tests at both loads, instead in the sample treated for three minutes with graphite after the test at 10 N the substrate can be seen on the surface due to the failure of the coating. In both the treatments performed at 1 minute with and without graphite nanoparticles the failure of the coating occurs already at 5N.

Summarizing the results regarding the tribological tests, was found that for both AZ91 and AZ80 magnesium alloy treated for one and three minutes the presence of graphite did not significantly improve the wear resistance and do not reduce the friction coefficient. This fact can be explained for the samples treated for one minute with the low thickness and the low quantity of graphite inside the coating, for the samples treated at three minutes with the high fragility of the oxide layer. Probably better results can be obtained with an intermediate treatment, about two minutes, in which a sufficient thickness could be obtained but also the fragility of the coating do not increase too much

5.6 CONCLUDING REMARKS

Samples of AZ91 and AZ80 magnesium alloy were used as substrate for PEO coatings using as electrolyte alkaline solutions containing graphite particles or nanoparticles. The use of graphite particles was early abandoned due to the too high dimensions of the particles that could not fill the pores of the PEO coatings. The use of graphite nanoparticles permit, instead, to obtain coatings with the pores almost totally filled by graphite. The presence of the graphite nanoparticles in the electrolyte produce also an increase in the thickness of the protective layer due to modification in the discharge phenomena produced by the conductive graphite particles. Moreover the samples containing graphite exhibits also an increase in the hardness of the oxide layer but also an higher fragility. Two different treatment times were tested: one minute and three minutes. Also the increase in the treatment time produce, as predictable from the literature, an increase in the thickness but also in the fragility of the coating. The microstructure of the coatings is the typical double layer structure of PEO coatings with the presence of the inner barrier layer that is more evident in the samples treated for three minutes due to the higher thickness. The coatings are mainly composed by magnesium and aluminum oxides, silicates and phosphates in accordance with the composition of the substrate and of the electrolyte. The presence of graphite is clearly evaluable inside the pores of the samples treated with an electrolyte containing graphite nanoparticles. The corrosion resistance of the different samples were tested with potentiodynamic polarization tests and EIS tests. All the PEO treated samples showed improved corrosion performances if compared with the untreated ones. The results showed also that the samples treated with graphite have improved corrosion performances, if compared with the ones treated for the same treatment time without graphite. This fact can be connected with the higher thickness of the oxide coating and with the increase in the barrier effect due to the sealing of the pores with the graphite. For AZ91 magnesium alloy the sample with the best corrosion performances is the one treated for three minutes with graphite nanoparticles instead for AZ80 alloy the samples treated with graphite for one and three minutes have a similar corrosion behavior from EIS tests. Tribological tests were also performed in order to evaluate the effect of the presence of graphite on the friction coefficient and on the maximum depth of wear. No significant differences in the friction coefficient were recorded for the different samples. For the samples of AZ91 only the samples treated without graphite present a decrease in the maximum depth of wear if compared with the untreated one instead for the samples of

AZ80 only the samples treated for three minutes exhibit improved wear resistance. The absence of significant improvements in the wear resistance is attributable for the samples treated at one minute to the low thickness of the coating and the consequent low quantity of graphite inside the oxide layer. Instead for the samples treated for three minutes the causes of this behavior can be found in the high fragility of the coating. Probably with an intermediate treatment time, for example two minutes, a good compromise between thickness and fragility could be obtained and the wear resistance maximized.

Chapter 6

Study of the addiction of silver particles in the PEO coating

In this chapter will be briefly discussed the possible addiction of silver particles in the electrolyte in order to produce a silver-containing oxide ceramic coating with an antimicrobial activity. The antimicrobial and disinfectant effect of silver is well known in literature [132-137]. Moreover the possible addition of silver particles and nanoparticles in the coatings permit to obtain an antimicrobial effect on various components without the use of detergents [138-140]. Also the post-treatment of anodized or PEO treated samples in order to insert in the coatings somewhat type of particles has been tested, and in the previous chapters the subject was detailed discussed. In this chapter will be described the preliminary results regarding the addiction of silver particles directly in the electrolyte used to produce PEO coating on aluminum alloys, in order to obtain an oxide coating that contain this silver particles. This could be very useful in the production of support devices (tray, furniture etc) used in the hospitals or however in the medical sphere because this particles could give an antimicrobial effect to the coated specimen without the use of detergents or additives. Moreover the particles will be directly put in the electrolyte used in PEO process and the production cycle will be so concluded in one step (two steps only if a sealing treatment is necessary).

6.1 PRODUCTION OF THE SILVER-CONTAINING PEO COATINGS

Samples of 7075 aluminum alloy were used as substrate for PEO coatings. The nominal composition of the alloy is reported in Tab.6.1 The behavior of the PEO treated samples was compared with the untreated sample and with a conventional anodized sample.

Tab. 6.1 Chemical composition of 7075 alloy (wt%).

Al	Mg	Zn	Cu	Others
90.7	3.1	4.1	0.9	1.2

The samples were polished following standard metallographic technique before the PEO treatment and then degreased using acetone in an ultrasound bath. The electrolyte used in the PEO process was constituted by an aqueous alkaline solution with 25 g/L of Na_2SiO_3 and 2.5 g/L of NaOH with two different addictions of silver particles. In detail in the first case was used a suspension of 25 ml in deionised water using as raw material 160mg of AgCl instead in the second case was employed a suspension of 25 ml in deionised water starting from 320mg of AgCl. These two samples are called sample A (the one obtained starting from 160mg of AgCl) and sample B (the one obtained starting from 320mg of AgCl). During the treatment, the substrate worked as anode and the cathode was a carbon steel mesh. The treatments were performed with the current density fixed at 0.3 A/cm^2 and the samples were treated for 4 minutes. After the treatment, the samples were washed with deionized water and ethanol and dried with compressed air. The two samples treated with silver particles in the electrolyte were analyzed and tested as produced but also after a treatment of sealing of the pores in boiling water (containing silver particles) for 15 minutes.

Also a sample treated with PEO process without silver particles in the electrolyte was produced and used as a reference in order to understand the possible modifications that the presence of the silver produce in the coating.

The conventional anodizing was performed maintaining the current density at 0.016 A/cm^2 for 25 minutes in a solution of sulfuric acid 20%. The temperature of the electrolyte was maintained constant at 18°C with the connection to a thermostatic bath. A lead plate was use as cathode. The convention anodized sample was produces in order to compare the properties of PEO coated samples with the one treated with the conventional anodizing technique. Also the addiction of silver particles in the electrolyte used in conventional anodizing was tested.

The surface of all the PEO treated and anodized samples can be observed in Fig.6.1 where a photographic analysis of the surfaces after the various treatments is reported.

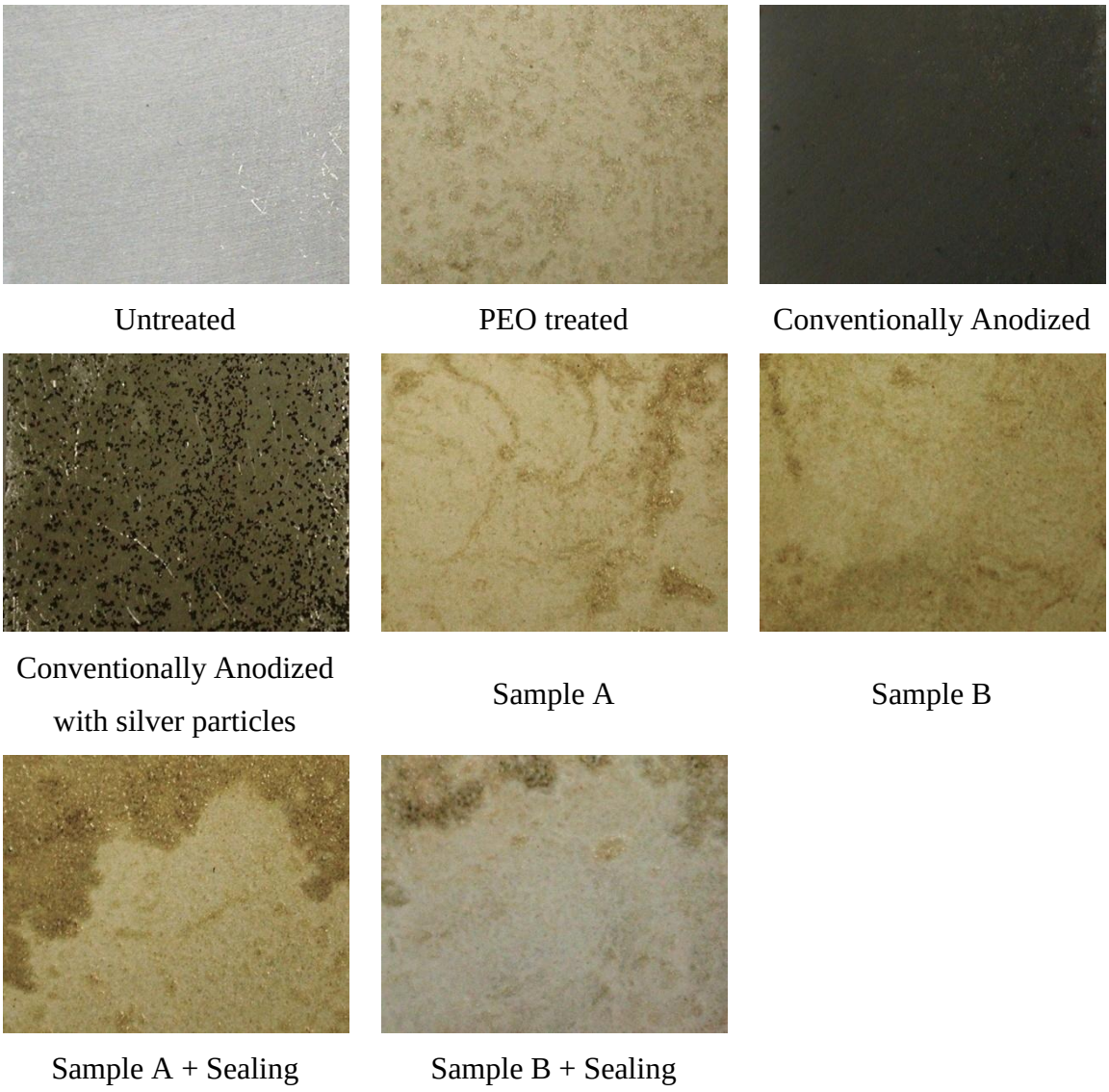

Fig.6.1 Photos of the surfaces of the different samples after the treatments

It can be observed the typical light grey color of PEO treated sample and the dark grey color of the anodized one. The presence of the silver particles cause the formation of a yellow layer on the surface but this is not present after the sealing treatment. Moreover it can be observed that on the sample conventionally anodized with silver particles in the electrolyte the oxide layer is not present and the start of pitting corrosion on the sample can be observed .

6.2 SURFACE ANALYSIS

The samples treated with PEO process using an electrolyte containing silver particles were first of all observed at the electron microscope in order to verify the presence of silver in the coating and in order to compare this samples with the ones obtained with PEO process without silver particles or conventional anodizing.

The surfaces and the cross sections of the reference samples, treated with PEO process with the same parameters but without silver particles, and treated with conventional anodizing are reported in Fig.6.2 and Fig.6.3 respectively.

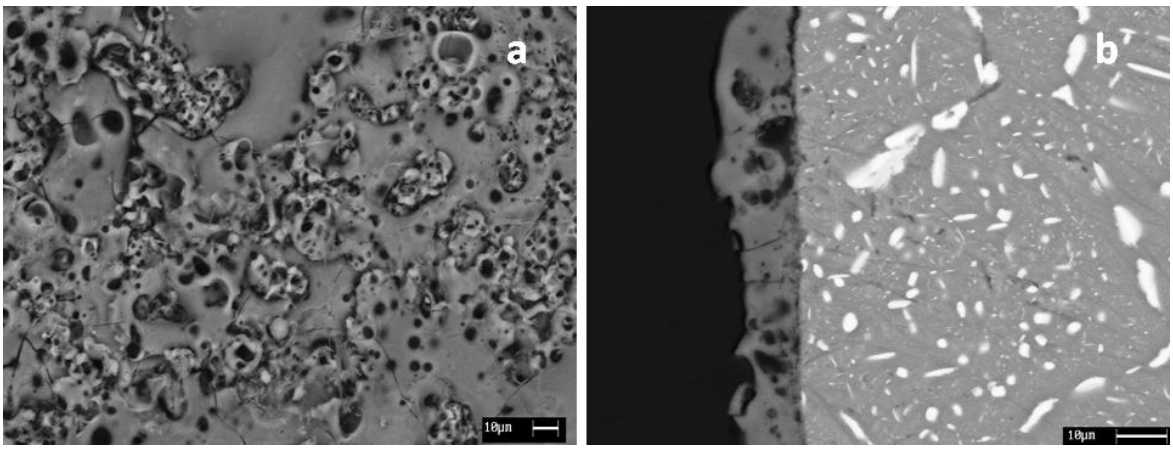

Fig.6.2 SEM images (BSE electrons) of the surface (a) and cross section (b) of the sample PEO treated without silver particles in the electrolyte

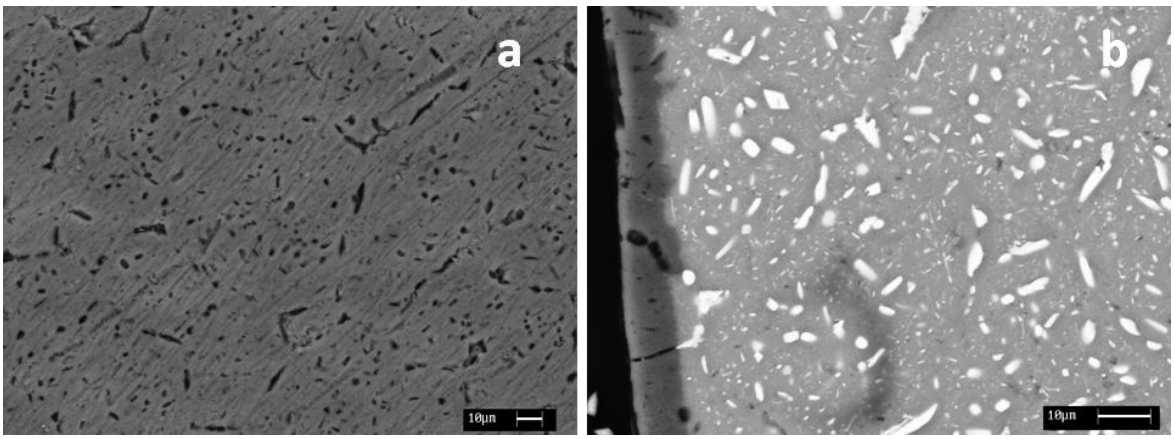

Fig.6.3 SEM images (BSE electrons) of the surface (a) and cross section (b) of the sample conventionally anodized

Regarding the PEO treated sample without silver particles in the electrolyte it can be observed the presence of a uniform and compact oxide coating with a thickness of about 11µm. The surface of the sample is the one typical of PEO coatings with a lot of pores and

micro-cracks. Also the anodized sample exhibit the conventional morphology found for this type of coating with an average thickness of about 9 microns and the presence of pores on the surface. The composition of the PEO coating obtained on 7075 AA without silver particles is in accordance with the composition of the substrate and of the electrolyte as reported in the EDS spectra in Fig.6.4 In detail it can be observed that the coating is mainly composed by aluminum and silicon oxides with the presence also of sodium oxide.

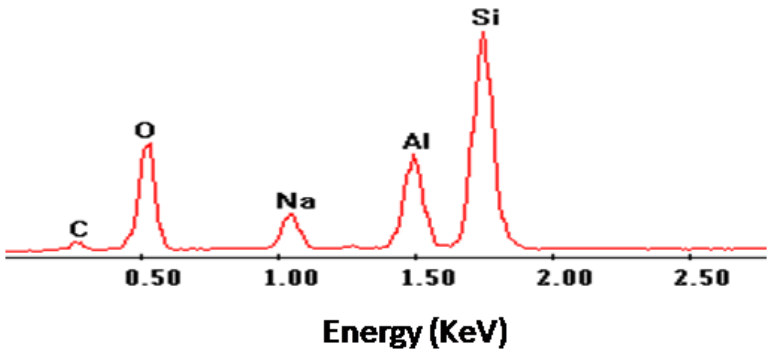

Fig.6.4 EDS analysis of the coating in the sample treated without silver particles in the electrolyte

The SEM micrographs of the surfaces and the cross sections of the sample called "sample A" (with the electrolyte containing a solution obtained starting from 160mg of AgCl) and of the "sample B" (electrolyte containing a solution obtained starting from 320mg of AgCl) are reported respectively in Fig.6.5 and Fig.6.6

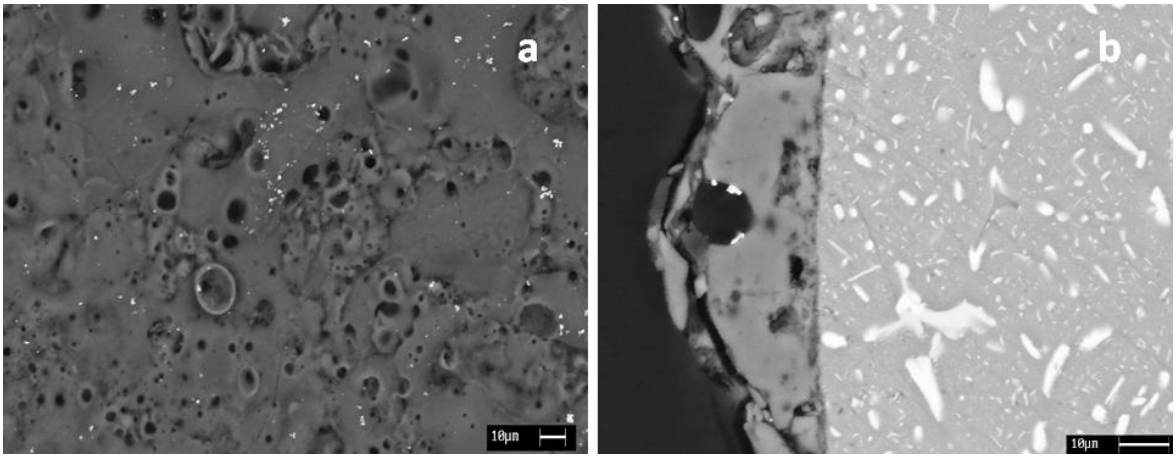

Fig.6.5 SEM images (BSE electrons) of the surface (a) and cross section (b) of the sample A (PEO treated with the electrolyte containing a solution obtained starting from 160mg of AgCl)

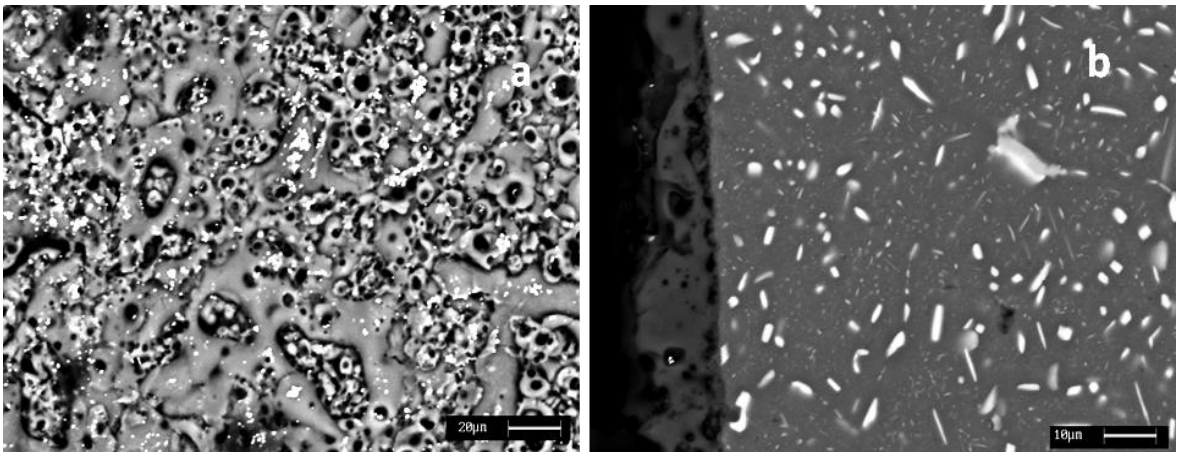

Fig.6.6 SEM images (BSE electrons) of the surface (a) and cross section (b) of the sample B (PEO treated with the electrolyte containing a solution obtained starting from 320mg of AgCl)

First of all it can be observed that the presence of silver particles in the electrolyte seem to not influence the formation of the oxide ceramic coating. In fact the protective layer, as was found for the sample PEO treated without silver particles, is adherent to the substrate and homogeneous for both the quantities of silver particles. The surfaces of the samples have also in this case the typical porous morphology of PEO coatings. The observation in backscattered electron mode allows to easily evaluate in both the samples the presence of the silver particles on the oxide coating (the white spots). However the nature of the white spots was also confirmed by EDS micro-analysis as reported in Fig.6.7 for the sample A. From the spectra result clear that the particles are constituted by Ag.

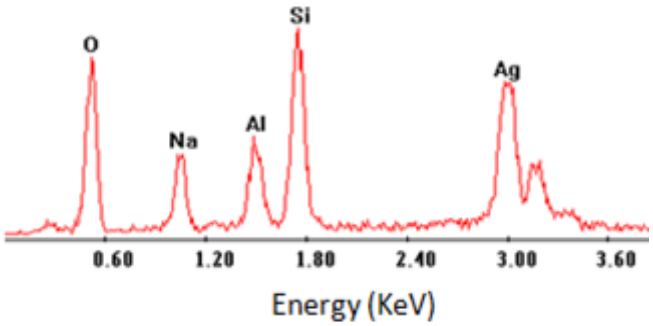

Fig.6.7 Punctual EDS micro-analysis on the surface of the sample A on a white spot

It can also be observed that the distribution of the silver particles on the surface of the sample is uniform, and that they go into the pores but also in the rest of the surface. This second remark is also more clear from the observation of the cross section of the coatings, where the white spots are mainly inside but also outside of the pores. Excluding the

presence of the silver particles, the composition of the oxide ceramic coating remain the same, as evidenced by the punctual EDS analysis in Fig.6.8, recorded in a zone of the surface without silver particles.

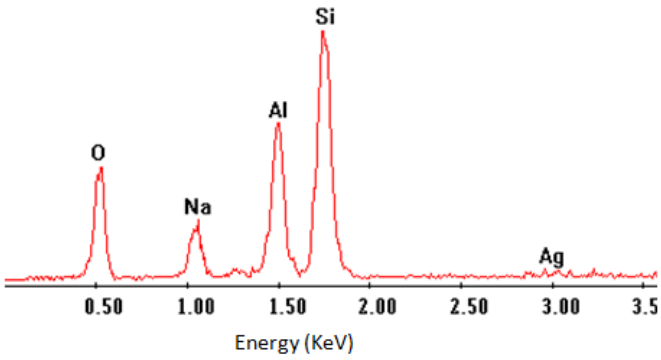

Fig.6.8 Punctual EDS micro-analysis on the surface of the sample A out of the white spots

Some further considerations regarding the average dimensions of the silver particles can be discussed observing the surfaces of the samples at higher magnifications as reported in Fig.6.9. In detail for both the samples A (Fig.6.9a) and B (Fig.6.9b) (and so regardless the concentration of silver particles) it can be observed the presence of some bigger agglomerates on the surfaces of the sample but also the presence of some sub micrometric particles.

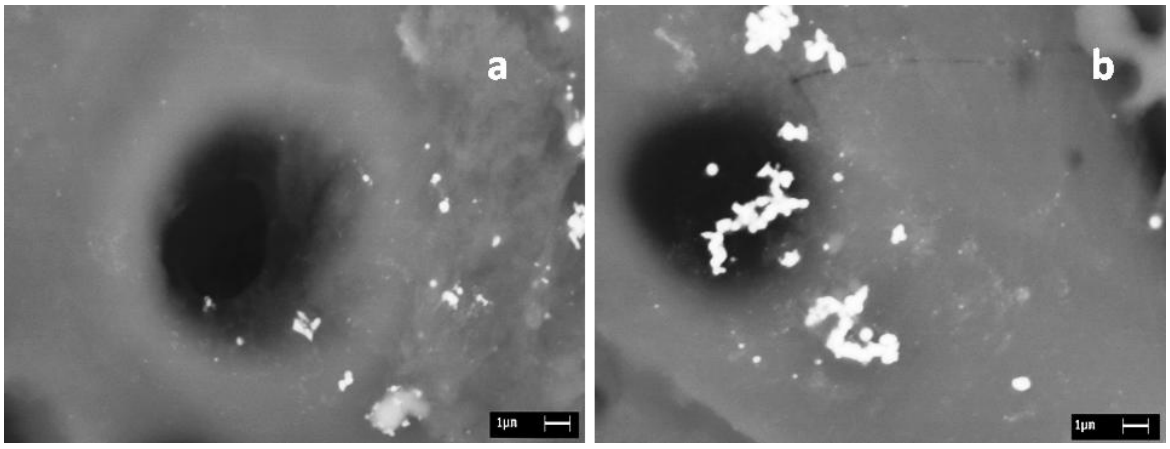

Fig.6.9 SEM images (BSE electrons) of the surface of the sample A (a) and B (b) at higher magnifications

Comparing sample A and sample B, it can be noted from the previously reported images that in sample B the quantity of silver particles on the surface is higher than in sample A. This is accordance with the composition of the electrolyte.

As was discussed in the previous chapters, the sealing of the pores that characterized the PEO coatings is always necessary if the specimen need good corrosion resistance. In fact without this type of treatment no protection against galvanic corrosion can be given by the oxide ceramic coating present on the surface. In the devices used in the medical sphere no corrosion is permitted so on this samples the sealing treatment must be performed. In this case a treatment of sealing in boiling water for 15 minutes minute was performed on sample A and sample B. Moreover silver particles are also put in the boiling water solution in order to produce a sealing treatment with silver particles.

After the sealing treatment the surfaces and the cross sections of the coatings were again observed with electron microscope in order to evidence some differences due to the performed treatment. The results are reported in Fig.6.10 for the sample A after the sealing and in Fig.6.11 for the sample B after the sealing.

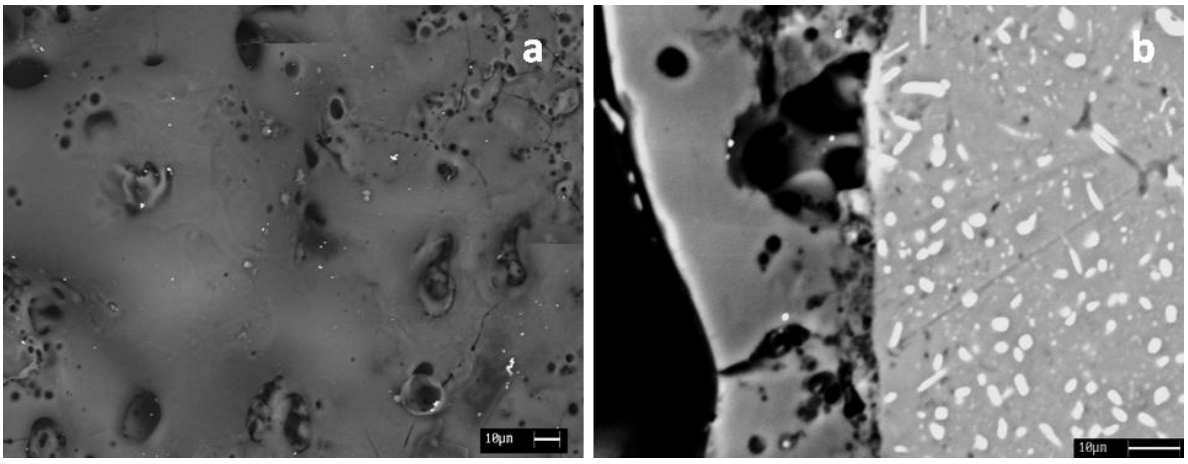

Fig.6.10 SEM images (BSE electrons) of the surface (a) and cross section (b) of the sample A after the sealing treatment

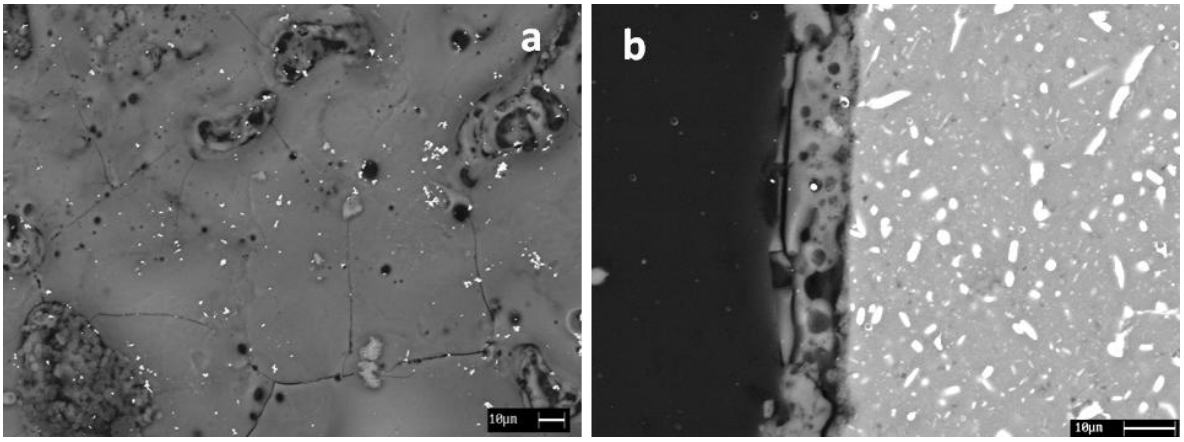

Fig.6.11 SEM images (BSE electrons) of the surface (a) and cross section (b) of the sample B after the sealing treatment

As can be seen, after the treatment the coating remains adherent to the substrate and the unique main difference is that the pores are now sealed as can be clearly seen especially for the sample B. This fact is very important because in this way the barrier effect of the oxide coating is significantly increased. The presence and distribution of silver particles seem not to be influenced by the sealing treatment and this fact is also confirmed by the observation of the surfaces at higher magnifications reported in Fig.6.12

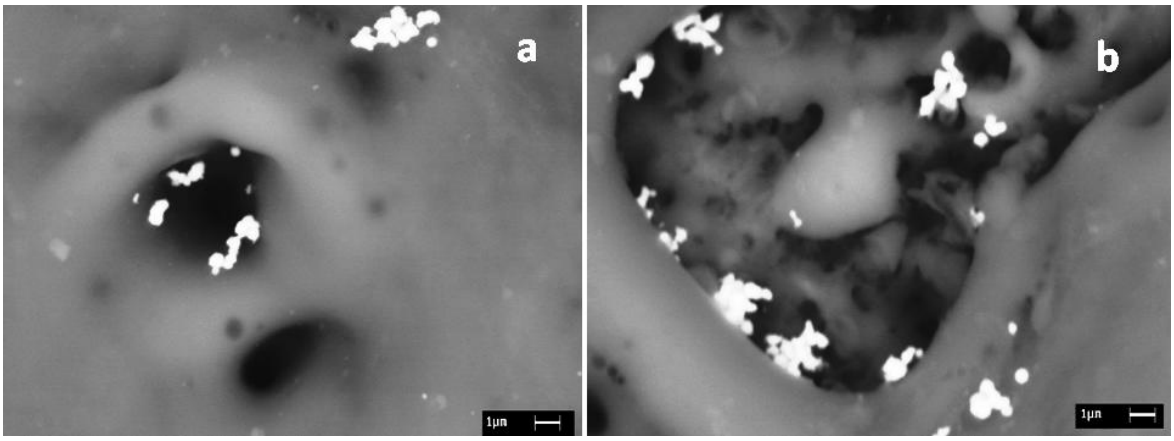

Fig.6.12 SEM images (BSE electrons) of the surface of the sample A+ sealing (a) and B+sealing (b) at higher magnifications

In detail, from the analysis at higher magnifications the presence of agglomerates and also sub micrometer silver particles is confirmed also after the sealing treatment. Moreover it is also more clear that the pores on the surface result sealed. The distribution of the particles is not influenced by the sealing treatment and remain homogeneous on the surface. In the cross section the particles can be observed mainly in the pores but are present also out of the pores.

The composition of the oxide ceramic coating do not result influenced by the sealing.

Also the addiction of silver particles in the electrolyte used for conventional anodizing process was tested, but the presence of the conductive silver particles influence the mechanism of formation of the anodized layer and do not permit to obtain a good coating. Moreover it causes pitting of the surface as can be observed in Fig.6.1.

This evidence is in accordance with the literature where is known that conventional anodizing require, if compared with PEO, a more strictly control of the process parameters.

In conclusion, the addiction of silver particles in the electrolyte used in PEO process allows to obtain an adherent and uniform coating that contain both inside and outside of the pores the silver particles. This particles are very important because they confer to the

PEO treated specimen an antimicrobial activity that permit to use these components for medical scopes. However for this type of applications the total absence of corrosion phenomena is required so, to improve the corrosion resistance, a treatment of sealing in boiling water with silver particles was performed. The treatment do not influence the coating or the distribution of the silver particles but produce the sealing of the pores and the increase in the barrier effect of the coating.

6.3 CORROSION BEHAVIOUR

To evaluate the effect of the different treatments on the corrosion resistance of the various sample potentiodynamic polarization tests were performed, in an electrolyte that simulate an aggressive environment containing both chlorides and sulfates (so in one of the worst condition for this kind of alloy). The corrosion resistance of the different samples was compared. The potentiodynamic polarization plots of the different samples are reported in Fig.6.13 and the corrosion current densities and corrosion potentials that could be extrapolated from the curves are summarized in Tab.6.2.

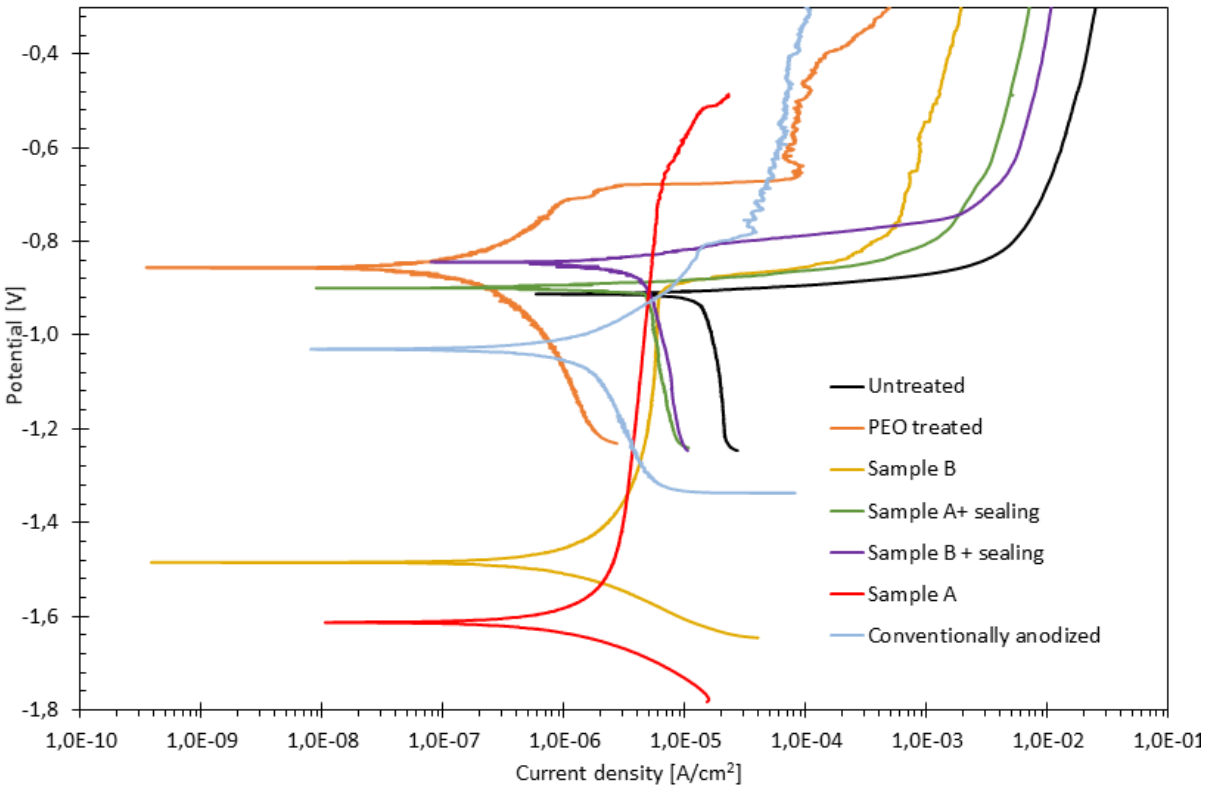

Fig.6.13 Anodic polarization plot for the different samples (test electrolyte: 0.1M Na_2SO_4 + 0.05M NaCl)

Regarding the corrosion resistance of the various samples, it can be firstly observed that the sample with the best corrosion performance is the one treated with PEO process but without silver particles in the electrolyte. In fact this sample is the one with the higher value of corrosion potential (that indicates the nobility of the sample) and the lower value of corrosion current density, directly connected with the corrosion rate with the Faraday law. In detail the corrosion current density of the sample treated with no silver particles in the electrolyte is about two order of magnitude lower than the untreated sample. The conventionally anodized sample has an intermediate corrosion behavior between the untreated sample and the PEO coated sample; this in accordance with the well known fact that the PEO coatings are characterized by improved corrosion resistance if compared with conventionally anodization.

Tab.6.2 Corrosion potentials and corrosion current densities for the different samples

	E_{corr} [V]	I_{corr} [A/cm^2]
Untreated	-0.9	$1.5x10^{-5}$
PEO treated No Silver	-0.86	$1.5x10^{-7}$
Anodized	-1.4	$1x10^{-6}$
Sample A	-1.62	$1x10^{-6}$
Sample B	-1.48	$1x10^{-6}$
Sample A + Sealing	-0.92	$3.5x10^{-6}$
Sample B + Sealing	-0.86	$3x10^{-6}$

Focusing now on the samples treated with silver particles in the electrolyte, it can be observed that the presence of silver cause a remarkable decrease in the corrosion potential in comparison with the sample treated without particles. This fact is confirmed both in sample A and sample B and is linked with the local galvanic couple that can be formed between the silver and aluminum causing galvanic corrosion. Also the current density increase of about one order of magnitude in the samples treated with silver particles. This behavior is due to the high difference in the scale of potentials between silver and aluminum that strongly favors the corrosion phenomena. The sealing treatment, as was previously remarked, allows to reduce the problems connected to galvanic corrosion enhancing the corrosion potential of the samples: in fact the samples after the sealing treatment are characterized by a corrosion potential similar than the sample treated without

silver particles. Moreover the corrosion current density is not influenced by the sealing treatment and remain the same both in the sample A and in the sample B after the treatment.

The addiction of silver particles cause a general decrease in the corrosion properties but thanks to the sealing treatment the corrosion resistance is still acceptable and in addition the coating have, thanks to presence of the silver particles, an antimicrobial effect. Comparing the two samples treated with different quantities of silver particles in the electrolyte it can be observed that the corrosion behavior of this samples is the same. So the silver particles content do not influence the corrosion resistance. Instead is know that the antimicrobial effect is connected with the silver content so the sample B (with the sealing) is preferable than sample A. It can also be remarked that the samples PEO treated and sealed with silver particles increased their corrosion performances if compared with the conventionally anodized sample: in fact the corrosion current density is the same but an increase in the corrosion potential can be observed. As was previously said, the test on the sample anodized with silver particles in the electrolyte wasn't possible because the presence of silver interact with the growing mechanism of the anodized layer.

6.4 CONCLUDING REMARKS

In this chapter was studied the effect of the addiction of silver particles in the oxide film formed with PEO process in order to give to the PEO treated specimens of 7075 aluminum alloy an antimicrobial activity. The antimicrobial effect of the silver particles is well know so the study focus on the mechanism to introduce these particles in the coating and on the corrosion resistance of the samples.

The introduction of the silver particles in the coating can be simply obtained by adding these particles to the electrolyte. The particles do not influence the mechanism of formation of the oxide coating during PEO process and can be found after the treatment both in the pores and out of the pores. The distribution of the silver particles is uniform and the obtained coatings are adherent and uniform. With conventional anodizing the simply addition of the particles to the electrolyte is not possible because their presence prevent the formation of a good-quality coating. The obtained samples exhibits a remarkable decrease in the corrosion resistance if compared with the sample PEO treated without silver particles due to the galvanic couple formed between silver and aluminum. This problem can be overcame with a sealing treatment in boiling water containing silver particles was

performed. The sealing treatment do not influence the distribution and the number of the silver particles, neither affect the oxide coating, but after the treatment from SEM observation the pores appears sealed. The corrosion resistance of the samples after the sealing treatment result improved: in fact the corrosion current density remain the same as before the treatment but a remarkable increase in the corrosion potential was recorded. This fact, connected with the improved barrier effect of the coating, reduces the problems of galvanic corrosion and permit to obtain coatings with antimicrobial effect with an acceptable corrosion resistance.

Chapter 7

Plasma electrolytic oxidation coatings on steels

Steel is one of the most used materials in industrial applications due to several good properties: high strength, high toughness good machining ability and low cost. In particular, carbon steels are often used in structural applications. However, this type of material is vulnerable to corrosion and the substitution with stainless steel is not always possible due to economic problems. Surface treatments on steels and in detail the production of oxide ceramic coatings for corrosion protection are one of the most common ways to solve these problems. Various techniques (PVD, CVD, arc-plasma discharge) have been employed to produce these ceramic coatings but most of these methods require high temperature on substrates, which seriously decreases their mechanical properties [141]. Plasma electrolytic oxidation (PEO) treatment seems to solve this problem since the whole substrate is nearly kept at room temperature. Compared to the light alloys, PEO studies on steels, which remain the most used metals in engineer, are relatively rare and only few works about the application of PEO treatment on carbon steel can be found in literature [142-144]. In this works some improvements in both physical and mechanical properties of sample were reported. The results obtained during these researches shown in particular that mechanical properties such as thermal shock resistance, bonding strength, friction coefficient and corrosion resistance of specimens were acceptably improved after PEO treatment. Also a work regarding the influence of PEO treatment on the corrosion resistance of Ck45 steel can be found [145] and the results shows that the corrosion properties resulted improved after PEO treatment. However PEO process was never applied in literature on alloyed steels.

In this chapter will be studied the effects of PEO treatment on a low-alloyed steel and in detail on the corrosion resistance of the material. In particular, the effectiveness of

different types of electrolytes was tested, using high current densities and relatively long treatment times.

7.1 PRODUCTION OF PEO COATINGS

Samples of 39NiCrMo3 were used as substrate for PEO coatings. The nominal composition of the alloy is reported in Tab. 7.1

Tab. 7.1 Nominal composition of the steel used as substrate for PEO process (%wt).

C	Cr	Mo	Ni	Si	Mn	Others	Fe
0.407	0.848	0.189	0.842	0.273	0.739	0.340	Bal.

Before the PEO treatment, the samples were polished following standard metallographic technique and then degreased using acetone in ultrasound. During the treatment, the sample worked as anode and a bar of SAF2507 stainless steel was used as cathode. The treatments were performed maintaining the current constant, letting the potential free to vary. The current density was fixed at 0.4 A/cm^2 and the samples were treated for 10 minutes. Different electrolytes were tested in order to optimize the amount of silicates and aluminates to obtain the better corrosion performances. In detail, the following solutions were tested: an electrolyte, called electrolyte A, containing 10 g/l of NaOH, 10 g/l of $NaAlO_2$ and 10 g/l of Na_2SiO_3; the electrolyte B containing 10 g/l of NaOH, 10 g/l of $NaAlO_2$ and 100 g/l Na_2SiO_3; the electrolyte C with 10 g/l of NaOH, 10 g/l of Na_2SiO_3 and 100 g/l of $NaAlO_2$. After the treatment, the samples were washed with deionized water and ethanol and dried with compressed air.

The starting potential was about 30 V for all the samples and the final potential is reported for the different samples in Tab. 7.2. It can be observed a higher value of the final potential for the sample obtained with electrolyte C, so with high concentrations of sodium aluminates. During the process, the formation of micro-discharges on the surface of the samples occurred and produced the growth of an oxide coating.

Tab. 7.2 Initial and final potential recorded for the different samples during PEO process

	Starting Potential [V]	Final Potential [V]
Electrolyte A	30	280
Electrolyte B	30	200
Electrolyte C	30	315

Also the number and intensity of micro-discharges is influenced by the final potential recorded during the treatment: samples with higher final potential shows a larger number of micro-discharges during the production process. The complete voltage vs time plot for the different PEO treated samples is reported in Fig.7.1.

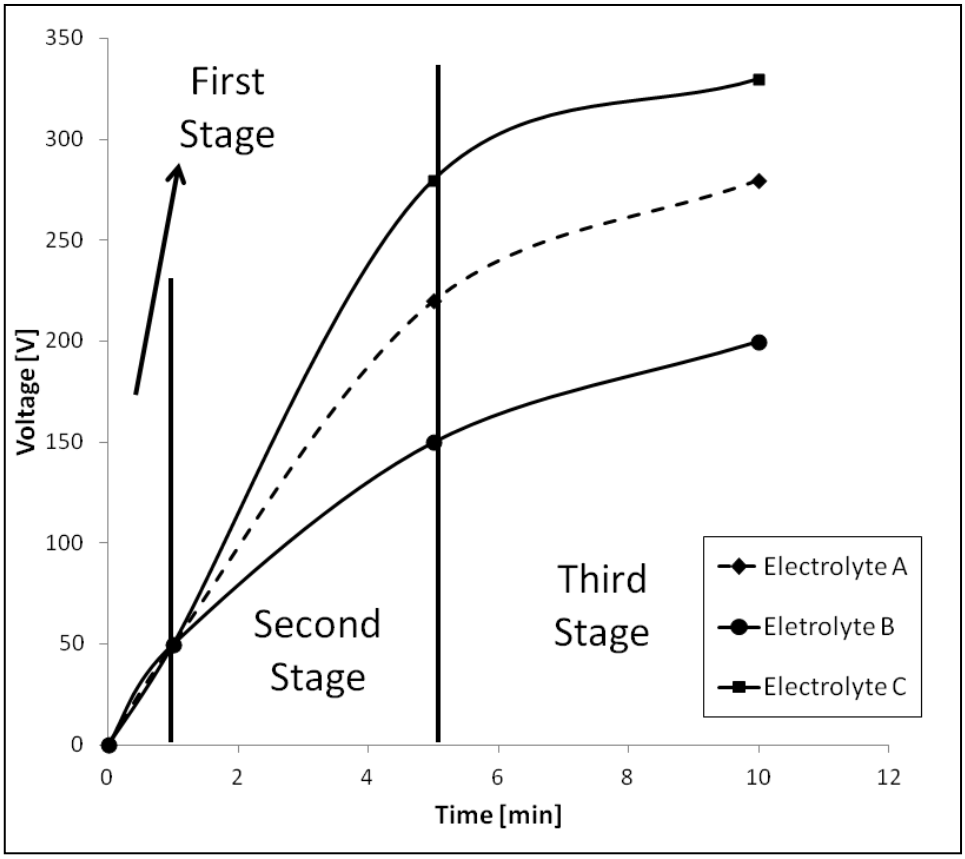

Fig.7.1 Voltage versus Time plot and different stages of PEO process for the samples treated with different electrolytes

It can be observed for all the samples the typical three stage evolution of PEO process but the sample treated with electrolyte C is characterized by an higher level of plateau of the potential during the third stage.

7.2 CORROSION BEHAVIOUR

The corrosion resistance of the obtained samples was studied with anodic polarization tests and EIS tests in an electrolyte containing both sulfates and chlorides.

The anodic polarization curves are reported in Fig. 7.2 and the values of i_{corr} and E_{corr} for the different samples are summarized in Tab. 7.3.

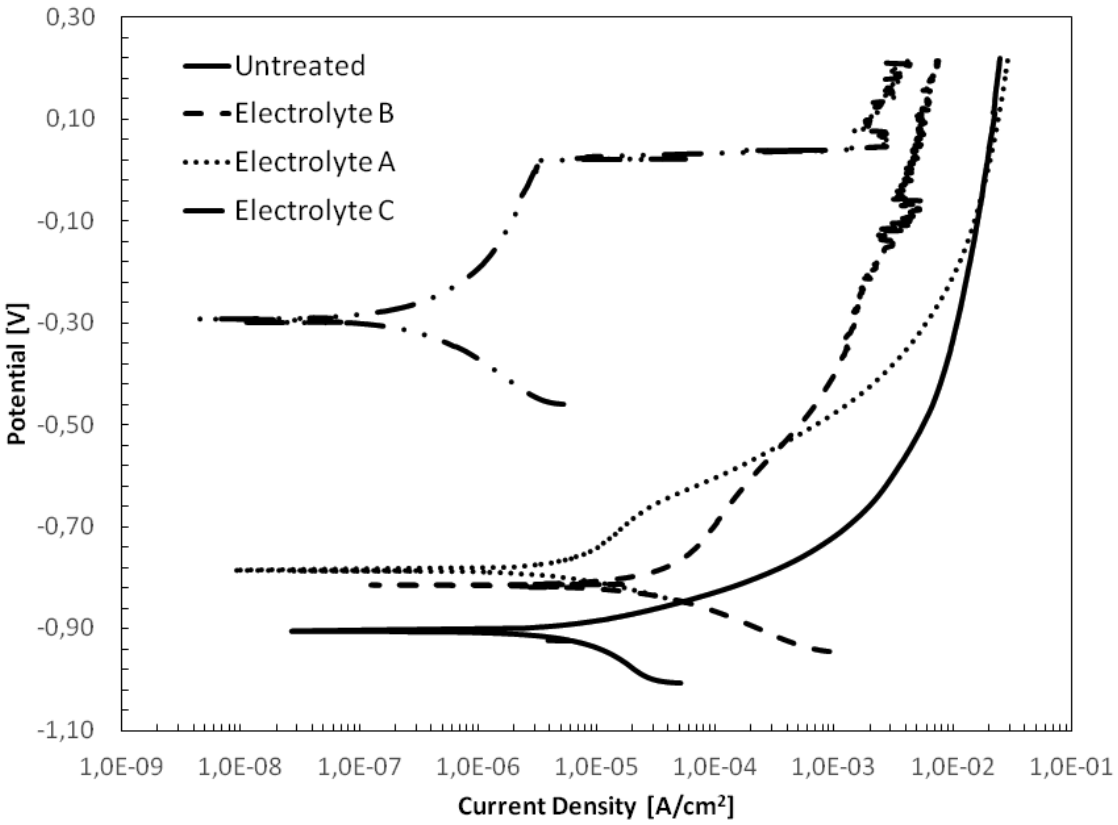

Fig. 7.2 Anodic polarization plots for the samples PEO treated in different electrolytes (test electrolyte: 0.1M Na_2SO_4 + 0.05M NaCl)

Tab. 7.3 Values of corrosion current density and corrosion potential for the different samples after anodic polarization test

	E_{corr} [V]	I_{corr} [A/cm^2]
Untreated	-0.9	$1x10^{-5}$
Electrolyte A	-0.78	$6x10^{-6}$
Electrolyte B	-0.83	$2x10^{-5}$
Electrolyte C	-0.3	$2x10^{-7}$

From the anodic polarization plots and the corrosion data previously reported a remarkable increase in the corrosion resistance can be observed for the sample obtained with the electrolyte C. In fact, the sample obtained with high concentrations of sodium aluminates

in the electrolyte is characterized by the lowest value of corrosion current density, about two order of magnitude lower if compared with the untreated sample. Moreover, the sample obtained with the electrolyte C is the one with the higher value of E_{corr}, about 0.6 V higher than the other samples. The sample obtained with the electrolyte B, with high concentrations of sodium silicate, has the same corrosion performances of the untreated sample. Therefore, this last treatment was not useful because an improvement in the corrosion performance was not observed. The sample treated with the electrolyte A, with the same concentration of aluminates and silicates, exhibits improved corrosion performances if compared with the untreated sample. However, the corrosion current density is one order of magnitude higher and the corrosion potential is 0.5 V lower, if compared with the sample obtained with electrolyte C.

To better understand the corrosion behavior also EIS tests were performed on the samples treated with the different electrolytes. Experimental data were fitted using the equivalent circuits reported in Fig.2.6. In particular, as explained in the previous chapters, the simpler circuit (Fig.2.6a) was used to fit data coming from the untreated sample and from the sample treated with electrolyte A and electrolyte B, where a single layer is formed as will be further discussed. The equivalent circuit reported in Fig.2.6b was instead used to fit data coming from the sample treated in electrolyte C, in order to consider also the presence of the typical double layer structure of PEO coatings. A good fitting quality was obtained for all samples, with chi-squared values varying between 0.005 and 0.03.

Nyquist impedance plots and results of the fitting of the experimental data for the samples treated using electrolytes containing different concentrations of sodium aluminates are reported in Fig. 7.3 and Tab. 7.4.

From the analysis of the data reported in Tab.7.4 it can be observed that the sample characterized by the higher value of polarization resistance R_3, that is a direct measure of the corrosion resistance offered by the internal barrier layer, is the sample obtained with electrolyte C so with high concentrations of sodium aluminates. In detail the value of R_3 of the sample treated with electrolyte C is two order of magnitude higher if compared with the untreated sample and over one order of magnitude higher if compared with the samples treated with electrolyte A and B. This result confirm the ones coming from anodic polarization tests where a remarkable decrease in the corrosion current density and increase in the corrosion potential was recorded for the sample treated with electrolyte C. For this sample also a value of R_2, representing the polarization resistance of the external porous

layer, was calculated with the fitting of the experimental data. This value cannot be compared with the other samples because only the sample treated with electrolyte C shows the typical double layer structure of PEO coatings as will be after reported. However can be observed that the value of R_2 is significantly lower than the one of R_3 and that indicates that the major protection against corrosion phenomena is given by the internal barrier layer.

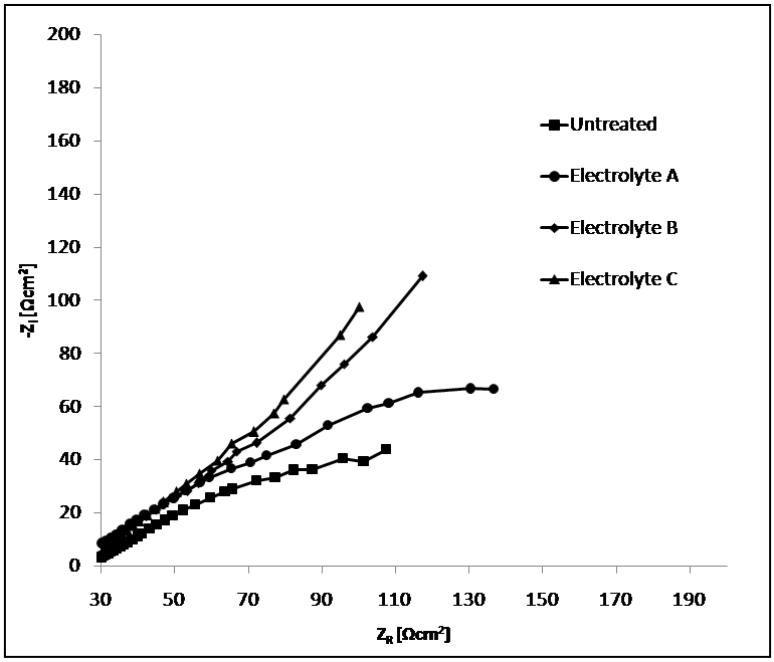

Fig. 7.3 Nyquist plots for 39NiCrMo3 samples PEO coated with different electrolytes (test electrolyte: 0.1M Na_2SO_4 + 0.05M NaCl)

Tab.7.4 Equivalent circuit data for the samples treated with different electrolytes obtained in a solution containing both sulphates and chlorides

	Untreated	**Electrolyte A**	**Electrolyte B**	**Electrolyte C**
R_1 [Ω*cm^2]	27.85	20.73	23.27	25.09
R_2 [Ω*cm^2]	-	-	-	1000
R_3 [Ω*cm^2]	184.9	800	483.7	20000
Q_1 [F*Hz^{1-n}]	-	-	-	3.12 x10^{-5}
n_1	-	-	-	0.68
Q_2 [F*Hz^{1-n}]	7.4 x10^{-4}	1.01 x10^{-4}	6.7 x10^{-4}	5.04 x10^{-5}
n_2	0.54	0.65	0.67	0.56

Moreover it can be observed that the minimum value of Q_1 and Q_2 was found for the sample treated with electrolyte C. The values of Q can be linked with the capacitance with Eq.4.1 and the values of Q (and so of the capacitances) calculated for the other samples, are significantly higher. The value of C can be correlated with the thickness of the protective oxide layer, using Eq.2.2, valid for a parallel-plate capacitor, corresponding to a homogenous oxide layer as was described in the previous chapters.

Therefore, the lower value of *C* calculated with the Eq.2.2 for the sample treated with electrolyte C, can be related to a thicker layer of this sample. This fact, as will be discussed, is confirmed by the surface characterization of the different samples.

7.3 SURFACE ANALYSIS

The thickness and morphology of the oxide layer formed during PEO process were analyzed by SEM. The cross section and the surface of the sample obtained with electrolyte C, that was the best in terms of corrosion performance, are reported in Fig. 7.4. The PEO process allowed the formation of a thick layer of about 50 µm, and this layer can be divided in an inner layer (grey color) mainly composed by iron and chromium oxides and a outer layer (white color), mainly composed by iron and aluminum, with a lower oxygen content, if compared with the inner layer (Fig. 7.4a). In the outer layer can be also observed some grey islands, rich in chromium and iron oxides. EDS semi-quantitative analysis of the outer and inner oxide layers are reported in Tab. 7.4

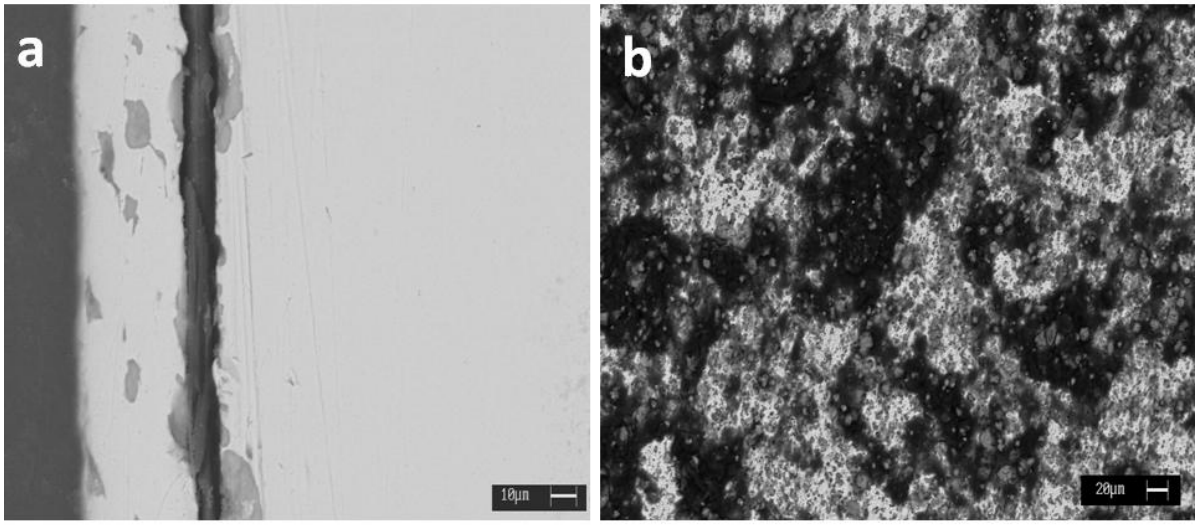

Fig. 7.4 BSE-SEM images of the cross section (a) and the surface (b) of the sample of 39NiCrMo3 PEO treated with electrolyte C

Tab.7.5 EDS semi-quantitative analysis of the cross section of PEO coated sample obtained with electrolyte C (%wt).

	Fe	Al	Cr	O
Inner layer	68.07	2.25	5.26	24.41
Outer layer	56.16	28.5	1.6	13.74

The formation of an inner and an outer layer is typical of the PEO coatings and the presence of chromium in the inner layer can be connected with the higher tendency of oxidation of this element. Moreover the presence of chromium in this layer can explain the improved corrosion performances of the sample treated with electrolyte C and also the evidence, coming from the fitting of the experimental data of EIS test, that the inner layer is more protective than the external layer.

The surface of the sample resulted rich of pores and micro-cracks and was not homogenous. In fact, two different zones can be found: a white zone, rich of pores, and a black zone rich of micro-cracks. From EDS analysis the white zone resulted mainly constituted by iron oxide, whereas the black zone by aluminum oxide, as reported in Tab.7.6

Tab. 7.6 EDS semi-quantitative analysis of the surface of PEO coated sample obtained with electrolyte C

	Fe%	Al%	Cr%	O%	Si%
White Zone	62.60	13.54	1	22.87	0
Black Zone	9.96	49.46	0.71	39.09	0.78

The cross section and the surface of the sample obtained with electrolyte B are reported in Fig. 7.5. The coating is about 15 μm thick and seems adherent and uniform. From EDS analysis, the protective layer resulted mainly constituted by silicon, aluminum, chromium and iron oxide, as is reported in Tab. 7.7.

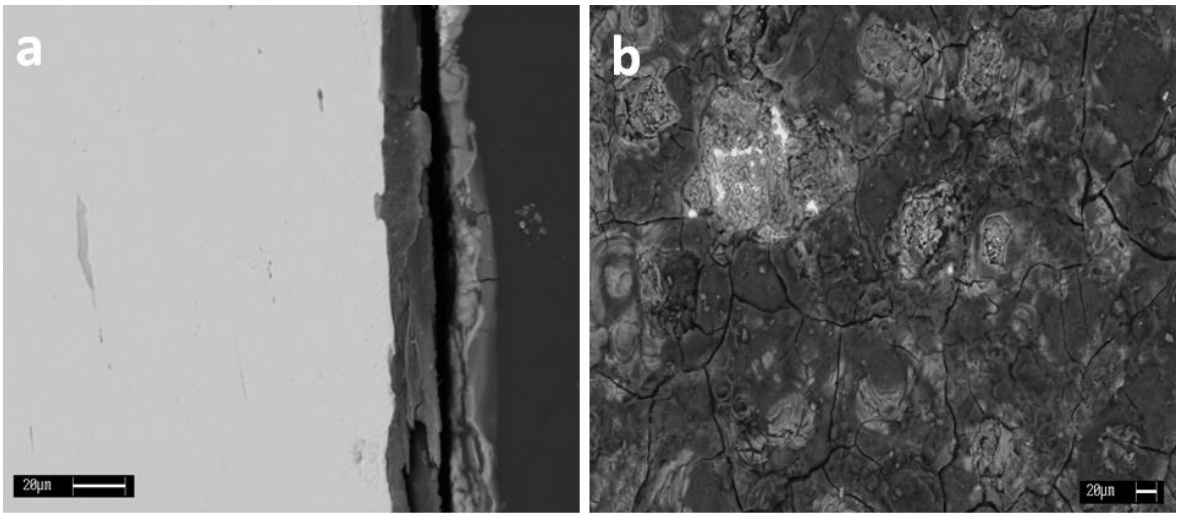

Fig. 7.5 BSE-SEM images of the cross section (a) and the surface (b) of the sample of 39NiCrMo3 PEO treated with electrolyte B

Tab.7.7 EDS semi-quantitative analysis of the cross section and the surface of PEO coated sample obtained with electrolyte B (%wt).

	Fe	**Al**	**Cr**	**O**	**Si**
Cross Section	70.38	8.13	1.55	10.37	9.57
Surface	32.18	9.76	0.57	33.07	23.80

The surface resulted constituted by two different zones: the darker zones, with a lot of cracks, rich in silicon and the lighter zones, with a lot of pores, rich in iron. The poor corrosion performances of the layer obtained with electrolyte B can be correlated with:

i) the thinner coating, if compared with the one on the sample obtained with electrolyte C;

ii) the increase in the number of micro-cracks in the zones of the surface with lower amounts of iron;

iii) the absence of the typical double-layer structure of PEO coatings.

In particular, the increase of the presence of micro cracks produced the decay of the barrier effect of the oxide coating. Moreover, the absence of the inner layer rich in chromium oxides, that typically give the major protection in steels against corrosion, negatively affect the corrosion properties.

The results of the SEM observation for the sample treated with electrolyte A is reported in Fig. 7.6.

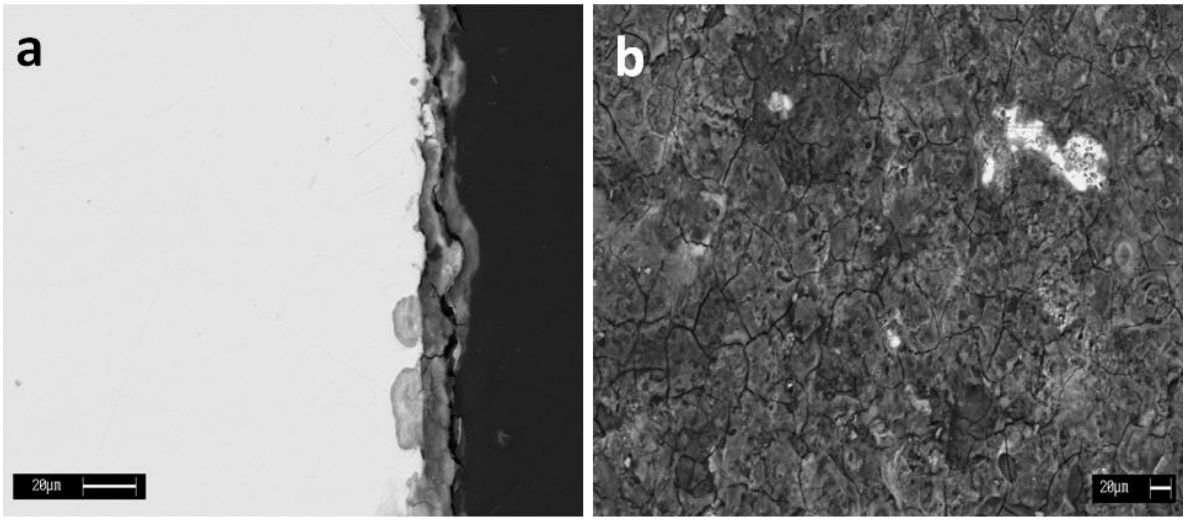

Fig. 7.6 BSE-SEM images of the cross section (a) and the surface (b) of the sample of 39NiCrMo3 PEO treated with electrolyte A.

The oxide layer resulted cracked and non homogenous with a thickness of about 23 µm, as can be seen in Fig. 7.6a. Moreover, the presence of some grey zones with the starting of corrosion phenomena on the substrate can be found. The surface, reported in Fig. 7.6b resulted porous and with a large number of cracks. The presence of white uncoated zones can be revealed. EDS semi quantitative results reported in Tab. 7.8 reported the composition of the surface and of the cross section of the coated sample.

Tab. 7.8 EDS semi-quantitative analysis of the cross section and the surface of PEO coated sample obtained with electrolyte A (%wt).

	Fe	**Al**	**Cr**	**O**	**Si**
Cross Section	56.44	25.03	1.71	9.02	7.81
Surface	27.14	23.89	0.55	35.21	13.21

As reported before, the coating obtained with electrolyte A produced only small improvement in the corrosion resistance, if compared with the uncoated sample and the results were significantly worse than the ones obtained with electrolyte C. This fact can be related also in this case to the morphology and the thickness of the protective layer. The oxide coating is in fact less thick and more cracked, if compared with the one obtained with electrolyte C. Moreover, the formation of the typical double layer of PEO coated samples was not observed. Also the presence of uncoated zones on the surface and the start

of corrosion phenomena during PEO process as reported in Fig.7.6 negatively affect the corrosion resistance of the obtained coating.

In order to study the different phases formed in the coating during PEO process also XRD analysis was performed on the samples treated with the three different electrolytes. XRD spectra, obtained with configuration for thin films, are reported in Fig.7.7

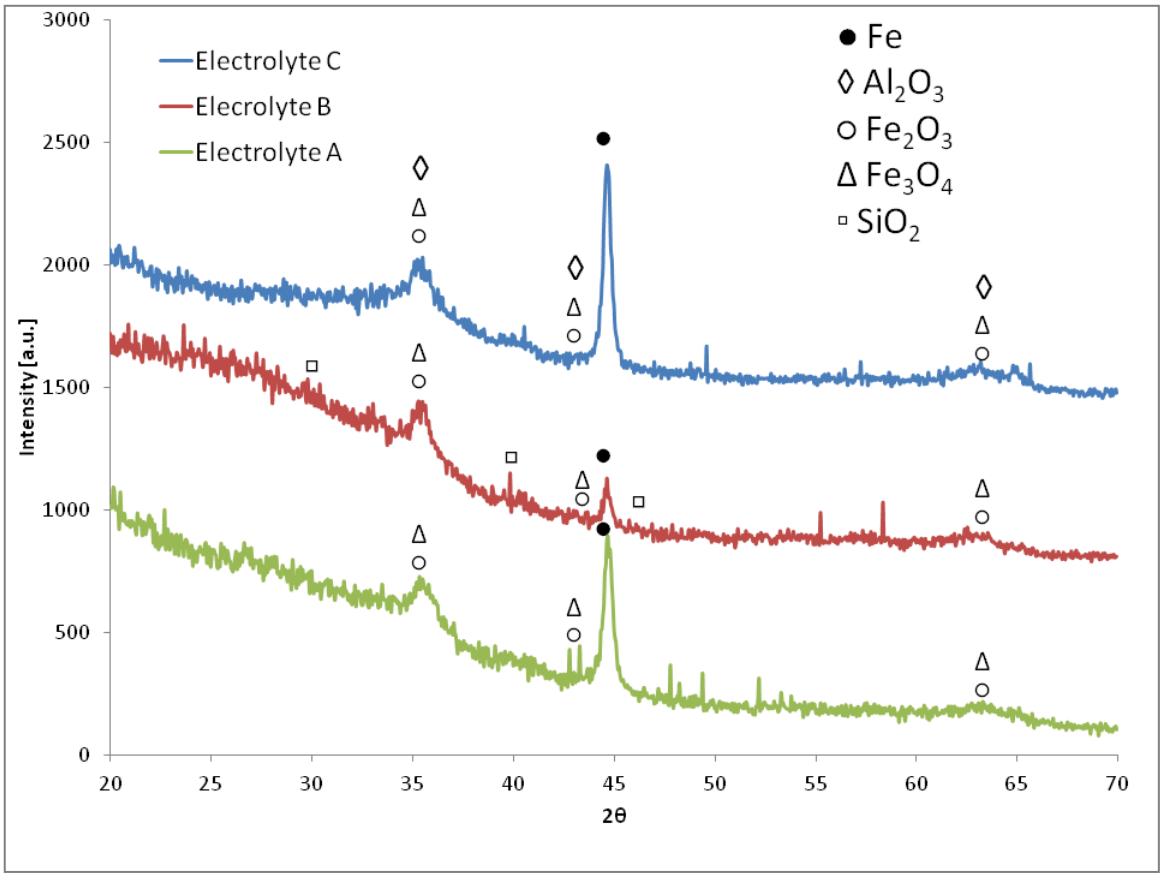

Fig. 7.7 X-ray diffraction patterns for 39NiCrMo3 samples PEO treated using electrolytes containing different quantities of sodium aluminates

It can be observed that the obtained coatings are mainly composed by iron oxides (from the substrate) and aluminum and silicon oxides in accordance with the composition of the electrolyte. The presence of the peaks of Fe can be ascribed to the reflection from the substrate. In the coating obtained with electrolyte A (so with equal low concentrations of sodium silicate and sodium aluminates) only the presence of the peaks of iron oxides magnetite and hematite can be revealed. The PEO coating obtained with electrolyte B, so with high concentrations of sodium silicates, shows again the presence of the peaks of iron oxides but also the presence of silicon oxide can be revealed due to the high silicon content in the electrolyte. As reported before the presence of this silicon oxide do not improve the

corrosion performance of the coating. In the sample obtained with the electrolyte containing high concentrations of sodium aluminates called electrolyte C besides the peaks of iron oxides also the peaks of Al_2O_3 can be revealed in accordance with the electrolyte composition.

7.4 CONCLUDING REMARKS

In this chapter was studied the application of PEO process on a 39NiCrMo3 steel in order to improve its corrosion performances. Different types of electrolytes containing different concentrations of silicates and aluminates were tested and the corrosion performances were evaluated in a solution containing both sulphates and chlorides. The best corrosion performances were obtained for the sample treated for 10 minutes at 0.4 A/cm^2 in a solution containing 10 g/l of NaOH, 10 g/l of Na_2SiO_3 and 100 g/l of $NaAlO_2$. The coating on this sample is mainly composed by iron oxides and aluminum oxide and exhibited a corrosion current density two order of magnitude lower than the untreated sample and an ennoblement in the corrosion potential of about 0.6 V. The obtained coating was about 50 μm thick and showed the typical double-layer structure of a PEO coating, with an inner layer rich in chromium oxide and an external layer rich in aluminum and iron oxides. The surface was rich of pores. Samples obtained with the same electric conditions but with different electrolytes, in particular with the reduction of the aluminates content and the increase in silicate amount, did not exhibit significant improvement in the corrosion properties, if compared with the uncoated sample. This fact can be correlated with a thinner oxide layer than the coating obtained with the solution rich of silicates. Moreover, the layer was rich of cracks and did not show the double layer structure, with the absence of the inner layer rich in chromium oxides that give the major protection against corrosion.

CONCLUSIONS

In this thesis work, after a brief discussion on the state of art regarding plasma electrolytic oxidation process (PEO), possible innovative modifications of the process were studied, in order to decrease the industrial costs of the treatment and to improve the properties of the obtained coatings. This achievements are in fact nowadays requested to extend the industrial applications of the process, from one hand reducing the costs, from the other obtaining specimens with improved characteristics. All the modifications of the process were studied in order to maintain the whole production cycle environmental friendly due to the fact that this is one of the more important advantages of PEO process than traditional anodizing process. All the experimental tests were performed using the PEO laboratory plant developed.

In the first part of the thesis were described the results regarding the modification of process parameters of PEO. In detail coating with good corrosion performances were obtained on magnesium and magnesium alloys working with high current densities and short treatment times. The results showed in fact that the corrosion resistance, evaluated with potentiodynamic polarization tests and EIS tests is strongly influenced by the current density and not so much by the treatment time. Working at higher values of current densities, in comparison with the ones present nowadays in literature and in the commercial processes, permit to reduce significantly the treatment time passing from several minutes to under one minute, maintaining good corrosion performances. This fact can be very important in future applications of PEO process because the total time of the production cycle (that strongly influence the cost of the final product) can be remarkably reduced.

During the second part of the experimental work the attention was focused on find particular additives that can be directly put in the electrolyte used for PEO process and that can enhance the properties of the coatings. This kind of modifications are one of the most studied nowadays from the researchers. In fact one of the main difference between PEO and conventional anodizing is that the process allows the formation of coatings composed of not only predominant substrate oxides but of more complex oxides containing the elements present in the electrolyte. Moreover particles suspended in the electrolyte can be incorporated inside of the coating. The direct addiction of the additives in the electrolyte

used in the process is also very promising in terms of industrial application because no additional steps and so no additional costs are required.

At first in this thesis were studied possible additives to improve the corrosion resistance of the obtained samples. Molybdenum and lanthanum salts were selected as possible additives due to their environmental friendly nature and due to their well known anti-corrosion and corrosion inhibition properties. The addition of molybdenum salts in the electrolyte used to produce PEO coatings on AZ91 magnesium alloy produce an improvement in the corrosion resistance as revealed by potentiodynamic polarization and EIS tests. However strong attention has to be put in the addition of the right quantity of molybdenum salts (0.3 g/l of sodium molybdate in our case), in fact a too high amount of this compound in the electrolyte produce the formation of a coating with poor corrosion performances. The presence of low quantities of molybdenum oxides and mixed magnesium-molybdenum oxides in the coating was revealed thank to advanced characterization techniques (XPS and SIMS).

Lanthanum salts were, instead, employed to improve the corrosion resistance of coatings obtained on a 7075 aluminum alloy (using also in this case high current densities and short treatment times). Also in this case corrosion tests evidenced that the presence of lanthanum produce a remarkable increase in the corrosion resistance. The improved corrosion performances can be both connected to an increase in the thickness of the coating and to the corrosion inhibition effect of lanthanum ions. Also in this case is very important the quantity of lanthanum salt in the electrolyte (0.075 g/l), because a too high amount of the compound cause a decrease in the corrosion properties. XPS permit to reveal the presence of $La(OH)_3$ in the oxide layer.

The reported results shows that the use of molybdenum and lanthanum salts could be a good way to improve the corrosion resistance of PEO coatings, but a strong attention must be used in the choice of the right quantity of the salt. The industrial application of this innovation so requires a lot of work in the control of the bath composition.

Also the addition of graphite particles and nanoparticles suspended in the electrolyte was studied in this thesis, in order to improve both the corrosion and wear resistance of PEO coatings. The protective layers were obtained on magnesium alloys with two different treatment times (one or three minutes) working with high current densities. Graphite particles resulted too big to be incorporated in the oxide coating so the main part of the study was performed with graphite nanoparticles. These nanoparticles from one hand fill the pores that characterize the typical surface of a PEO coating, from the other, due to their

conductive nature, modify the discharge phenomena during the oxide film formation and permit to obtain thicker protective coatings. Due to this modifications, induced by the presence of the graphite nanoparticles, the graphite-containing samples are characterized by improved corrosion resistance if compared with the ones obtained without graphite in the electrolyte. The presence of the graphite cause also an increase in the hardness of the oxide coating but also in the fragility of the protective layer. The tribological tests performed of the various samples evidenced that the presence of graphite did not cause an improvement of the wear resistance or a decrease of the friction coefficient. This fact can be related, for the samples treated for one minute, to the low quantity of graphite into the thin oxide layer and, for the samples treated for three minutes, to the high fragility of the coating. For a technological application of the addition of graphite nanoparticles to the electrolyte that combines an improvement both in the corrosion and wear resistance probably an intermediate treatment (two minutes) is necessary. With this kind of treatment a good compromise between thickness and fragility can be obtained and an increase in the wear properties reached. Instead was demonstrated that the presence of the graphite particles themselves already produce an increase in the corrosion resistance in the samples treated for one or three minutes.

In order to give to the oxide ceramic coating new properties also the study of the addiction of silver particles in the electrolyte was performed in this thesis. This silver particles, if incorporated inside the oxide coating, give to the final specimen an antimicrobial activity that permit its use for medical devices. In fact the antimicrobial activity of silver is well known in literature. In this work was studied the incorporation of the silver particles in the PEO coating produced on a 7075 aluminum alloy. The electron microscope observation evidences that the particles dispersed in the electrolyte can be found both inside and outside of the pores of PEO coated samples. The final objective was also to obtain specimen with acceptable corrosion resistance, and this could be a problem due to the galvanic couple formed between aluminum and silver. However after a treatment of sealing of the pores in boiling water the silver-containing PEO treated samples exhibits a corrosion resistance only slightly lower than the sample PEO treated without silver particles, especially in terms of corrosion potential. The addiction of silver particles in the electrolyte permit so to obtain, after a sealing treatment, specimens with good corrosion performances (better than the untreated sample and the conventionally anodized sample) and with an intrinsic antimicrobial activity.

In the last experimental part of this thesis the study of the possible application of PEO process on low alloyed steels was performed. The application of PEO process on steels could be very important for the wide technological applications of this material and PEO process could increase the corrosion resistance of the substrate without altering the microstructure of the base material. However a lack of researches in this sector was found in literature. In this thesis was described the successfully application of the PEO process on a low alloyed steel using an electrolyte containing mainly sodium aluminates. The obtained coated sample exhibit improved corrosion performances than the untreated one and the oxide ceramic coating, mainly composed by iron, aluminum and silicon oxides, has the typical double layer structure of PEO coatings.

Concluding this thesis work was devoted to the research of new solutions that permit the use of PEO process in a wider range of industrial applications. The experimental work shows that the modification of the process parameters and the formulation of additives for the electrolyte, could improve the properties of the final products and could also reduce the overall cost of the process. So the results reported in this thesis permit to extend the knowledge regarding PEO process and to open new ways for the industrial applications of the process.

REFERENCES

[1] Li Q, Linag J, Wang Q. *Plasma Electrolytic Oxidation coatings on lightweight metals*, Modern Surface Engineering Treatments, Chapter 4, 75-99

[2] *Surface Engineering of Light Alloys*, Chapters 5 and 6, 110-180, Woodhead Publishing Limited, 2010

[3] Wernick S, Pinner R, Sheasby PG. *The surface treatment and finishing of aluminum and its alloys*, 5th edn; 1987, Teddington, Finishing Publications Ltd.

[4] Henley V F. *Anodic oxidation of aluminium and its alloys*, 1982, Oxford, Pergamon Press.

[5] Walsh F C, Low C T J, Wood R J K, Stevens K T, Archer J, Poeton A R, Ryder A. *Plasma electrolytic oxidation (PEO) for production of anodised coatings on lightweight metal (Al, Mg, Ti) alloys*, Transactions of the Institute of Metal Finishing, 2009; 87: 122–135.

[6] Patel J L, Saka N. *Microplasmic coatings*, Am Ceram Soc Bull, 2001; 80: 27–29

[7] Chigrinova N M, Chigrinova V E, Kukharev A A. *Formation of coatings by anodic microarc oxidation and their operation in thermally-stressed assemblies*, Powder Metallurgy and Metal Ceramics, 2001; 40: 213–220

[8] Atroshchenko E S, Chufistov O E, Kazantsev I A, Kamyshanskii S I. *Formation of structure and properties of coatings developed by microarc oxidizing on parts fabricated from aluminum alloys*, Metal Science and Heat Treatment, 2000; 42: 411–415

[9] Hirohata Y, Nakamura T, Aihara Y, Hino T. *Dependence of surface oxidation on hydrogen absorption and desorption behaviors of Ti6al4V alloy*, J Nucl Mater, 1999; 266–269, 831–836

[10] Günterschultze A, Betz H. *Die electronenstromung in isolatoren bei extremen feldstarken*, Z Phys, 1934; 91: 70–96

[11] Mcniell W, Gruss L L (1966), US Patent, 3293158

[12] Mcniell W, Nordbloom G F (1958),US Patent, 2854390

[13] Yerokhin A L, Nie X, Leyland A, Matthews A, Dowey S J. *Plasma electrolysis for surface engineering*, Surf Coat Tecn, 1999; 122: 73-93

[14] Duradzhy V N, Parsadanyan A S. *Metal Heating in Electrolytic Plasma*, Shtiintsa Kishinev, 1988

[15] Tchernenko V I, Snezhko L A, Papanova I I. *Coatings by Anodic Spark Electrolysis*, Khimiya Leningrad, 1991

[16] Ikonopisov S. *Theory of electrical breakdown during formation of barrier anodic films*, Electrochim Acta, 1977; 22: 1077-1082

[17] Monterro J, Fernandez M, Albella J M. *Pore formation during the breakdown process in anodic Ta_2O_5 films*, Electrochim Acta, 1987; 32: 171-174

[18] Krysmann W, Kurze P, Dittrich K H, Schneider H G. *Process characteristics and parameters of Anodic Oxidation by spark discharge (ANOF)*, Cryst Res Technol, 1984; 19: 973-979

[19] Snizhko L O, Yerokhin A L, Pilkington A, Gurevina N L, Misnyankin D O, Leyland A, Matthews A. Anodic *processes in plasma electrolytic oxidation of aluminium in alkaline solutions*, Electrochim Acta, 2004; 49: 2085-2095

[20] Cao F H, Lin L Y, Zhang Z, Zhang J Q, Cao C N. *Environmental friendly plasma electrolytic oxidation of AM60magnesium alloy and its corrosion re-sistance*, Trans Nonferrous Met Soc China, 2008; 18: 240-247

[21] Martin J, Melhem A, Shchedrina I, Duchanoy T, Nominè A, Henrion G, Czerwiec T, Belmonte T. *Effects of electrical parameters on plasma electrolytic oxidation of aluminium*, Surf Coat Technol, 2013; 221: 70-76

[22] Li J Z, Shao Z C, Tian Y W, Kang F D, Zhai Y C. *Application of microarc oxidation for Al、Mg, Ti and their alloys*, Corrosion Science and Protection Technology , 2004; 16: 218–221

[23] He J, Cai Q Z, Luo H H, Yu L and Wei B K. *Influence of silicon on growth process of plasma electrolytic oxidation coating on al-Si alloy*, J Alloys Compd, 2009; 471:395-399

[24] Shin K R, Ko Y G, Shin D H. *Effect of electrolyte on surface properties of pure titanium coated by plasma electrolytic oxidation*, Journal of Alloys and Compounds, 2011; 509:478–481

[25] Becerik D A, Ayday A, Kumruoğlu L C, Kurnaz S C, Őzel A. *The Effects of Na_2SiO_3 Concentration on the Properties of Plasma Electrolytic Oxidation Coatings on 6060 Aluminum Alloy*, JMEPEG, 2012; 21:1426–1430

[26] Forno A D, Bestetti M. *Effect of the electrolytic solution composition on the perform-ance of micro-arc anodic oxidation films formed on AM60B magnesium alloy*, Surface and Coatings Technology, 2010; 205: 1783–1788

[27] Shi X L, Wang Q L, Wang F S, Ge S R, *Effects of electrolytic concentration on properties of micro-arc film on Ti6Al4V alloy*, Mining Science and Technology, 2009; 19: 20– 224

[28] Hussein R O, Nie X, Northwood D O. *Influence of process parameters on electrolytic plasma discharging behaviour and aluminum oxide coating microstructure*, Surface and Coatings Technology, 2010; 205: 1659–1667

[29] Yang Y, Wu H. *Effects of Current Frequency on the Microstructure and Wear Resistance of Ceramic Coatings Embedded with SiC Nano-particles Produced by Micro-arc Oxidation on AZ91D Magnesium Alloy*, Journal of Material Science Technology, 2010; 26: 865–871

[30] Khan R H U, Yerokhin A, Li X, Dong H, Matthews A. *Surface characterisation of DC plasma electrolytic oxidation treated 6082 aluminium alloy: Effect of current density and electrolyte concentration*, Surface and Coatings Technology, 2010; 205: 1679–1688

[31] Huang P, Wang F, Xu K W, Han Y. *Mechanical properties of titania prepared by plasma electrolytic oxidation at different voltages*, Surface and Coatings Technology, 2007; 201: 5168 -5171

[32] Liang J, Guo B G, Tian J, Liu H W, Zhou J F, Xu T. *Effect of potassium fluoride in electrolytic solution on the structure and properties of microarc oxidation coatings on magnesium alloy*, Applied Surface Science, 2005; 252: 345–351

[33] Blawert C, Heitmann V, Dietzel W, Nykyforchyn H M, Klapkiv M D. *Influence of electrolyte on corrosion properties of plasma electrolytic conversion coated magnesium alloys*, Surface and Coatings Technology, 2007; 201: 8709–8714

[34] Blawert C, Heitmann V, Dietzel W, Nykyforchyn H M, Klapkiv M D. *Influence of process parameters on the corrosion properties of electrolytic conversion plasma coated magnesium alloys*, Surface and Coatings Technology, 2005; 200: 68–72

[35] Curran J, Clyne T W.*Porosity in plasma electrolytic oxide coatings*, Acta Materialia, 2006; 54:1985–1993

[36] Popova N E, Popova S S and Povolotskii E G. Proceedings of the All- Russian Conf 'Electrochemistry of Membranes and Processes in Thin Ion-conducting Films on Electrodes', ECHM-99, 1999, 68

[37] Liang J, Hu l, Hao J. *Characterization of microarc oxidation coatings formed on AM60B magnesium alloy in silicate and phosphate electrolytes*, Applied Surface Science, 2007; 253: 4490–4496

[38] Arrabal R, Matykina E, Viejo F, Skeldon P, Thompson G E. *Corrosion resistance of WE43 and AZ91D magnesium alloys with phosphate PEO coatings*, Corrosion Science, 2008; 50: 1744–1752

[39] Liang J, Bala Srinivasan P, Blawert C, Störmer M, Dietzel W. *Electrochemical corrosion behaviour of plasma electrolytic oxidation coatings on AM50 magnesium alloy formed in silicate and phosphate based electrolytes*, Electrochimica Acta, 2009; 54: 3842–3850

[40] Liang J, Hu L, Hao J. *Improvement of corrosion properties of micro arc oxidation coating on magnesium alloy by optimizing current density parameters*, Applied Surface Science, 2007; 253: 6639–6645

[41] Bala Srinivasan P, Liang J, Blawert C, Störmer M, Dietzel W. *Effect of current density on the microstructure and corrosion behaviour of plasma electrolytic oxidation treated AM50 magnesium alloy*, Applied Surface Science, 2009; 255: 4212–4218

[42] Bala Srinivasan P, Blawert C, Störmer M, Dietzel W. *Characterization of tribological and corrosion behavior of plasma electrolytic oxidation coated AM50 magnesium alloy*, Surface Engineering, 2009, 26:340-346

[43] Blawert C, Dietzel W, Ghali E, Song G. *Anodizing treatments for magnesium alloys and their effect on corrosion resistance in various environments*, Advanced Engineering Materials, 2006; 8: 511-533

[44] Yerokhin A L, Nie X, Leyland A, Matthews A. *Characterization of oxide films produced by plasma electrolytic oxidation of a Ti–6Al–4V alloy*, Surf Coat Technol, 2000; 130: 195–206

[45] Gnedenkov S V, Khrisanfova O A, Zavidnaya A G, Sinebrukhov S L, gordienko P S, Iwatsubo S and Matsui A. *Composition and adhesion of protective coatings on aluminum*, Surf Coat Technol, 2001; 145: 146–151

[46] Huang P, Xu K W, Han Y. *Character and Mechanism of the Film by Microarc Oxidation on Titanium alloy*, Rare Metal Mat Eng, 2003; 32: 272–275

[47] Wang Y M, Jiang B L, Lei T Q, Guo L X. *Microarc oxidation and spraying graphite duplex coating formed on titanium alloy for antifriction purpose*, Appl Surf Sci, 2005; 246: 214–221

[48] Wang Y M, Lei T Q, Jiang B L , Guo L X. *Growth, microstructure and mechanical properties of microarc oxidation coatings on titanium alloy in phosphate containing solution*, Appl Surf Sci, 2004; 233: 258–267

[49] Khan R H U, Yerokhin A L, Pilkington T, Leyland A, Matthews A. *Residual stresses in plasma electrolytic oxidation coatings on al alloy produced by pulsed unipolar current*, Surf Coat Technol, 2005; 200: 1580–1586

[50] Guan Y J, Xia Y , Xu F T. *Interface fracture property of PEO ceramic coatings on aluminum alloy*, Surf Coat Technol, 2008; 202: 4204–4209

[51] Ishizawa H, Ogino M. *Formation and characterization of anodic titanium oxide coatings containing Ca and P*, J Biomed Mater Res, 1995; 29: 65–72

[52] Ishizawa H, Ogino M. *Characterization of thin hydroxyapatite layers formed on anodic titanium oxide coatings containing Ca and P by hydrothermal treatment*, J Biomed Mater Res, 1995; 29: 1071–1079

[53] Ishizawa H, Ogino M. *Hydrothermal deposition of hydroxyapatite on anodic titanium oxide coatings containing Ca and P*, J Mater Sci, 1999; 34: 5893–5898

[54] Li L H, Kong Y M, Kim H W. *Improved biological performance of Ti implants due to surface modification by micro-arc oxidation*, Biomaterials, 2004; 25: 2867–2875

[55] Zhu X L, Kim K H, Jeong Y S. *Anodic oxide films containing Ca and P of titanium biomaterial*, Biomaterials, 2001; 22: 2199–2206

[56] Zhu X L, Ong L G, Kim S Y, Kim K H. *Surface characteristics and structure of anodic oxide films containing Ca and P on titanium implant material*, J Biomed Mater Res, 2002; 60: 333–338

[57] Song W H, Jun Y K, Han Y, Hong S H. *Biomimetic apatite coatings on micro-arc oxidized titania*, Biomaterials, 2004; 25: 3341–3349

[58] Sun J F, Han Y, Cui K. *Microstructure and apatite-forming ability of the MAO-treated porous titanium*, Surf Coat Technol, 2008; 202: 4248–4256

[59] Gray J E, Luan B. *Protective coatings on magnesium and its alloys- A critical Review*, Journal of Alloys and Compounds, 2002; 336: 88-113

[60] Curran J A, Clyne T W. *The thermal conductivity of plasma electrolytic oxide coatings on aluminium and magnesiu*', Surf Coat Technol, 2005; 199: 177–183

[61] Curran J A, Kalkanc H, Magurova Y, Clyne T W. *Mullite-rich plasma electrolytic oxide coatings for thermal barrier applications*, Surf Coat Technol, 2007; 201: 8683–8687

[62] Ghasemi A, Raja V S, Blawert C, Dietzel W, Kainer K U. *Study of the structure and corrosion behavior of PEO coatings on AM50 magnesium alloy by electrochemical impedance spectroscopy*, Surf Coat Technol, 2008; 202: 3513–3518

[63] Mizutani Y, Kim S J, Ichino R, Okido M. *Anodizing of Mg Alloys in Alkaline Solutions*, Surf Coat Technol, 2003; 143: 169–170

[64] Olbertz B. Jahrbuch Oberflächentechnik,1989; 45: 262–273

[65] Khaselev O, Yahalom J. *Constant voltage Anodizing of Mg-Al alloys in KOH-Al(OH)$_3$ solutions*, J Electrochem Soc, 1998; 145: 190-193

[66] Khasalev O, Weiss D, Yahalom J. *Structure and composition of anodic film formed on binary Mg-Al alloy in KOH-aluminate solution under continuous sparking*, Corros Sci, 2001; 43: 1295-1307

[67] Zozulin A J, Bartak D E. *Anodized coatings for magnesium alloys*, Met Finishing, 1994; 92: 39-44

[68] Shrestha S, Sturgeon A, Shashkov P, Shatrov A. *Improved corrosion performances of AZ91D magnesium alloy coated with KeroniteTM process*, Magn Technol, 2002; TMS 2002, 283–287

[69] Blawert C, Heitmann V, Dietzel W, Nykyforchyn H M, Klapkiv M D. *Influence of process parameters on the corrosion properties of electrolytic conversion plasma coated magnesium alloys* ,Surf Coat Technol, 2005; 200: 68-72

[70] Wang G G, Stewart K, Berkmortel J, Skar I. *SAE Paper 2001-01-0421*, SAE 2001, 397–405

[71] Srinivasan P B, Blawert C, Dietzel W. *Dry sliding wear behaviour of plasma electrolytic oxidation coated AZ91 cast magnesium alloy*, Wear 2009, 2009; 266: 1241–1247

[72] Chen F, Zhou H, Chen C, Xia Y J. *Study on the tribological performance of ceramic coatings on titanium alloy surfaces obtained through microarc oxidation*, Progress in Organic Coatings, 2009; 64: 264–267

[73] Tian J, Luo Z Z, Qi S K, Sun X J, *Structure and antiwear behavior of micro-arc oxidized coatings on aluminum alloy*, Surface and Coatings Technology, 2002; 154: 1–7

[74] Ross P N, MacCulloch J A, Esdaile R J. 20th Int. Die Casting Congress and Exp. Cleveland, USA, Nov. 1–4, 1999,p. 213–218, Paper-Nr. T99-063

[75] http://www.magnesium.co.nz/Magnesium/

[76] Moulder J F, Stickle W F, Sobol P E, Bomben K D, Chastain J (1992) Handbook of X-Ray Photoelectron Spectroscop. Perkin Elemer Corp, Eden Prairie, MN

[77] X-ray Photoelectron Spectroscopy Database 20, Version 3.0, National Institute of Standards and Technology, Gaithersburg

[78] http://srdata.nist.gov/XPS

[79] Glisenti A, Frasson A, Galenda A, Natile M M. *Au/CeO2 Supported Nanocatalysts: Interaction with Methanol*, Nanoscie Nanotechn Letters 2, 2010; 3: 213-219

[80] Natile M M, Tomaello F, Glisenti A. *WO3/CeO2 nanocomposite powders; synthesis, characterization, and reactivity*, Chem Mater, 2006; 18: 3270-3280

[81] Teterin Y A, Teterin A Y, Lebedev A M, Utkin I O. *The XPS spectra of Cerium compounds containing oxygen*, J Electron Spectr Rel Phenom, 1998; 88-91: 275-279

[82] Wang S, Qiao Z, Wang W, Qian Y. *XPS studies of nanometer CeO2 thin films deposited by pulse ultrasonic spray pyrolysis*, J Alloys Compd, 2000; 305: 121-124

[83] D. A. Shirley, *Phys Rev B*, 1972; 55, 4709.

[84] Guo H L, Huan C, Xing Q W,Hua P, Gu L Z, Bin Z, Heon J L,Si Z Y. *Effect of additives on structure and corrosion resistance of plasma electrolytic oxidation coatings on AZ91D magnesium alloy in phosphate based electrolyte* Surf Coat Technol, 2010; 205: 36-40

[85] Sreekanth D,Rameshbabu N,Venkateswarlu K. *Effect of various additives on morphology and corrosion behavior of ceramic coatings developed on AZ31 magnesium alloy by plasma electrolytic oxidation,* Ceram Int, 2012; 38:4607-4615

[86] Duan H, Yan C, Wang F. Effect of electrolyte additives on performance of plasma electrolytic oxidation films formed on magnesium alloy AZ91D, Electrochim Acta, 52 : 3785-3793

[87] Junghoon L,Yonghwan K, Wonsub C (2012) *Effect of Ar bubbling during plasma electrolytic oxidation of AZ31B magnesium alloy in silicate electrolyte*, Appl Surf Sci, 2007; 259: 454-459

[88] Li W, Li C, Wen F. *Characterization of Plasma Electrolytic Oxidation Films Formed on AZ31 Magnesium Alloys by Different Voltage Parameters*, Adv Mat Res, 2011; 168-170: 1203-1208

[89] Hussein R O, Northwood D O, Nie X. *The Influence of Pulse Timing and Current Mode on the Microstructure and Corrosion Behaviour of a Plasma Electrolytic Oxidation (PEO) Coated AM60B Magnesium Alloy*, J Alloy Compd, 2012; 541: 41-48

[90] Kazanski B, Kossenko A, Zinigrad M, Lugovskoy A. *Fluoride ions as modifiers of the oxide layer produced by plasma electrolytic oxidation on AZ91D magnesium alloy,* Appl Surf Sci, 2013; 287: 461-466

[91] Ma C, Zhang M, Yuan Y, Jing X, Bai X. *Tribological behavior of plasma electrolytic oxidation coatings on the surface of Mg-8Li-1Al alloy*, Tribol Int, 2012; 47: 62-68

[92] Gun K Y, Seok L E, Hyuk S D. *Influence of voltage waveform on anodic film of AZ91 Mg alloy via plasma electrolytic oxidation: Microstructural characteristics and electrochemical responses*, J Alloy Compd, 2014; 586: 356-361

[93] Ma C, Lu Y, Sun P, Yuan Y, Jing X, Zhang M. *Characterization of plasma electrolytic oxidation coatings formed on Mg–Li alloy in an alkaline polyphosphate electrolyte*, Surf Coat Technol, 2011; 206: 287–294

[94] Felker D L, Sherwood P M A. *Magnesium Phosphate (Mg3(PO4)2) by XPS*, Surf Sci Spectra, 2002; 9: 83-90

[95] Cai J, Cao F, Chang L, Zheng J, Zhang J, Cao C. *The preparation and corrosion behaviours of MAO coating on AZ91D with rare earth conversion precursor film,* Appl Surf Sci, 2011; 257: 3804-3811

[96] Jianzhong L, Yanwen T, Zuoxing C, Zenqi H. *Effect of rare earths on the microarc oxidation of a magnesium alloy*, Rare Metals, 2008; 27: 20-54

[97] Salaman S A, Ichino R, Okido M. *Improvement of corrosion resistance of AZ91 Mg alloy by anodizing with co-precipitation of cerium oxide*, Transactions of Nonferrous metals society of China, 2009; 19: 883-886

[98] Lim T S, Ryu H S, Hong S H. *Electrochemical corrosion properties of CeO_2-containing coatings on AZ31 magnesium alloys prepared by plasma electrolytic oxidation*, Corros Sci, 2012; 62: 104-111

[99] Laleh M, Kargar F, Sabour Rouhaghdam A. *Investigation of rare earth sealing of porous micro-arc oxidation coating formed on AZ91D magnesium alloy*, Journal of rare earths, 2012; 30: 1293-1297

[100] Armour A W, Robitaille R D. *Corrosion inhibition by sodium molybdate*, J Chem Technol Biot, 1979; 29: 619-628

[101] Stranick M A, NACE 8, 1985, 1-380

[102] Lopez-Garrityz O, Frankel G S. *Corrosion inhibition of aluminum alloy 2024-T3 by sodim molybdate*, J Electrochem Soc, 2014; 161: C95-C106

[103] Bi-Lan L, Jin-Tang L, Gang K. *Effect of molybdate post-sealing on the corrosion resistance of zinc phosphate coatings on hot-dip galvanized steel*, Corros Sci, 2008; 50: 962-967

[104] Feng L, Guo-Xi L, Jing Z, Gui-Hong G. *Molybdate-doped copolymer coatings for corrosion prevention of stainless steels*, J Appl Polym Sci, 2014; 131

[105] Brunelli K, Magrini M, Dabalà M. *Method to improve corrosion resistance of AA5083 by cerium based conversion coating and anodic polarization in molybdate solution*, Corr Eng Sci Technol, 2012; 47: 224-232

[106] Yingwu Y, You Z, Chunmei Z, Yuxiang H, Chunxia Z. *Preparation and corrosion resistance properties of molybdate conversion coatings containing SiO_2 nanoparticles*, J Electrochem Soc, 2013; 160: C185-C188

[107] Yingwu Y, You Z, Liang H. *Corrosion behavior of molybdate conversion coatings on AZ31 magnesium alloy in NaCl solution*, Anti-Corros Method M, *2013;* 60: 307-311

[108] Zhao C M, Yao Y W, Zhou Y. T I Met Finish, 2013; 91:330-335

[109] Sun P, Lu Y, Yuan Y, Jing X, Zhang M. *Preparation and characterization of duplex PEO/ MoC coatings on Mg-Li alloys*, Surf Coat Technol, 2011; 205: 4500-4506

[110] Li Z J, Yuan Y ,Jing X Y. *Comparison of plasma electrolytic oxidation coatings on Mg-Li alloy formed in molybdate/silicate and aluminate/silicate composite electrolytes*, Materials and Corrosion, 2014; 65: 493-501

[111] Xiajun W, Xiangdong L, Yongzhen L, Chunxia H, Yuehe D. *Effects of Ce (III) on rate of formation and phase composition of ceramic coating formed on surface of ZAlSi12CuMg1 by microarc oxidation*, Journal of rare earths,2007; 25: 82-85

[112] Liu J, Lu Y, Jing X, Yuan Y, Zhang M. *Characterization of plasma electrolytic oxidation coatings formed on Mg–Li alloy in an alkaline silicate electrolyte containing silica sol* Materials and Corrosion, 2009; 60: 865-870

[113] Blawert C, Heitmann V, Dietzel W, Nykyforchyn H M, Klapkiv M D *Influence of electrolyte on corrosion properties of plasma electrolytic conversion coated magnesium alloys,* Surf Coat Technol, 2007 201: 8709-8714

[114] Dehnavi V, Shoesmith D W , Li Luan B, Yari M, Yang Liu X, Rohani S. *Corrosion properties of plasma electrolytic oxidation coatings on aluminum alloys-The effect of the PEO process stage,* Mat Chem Phy, 2015; 161: 49-58

[115] Sreekanth D, Rameshbabu N , Venkateswarlu K. *Effect of various additives on morphology and corrosion behavior of ceramic coatings developed on AZ31 magnesium alloy by plasma electrolytic oxidation,* Ceramics Intern, 2012; 38: 4607-4615

[116] Kang L, Gao J, Xu H R, Zhao S Q, Chen H, Wu P H. *Epitaxial Mg2SiO4 thin films with a spinel structure grown on Si substrates,* J Cryst Growth, 2006; 297: 100–104

[117] Yoo B, Shin K R, Hwang D Y, Lee D H, Shin D H. *Effect of surface roughness on leakage current and corrosion resistance of oxide layer on AZ91 Mg alloy prepared by plasma electrolytic oxidation,* Appl Surf Sci, 2010; 256: 6667-6672

[118] Martinez S, Metikosˇ-hukovic M. *A nonlinear kinetic model introduced for the corrosion inhibitive properties of some organic inhibitors* J Appl Electrochem, 2003; 33: 1137-1142

[119] Lebrini M, Lagrenee M, Vezin H, Traisnel M, Bentiss F. *Experimental and theoretical study for corrosion inhibition of mild steel in normal hydrochloric acid solution by some new macrocyclic polyether compounds,* Corros Sci, 2007; 49: 2254-2269

[120] Snizhko L O, Yerokhin A L, Pilkington A, Gurevina N L, Misnyankin D O, Leyland A, Matthews A. *Anodic processes in plasma electrolytic oxidation of aluminium in alkaline solutions,* Electrochim Acta, 2004; 49: 2085-2095

[121] Pezzato L, Brunelli K, Gross S, Magrini M, Dabalà M. *Effect of process parameters of plasma electrolytic oxidation on microstructure and corrosion properties of magnesium alloys,* J Appl Electrochem, 2014; 118: 867-879

[122] Wannaparhun S, Seal S, Desai V. *Surface chemistry of Nextel-720, alumina and Nextel-720/alumina ceramic matrix composite (CMC) using XPS–A tool for nano-spectroscopy,* Appl Surf Sci, 2002; 185: 183–196

[123] Sunding M F, Hadidi K, Diplas S, Løvvik O M, Norby T E, Gunnæs A E. *XPS characterisation of in situ treated lanthanum oxide and hydroxide using tailored charge referencing and peak fitting procedures, J Electron Spectrosc Relat Phenom,* 2011; 184: 399-409

[124] Montemor M F, Simões A M,Carmezim M J. *Characterization of rare-earth conversion films formed on the AZ31 magnesium alloy and its relation with corrosion protection*, Appl Surf Sci, 2007*;* 253: 6922–6931

[125] Mu W, Han Y. *Characterization and properties of the MgF_2/ZrO_2 composite coatings on magnesium prepared by micro-arc oxidation*, Surface and Coatings Technology, 2008; 202: 4278–4284

[126] Matykina E, Arrabal R, Monfort F, Skeldon P, Thompson G E. *Incorporation of zirconia into coatings formed by DC plasma electrolytic oxidation of aluminium in nanoparticle suspensions*, Applied Surface Science, 2008; 255: 2830–2839

[127] Aliofkhazraei M, Rouhaghdam A S, Shahrabi T. *Abrasive wear behaviour of Si_3N_4/TiO_2 nanocomposite coatings fabricated by plasma electrolytic oxidation*, Surface and Coatings Technology, 2010; 205: S41–S46

[128] Aliofkhazraei M, Rouhaghdam A S. *Fabrication of functionally gradient nanocompo-*
site coatings by plasma electrolytic oxidation based on variable duty cycle, Applied Surface Science, 2012; 258: 2093–2097.

[129] Wu X H, Qin W, Guo Y, Xie Z Y. *Self-lubricative coating grown by micro-plasma oxidation on aluminum alloys in the solution of aluminate–graphite*, Applied Surface Science, 2008; 254: 6395–6399.

[130] Mu M, Zhou X J, Xiao Q, Liang J, Huo X D, *Preparation and tribological properties of self-lubricating TiO_2/graphite composite coating on Ti6Al4V alloy*, Applied Surface Science, 2012; 258: 8570–8576

[131] Mu M, Liang J, Zhou X J, Xiao Q. *One-step preparation of TiO2/MoS2 composite coating on Ti6Al4V alloy by plasma electrolytic oxidation and its tribological properties*, Surface and Coatings Technology, 2013; 214: 124–130

[132] Sondi I, Salopek-Sondi B. *Silver nanoparticles as antimicrobial agent: a case study on E. coli as a model for Gram-negative bacteria*, Journal of Colloid and Interface Science, 2004; 275: 177–182

[133] Prabhu S, Poulose E K. *Silver nanoparticles: mechanism of antimicrobial action, synthesis, medical applications, and toxicity effects*, International Nano Letters, 2012

[134] Yin L, Cheng Y, Espinasse B, Colman B P, Auffan M, Wiesner M, Jerome Rose, Liu J, Bernhardt E S. *More than the Ions: The Effects of Silver Nanoparticles on Lolium Multiflorum*, Environ Sci Technol, 2011; 45

[135] Chernousova S, Epple M. *Silver as Antibacterial Agent: Ion, Nanoparticle, and Metal*, Angew Chem Int Ed, 2013; 52: 1636 - 1653

[136] Wesley Alexander J. *History of the Medical Use of Silver*, Surgical Infection, 2009; 10

[137] Young-Ki J, Byung H K, Geunhwa J. *Antifungal Activity of Silver Ions and Nanoparticles on Phytopathogenic Fungi,* Plant Disease, 2009; 10

[138] Gokdeniz N, Asli K. *The antifouling performance of gelcoats containing biocides and silver ions in seawater environment,* J Coat Technol Res, 2010; 7: 139–143

[139] Liu T, Dong Y, He T, Guo N, Zhang F. *Films with nanosilvers improve biocorrosion resistance of aluminium in sea water,* Surface Engineering, 2014; 30: 6-10

[140] Knetsch M L W, Koole L H. *New Strategies in the Development of Antimicrobial Coatings: The Example of Increasing Usage of Silver and Silver Nanoparticles,* Polymers, 2011; 3: 340-366

[141] Meletisa E I, Nie X, Wang F L, Jiang J C. *Electrolytic plasma processing for cleaning and metal-coating of steel surfaces,* Surf Coat Tecnol, 2002; 149: 245-251

[142] Wang Y, Jiang Z, Yao Z, Tang H. *Microstructure and corrosion resistance of ceramic coating on carbon steel prepared by plasma electrolytic oxidation*, Surf Coat Tecnol, 2010; 204:1685-1688

[143] Wang Y, Jiang Z, Yao Z. *Preparation and properties of ceramic coating on Q235 carbon steel by plasma electrolytic oxidation*, Curr Appl Phy, 2009; 9: 1067-1071

[144] Wang Y, Jiang Z, Yao Z. *Microstructure, bonding strength and thermal shock resistance of ceramic coatings on steels prepared by plasma electrolytic oxidation*, Appl Surf Sci, 2009; 256: 650-656

[145] Abuali Galedari S, Mousavi Kohei M. *Characterization of Oxide Film Formed on Ck45 Steel by Plasma Electrolytic Oxidation Method,* Journal of Mechanical research and application, 2012; 4: 57-61

LIST OF PUBLICATIONS

Published Papers

-Pezzato L, Taverna B, Magrini M (2016). *Corrosione per pitting di strumenti chirurgici in ambiente disinfettante*, LA METALLURGIA ITALIANA, vol 1, p. 5-14

-Pezzato L, Brunelli K, Napolitani E, Magrini M, Dabalà M (2015). *Surface properties of AZ91 magnesium alloy after PEO treatment using molybdate salts and low current densities*. APPLIED SURFACE SCIENCE, vol.357, p. 1031-1039

- Cason C, Pezzato L, Breda M, Furlan F, Dabalà M, (2015) *Effect of microstructure and residual stresses, generated from different annealing and deformation processes, on the corrosion and mechanical properties of gold welding alloy wires*, GOLD BULLETIN, vol.48, p.135-145

-Pezzato L, Brunelli K, Dabalà M (2014). *Cromatura esavalente vs Cromatura Trivalente*. TRATTAMENTI & FINITURE

-Breda M, Pezzato L, Mészáros I, Calliari I (2014). *Duplex stainless steels: micro structural transformations induced by cold rolling*. PRAKTISCHE METALLOGRAPHIE, vol. 46, p. 253-258

-Breda M, Pezzato L, Pizzo M, Calliari I (2014). *Effect of cold rolling on pitting resistance in duplex stainless steels*. LA METALLURGIA ITALIANA, vol. 6, p. 15-19

- Pezzato L, Brunelli K, Gross S, Magrini M, Dabalà M (2014). *Effect of process parameters of plasma electrolytic oxidation on microstructure and corrosion properties of magnesium alloys*. JOURNAL OF APPLIED ELECTROCHEMISTRY, vol. 44, p. 867-879

-Brunelli K, Pezzato L, Napolitani E, Gross S, Magrini M, Dabalà M (2014). *Effects of atmospheric pressure plasma JET treatment on aluminum alloys*. SURFACE ENGINEERING, vol.30, p. 636-642

-Brunelli K, Pezzato L, Napolitani E, Gross S, Magrini M, Dabalà M (2014). *Influence of atmospheric pressure plasma treatments on the corrosion resistance of stainless steels*. LA METALLURGIA ITALIANA, vol. 7-8, p. 35-40

Submitted and accepted

-Pezzato L, Magnabosco M, Breda M, Brunelli K, Dabalà M, *Microstructure and mechanical properties of a 18kt 5N gold alloy after different heat treatments*, Metallography, Microstructure and Analysis

-Pezzato L, Brunelli K, Dabalà M , *Grey anodizing of a grade 5 titanium alloy: study of process parameters*, Materials Science Forum

-Pezzato L, Brunelli K, Dabalà M , *Corrosion properties of plasma electrolytic oxidation coated aa7075 treated using an electrolyte containing lanthanum salts*, Surface and Interface Analysis

Conference Proceedings

- Pezzato L, Brunelli K, Dabalà M (2015). *Effect of process parameters on type II anodization of a Ti6Al4V Titanium alloy*. In: Atti del convegno. EUROMAT 2015, Varsavia, 21-25 Settembre 2015

- Pezzato L, Brunelli K, Magrini M, Dabalà M (2015). *Effetto del nitrato di lantanio sulla resistenza a corrosione e le caratteristiche superficiali di una lega d'alluminio 7075 trattata mediante peo*. In: Atti del Convegno. Giornate Nazionali sulla Corrosione e Protezione, Ferrara, 15-17 giugno 2015

- Cason C, Pezzato L, Breda M, Dabalà M, *Effect of microstructure and residual stresses, generated from different annealing and deformation processes, on the corrosion and mechanical properties of gold welding alloy wires* In: Atti del convegno. EUROMAT 2015, Varsavia, 21-25 Settembre 2015

- Pezzato L, Brunelli K, Dabalà M (2015). *Corrosion resistance and surface characteristics of plasma electrolytic oxidation coating produced on steels*. In: Atti del convegno. EUROCORR 2015, Graz, 6-10 Settembre 2015

- Pezzato L, Magnabosco G, Brunelli K, Dabalà M (2015). *Effect of different heat treatments on the microstructure and the mechanical properties of a 750 gold alloy* . In: Atti del convegno. ECHT 2015, Venezia, 20-22/05/2015

- Pezzato L, Brunelli K, Dabalà M (2015). *Corrosion properties of PEO coated 7075 aluminum alloy treated using lanthanum-salts containing electrolyte*. In: Atti del convegno. ASST 2015, Madeira, Portugal, 17th - 21st May 2015

-Pezzato L, Brunelli K, Dabalà M (2014) *Resistenza a corrosione e caratteristiche meccaniche di componenti cromati: un confronto tra cromatura esavalente e trivalente*. In: Atti del convegno. Convegno Nazionale AIM, Roma 2014

-Pezzato L, Brunelli K, Magrini M, Dabalà M (2014). *Corrosion properties of PEO coatings obtained on Mg alloys with an electrolyte containing different concentrations of molybdate*. In: Atti del convegno. EUROCORR 2014, Pisa, 08-12 Settembre 2014

- Breda M, Pezzato L, Pizzo M , Calliari I (2013). *Effetto della deformazione plastica a freddo sulla resistenza al pitting negli acciai inossidabili Duplex*. In: Atti del convegno. Giornate Nazionali sulla Corrosione e Protezione , Napoli, luglio 2013

-Brunelli K, Pezzato L, Dabalà M, Magrini M (2013*). Influenza di trattamenti con plasma atmosferico sulla resistenza a corrosione di acciai inossidabili*. In: Atti del convegno. Giornate nazionali sulla corrosione e protezione. Napoli, 10-12 luglio 2013

-Pezzato L, Brunelli K, Dabalà M (2013). *Study of the corrosion properties of coatings obtained by plasma electrolytic oxidation on Mg alloys*. In: Atti del convegno. EUROMAT 2013, Siviglia, 8-13 september 2013

-Breda M, Calliari I, Pezzato L, Magrini M, Mészàros I, Pizzo M (2013). *Effect of cold deformation in duplex stainless steels*. In: Atti del convegno. EUROMAT 2013, Siviglia, 8-13 September 2013

-K. Brunelli, L. Pezzato, E. Napolitani, M. Magrini (2012). *Influenza di trattamenti con plasma atmosferico sulla resistenza a corrosione di leghe d'alluminio*. In: Atti del convegno. Convegno Nazionale AIM 2012, TRENTO, 7-9 Novembre 2012

ACKNOWLEDGMENTS

At the end of this thesis work some acknowledgments are dutiful. First of all I want to thank my family for always supporting me in my decisions during this Ph.D and all my friends from Padua and Schio zones for always being next to me in this period.
I clearly thank my supervisor prof. Manuele Dabalà for guiding me for this years and for having always given me great autonomy and confidence. A big thank also to Katya for all the work performed together and the lots of teachings and to prof. Magrini for the always helpful words.
I thank also Marco, Pierre, Claude e Totò for being friends as well as colleagues, for the collaboration, the support and all the nice moments during this years. A thank also to Spezza for being a Ph.D student with me after the degree and to all the others Ph.D students that have worked with me in this years.
Thanks also to all the current and past members of the metallurgy group: Prof.ssa Calliari, Giulia, Massimiliano, Rodrigo and the ones that I'm forgetting, each of you was important for me.
A mention to all the students that do their thesis with me, especially the ones whose work involve PEO: Marco, Fabio and Giulia.

RINGRAZIAMENTI

Giunti alla fine di questo lavoro di tesi che conclude e riassume il mio percorso di dottorato desidero ringraziare tutti quelli che mi sono stati vicini e mi hanno aiutato in questi anni. Bisogna però essere brevi, cosa per me non facile, ma farò del mio meglio.
Il primo ringraziamento va quindi alla mia famiglia che mi ha sempre sostenuto nelle mie decisioni lungo questo percorso e che mi ha sempre aiutato.
Un ringraziamento va chiaramente al prof. Manuele Dabalà per l'aiuto e la guida durante il dottorato, per la fiducia sempre dimostrata nonché per avermi dato, dopo la laurea, la possibilità di svolgere questo percorso; con lui mi sono sempre trovato benissimo sia dal punto di vista umano che lavorativo. Un grazie anche a Katya per tutto il lavoro svolto insieme e i tanti insegnamenti in laboratorio e al prof. Maurizio Magrini per i sempre utili consigli.

Grazie anche a Marco che mi ha insegnato a "fare il dottorando" e mi ha guidato e aiutato molto durante i miei primi anni in laboratorio. Grazie anche ovviamente a Pierre, Claude e Totò, coloro che rimangono dottorandi (al momento); grazie per essere stati amici prima ancora che colleghi e per l'aiuto, collaborazione e sostegno quotidiano sia in laboratorio che fuori. Con alcuni di voi ci si conosceva da tempo, con altri ci siamo conosciuti durante il dottorato, di certo senza di voi il lab sarebbe un luogo più noioso. Un doveroso ringraziamento anche all'amico Spezza con il quale dopo gli anni della laurea ho condiviso anche questi di dottorato, anche se in laboratori diversi, e con il quale il confronto sui più disparati temi non è mai mancato; sarà strano non recarsi più a Padova insieme.

Un grazie anche a tutti gli amici di Schio e dintorni per essermi stati vicino e avermi sostenuto e anche grazie a voi che sono riuscito a concludere questo dottorato in maniera positiva.

Un grazie anche a tutti gli altri dottorandi, in particolare quelli a meccanica e al "piano di sotto" con cui ho cominciato questo percorso e che ora con me concludono oppure che rimangono, ci siamo spesso aiutati nelle varie faccende e questo ha reso più facile l'intero percorso.

Un grazie a tutti coloro che fanno parte o che hanno fatto parte del gruppo di metallurgia: prof. Calliari, Massimiliano, Giulia, Rodrigo, Caterina e qualcun altro che sicuro sto dimenticando, ognuno di voi è stato importante durante questo mio percorso e mi avete aiutato molto.

Infine (ma non ultimi) vanno certamente ricordati e ringraziati tutti gli studenti che ho seguito durante la loro tesi di laurea, ognuno mi ha sicuramente dato qualcosa dal punto di vista personale e io spero di essere stato un valido aiuto per ciascuno di loro. Non essendo possibile ricordarli tutti citiamo solamente quelli la cui tesi ha riguardato il PEO è che hanno quindi direttamente contribuito con il loro operato in laboratorio a questo lavoro di tesi: Marco, Fabio e Giulia.